Structural investigations on the interaction and phosphorylation of TAp63

Dissertation

zur Erlangung des Doktorgrades

der Naturwissenschaften

vorgelegt beim Fachbereich

Biochemie, Chemie und Pharmazie (FB 14)

der Johann Wolfgang Goethe-Universität

in Frankfurt am Main

von

Jakob Gebel

aus Solingen

GOETHE

UNIVERSITÄT

FRANKFURT AM MAIN

Frankfurt am Main, 2018

(D30)

Vom Fachbereich Biochemie, Chemie und Pharmazie (FB 14) der

Goethe-Universität als Dissertation angenommen.

Dekan: Prof. Dr. Clemens Glaubitz

Gutachter: Prof. Dr. Volker Dötsch

              Prof. Dr. Clemens Glaubitz

Datum der Disputation: _____

*"Failure is **always** an option."*

Adam Savage

Eidesstattliche Erklärung

Ich erkläre hiermit an Eides statt, dass ich die vorgelegte Dissertation über „Structural investigations on the interaction and phosphorylation of TAp63" selbständig angefertigt und mich anderer Hilfsmittel als der in ihr angegebenen nicht bedient habe. Ich erkläre weiterhin, dass Entlehnungen aus Schriften, soweit sie in der Dissertation nicht ausdrücklich als solche bezeichnet sind, nicht stattgefunden haben. Ich habe bisher an keiner anderen Universität ein Gesuch um Zulassung zur Promotion eingereicht oder die vorliegende oder eine andere Arbeit als Dissertation vorgelegt.

Frankfurt am Main, den 26.09.2018

_____

Jakob Gebel

Inhaltsverzeichnis

Abbreviations

9aaTAD	9 amino acid Transactivation Domain
AEC	ankyloblepharon-ectodermal dysplasia-clefting syndrome
Akt	Protein Kinase B
AL	Activation Loop
AML	Acute myeloid leukemia
APBS	Adaptive Poisson-Boltzmann Solver
APE1	AP endonuclease 1
ASPP	Apoptosis-stimulating of p53 protein
Bcl-2	B-cell lymphoma 2
BAX	Bcl-2-associated X protein
BER	Base Excision Repair
BEST	Band-selective Excitation Short-Transient
BN	Blue Native
BRD	Bromo domain
CBP	shorer form of CREBBP
CEX	Cation Exchange
CIMD	Caspase-Independent Mitotic Death
CLOCK	Circadian locomoter output cycles protein kaput
CoA	Co-Enzyme A
CREB	cAMP response element-binding protein
CREBBP	CREB Binding Protein
Cryo-EM	Cryogenic Electron Microscopy
CSP	Chemical Shift Perturbation
CTD	C Terminal Domain
CV	Column Volume
DBD	DNA binding domain
DMSO	Dimethyl sulfoxide
DNA	Deoxyribonucleic acid
dNTP	Deoxynucleoside triphosphate
DOX	Doxorubicin
DSS	4,4-dimethyl-4-silapentane-1-sulfonic acid
EDTA	Ethylenediaminetetraacetic acid

EEC	Ectrodactyly-ectodermal dysplasia-cleft
FBS	Fetal bovine serum
GB1	Protein G B1 Domain
GFP	Green Fluorescent Protein
GNAT	Gen5-related acetyl-transferases
GST	Glutathione S-transferase
HAT	Histone Acetylase
HEPES	4-(2-hydroxyethyl)-1-piperazineethanesulfonic acid
HMBC	Heteronuclear Multibond Correlation
HMGB1	high-mobility group protein 1
IBiD	Interferon Binding Domain (also known as NCBD)
IMAC	Immobilized Metal Affinity Chomatography
IR	Ionizing Radiation
IRF	Interferon
KAT	Lysine acetyltransferase
KET	old name for p63
KID	(pKID) Kinase Inducible Domain
Kix	KID interacting domain
KO	Knock Out
LSM	Light Sheet Microscope
MBP	Maltose Binding Protein
MCC	Motile Multiciliated Cells
MDM2	Murine Double Minute 2
MDM4	Murine Double Minute 4
MED15	Mediator of RNA polymerase II transcription subunit 15
MEF	mouse embryonic fibroblasts
MLL	mixed-lineage leukemia
MSY-2	Y-box-binding protein 2
MTSL	S-(1-oxyl-2,2,5,5-tetramethyl-2,5-dihydro-1H-pyrrol-3-yl)methyl methanesulfonothioate
NCBD	nuclear receptor coactivator binding domain, alternative name of the IBiD domain
NEIL1/2	Nei-like 2 DNA glycosylases
NER	Nucleotide Excision Repair
NES	Nuclear Export Signal
NIH	National Institute of Health
NLS	Nuclear Localization Signal
NMR	Nuclear Magnetic Resonance
NOESY	Nuclear Overhauser Effect Spectroscopy
Noxa	Phorbol-12-myristate-13-acetate-induced protein 1
NP	Native Page

OD	Oligomerization domain
OGG1	8-Oxoguanin DNA glycosylase 1
OL	Overlap extension
P21	cyclin-dependent kinase inhibitor 1
PAD	Phospho-Activation Domain
PAGE	Polyacrylamide Gelelectrophoresis
PARP-1	Poly ADP-ribose polymerase 1
PBS	Phosphate Buffered Saline
PCAF	p300/CBP Associated Factor
PCR	Polymerase Chain Reaction
PDB	Protein Databank
PFA	Para-Formaldehyde
PHD	Plant Homeo Domain
PKC	Proein Kinase C
PML	promyelocytic leukemia
PRE	paramagnetic relaxation enhancement
PUMA	p53 upregulated modulator of apoptosis
RecQ	ATP-dependent DNA helicase
re-IMAC	reverse Immobilized Nickel Affinity Chromatography
RING	Really Interesting New Gene
RPA	Replication Protein A
RPA	Replication protein A
RT	Room Temperature
SAC	Spindle Assembly Checkpoint
SCC	Squamous Cell Carcinoma
SDS-PAGE	SDS Polyacrylamide Gel Electrophoresis
SDS	Sodium Dodecyl-sulfate
SIRT1	Sirtulin-1
SRC1	nuclear receptor coactivator 1
SSRP1	Structure specific recognition protein 1
STAT	Signal transducer and activator of transcription
SUMO	Small Ubiquitin like Modifier
TAD	Transactivation Domain
Taz	Transcription Adaptor putative Zinc finger
TBP	TATA-binding protein
TD	Tetramerization Domain
TDG	Thymine DNA Glycosylase
TFIIH-PH	Transcription Factor II subunit H Pleckstrin homology domain
TSA	Thermal Shift Assay

TI	Transactivation Inhibition Domain
TOCSY	Total Correlation Spectroscopy
TROSY	Transverse Relaxation Optimized Spectroscopy
VDAC	mitochondrial voltage-dependent anion channel
WB	Western Blot
WRN	Werner Protein
XPA	DNA repair protein complementing XP-A cells
XPG	DNA repair protein complementing XP-G cells

Summary

The p53 family of transcription factors is composed of three members, p53, p63 and p73. p53 was discovered first in 1979 and described as an oncogene, because it was frequently found in higher quantities in tumor tissue compared to normal somatic cells. Soon after it was recognized that these highly expressed variants were in fact mutated, non-functional proteins. Additionally it was discovered that native p53 expression leads to senescence and/or apoptosis. It became clear that p53 is in fact a potent tumor suppressor protein, becoming activated though DNA damage sensing. Later two homologs of p53 were discovered. Due to their larger size they were termed p73 and p63. All three members of the family consists of several conserved domains with folded linkers in between them. p53 contains three distinct domains, the amino-terminal Transactivation Domain (TAD), the central DNA binding domain (DBD) and the carboxy-terminal Oligomerization Domain (OD). In case of p63 and p73 the protein is elongated and contains a Sterile Alpha Motif (SAM) Domain as well as a carboxy-terminal Transcription Inhibition Domain (TID). Furthermore p63 and p73 are present in a variety of different isoforms, due to alternative splicing in the carboxy-terminus as well as two different promoters, giving rise to two amino-terminal variants (TA- and ΔN-variants). In case of p63 two even more N-terminally elongated isoforms have been described recently (TA* and GTA). ΔN-variants of p63 and p73 lack the N-terminal TAD and are therefore unable to lead to transactivation on classical p53 promoters. ΔN-isoforms are thereby considered to functional repressors and potential oncogenes. All isoforms of the family form tetramers and the tetramerization is required for the proper activity of the proteins. TAp63α is the longest p63 isoform and is the outstanding exception, as it is inherently a dimeric protein (see below). The activity of p53 in somatic cells is regulated via a feedback loop with the E3 ligase Mouse Double Minute 2 (MDM2). The MDM2 promoter features a p53-response element, leading to a higher MDM2 expression as a response to an increase in p53 levels. This ensures that p53 underlies a fast turnover, thereby preventing the induction of senescence or cell death. Upon DNA damage the p53 transcriptional potential is massively increased by phosphorylation of residues within the TAD, leading to a massive increase of affinity to transcriptional co-activators while only having a moderate effect on the affinity to MDM2. The regulation of TAD-containing p73 isoforms is related to the p53 regulation, with the exception that p53 shows a high basal activity even without any phosphorylations in the TAD while p73 is transcriptionally almost dead and needs to be modified to increase the transactivation potential. In general p73 is present in the differentiating epidermis and plays a role in the development of the brain. Additionally mice lacking p73 have a chronically inflamed lung and the

males are almost sterile due to failure of correct formation of the blood-testis-barrier. TAp63α is regulated in a totally different way, compared to the other two proteins. It is present in high quantities in primordial oocytes, where it is in a completely inactive dimeric state. Irradiation of ovaries or treatment with DNA double strand break inducing agents leads to subsequent phosphorylation events in the protein by two independent kinases and as a result tetramerization. The resulting tetramer is fully active and is able to bind pro-apoptotic promoters, inducing cell death. This ensures the genetic integrity of the female germline by eliminating all oocytes that have been damaged. The acetylation of proteins is the most abundant chemical modification of proteins, besides phosphorylation. Originally acetylation was described for histones thereby the acetylating enzymes are termed Histone Acetylases and the deacetylating enzymes Histone Deacetylases (HDACs). Acetylation of proteins other than histones is relevant for a great variety of processes in cells such as protein localization or enzymatic activity. In humans five different families are distinguished (KAT1 to KAT5) varying greatly in structure and functionality. The most prominent family is the KAT3 family with its two members p300 and CBP. Both are large proteins of $\approx$2400 amino acids which are largely unfolded with several domains arranged in a pearls-on-a-string-like arrangement. Four of these domains (Taz1, Kix, Taz2 and IBiD) have been shown to interact with TADs of transcription factors such as the p53 family. Additionally the proteins harbor the catalytic Histone acetyltransferase enzymatic domain (HAT), an acetyl-lysine binding Bromo domain, a methyl-lysine binding Plant Homeo Domain (PHD) with an interspersed Really Interesting New Gene (RING) domain as well as a SUMO1 binding ZZ-domain. Both Taz-type domains are zinc-finger domains where the structure is stabilized by three zinc ions in total. Of all four TAD interacting domains the Taz2 domain is generally the strongest binder of p53 family TADs. CBP and p300 are highly homologous proteins, with an almost complete conservation within folded domains. Unsurprisingly differences in protein function are not well understood. The Rubinstein-Taybi syndrome (RTS) is the only known genetic disorder for either CBP or p300 where an obvious phenotype is seen in patients. Generally it is the result of deletion or loss of function mutation within one allele of CBP. Deletion or loss of function of p300 is rarely described and generally seems to lead to a less severe phenotype in patients. The phenotypes are a general severe learning disability. Deletion or inactivation of more than one of the two alleles of both proteins in any combination is considered to be embryonic fatal. One aim of this thesis was to structurally characterize the interaction of the Taz2 domain with the TAD of p63 as well as p73 as a comparison. Furthermore the results of direct acetylation within the p63 in context of oligomeric state, transactivation capabilities and protein turnover were investigated.

As a first step several potential transcriptional co-activators known to interact with p53 were tested for potential interaction with TAp63 and TAp73 via pull-down assay. Neither the middle domain of SSRP1, the Kix domain of MED15 nor the HMGB1 BoxA showed significant interaction with the TAD of p63 or p73. The SSRP1 domain showed interaction with the TID of both proteins. This however could only be due to unspecific interaction with the highly hydrophobic amino acids of these domains. Furthermore Taz1 and Taz2 of p300 were tested for interaction

with the longest isoform of p63 and p73 (TAp63α and TAp73α) as well as a truncated variant of both proteins which lacks the TID (γ-isoform in case of p63 and β-isoform in case of p73). Interestingly interaction with both p300 domains could be detected for all tested variants except TAp63α. This indicates that the TAD of the dimeric p63 variant is completely buried within the protein and totally unavailable for transactivation. The lack of transactivation activity for the dimeric isoform has been previously reported, which fits nicely to this result. As a next step the TAD of p63 was further characterized via peptide-spot membrane with the Taz2 domain. Interestingly the resulting Taz2 binding peptide is not completely identical to the MDM2 binding motif as suspected earlier, but shifted further to the N-terminus of the protein. This result was verified by performing NMR titration experiments with two short peptides, both including the MDM2 binding motif, elongated N-terminally or C-terminally. Here the N-terminally elongated peptide showed much stronger CSPs, indicating that this sequence is indeed As a next step the complete peptide sequence shown to interact with the peptide membrane was expressed and titrated onto ^{15}N-labeled Taz2 domain. The resulting spectra showed extensive line-broadening, indicating intermediate exchange. To circumvent the problem the length of the peptide was reduced, resulting in smaller linewidth. Unfortunately a stable complex was not attainable as the peptide showed additional binding at a 2nd site after almost reaching saturation at the first binding site, resulting in a reduced protein stability as well. To solve the intermediate exchange issue as well as the 1:1 complex formation a fusion construct between Taz2 and the p63 TAD was constructed. The attained spectra showed line shapes in agreement with the size of the protein and extraordinary protein stability at millimolar concentrations. Two similar constructs of the Taz2 domain with the p73 TAD were constructed, as intermediate exchange for Taz2:p73 TAD interaction was reported, as well. The structure of Taz2-p63TAD shows a structure comparable to a previously solved Taz2-p53TAD2 structure, whereas the Taz2-p73TAD1 structure seems to indicate a different organization of the p73 TAD. Generally TADs interacting with the Taz2 domain form a single helix on the surface of helices 1-3 of Taz2. The p63 peptide is shows an extremely long helix with similar orientation to the p53 TAD2. In contrast to this the p73 TAD1 peptide forms a short helix but the majority of the interaction is mediated by two aromatic residues in a stretched conformation. Mutation of these two residues in a p73 TAD1 peptide does not completely abolish the interaction with the Taz2 domain but decreases the affinity at least 50-fold. To further understand the differences in the transactivation domains of p73 and p63 the binding affinities of several peptides with the Taz2 domain were tested by fluorescence anisotropy. A p63 peptide showed a K_D comparable to that of the p53 TAD2 (200 nM) whereas the p73 affinity was much lower ($\approx$1 μM). This effect is rescued by phosphorylation of two residues within the p73 TAD preceding the two aromatic residues described above. Additionally the affinity of the p63 TAD can be transferred to the p73 TAD1 by exchanging the homologous amino acids to the amino acids of the N-terminal elongated short peptide discussed above. This exchange also drastically increases the transactivational capabilities of TAp73β as seen in a transactivation assay, indicating that this exchange most likely leads to a switch from the p73 conformation

seen in the structure to a more p63-like conformation. Furthermore the inhibition of p300/CBP in mouse ovaries during genotoxic stress was tested. 3D ovary staining revealed a rescue of the primordial oocytes, indicating that p300/CBP in oocytes is necessary for the efficient induction of apoptosis as a result of DNA damage. Lastly the direct acetylation of TAp63α within H1299 under DNA damaging conditions was analyzed. In total 12 direct acetylation events could be found in mass spectrometry data from a related project. The acetylation sites were found dispersed throughout the protein with a cluster in an unfolded region between the DBD and the TD. Additionally several residues of the DBD and TD were found to be acetylated. The acetylation sites were examined for transactivation potential, protein turnover rates and oligomeric state within the TAp63α dimer by introducing selective mutations to either mimic acetylation (K$\rightarrow$Q) or inhibit acetylation (K$\rightarrow$R). All tested mutants of TAp63α were seen to be dimeric, thereby the mutations, even within the TD do not affect the protein oligomeric state. To test the transactivation potential the mutations were introduced into the constitutive tetrameric isoform TAp63γ and were subject to a transactivation assay on the p21 promoter. All tested variants showed similar transactivation potential but grossly different total protein level. TAp63γ mutants were also subject to a cycloheximide chase experiment to determine the turnover of the protein within the cells. Three of the mutated constructs showed greatly increased protein stability, independent of the type of mutation (acetyl-mimic or acetyl-dead), thereby suggesting that these lysines are relevant for ubiquitination and subsequent degradation of the protein. Moreover acetylation events within the TD showed drastically reduced protein stability in the cycloheximide chase experiment as well as the transactivation assay. The isolated TDs harboring one acetyl-mimic mutation each showed a reduction in melting temperature by 20°C, raising the question if the proteins are stable tetramers at the cellular expression levels at all. The nuclear export signal (NES) of p63 is located within the first helix of the tetramerization domain and is buried within the folded TD in the active state of the protein. Instability of the TD due to acetylation might lead to the export of the protein from the nucleus to the cytoplasm where it is then rapidly degraded. Adding to this, one of the acetylation sites was found to be located directly within the nuclear localization signal (NLS), probably reducing the tendency of the protein to be re-imported to the nucleus again.

Additionally the kinetics of activation of TAp63alphaα by phosphorylation was investigated. Isotopically-labeled, MK2 pre-phosphorylated (S582), peptide was phosphorylated with CK1δ kinase at 25°C during an NMR-titration experiment. The results reveal residues that are phosphorylated and at which time scale. CK1δ phosphorylates in +3 position of a given phosphorylated serine or threonine. In the given p63 sequence four amino acids fit this sequence (S585, S588, S591, T594). Interestingly the phosphorylation is not processive, S585 and S588 become phosphorylated much faster than S591 and T594 ($\approx$30-fold faster). The phosphorylation of S585 and S588 is almost equally fast. Additionally another threonine (T586) gets phosphorylated, matching the slower kinetic of S591 and T594.

Mutational analysis showed that the different kinetics within this sequence might be a feature

of the sequence itself and not of the kinase, as mutation within the sequence can almost remove the staggering effect completely. Finally X-ray crystallography shows that the S582, S585, S588 phosphorylated peptide is preferentially bound in a product-state within the kinase, thereby leading to stalling of the phosphorylation process.
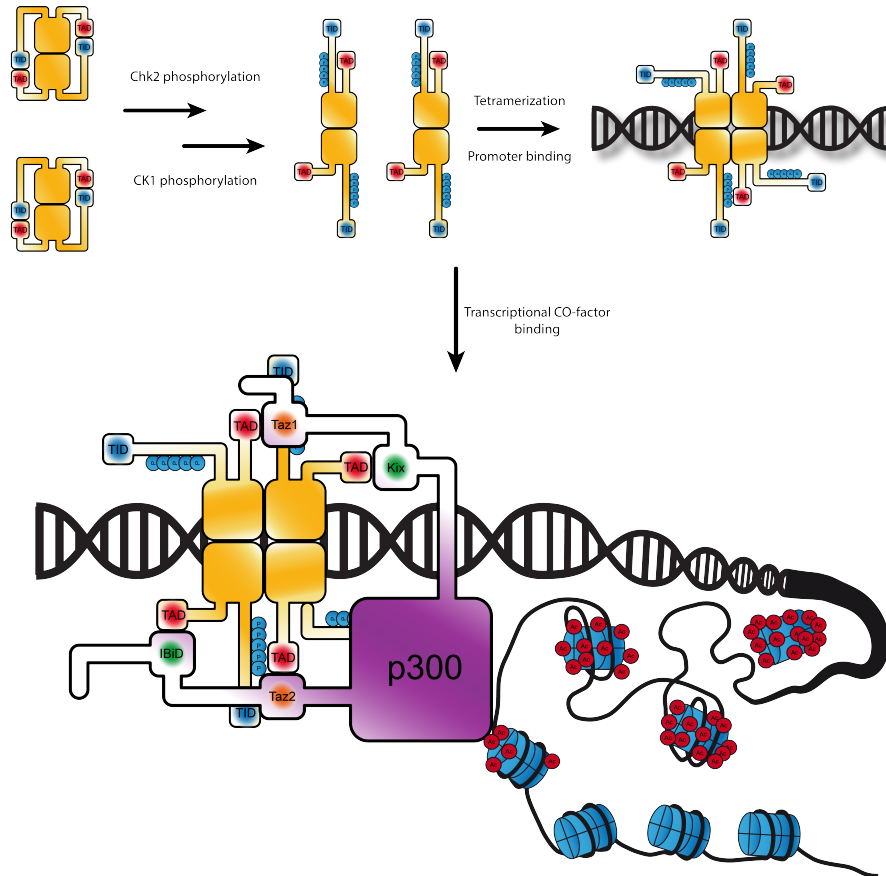
Model of the activation of TAp63α.

Zusammenfassung

Die Tumorprotein-Familie des Proteins p53 besteht aus den drei Familienmitgliedern p53, p63 und p73 mit diversen Funktionen. Als Transkriptionsfaktoren übernehmen die DNA-bindenden Proteine diverse Funktionen in verschieden zellulären Kontexten. p53 war das erste Mitglied dieser Familie, das im Jahre 1979 entdeckt wurde und hat, wie der Name impliziert, ein Molekulargewicht von etwa 53 kDa. p53 wurde zunächst als krebsverursachendes Protein eingeordnet (Oncogen), weil es in vielen Tumorgeweben in erhöhter Menge vorgefunden wurde. Einige Zeit später wurde allerdings festgestellt, dass der Großteil dieser gefundenen p53 Proteine Mutationen in ihrer Aminosäure-Sequenz aufwiesen und daher so nicht mehr funktionsfähig waren. Unmutiertes p53 hingegen führt zu einem Stopp von Zellteilung oder sogar Zelltod, sofern die Zellen genetischem Stress erfahren. Dieser wird durch DNA-Doppelstrangbrüche verursacht, wenn die Zellen Strahlung oder mutagenen Chemikalien ausgesetzt sind. Heute wird p53 als eines der wichtigsten Tumor-Unterdrückungsproteine betrachtet. Die beiden anderen Familienmitglieder p63 und p73 existieren in einer Vielzahl von Isoformen. Neben carboxy-terminaler alternativen mRNA-Prozessierung (Splicing, α,β,γ) führen zwei unabhängige Promotoren auch zu zwei unterschiedlichen Amino-Termini. Hier wird zwischen ΔN und TA-Isoformen unterschieden. Im Falle von p63 treten zwei dominante Isoformen auf, ΔNp63α und TAp63α. Während ΔNp63α eine Rolle in der Differenzierung von Haut spielt, wurde TAp63α bisher ausschließlich in Eizellen gefunden. Dort hat es die Funktion eines Sensors, der die genetische Integrität der weiblichen Keimbahn sicherstellt. Es liegt in Eizellen in hoher Konzentration vor, allerdings in einer komplett inaktiven Form. Werden Schäden im der Erbgut der Eizelle festgestellt, so wird das Protein aktiviert und aktiviert den Prozess des Zelltods in der Eizelle. Mutationen oder das Fehlen des p63 Genes führt zu Missbildungen während der Entwicklung und zu unvollständig ausgebildeter Haut. Im Falle von p73 gibt es ebenfalls mehrere Isoformen, wobei die Funktionen und Relevanzen der einzelnen Isoformen bisher nicht komplett geklärt werden konnten. Eine genotypisch p73-negative Maus hat einen diffusen Phänotyp, der sich durch niedrige Intelligenz, fast sterile Männchen und chronische bronchiale Infektion auszeichnet. Generell sind alle Mitglieder der p53 Familie tetramere Proteine und sind nur in diesem Zustand auch aktiv. Die einzige Ausnahme stellt, wie oben beschrieben, TAp63α dar, das in einem inaktiven dimeren Zustand vorliegt und nur durch Modifikation durch zwei unabhängige Kinasen aktiviert werden kann. Die Interaktion von zwei Domänen im Protein wird so unterbrochen, sodass eine Öffnung und Mulitmerisierung möglich ist. Im tetrameren Zustand ist TAp63alpha daraufhin aktiv.Dabei geht es in den tetrameren Zustand über und ist daraufhin aktiv. Alle drei Proteine haben (anhand

der längsten Isoformen beschrieben) eine konservierte Domänenstruktur. Am Amino-Terminus befindet sich zunächst die transaktivierende-Domäne (TAD), die für Interaktionen mit transkriptionellen Koaktivatioren relevant ist. Danach folgt die stark konservierte Desoxyribonukleinsäure (DNA) bindende Domäne (DBD). Sie stellt sicher, dass der Transkriptionsfaktor sequenzspezifisch an der richtigen Stelle auf die DNA bindet. Weitergehend folgt die Tetramerisierungsdomäne (TD), welche den oligomeren Zustand des Proteins herstellt. Im Falle von p53 endet das Protein an dieser Stelle, bei p63 und p73 folgen noch das Sterile-Alpha-Motiv (SAM) und die Transkription-inhibierende Domäne (TID). Die SAM-Domäne wird generell als Interaktionsdomäne beschrieben, hat in beiden Proteinen allerdings eine unbekannte Funktion, da bis dato kein Interaktionspartner gefunden werden konnte. Die TID hat einen negativen Einfluss auf die transkriptionelle Aktivität der Proteine. Im Falle von TAp63α kommt noch eine Interaktion mit der TAD hinzu, welche maßgeblich zur Ausbildung des inaktiven Dimers beitägt. Diese Arbeit behandelt verschiedene Aspekte der Funktion von TAp63α, welche sich aus Fragestellungen aufgrund der speziellen Struktur ergeben.

Die Acetylierung von Histonen ist neben deren Methylierung die wichtigste Modifikation. Sie ist essenziell für die Transkription innerhalb aller eukaryontischen Lebewesen, da sie durch die Modifikation von Histonen die DNA für DNA-Polymerase II zugänglich macht. Es gibt insgesamt fünf verschiedene, nicht näher miteinander verwandte Familien von Histonacetylasen. Diese Studie beschäftigt sich mit der KAT3 Familie, bestehend aus den Proteinen p300 und CBP. Beide sind hochgradig konserviert, in gefalteten Bereichen der Proteine erreicht die Sequenzidentität fast 100%. Beide Proteine scheinen sehr ähnliche Aufgaben zu erfüllen, die jedoch nicht komplett identisch sind. Während eine Fehlfunktion von CBP auf nur einem Allel zum Krankheitsbild des Rubinstein-Taybi-Syndrom (RTS) führt, wirkt sich ein Mangel am p300 in Mäusen auf das Gedächtnis aus. Jedoch weisen RTS Patienten ebenfalls eine geringe Intelligenz und einen sehr schleppenden Lernverlauf auf. Der komplette Verlust beider Allele eines der Proteine ist immer tödlich, genauso wie auch der gemeinsame Verlust jeweils eines Allels von p300 und CBP. Insgesamt vier unabhängige Domänen in p300/CBP sind in der Lange die transaktivierende-Domänen der p53 Familie zu binden. Bei zwei der Domänen handelt es sich um Zinkfinger-Proteine (Taz1 und Taz2), die anderen beiden sind kleine, ausschließlich α-helikale Domänen (Kix und IBiD). Diese Studie beschäftigt sich mit der Lösung von Strukturen von der transaktivierenden-Domäne von p63 und p73 mit der p300-Domäne Taz2. Zusätzlich wurden die Auswirkungen von direkten Acetylierungen in TAp63α charakterisiert und der Effekt von einem potenten p300/CBP Inhibitor auf Oozyten unter genotoxischem Stress analysiert.

Zunächst wurde die Bindung von verschiedenen p63- und p73-Isoformen an Domänen von unterschiedlichen p53-Interaktionspartnern untersucht. Während die Interaktionen für die untersuchten Proteine für p53 bestätigt werden konnten, so konnte für p63 und p73 nur gezeigt werden, dass der Carboxyterminus der α-Isoformen für die Interaktion verantwortlich zu sein scheint. Dieses Ergebnis ist nicht sicher als direkte Bindung zu verstehen, da die TID zu Ag-

gregation neigt und somit eine unspezifische Interaktion der Auslöser für dieses Resultat sein könnte. Die einzige Ausnahme waren die p300-Domänen Taz1 und Taz2, wo eine eindeutige Interaktion mit der TAD gezeigt werden konnte. Weitergehend wurde die tatsächliche TAD von p63 mittels einer Peptid-Punkt-Membran-Analyse charakterisiert. Das Ergebnis wurde mit der bereits identifizierten Sequenz aus p73 verglichen. Die ermittelte Sequenz wurde bakteriell exprimiert und eine Kernspinresonanz-Titration mit Taz2 als Bindungspartner durchgeführt. Dabei wurde beobachtet, dass sich der Peptid:Protein Komplex in der Nähe des intermediären Austauschs befindet und daher die Linienbreite sehr hoch war. Eine Kürzung des Peptids hat die Austauschrate erhöht und somit die Linienbreite verringert. Allerdings konnte dabei festgestellt werden, dass ein Taz2-Protein in der Lage ist multiple p63-Peptide simultan zu binden. Neben der massiven Erhöhung der Komplexität der Strukturlösung wies dieser komplex auch noch eine sehr niedrige Stabilität auf und starkem Proteinverlust durch Ausfallen wurde während der Messung beobachtet. Um dieses Problem zu umgehen wurde ein Fusionskonstrukt entwickelt, sodass eine Taz2-Domäne stets im Komplex mit einem p63/p73-TAD-Peptid vorliegt. Die resultierenden Proteine zeigten eine gute Stabilität bei hohen Konzentrationen, sodass entschieden wurde die Struktur mit diesen Konstrukten zu lösen. Im Falle von p73 wurden zwei verschiedene Peptidlängen verwendet, da bekannt ist, dass sich innerhalb der ersten 70 Aminosäuren von p73 zwei Interaktionstellen für die Taz2-Domäne befinden. Beide resultierenden Strukturen zeigen eine helikale Konformation des Peptides, gebunden auf die Helices 1-3 der Taz2-Domäne. Die auf der Taz2 gebundene p63-TAD formt mit 13 Aminosäuren die längste bisher charakterisierte Helix der p53-Familie. Im Falle von p73 ist die Helix mit 9 Aminosäuren deutlich kürzer, allerdings befindet sich auf der carboxyterminalen Seite der Helix noch eine auf die Taz2 gebundene gestreckte Aminosäuresequenz. Diese scheint essenziell für die Taz2-Bindung zu sein, da zwei aromatische Seitenketten in dieser Sequenz tief in der Taz2-Domäne binden und deren Mutation zu Alanin zu einem starken Verlust von Bindungsaffinität führen. Die Struktur des längeren Taz2-p73 Konstruktes konnte nicht zufriedenstellend gelöst werden, da die Interaktion des Carboxyteminus des Peptids eine zu kurzlebige Interaktion zur Taz2-Domäne hat und daher keine eindeutigen Signale im Kern-Overhauser-Effekt-Spektrum (NOESY) detektiert werden konnten. Die Affinitäten der p63-TAD liegen im erwarteten Bereich für eine transkriptionell aktive Transaktivierungsdomäne ($\approx$200 nM für die Taz2-Bindung). Interessanterweise ist die TAD nur an einer Stelle durch Phosphorylierung modifizierbar. Im Vergleich dazu hat die entsprechende p73-Sequenz im gleichen Bereich sieben phosphorylierbare Reste. p73 zeigt eine sehr geringe intrinsische transkriptionelle Aktivität, welche vermutlich durch Phosphorylierung gesteigert werden kann. Um dies zu testen wurde, basierend auf der Struktur, ein doppelt phosphoryliertes Peptid synthetisiert und die Affinitäten zu Taz2 gemessen. Wie erwartet hat sich die Affinität um fast einen Faktor zehn verbessert, zu einem p63-TAD-ähnlichen Wert. Dies wird sich vermutlich im gleichen Maße auf die transkriptionelle Aktivität von phosphoryliertem p73 auswirken. Zusätzlich wurde ein Hybrid-Peptid getestet, bei welchem die Aminosäuren 8-15 von p63 in die TAD von p73 integriert wurde. Dabei konnte beobachtet werden, dass die Affinität dieses Peptides

vergleichbar mit der Affinität des p63-TAD-Peptids ist. Generell erscheint der unterschiedliche Aufbau von beiden TADs sinnvoll, da TAp63α als inaktives Dimer vorliegt und nicht in der Lage ist transkriptionell aktiv zu sein. Wird es aufgrund von DNA-Schäden aktiviert so verändert es seinen oligomeren Zustand und ist schlagartig voll aktiv, ohne auf weitere Modifikationen angewiesen zu sein. Im Gegensatz dazu scheint TAp73 als Integrator von zellulären Zuständen eine sehr feingliedrige Aktivierung zu durchlaufen, vermutlich da es die Expression von Proteinen kontrolliert, die weder zu wenig noch zu viel vorhanden sein dürfen um so eine korrekte Funktionalität zu gewährleisten.

TAp63α wird in kultivierten H1299 Zellen unter DNA-Stress Bedingungen an mehreren Stellen selbst acetyliert. Alle Acetylierungen wurde einzeln auf transkriptionelle Aktivität getestet und es konnte kein Unterschied festgestellt werden. Allerdings konnte gezeigt werden, dass zwei Lysine-Seitenketten durch Acetylierung die Proteinlebensdauer stark erhöhen. Zusätzlich wurden zwei acetlyierte Lysine innerhalb der Tetramerisierungsdomäne gefunden. Hier führt Acetylierung zu einer massiven Destabilisierung der Faltung des Proteins. Acetylierungen dieser Aminosäuren haben daher auch einen stark negativen Effekt auf die Lebensdauer des Proteins, obwohl sie augenscheinlich keinen Einfluss auf die transkriptionelle Aktivität haben.

Abschließend wurde der Effekt der Inhibierung von p300/CBP mittels des neuartigen Inhibitors A-485 getestet. Es wurden dreidimensionale proteinspezifische Zellfärbungen angefertigt und mittels eines Lichtscheibenmikroskops analysiert. Dabei hat sich gezeigt, dass die Inhibition von p300/CBP zunächst ausreichend ist um Oozyten vor DNA-Schäden induziertem Zelltod zu schützen. Dabei ist allerdings fraglich, ob dies ein valider Ansatz für die Erhaltung der weiblichen Fruchtbarkeit unter Chemotherapie ist, da p300/CBP sowohl entscheidend für die Funktion vieler Tumorsuppressoren, als auch eine wichtige Rolle in der Regulierung der DNA Reparatur spielt.

Als weiteres Projekt wurde die Phosphorylierungskinetik von TAp63α analysiert um ein Verständnis der Geschwindigkeit der Aktivierung des Proteins zu bekommen. Dazu wurde zunächst die Sequenz, welche von unserer Gruppe als relevant identifiziert wurde[1], isotopenmarkiert exprimiert, gereinigt und mittels NMR Experimenten zugeordnet. Im nächsten Schritt wurde das Peptid mit MK2-Kinase an Serin 582 vor-phosphoryliert und erneut gereinigt. MK2 wurde hierbei als Surrogat für die *in vivo* relevante Kinase Chk2 verwendet, da es sich in *E. coli* in aktiver Form produzieren lässt. Sie zeigt die gleiche Erkennungssequenz wie Chk2 und kann daher für alle *in vitro* Experimente verwendet werden. S582 Phosphorylierung ist notwendig, da CK1δ eine phosphorylierte Aminosäure erkennt und dann, sofern möglich, in +3 Position eine weiter Phosphorylierung durchführt. Anschließend wurden Kinetiken der CK1δ Phosphorylierungen mittels NMR aufgezeichnet. Zu erwarten war, dass insgesamt vier Phosphorylierungen zu beobachten sind (S585, S588, S591 und T594). Dabei konnte beobachtet werden, dass T594 phosphoryliert wird, was bisher nicht bekannt war, da diese Phosphorylierung in der Massenspektroskopie nicht gefunden wurde. Weitergehend wurde T586 phosphoryliert gefunden, welches außerhalb der eigentlichen Sequenz liegt. Interessanterweise konnte gezeigt werden, dass die ins-

gesamt vier Phosphorylierungen mit zwei unterschiedlichen Geschwindigkeiten ablaufen, wobei die Phosphorylierung der ersten beiden Stellen (S585 und S588) bei 25°C circa 30-mal schneller ablaufen, als die Letzen beiden Phosphorylierungen. Mittels Röntgenkristallograpie konnte gezeigt werden, dass ein dreifach phosphoryliertes Peptid der relevanten p63-Sequenz einen Produktkomplex mit der Kinase bildet. Zusätzlich konnte durch Mutagenese im zweiten Teil der Sequenz der Effekt der zwei unterschiedlichen Phosphorylierungsgeschwindigkeiten auf einen Faktor zwei reduziert werden, was darauf hindeutet, dass die Sequenz evolutionär eine Funktion erfüllt. Weitergehend wurde eine TAp63α-Mutante erzeugt, die es erlaubt das relevante Peptid aus dem Protein heraus zu schneiden und abzutrennen. Dies erlaubt zu ermitteln, ob es relevante kinetische Unterschiede zwischen der Phosphorylierung des Peptids und dem kompletten Protein gibt. Hier zeigte sich, dass die initiale Phosphorylierung von MK2 sehr ähnlich zum Peptid verläuft, CK1δ allerdings stark verringerte Spezifität zeigt und scheinbar weitere Phosphorylierungen durchführt, die im Peptid nicht zu beobachten sind. Weitergehende Experimente sind notwendig um diesen Prozess genauer zu verstehen.
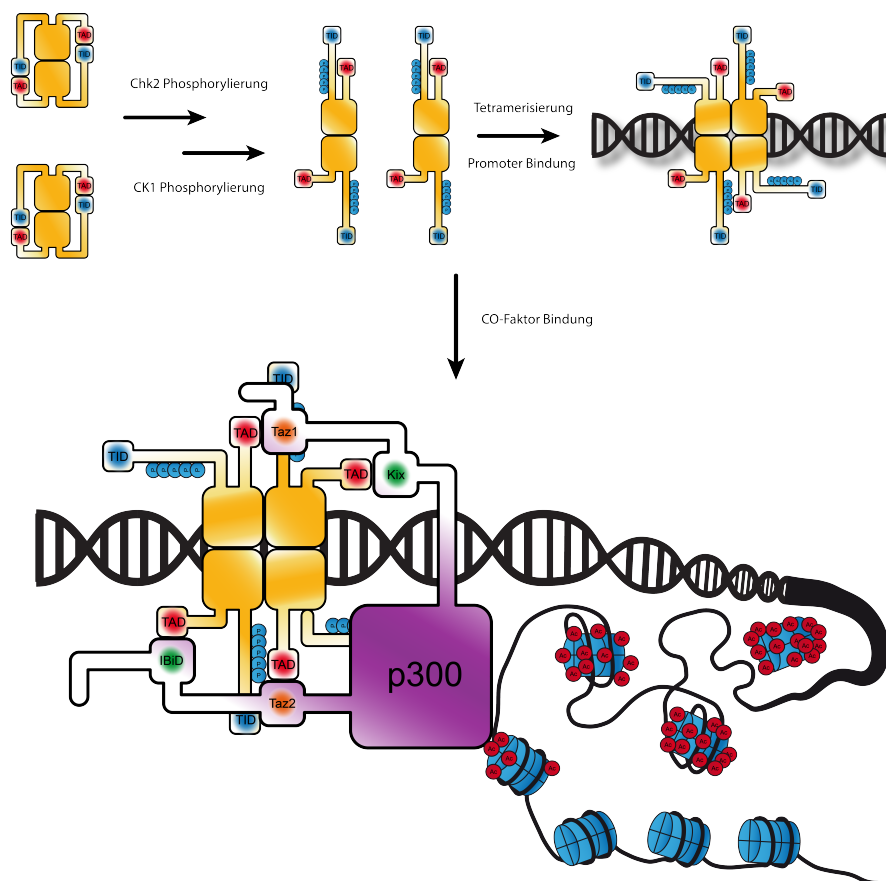
Modell der Aktivierung von TAp63α. TAp63α wird zunächst im C-Terminus an mindestens vier Aminosäuren phosphoryliert. Dies führt zu einer Öffnung des Proteins und schlussendlich zur Tetramerisierung. Durch die Öffnung wird die Transaktivierungsdomäne zugänglich und kann Kofaktoren wie p300 binden. Im Falle der Bindung von p300 führt dies dann zur Öffnung des Chromatins durch die Histonacetylaseaktivität des Enzyms.

1 Introduction

1.1 The p53 family of proteins

The p53 protein family consists of three different members in mammals, namely p53, p63 and p73. All three members are transcription factors with a variety of different functions. A transcription factor is a protein with sequence specific DNA binding capability, controlling the activity of proteins, ultimately leading to the recruitment of DNA dependent RNA polymerase II and the production of messenger RNA for protein synthesis. To achieve this function, all transcription factors include a Transactivation Domain (TAD), which serves as a binding interface for different co-activator with varying functions. The most important co-factors are chromatin remodeling enzymes, such as histone acetylases, the mediator complex or the TATA-Binding Protein (TBP). While p53 has been described early on as a potent tumor suppressor protein[2], the existence and function of p63 and p73 has been described much later[3;4;5]. All three proteins are believed to have been the result of two different gene-duplication events, a p63-like protein being the original ancestor[6;7]. The original function of the p63-like protein is believed to be that of a protein protecting the integrity of germ cells. Only much later a protein protecting the organism from cancer, induced by somatic-cell DNA damage, became relevant due to the longevity of the organisms (reviewed in[8]). The structure of the family members will be discussed in section 1.1.1 while function and regulation will be discussed in section 1.2.

1.1.1 Structural organization of the p53 family

All three family members have been reported in a number of different splice variants (Figure 1.1.1)[3;9;10]. Until recently only one splice variant of p53 was known, but this has changed with reports of several different variants present on mRNA level, leading to deletions within the protein or truncations at the N- or C-terminus[11;12]. In case of p63 and p73 alternative promoters give rise to different N-terminal variants as well[5;13;14]. Generally two different variants are described, one containing the transactivation domain (TAD, TA-isoforms) and one lacking the domain (ΔN-isoforms). In case of p63 two even more N-terminally elongated isoforms have been reported: GTA-isoforms[15;16] and TA*-isoforms[5]. Both sequences have so far only been described on mRNA level. TA*p63 could recently be identified on protein level in in a breast cancer cell line (Sum159) by our group via Mass Spectrometry analysis (unpublished). The general consensus architecture of the p53 family consists of three individual domains con-

nected via flexible linkers (Figure 1.1.1). At the N-terminus of all TAD containing p63/p73 iso-forms as well as wild type p53 a transactivation domain of the "9 amino acid transactivation domain" (9aaTAD) can be found[17]. Recently several p53 isoforms have been described, lacking either parts or the complete TAD of p53 (reviewed in[18]). In case of wild type p53 and p73 two independent transactivation domains are present within the first 70 amino acids of the protein[19;20]. Following the TAD a highly conserved DNA binding domains (DBDs) is present in all members. The DNA binding domains are highly conserved and adopt a immunoglobulin fold[21]. C-terminally to the DBD a conserved oligomerization/tetramerization domain (OD/TD) is present. This domain consists only of a single beta-sheet and one alpha-helix in case of p53, while p63 and p73 feature a second helix C-terminal to the first helix. The TDs of p63 and p73 are highly similar and readily form hetero-tetramers if both proteins are present[22;23;24]. In case of p53 C-terminal to the TD a small C-terminal domain domain (CTD) can be found. This domain is highly basic and has been implied be DNA binding and modulating the DNA affinity of the whole protein[25;26]. The other two members feature an additional folded domain, a Sterile Alpha Motif (SAM) domain, as well as an unfolded C-terminal Transcription Inhibition Domain (TID)[27;28]. The structure and function of the different domains will be described in more detail in the following sections.
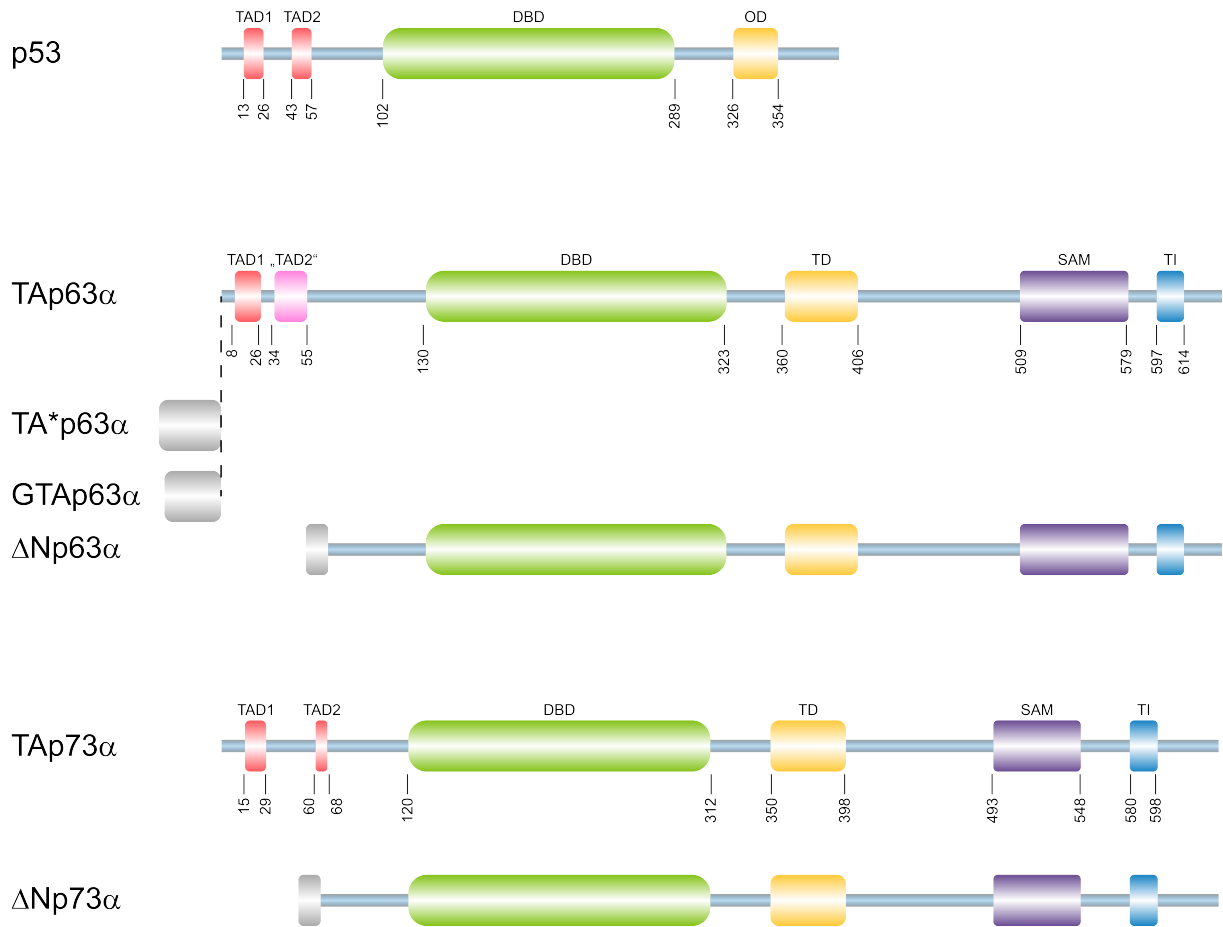
Figure 1.1.1: Protein variants of the p53 family. The domain architecture of all members of the p53 family is shown with their longest respective C-terminal splice variants. p53 and p73 feature two independent transactivation domains (TAD1 and TAD2), whereas p63 does only have one. The p63 "TAD2" domain is instead involved in maintaining the dimeric state in the inactive protein and does not seem to be relevant for transactivation. Shorter splice variants of p63 and p73 have been omitted for clarity reasons. Domains are colored according to their function: Transactivation domain: red; DNA binding domain: green; oligomerization/tetramerization: orange; Sterile alpha motif: purple; transcriptional inhibition: blue; additional important unfolded regions: grey.

1.1.2 Transactivation Domain

The transactivation domain of the p53 family has been characterized mainly on the basis of the p53 protein. p53 features two independent 9aaTAD sequences with a spacing of 18 amino acids between them. Both domains have been extensively structurally characterized (Figure 1.1.2). The consensus sequence of a 9aaTAD features a peptide sequence corresponding to an amphipathic alpha-helix with preferentially negatively charged amino acids on the outer side of the helix (consensus sequence: XXΦXXΦΦXX, where X are preferentially hydrophobic or negatively charged and Φ are hydrophobic residues)[29]. In all available structures featuring the TAD of p53 such a helix can be found, with the exception of a complex structure with the general transcription factor II H Pleckstrin homology domain (TFIIH PH) where a stretched conformation was observed (Figure 1.1.2)[30]. Generally the p53 TAD has been shown to bind to a large mag-

25

nitude of proteins (e.g. KAT3 family of histone acetylases[31;32], TFIIH[33;34], Mediator of RNA polymerase II transcription subunit 15 (MED15)[35], high-mobility group protein 1 (HMGB1)[36], TATA-binding protein (TBP)[37], Replication protein A (RPA)[38]). The binding mode of KAT3 histone acetylases with the 9aaTAD is discussed in section 1.3.2.
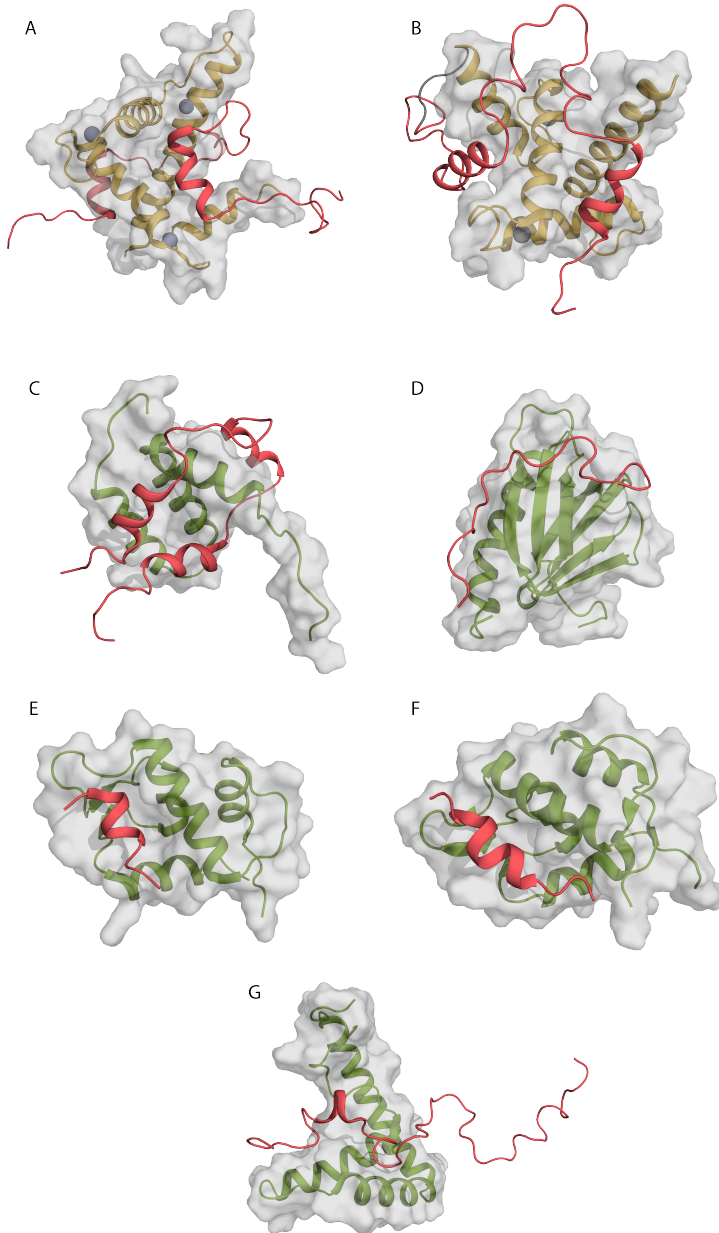
Figure 1.1.2: Known structures of p53 TAD complexes. All known structures with the TADs of p53 in complex with the respective interaction partner are shown. The p53 chain is always shown in red, the corresponding interaction partner in green or orange.
(A) CBP Taz1 with both TADs of p53 (PDB 5HOU), (B) CBP with both TADs of p53 (PDB 5HPD), (C) CBP IBiD with both TADs of p53 (PDB 2L14), (D) TFIIH PH domain with S46/T55 phosphorylated TAD2 of p53 (PDB 2RUK), (E) MDM2 with TAD1 of p53 (PDB 1YCR), (F) MDMX/MDM4 with TAD1 of p53 (PDB 2Z5S), (G) HMGB1 Box A with both TADs of p53 (PDB 2LY4).

The first TAD of p53 and p73 have a high sequence identity of with a conserved "FWL"-motif (F19, W23, L26 of p53 and F15, W19, L22 of p73) essential for the binding of the E3 ligases murine double minute 2 (MDM2) and murine double minute 4 (MDM4)[39;40]. p63 features a similar sequence (F16, W20, L23), but the binding to MDM2 is diminished by more than a factor of ten[41]. The putative MDM4/TAp63 interaction is not characterized so far. The interaction of p53 TADs with the transcriptional co-activator family p300/CBP have been characterized both structurally and functionally[32;42;43;44;45]. Interestingly two structures of Transcription Adaptor

putative Zinc finger 2 (Taz2) domains with the first TAD of p53 have been published, directly disagreeing with one another. An older structure of Taz2 with an isolated p53 TAD1 peptide (PDB 2K8F) shows binding to a region where p53 TAD2 is bound in case of a long peptide including both domains (PDB 5HPD)[45]. An overlay of both structures in question is shown in 1.1.3.

Figure 1.1.3: Overlay of disagreeing structures of p300 Taz2/p53 TAD1 (PDB 2K8F) and CBP Taz2-p53 TAD1-TAD2 (5HPD). The Taz2 domain in both structures shows the expected conserved fold (CBP Taz2 in yellow, p300 Taz2 in blue). However in both structures the position of the TAD1 sequence of p53 varies significantly. In absence of p53 TAD2 the p53TAD1 occupies a binding site formed by helices 1-3 of the Taz2 domain form a binding surface for the TAD1 sequence (yellow ellipse). When p53 TAD2 is present the p53TAD1 peptide moves to a secondary binding site formed by helices 3 and 4, as the primary binding site is then occupied by the TAD2 peptide of p53. Peptide sequences are color coded TAD1: red; TAD2: green.

This indicates that mutual binding of both TADs to one Taz2 domain is possible, although tertiary complexes between p300 Taz2 binding to the p53 TAD2 and MDM2 p53 TAD1 could be possible as well. A complex of the p53 TAD with MDM2 and p300 Taz1 domain has been reported in the past[46]. Additionally a complex composed of MDM2, p300 and p53 full-length constructs has been reported as well, however the experiments have been performed in presence of zinc-chelating agents, therefore rendering the results questionable as the experimentalists might have seen co-aggregation instead of real interaction[47]. The interaction of the p73 TADs with p300 has been characterized in much less detail[48]. However a Nuclear Magnetic Resonance (NMR) study revealed two independent interacting regions in the first 70 amino acids of p73[20]. Besides MDM2[41], and potentially p300[49;50] no direct interaction partners of the p63 TAD have been described.

1.1.3 DNA Binding Domain

The DNA binding domain forms the central structural element of all p53 family members. The structure is highly conserved between all three members, binding onto very similar DNA sequences[51]. Sequence-wise the p53 DBD is evolutionary the most distant family member, as sequence the identity ranges from ≈55% for p53/p63 to ≈86% for p63/p73. Binding occurs to the conserved p53-consensus sequence 5'-PuPuPuC(A/T)(T/A)GPyPyPy-3' (where Pu = Purine/ Py = Pyrimidine)[52]. p53 family members bind to DNA as tetramers in a cooperative manner, therefore the p53 response elements (p53-RE) described above is present in two copies, spaced by several base pairs on the DNA (so-called "half-sites")[53]. Recently a study by cryo-electron microscopy suggests that under DNA damage conditions a p53-tetramer binds to one p53-RE, therefore freeing the second response element for an additional p53-tetramer to bind[54]. This would likely lead to an amplification of DNA-damage signaling as it increases the available TA domains for co-factor binding on a given promoter by a factor of two. Structurally p53 family DBDs consists of a immunoglobulin s-type fold, thereby forming a flattened β-barrel like arrangement (β-sandwich)[55;21]. Structures are highly conserved, reaching a maximum RMSD of 1.04 Å between p53 and p63 (excluding the more flexible C-terminal helix; compare 1.1.4).
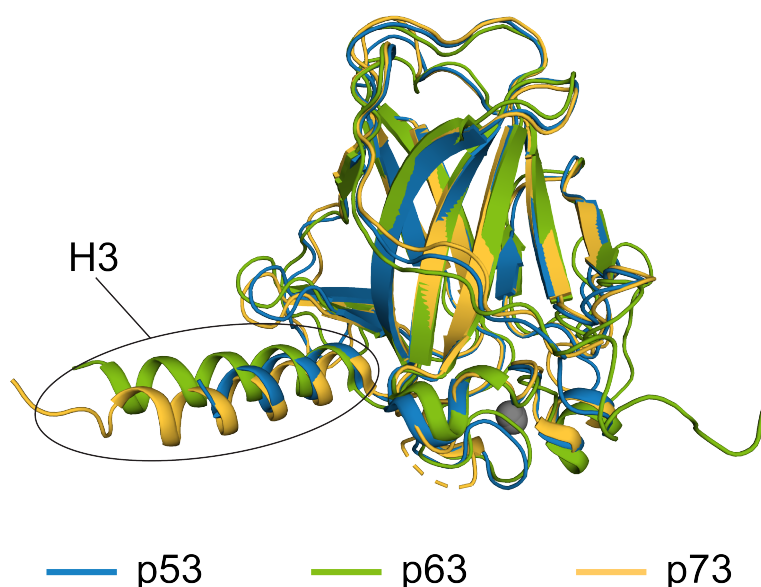
Figure 1.1.4: Overlay of DNA binding domains of all p53 family members. The immunoglobulin s-type fold is highly conserved, with almost no visible differences in structure between all three domains. The most prominent difference is the helix orientation of the C-terminal helix in p63. However this orientation might misleading as the p63 structure is derived from solution NMR while the other two structures were solved by crystallography. Besides this difference, some minor deviations in loop orientation around the single zinc finger can be observed. This might have implications in specificity of DNA binding, as the major DNA contacts are formed by these loops as well as the C-terminal helix. Zinc ions are depicted as grey sphere. PDB: 1TSR (p53), 2RMN (p63), 2XWC (p73)

Sequence specific DNA contacts are mainly formed by the C-terminal helix (H3) and loops, structurally defined by a single zinc finger. The main DNA contacts are conserved in all three proteins (S272, R279, R304, C308, R311 in p63 nomenclature)[56]. Helix H3 is lying in the major groove of the DNA contributing to DNA affinity by electrostatic as well van-der-Vaals interactions. S272 forms a hydrogen bond interaction to a backbone phosphate group of the DNA, R279 intercalates into the minor groove of the DNA helix thereby directly attaching the zinc-finger motif to the DNA[57].

A

B
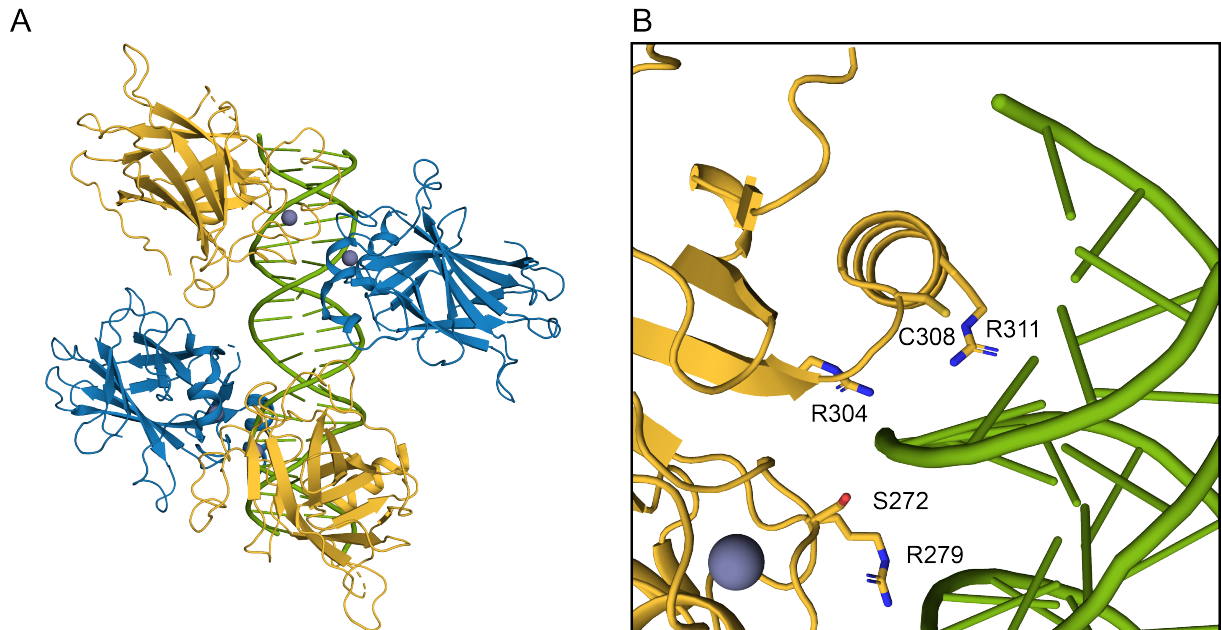
Figure 1.1.5: Structure of p63 DBDs bound to DNA.(A) The tetramerization domains of p63 crystallized on a double-stranded DNA fragment with the consensus nucleotide sequence. (B) Closeup of the DNA contacts of a single DBD with DNA. Three arginine residues (R279, R304 and R311) as well as S272 and C308 mediate the interaction.

The fold of the domains is virtually identical between all family members, as already suggested by the highly conserved DNA response element. Only minuscule differences DNA binding preferences have been reported between the DBDs of p53 and p63[58]. One major difference between the three domains is their thermal stability, p53 DBD being the least stable, followed by p73 DBD and p63 DBD being the most stable[59]. The majority of disease relevant DBD mutations found in p63 decrease the protein stability or impair the ability of the domain to bind DNA[57]. Most cancer associated p53 mutations can be found in the DBDs. They can be subdivided into two distinct categories loss of function or gain of function. Loss of function mutations can be further sub-divided into DNA contact mutants, abrogating DNA binding or mutants either destabilizing or destroying the fold of the DBD entirely[60;61]. Gain of function mutants include DBD mutants that enable p53 to co-aggregate with other proteins (reviewed in[62]). In case of p73 not much is known about the prevalence of mutations in the DBD in the context of cancer. One study indicates that a G264W mutation displays a dominant negative phenotype in some cancer cell lines, thereby suppressing the transactivation potential of WT alleles[63].

1.1.4 Tetramerization Domain

All p53 family members are active as tetrameric proteins, thereby requiring an oligomerization/tetramerization domain. The basic fold of the oligomerization domain is highly conserved throughout all organism with p63-like proteins[7;64]. The fold of the complete domain with four strands can be considered a dimer of dimers. In case of p63 and p73 a single chain consists of an N-terminal β-sheet and two α-helices (termed tetramerization domain, TD). The p53 oligomerization domain has the same overall fold but lacks the C-terminal α-helix (oligomerization domain, OD). All three domains are shown in figure 1.1.6. The major difference between the p63 and p73 structure is the extended second helix in case of p63. While the second helix of p73 seems to be firmly bound onto the structure, the p63 helix has additional flexibility at its C-terminus[65].
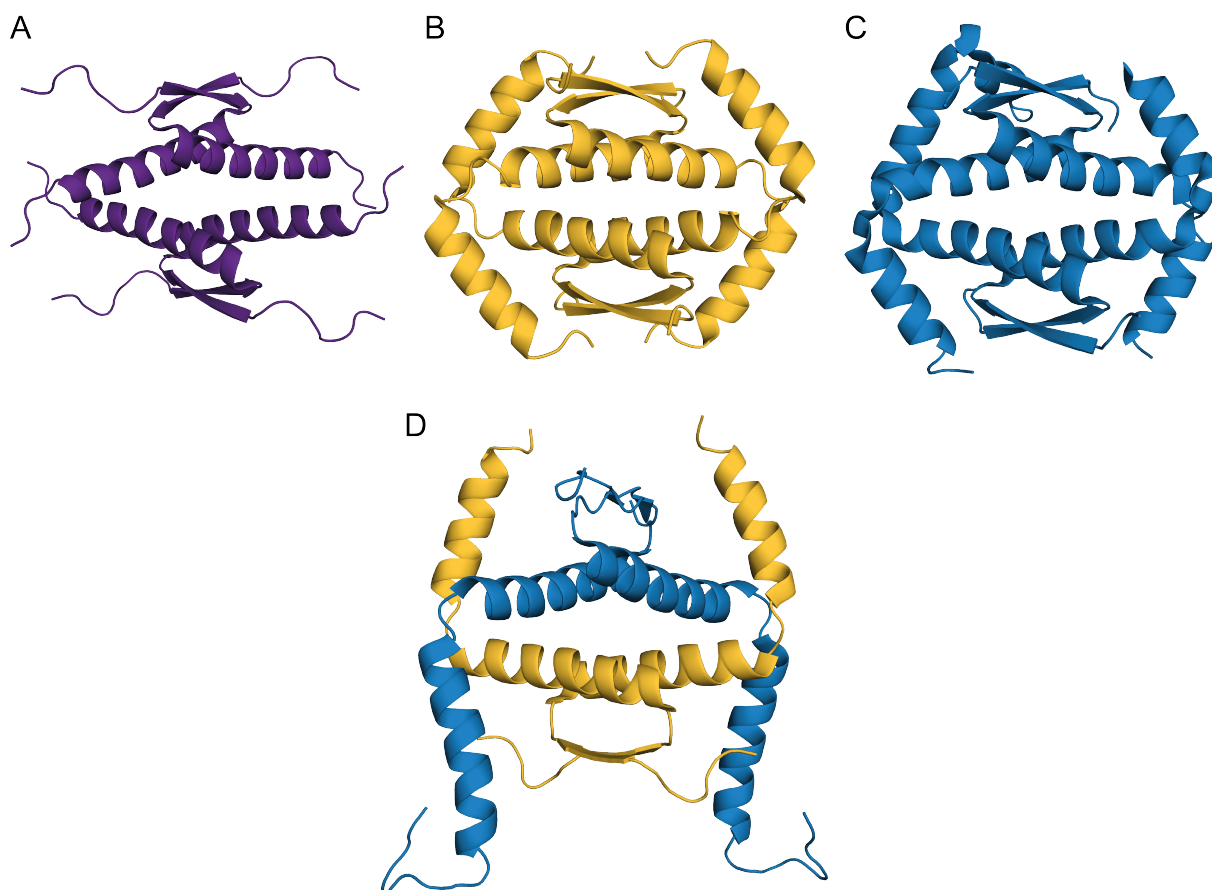
Figure 1.1.6: Oligomerization/Tetramerization Domains in the p53 family. All oligomerization domains share the similar basic architecture of one N-terminal β-sheet and one α-helix per chain. p63 (PDB 4A9Z, B) and p73 (PDB 2KBY, C) feature an additional C-terminal helix whereas p53 (PDB 1OLG, A) does not. The hetero-oligomerization of p63/p73 domain is shown for comparison (PDB 2NB1, D), with coloring according to the homo-tetramers.

Due to the architecture as a dimer of dimers, greatly different thermodynamic and kinetic association constants could be observed. In case of p53 the dissociation constant tetramer/dimer dissociation was determined to be an order of magnitude higher than that of dimer/monomer

(50 nM/0.55 nM). Therefore the exchange rates of different dimers within a tetramer are almost an order of magnitude higher compared to the exchange of a monomer[66]. Sequence-wise the tetramerization domains of p63 and p73 are highly homologous while the p53 tetramerization domain is more distally related. This is reflected in the ready formation of hetero-tetramers by p63/p73 while none of these domains interact with p53 in wild type proteins[24]. However interaction has been observed between p73 and mutant p53, potentially through co-aggregation[67;68]. Interestingly the interaction of two homo-dimers of p63 and p73 is the most favored tetramer, accounting for almost 40% of all detected tetramers (1.1.7).
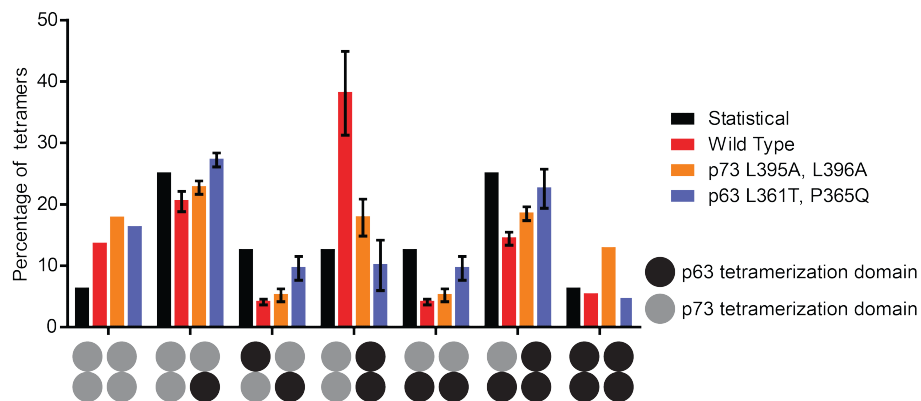
Figure 1.1.7: Distribution of all possible tetramers in a 1:1 molar mixture of p63 TD and p73 TD. The wild type proteins (red bars) tend to form hetero tetramers of homo dimers contributing roughly 40% of all tetramers found in solution. Point mutation of several key residues within the TDs (orange/blue bars) of either one of the proteins restores the levels to close to statistical levels (black bars). The type of tetramer belonging to the specific bar is indicated underneath the diagram. Modified from[24].

By selective stabilization of hetero-tetramer salt-bridge interactions while destabilizing homo-tetrameric salt-bridges it was possible to solve a structure of the hetero-tetramerization domain of p63/p73 in our group (1.1.6). Hetero-tetramerization between both proteins may play an important role within differentiation of epithelial stem cells, as a co-expression of ΔNp63α and a p73 isoform has been observed in these cells in vitro as well as in vivo[69;70;24]. Additionally Squamous Cell Carcinoma (SCC) cells frequently express ΔNp63 and a TAp73 isoform as well[71]. In the latter case suppression of ΔNp63α by siRNA rescues the pro-apoptotic properties of p73. This could mainly be attributed to promoter squelching of ΔNp63α and not hetero-oligomerization[24]. Germline mutations within the oligomerization domain of p53 (L344P and R337C) have been reported in several patients, leading to a Li-Fraumeni or Li-Fraumeni like syndrome[72]. While L344P destroys the α-helix, making oligomerization impossible, R344C removes one crucial inter-dimer salt-bridge, thereby greatly destabilizing the dimer. For neither p63 nor p73 any mutations within the tetramerization domains have been published. Although in case of p63 there are two mutations known within the TD that destabilize the structure (V366M and R369H) leading to orofacial-clefting. The R369H mutation only has a minor effect on the thermal stability and no effect on the oligomeric state while the V366M has a massive destabilizing effect on both oligomeric state and thermal stability (submitted, currently under review at

Human Molecular Genetics).

1.1.5 Sterile Alpha Motif (SAM)

Sterile Alpha Motifs (SAM) are small domains consisting of five short helices forming a globular fold of approximately 70 amino acids (Figure 1.1.8). They are present in a wide range of proteins and are generally considered to be interaction platforms for homo-[73] or hetero-multimerization[74]. Additionally SAM domains in general can bind a variety of other protein folds as well as RNA[75].
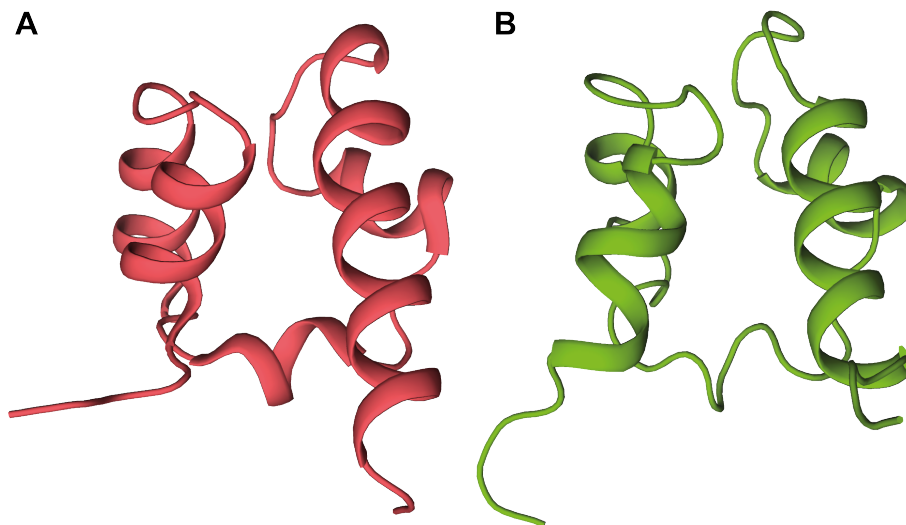
Figure 1.1.8: Sterile Alpha Motif (SAM) domains of p63 (A) and p73 (B). Both domains share the conserved SAM domain fold. Both of these domains lack a confirmed protein interaction partner. Lipid binding of both domains was described, although the authors are unsure if this interaction is relevant in vivo[76]. PDB IDs: 1RG6 (p63) and 1COK (p73).

The α-isoforms of p63 and p73 have a SAM domain located C-terminally to the tetramerization domain p53 does feature a SAM domain neither do truncated isoforms of p63/p73 such as β,γ or δ. Recently DLC2 was identified as a potential interaction partner of the p73 SAM domain, with a proposed impact on the relative expression levels of ΔNp63 and TAp73[77]. In case of p63 no interaction partner could be identified up to this point. However lipid binding of both domains was described, although the authors are unsure if this interaction is relevant in vivo[76]. In case of p63 germline mutations within the SAM domain display a striking phenotype in vivo. The ankyloblepharon-ectodermal-dysplasia clefting syndrome (AEC syndrome, also called Hay-Wells syndrome) leads to skin fragility, hypo pigmentation, severe skin erosions and is considered a life threatening disease. Most of the mutations found within the domain lead to aggregation of the protein and co-aggregation with other protein such as p73 and therefore can be described as gain-of-function mutations rather than simple loss of function mutations[78].

1.1.6 C-terminal Domains (TID and CTD)

p63 as well as p73 feature a conserved C-terminal peptide sequence in their α-isoform dubbed the Transcription Inhibition Domain (TID). The presence of the TID lowers the transcriptional activity on pro-apoptotic promoters such as p21 or BAX (B-cell lymphoma 2 (Bcl-2)-associated X protein)[79;80;81]. In case of p63 it could be shown that a direct interaction between the TAD and the TID is responsible for a change in the oligomerization state from the expected tetramer towards a closed inactive dimeric state[82]. For p73 the TID does not change the oligomeric state of the protein, although presence of the domain still has a negative effect on transcription[81]. p53 does not feature a TID albeit the extreme C-terminus (CTD) of the protein was implicated in transcriptional regulation as well. The CTD is highly basic, containing six lysines within 24 amino acids, and is therefore massively acetylated by PCAF and p300 in vitro and in vivo in response to DNA damage[83]. Acetylation of these residues seems to influence the DNA binding preference of p53 enabling of-consensus DNA binding[84]. Truncation of the CTD seems to overall increase transcriptional activity of p53 but also leads to impairment in development of mice due to hyperactivity of p53 on the p21 promoter (cyclin-dependent kinase inhibitor 1 promoter) and resulting premature senescence in developing tissues[85].

1.2 Regulation of the p53 family

All members of the p53 family are mainly regulated through protein expression, protein localization and post-translational modification (Figure 1.2.1). p53 underlies a regulation network where the protein is constantly expressed and rapidly ubiquitinated by the E3 ligase MDM2. Additionally the MDM2 promoter features a p53 response element, forming a negative feedback loop to control p53 levels[86;87]. MDM2 knock out mice are not viable and die in utero due to the strong p53 response. This effect can be rescued by a double knock out with p53[88]. Phosphorylation of p53 in the transactivation domains has been reported for several kinases (reviewed in[89;90]). In vitro phosphorylation of the TADs of p53 increases the affinity of the domain towards transcriptional co-activators such as p300/CBP while decreasing the affinity towards MDM2[44]. Acetylation of p53 has been shown to occur at several sites within the DBD as well as in the CTD (described in 1.1.6). Additionally it has been shown that ubiquitination of p53 by MDM2 can be suppressed by acetylation of ubiquitin acceptor lysines[91]. p53 localization has been studied extensively and is poorly understood. p53 is by itself a nuclear protein to fulfill its function as transcription factor. However ubiquitination of residues within the DBD or the CTD leads to exposition of the nuclear export signal (NES) and subsequent shuttling to the cytoplasm for proteasomal degradation[92]. Upon DNA damage cytoplasmatic p53 can localize to mitochondria[93] where it enhances the induction of apoptosis[94]. Furthermore p53 has been shown to be located in promyelocytic leukemia (PML) bodies upon DNA damage. The localization to these bodies has shown to enhance the transcriptional activity on p53 target promoters[95].

Phosphorylation of TAp63α leading to activation of the protein in oocytes is described below in 1.2.2. Besides phosphorylation in its C-terminus, other phosphorylations potentially relevant for activation in TAp63α have been reported as well[96]. Degradation of TAp63 via the ubiquitin-proteasome pathway is still poorly understood. Although the classical MDM2 binding motif "FWL" is conserved the actual binding affinity observed in vitro of the p63 TAD towards MDM2 is an order of magnitude weaker than of the other two family members[41]. This makes an effective regulation of p63 by MDM2 questionable. The E3 ligase p53-induced RING-H2 (Pirh2) has been shown to be able to interact and ubiquitinate ΔNp63α in keratinocytes. Additionally the E3 ligase Itch has been described to control the stability of both TAp63α and ΔNp63α[97]. New results also indicate an interplay between SUMOylation and ubiquitination for the efficient degradation of ΔNp63α[98]. Both p63 and p73 α-isoforms feature a SUMO-consensus binding site at the extreme C-terminus (ΦKXE sequence). In case of p63 it could be shown that SUMO-1 conjugation has an influence on protein stability[99;100].

The regulation of p73 isoforms can be subdivided into the two N-terminal transcript variants. TAp73 isoforms are ubiquitinated by MDM2 without leading to its degradation[101;102], while TAp73 isoforms seem to be targeted for degradation by Pirh2[103;104]. Both isoforms may also be regulated by Itch[105]. Similar to the regulation of the MDM2-p53 feedback loop, TAp73 expression leads to an upregulation of another ubiquitin E3 ligase, TRIM32, which in turn ubiquitinates TAp73 and targets degradation. ΔNp73 on the other hand can effectively repress the TRIM32 promoter thereby effectively regulating the TAp73:ΔNp73 ratio[106]. Known post-translational modifications were reviewed in[107].
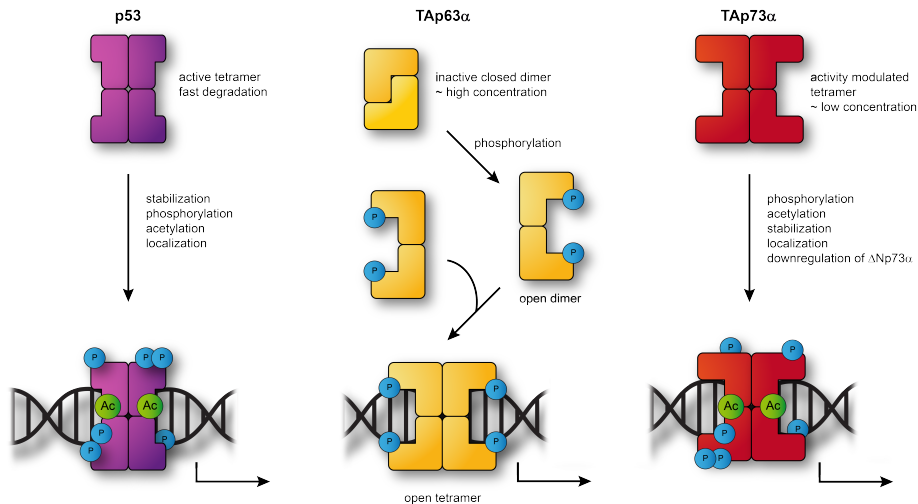
Figure 1.2.1: Regulation of protein activity and stability within the p53 family. Although the p53 family is highly conserved throughout its members, several different strategies for controlling the protein activity of the specific member have evolved depending on the specific purpose of the protein. p53 (left panel, purple) is a constitutive tetramer of high transcriptional activity. To suppress its transactivation potential in non-damaged cells, it is rapidly ubiquitinated and degraded. Additionally it can be targeted to the cytoplasm to inhibit its transactivation potential. In case of DNA damage the protein becomes stabilized by post-translational modifications such as phosphorylation and acetylation. Phosphorylation in the TADs of p53 have been shown to increase the affinity for co-activators even further and acetylation has been shown to prevent degradation and change the DNA binding preferences. TAp63α (orange, center panel) is expressed in a high quantity in primordial oocytes, being totally inert and without any transcriptional activity in a dimeric state. Upon DNA damage phosphorylation events open the dimer, which leads to subsequent tetramerization and high transcriptional activity without further modification of the protein. Furthermore the TAD of p63 is much less susceptible to MDM2 mediated ubiquitination. TAp73α (right panel, red) seems to be a constitutive tetramer which is present in low concentrations and a low intrinsic transactivation potential. Protein activity can be mediated by post-translational modification and localization. Modified from[108]

1.2.1 Function of p53

p53 was originally described as an oncogene, as elevated protein levels were observed in tumor tissue[109]. Sometime later it became clear that these elevated protein level were the result of mutations within the gene[110;111;112]. Furthermore it could be shown that p53 efficiently inhibits spontaneous cell immortalization by inducing apoptosis[113;114]. p53 functions as a transcription factor and gets activated in response to several different stimuli such as DNA damage[115], nutrient depletion[116], hypoxia[117], Reactive Oxygen Species[118], and others stressors (recently reviewed in[119]). p53 activation is mediated by stabilization of the protein otherwise undergoing rapid turnover (see section 1.2. Activated p53 binds to promoters featuring the p53-RE, thereby inducing transcription of these genes. The most well-known promoters for p53 are the p21 and BAX promoter, p53 upregulated modulator of apoptosis (PUMA) and Phorbol-12-myristate-13-acetate-induced protein 1 (Noxa) promoters. The p21-gene codes for the protein "cyclin-dependent kinase inhibitor 1" (also called p21) which inhibits a kinase necessary for progression

of the cell cycle and thereby inducing senescence[120;121]. This allows the cell to repair minor DNA damage or sustain nutritional stress/hypoxia. In case of more severe stress/damage on the cell the transcription of BAX, PUMA and Noxa is switched on[122;123;124]. All three proteins are members of the Bcl-2 family and are mitochondrial membrane associated proteins. The general understanding of their functioning is an association and activation of the mitochondrial voltage-dependent anion channel (VDAC) leading to subsequent rupture of the mitochondrial membrane and cytochrome-C release[125]. Recently there is growing evidence that the Bcl-2 family members might be able to form pores in the mitochondrial membrane by themselves, thereby being independent of VDACs[126]. Interestingly p53 knock out mice are completely viable, without any obvious defects in development, albeit with a high tumor incidence by the age of ten month[127] similar to the Li-Fraumeni syndrome in humans[111] (compare section 1.3.4). Fertility of the mice This indicates that p53 is completely dispensable in development and only required as a guardian of the genomic integrity in long-lived animals.

1.2.2 Function of p63

As p63 is present as two different N-terminal isoforms (Figure 1.1.1) with two completely different functions they have to be discussed separately. The TAD containing TAp63α isoform is expressed in high levels in mammalian oocytes and will be discussed in section 1.2.2, while the dominant isoform lacking the TAD, ΔNp63α is expressed predominantly in the basal layer of the epithelium and will be discussed in section 1.2.2.

Function of TAp63

TAp63α is the protein isoform which embodies the original function of the p53 protein family as closely as currently known, namely being a quality control factor that ensures the integrity of the germline. It is highly expressed in primordial oocytes, rendering these cells sensitive to ionizing radiation or other genotoxic stress[128]. Early on it could be shown that TAp63α becomes phosphorylated in vitro in response to stress stimuli, which increases p63s DNA binding affinity 20-fold. Subsequent λ-phosphatase treatment removed the phosphorylations but not lower the DNA binding affinity. Later our group could show that TAp63α is trapped in a dimeric conformation *in vitro* and *in vivo* and switches oligomeric states upon DNA damage[82]. The tetramerization event is unidirectional, therefore once tetramerized TAp63α can only be removed by degradation. This is attributed to a spring-loaded mechanism whereby an autoinhibitory complex keeps the protein complex in a dimeric state and upon phosphorylation the complex is destroyed by charge repulsion[129]. The subsequently formed tetrameric TAp63α is the thermodynamically favored variant and even dephosphorylation seems to be insufficient to reverse the process. It could be shown that activation of TAp63α is dependent on phosphorylation by Checkpoint kinase 2 (Chk2)[130]. Chk2 displays a very specific consensus sequence (LXRXXS/T) which can be found within the C-terminus of TAp63α. A S582A mutation abolished phosphorylation of

overexpressed TAp63α in vitro.

Recently the process of TAp63α activation upon DNA damage was revealed in more detail by our group[1]. TAp63α phosphorylation by Chk2 is not sufficient to trigger tetramerization but another kinase is required to break the auto-inhibitory complex. The kinase was identified to be Casein Kinase I (CKIδ) which attaches at least another three phosphates in a +3 pattern to TAp63α. During the development of the mouse female germline TAp63α expression starts in primordial oocytes at around birth, after SPO11 induced meiotic double strand breaks (DSBs) have been repaired by the cells (Figure 1.2.2)[131]. This ensures that homologous recombination for genetic shuffling can take place without restricting the ability to detect DNA damage later on. As expected selective TAp63$^{(-/-)}$ female mice are fully fertile after irradiation[128]. This might also be true for full p63 knockouts, however as the animals die shortly after birth due to developmental defects this cannot be readily assessed[131] (see below).
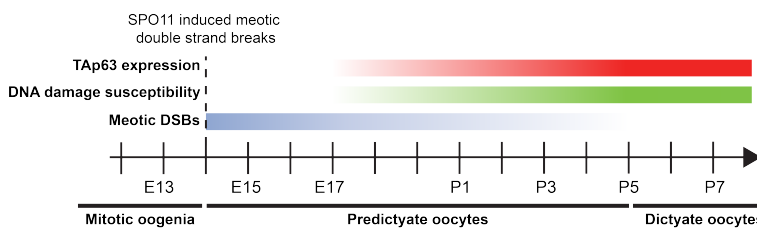
Figure 1.2.2: Meiotic Double Strand Breaks (DSBs) during mouse development. Meiotic double strand breaks are induced at around day 2L14 of the embryonic development. At this point the oogonia are not sensitive to DNA damage. The DNA damage is repaired and expression of TAp63α commences. With increasing protein concentration the predictyate oocytes become sensitive to DNA damage. Modified from[108]

Function of ΔNp63

ΔNp63α has been described as a master regulator of epidermal development[132]. As it lacks the N-terminal transactivation domain entirely, it has been mainly described as a repressive factor, albeit having some transactivation potential on certain promoters involved in differentiation of keratinocytes[133]. In vitro differentiation of keratinocytes leads to a gradual loss of ΔNp63α throughout the process. During the differentiation a (TA)p73 isoform can be observed co-localizing with p63. This might indicate a potential hetero-tetramer formation[24]. ΔNp63α is described to function as an oncogene in several types of cancers, as it can bind p53-RE promoters without leading to actual expression, as well and inhibit the function of p53 or p73 by promoter squelching[71]. Complete loss of ΔNp63α, due to loss of function or gain of function mutations, however leads to severe phenotypes such as Ectrodactyly-ectodermal dysplasia cleft (EEC) syndrome or Hay-Wells syndrome (also called Ankyloblepharon-ectodermal defects-cleft lip/palate (AEC))[134;135]. This indicates a vital role for ΔNp63α during embryonic development

as well as maintenance of the skin. The function of ΔNp63α in epidermal development has recently been reviewed[136].

1.2.3 Function of p73

p73 is the third member of the p53 family. Like p63 it has two different promoters giving rise to a potential tumor suppressing TAp73 isoform as well as a dominant negative ΔNp73 variant. The function of both variants are still a matter of debate, as isoform specific as well as global knock-out mice display diffuse phenotypes[14]. ΔNp73 knockout mice are fertile and healthy but show signs of neurodegeneration[137]. Additionally cells derived from these mice show increased sensitivity towards p53 mediated apoptosis as response to DNA damage. This hints at a repressive function of ΔNp73 similar to ΔNp63 in Squamous Cell Carcinoma (SCC)[71]. In a non-oncogenic context ΔNp73 seems to be important for the maintenance of neuron-development and proliferation. ΔNp73$^{(-/-)}$ mice exhibit increased Neural Stem Cell (NSC) senescence and impaired ability of NSCs to generate mature neurons[138]. In contrast to this TAp73$^{(-/-)}$ mice exhibit a clear, but mild phenotype related to its tumor suppressor function. They show impaired genomic stability resulting in lower life expectancy as well as infertility[139]. Female infertility in the KO mice has been attributed to spindle defects which seems to correlate with an increase of spindle defects in women throughout their fertile lifespan[140]. TAp73α has been implicated in direct non-transcriptional binding of BUB1, BUB3 and BUBR1 of the Spindle Assembly Checkpoint complex (SAC). Deletion or knock down of TAp73 leads to impaired functioning of the SAC as well as a rescue of cells undergoing caspase-independent mitotic death (CIMD) in response to spindle defects[141;142]. On the other hand overexpression of TAp73α leads to aneuploidy[143] thereby indicating that the protein level needs to be subtly balanced for proper functioning. Male TAp73$^{(-/-)}$ mice show strongly reduced fertility as well. This went almost unnoticed as they retain some fertility. However immunohistological stainings revealed that the mice display a "near-empty seminiferous tubule" phenotype where the blood-testis-barrier (BTB) as well as the apical ectoplasmic specialization (apical ES) complex are dysfunctional due to a misbalance in the expression of several extracellular proteases[144].

+TAp73   -TAp73

mature spermatid

elongating spermatid

spermatocytes

spermatogonia

Sertoli cell

Blood testis barrier (BTB) adhesion protein complex

Gap junction protein complex/Desmosome protein complex

Apical ES protein complex
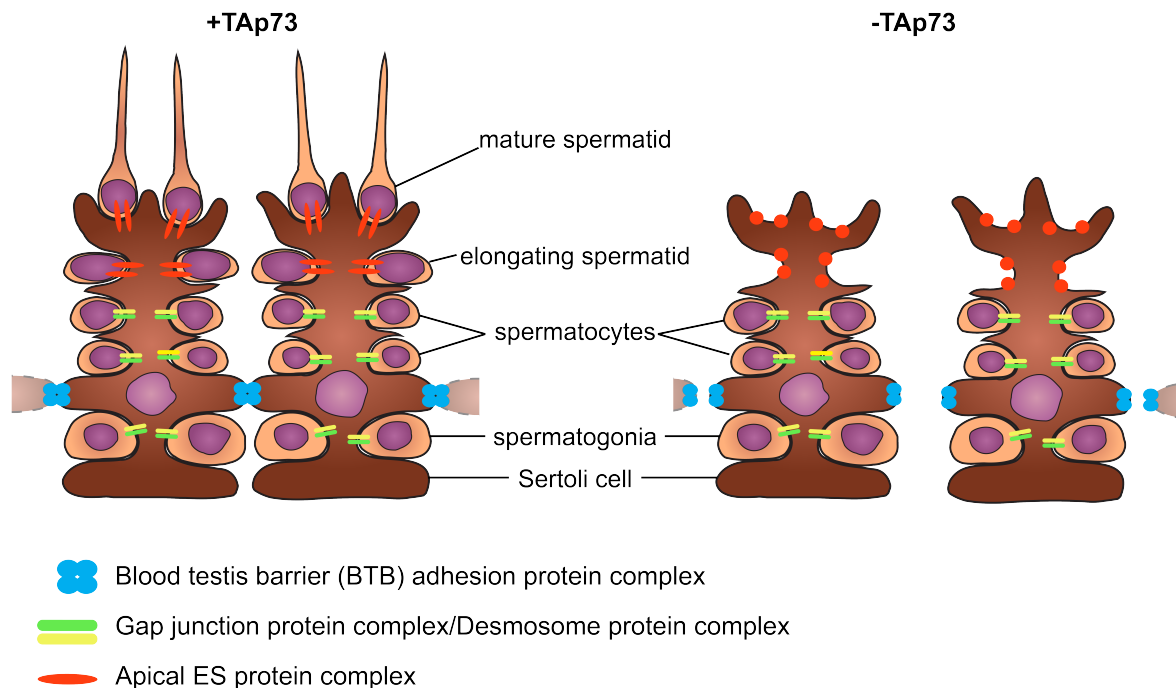
Figure 1.2.3: The blood-testis-barrier and apical ES complex are compromised under TAp73 knock out conditions. TAp73 plays a role in the transcription of several extracellular proteases involved in formation of the BTB as well as the apical ES complex. Due to a misbalance in the levels of these proteins spermatids fail to attach to nursing Sertoli cells and are therefore almost depleted from the seminiferous tubule. Modified from [108]

Furthermore TAp73$^{(-/-)}$ mice display chronic respiratory tract infections due to a lack of Motile multi-ciliated cells (MCCs). In this case the effect could be narrowed down to a lack of expression of genes required for cilia formation such as Foxj1 [145;146]. Recently TAp73 has been implicated in the response to oxidative stress by enhancing transcription of enzymes needed for antioxidant biosynthetic pathways [147;148].

1.3 Histone Acetylases

Histone acetylases (HAT) are enzymes which catalyze the transfer of acetate-groups to lysine side chains [149]. Acetylation of lysines represents one important type of post-translational modification of proteins. Histone acetyl-transferases are generally known as factors for chromatin remodeling during transcription, although they frequently have a multitude of different targets as well. Histones are octameric protein complexes and important DNA organizers, as they condense the elongated DNA into more compact nucleosomes. Acetylation of histone-tails leads to a reduction in binding affinity of the histones towards the DNA and in turn to opening of the nucleosome, enabling transcription. In mammals three different families of HATs are found (reviewed in [150]):

- Gen5-related acetyl-transferases (GNATs)

- MOZ, Ybf2, Sas2, Tip60-related (MYST)

- p300/CBP (also known as KAT3 family)

Additionally several other histone-acetylases with varying homology towards the three families are found. Generally all lysine-acetylating enzymes work in a similar fashion as they use acetyl-Co-enzyme A (acetyl-CoA) as an activated acetyl-donor to catalyze the reaction. The reaction is catalyzed as a ternary complex of enzyme, acetyl-CoA and substrate. The GNAT family fold is highly conserved and can be found in all domains of life. The enzymes of this family use a ternary complex transfer mechanism to transfer the acetyl from CoA to a lysine residue (reviewed in[151]). The KAT3 family transfer acetyl-rests via a ternary complex transfer mechanism. It relies on a sequential binding of acetyl-CoA and the substrate peptide sequence. As soon as the substrate peptide is encountered the acetyl-rest is transferred and the product peptide can diffuse away. This mechanism has been dubbed "hit-and-run"[152]. For the Efa1 enzyme of the MYST family a covalent acetyl-enzyme intermediate was discussed[153], but this result has been challenged by another study in favor of a ternary complex mechanism[154]. This study focusses on the KAT3 family, therefore the other HAT-families will not be discussed in further detail.

1.3.1 p300/CBP

p300 (also known as KAT3a) and CREB binding protein ('cAMP response element-binding protein' binding protein in short CBP or KAT3b) are two closely related histone acetyltransferase enzymes, defining the KAT3 family of lysine acetyl transferases. They have first been identified as acetyl-transferase enzymes by autoradiography in 1996[155]. Prior to this discovery it was assumed that the proteins act as a scaffold protein between the transcription factors and proteins required further down-stream[156]. The protein family is conserved in all metazoan and even holozoan animals[157], as well as plants[158]. Fungi use different, non-homologous, histone acetylase enzymes such as Rtt109[159]. While p300 and CBP amino acid sequences are almost completely identical within the folded domains (88% sequence identity), unfolded regions vary greatly in sequence between the two proteins (42% sequence identity). The KAT3 family of histone acetylases is the most prominent family in mammals, due to the confirmed binding of several important proteins such as p53[160], the Apoptosis-Stimulating of p53 Protein (ASPP) family[161] and the Circadian Locomotor Output Cycles Kaput complex (CLOCK)[162]. Although the protein family is hugely important for transcription, only very few germline mutations have been observed in humans. Heterozygous loss or reduction of function mutations within CBP are associated with the Rubinstein-Taybi-Syndrome (RTS)[163]. Loss or reduction of function within one allele of CBP leads to short stature and different degrees of learning disability. Homozygous deletion of either p300 or CBP can be considered embryonic lethal[164]. Additionally heterozygous deletion of one allele of both proteins at the same time is lethal as well[164] (see section 1.3.4).

From an evolutionary standpoint the essential domains within the KAT3 family are a Histone Acetylase enzyme (HAT), a Transcription Adaptor putative Zinc finger domain (Taz), a Plant Homeo Domain (PHD) and a ZZ-type zinc finger[165]. In mammalian KAT3 enzymes these domains are complemented by a second Taz-type zinc finger domain, a Kinase Inducible domain interacting domain (Kix)[166], an Interferon Binding Domain (IBiD)[167] and a Bromo domain. Within the fold of the PHD domain another Ring-finger domain is introduced into a loop structure[168]. A construct consisting of Bromo-, PHD/Ring-, HAT-, and ZZ-domains is commonly referred to as p300/CBP core domain (see section 1.3.3). In case of the human sequences only 23% are folded into domains, whereas the remaining 58% are intrinsically disordered. The general architecture of human p300/CBP proteins is depicted in figure 1.3.1. A long unfolded N-terminus is followed by the first of two Taz-type zinc fingers, named Taz1. This N-terminal region also contains the nuclear localization signal (NLS) for the protein.[169] The next folded domain is the Kix domain, followed by the p300/CBP core domain. C-terminally to the core domain a second Taz-type zinc finger (Taz2) can be found[170], followed by an interferon binding domain (IBiD), which is also referred to as nuclear receptor coactivator binding domain (NCBD)[167]. In older publications regions are dubbed as Cysteine-Histidine rich regions (CH1, CH2, CH3)[170]. Here CH1 represents the Taz1, CH2 the HAT domain with the PHD/Ring domain and CH3 a combination of ZZ and Taz2 domain[32]. The domains and their functions are described in more detail in the following section and 1.3.2.
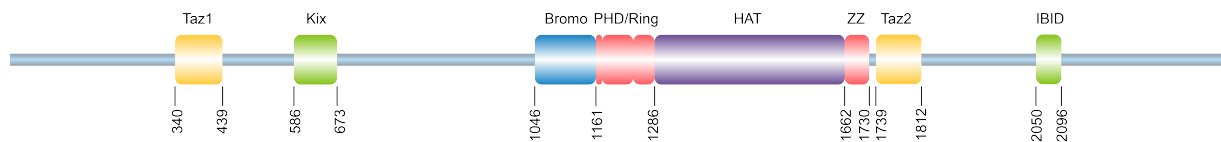
Figure 1.3.1: General domain architecture of p300/CBP. Both members of the KAT3 family consist of a single chain of ≈2400 amino acids. Amino acid numbering in this image corresponds to human p300. Besides its enzymatic activity it functions as a framework for further transcriptional co-factor binding. Four domains are known to be transcription factor binding: Taz1, Kix, Taz2 and IBiD. The CBP/p300 "core domain" consists of an acetyl-lysine binding Bromo-domain, a PHD domain with an inbuilt RING finger domain the enzyme itself and a SUMO (Small Ubiquitin like Modifier) binding ZZ finger domain. Within the unfolded regions several important motifs can be found, such as SUMOylation sites, phosphorylation sites and sites of lysine auto-acetylation.

1.3.2 Transcription factor binding domains

CBP and p300 feature four distinct transcription factor interacting regions, distributed over the complete protein.[32] All four domains are depicted in figure 1.3.2. The domains are completely alpha-helical in nature and two of them are Taz-type zinc fingers.
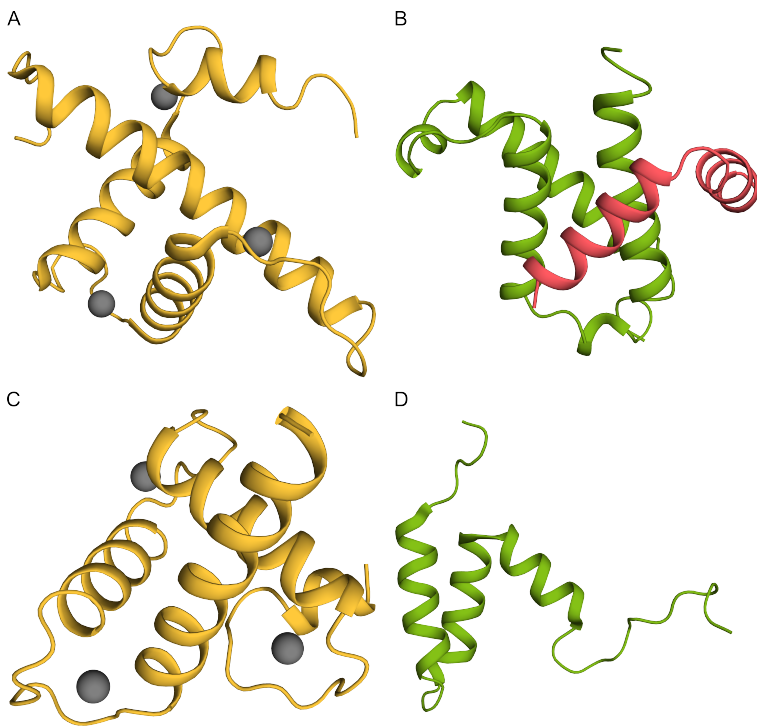
Figure 1.3.2: p300/CBP domains shown to interact with 9aaTAD transcription factors. All four domains of p300/CBP known to interact with transcription factors are shown. The Taz1 (A) and Taz2 (C) are zinc finger domains of a similar fold. Both of them are composed of four α-helices and feature 3 C_3H zinc binding loops. Both Kix (B) and IBiD (D) are helical only domains consisting of three helices. The Kix domain of p300/CBP is very unstable in its apo-form, therefore only complex structures are available (Kix domain is shown in green, interaction partner in red).

These domains are able to bind so called nine amino acid transactivation domains (9aaTAD, reviewed in[29]). The affinity of binding to each individual domain varies greatly over the specific domain and interaction partner, however in case of p73 and p53 the Taz2 domain is by far the strongest binder[20;32]. Besides in p300/CBP structures the amphipathic helix of the TAD can be formed on other co-activators such as TAF9[171] as well as on E3 ligases of the MDM family[172]. The helix formed contains at least two hydrophobic amino acids in subsequent helix turns[29]. The outward facing side of the helix contains mostly hydrophilic amino acids. Additionally in many cases the residues are either glutamate/aspartate or serine/threonine/tyrosine[173;29], the latter being phosphorylatable and the former carrying a negative charge. A negative net-charge of the transactivation domain enhances the binding to most of the highly basic interaction domains[17]. Binding to proteins of the MDM family is restricted to amino acid sequences which carry an "FWL"-motif on the hydrophobic side of the formed helix, as this exact sequence is needed for binding[174].

Taz1

The Taz1, also called CH1 region, consists of $\approx$100 amino acids (amino acids 327-424 of human p300), forming a stable structure of four short amphipathic helices, connect via linkers and stabilized by zinc ions within these linkers[175]. The zinc ions are coordinated by three cysteines and one histidine in a tetragonal C_3H type configuration[175]. Older studies initially suggested that the domain by itself is unstable and only forms a molten globule[176]; upon binding of an interaction partner a stable fold would be found. However this could be traced back to over-titration with zinc ions in a later study[175]. The most important interaction partners of the Taz1 domain

are the Hypoxia Inducing Factor 1α (HIF-1α)[177] and CBP/p300-interacting transactivator 2 (CITED2)[178].

Kix

The Kix domain of p300 consists of 90 amino acids (amino acids 567-651 of p300), divided into three almost equally long helices[179]. The protein fold itself is unstable, described as molten globule[180], and thus no structure of the isolated human Kix domain of either CBP or p300 have been reported to date. However structures of other isolated Kix domains from human[181] and yeast[182] proteins have been solved. The structures show that all three helices of the fold are arranged in a nearly parallel fashion. This is in contrast to the reported structures of the human p300/CBP Kix domains with interaction partners. In these structures the helices of the Kix domains adopt an angle towards each other[179]. It has been shown that this structural rearrangement enables multiple transactivation domains to bind simultaneously onto the surface of Kix. For transactivation domains of mixed-lineage leukemia (MLL) and the phosphorylated kinase-inducible domain (pKID) of the cAMP response element-binding protein (CREB) it could be shown that the binding occurs in a cooperative manner[183].

Taz2

The Taz2 domain is a 90 amino acid long domain (amino acids 1723-1836 of p300) of similar fold as the Taz1 domain, albeit having only 34% sequence identity[165]. It forms a stable protein, resulting in numerous structures with[42;184] and without[185] interaction partners. The Taz2 domain is the most studied p300/CBP in context with p53, as it is the domain with the highest affinity towards these transactivation domains[186;44;187]. Additionally it binds the Signal Transducer and Activator of Transcription (STAT) family of proteins[184], which are required for interferon signal transduction from cell membrane associated kinases to the nucleus (reviewed in[188]). Besides the acetyl-transferase domain itself the Taz2 domain is the only domain conserved in all organisms with a KAT3 type histone acetylase, and therefore belongs to the required domains of p300/CBP[189;158].

IBiD

The interferon binding domain (IBiD), also called nuclear receptor co-activator binding domain (NCBD) is a very small alpha helical domain, consisting only of 44 amino acids (amino acids 2050-2094 of p300)[190;167]. These amino acids form three very small separate alpha helices[180]. It can directly bind to interferons such as IRF-3[191] or transcriptional co-activators such as nuclear receptor coactivator 1 (p160/SRC1)[192].

All of these domains show affinity towards the transactivation domains of p53, with affinities varying from lower nano molar (Taz2) to micro molar (IBiD) regions[32]. The affinity towards the domains can be greatly increased by phosphorylation of the p53 transactivation domains[187]. In case of Taz2 the affinity of a p53 peptide spanning both transactivation domains (1-57) can be increased from 20 nM to 0.5 nM by phosphorylation of all serine/threonine residues[44]. This indicates that the transcription-factor binding of these domains is at least partly dependent on electrostatic interactions and that the phosphorylation state of the p53 TADs matters in terms of co-activator binding[43].

1.3.3 p300/CBP core

The catalytic core of p300/CBP can be separated in several subdomains with varying functions. In mammals it consists of an acetyl-lysine binding domain (BRD)[193], a Plant Homeo Domain (PHD)[170;194] with an interspersed "Really Interesting New Gene" zinc finger domain (RING finger domain)[194;195], the catalytically active Histone Acetylase domain (HAT) and a potentially Small Ubiquitin like Modifier 1 (SUMO1) binding ZZ-domain[196]. Additionally a lysine rich Activation Loop (AL) between the HAT enzyme and the ZZ domains controls the activity of the enzyme via auto-acetylation[195]. Since last year, X-ray crystallography structures of the p300 as well as the CBP core are available.[168;195]. Previously only the p300 core structure was available. Both structures look virtually identical (overlay: Figure 1.3.3). One notable difference is the attachment of the BRD to the HAT domain, where the BRD is more closely connected to the HAT in the CBP structure. This might be a relevant difference, as the acetylation patterns vary between both proteins, although they are almost identical sequence-wise[197].
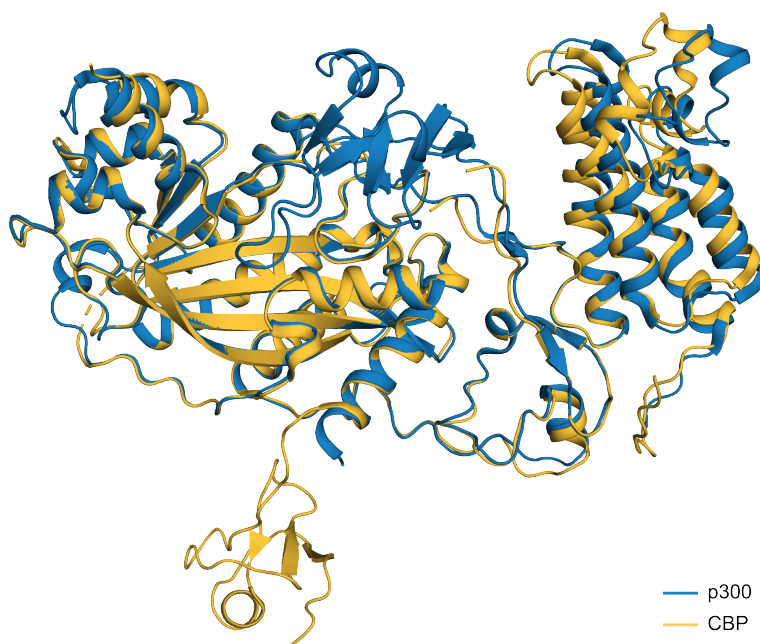
Figure 1.3.3: Overlay of CBP and p300 "core domain". Both proteins adopt an identical fold with minuscule differences. The p300 construct was truncated before the ZZ domain, therefore it is not present in the structure. Additionally no electron density was observed for the PHD/RING domain in CBP. Besides this the most intriguing difference between the structures is the different angle between the Bromo domain and the enzyme. PDB: 4BHW (p300) and 5U7G (CBP)

PHD finger domains have originally been discovered as a novel fold in the HAT3.1 protein of *Arabidopsis*[198]. By structural analysis it was determined that PHD domains recognize the

methylation state of lysine (reviewed in[199]). This allows for a sophisticated interplay between Histone acetylation and methylation. In respect to p300/CBP the PHD domain was found to be necessary for enzymatic function of CBP but dispensable in case of p300[170]. The function of the interspersed RING domain is currently unknown. Speculatively it is involved in SUMO or ubiquitin binding as well[195].

1.3.4 Physiological Functions of p300/CBP

The p300/CBP family of HATs has been implicated in diverse cellular functions. To date over 400 direct interaction partners/acetylation targets have been found[200]. The most prominent function of both enzymes is the acetylation of histones in response to stimuli by transcription factor binding. Acetylation of all four major histones has been found for p300 and CBP, although the frequency of acetylation seems to vary with the specific enzyme[201]. The predominant acetylation occur at K18 and K27 of histone H3 in vivo[202]. Additional modifications have been found at H3 (K14), H4 (K5, K8), H2A (K5) and H2B (K12, K15)[203].

p300/CBP related diseases

Haploinsufficiency by inactivation of one allele of both proteins (CBP$^{(+/-)}$/p300$^{(+/+)}$ or CBP$^{(+/+)}$/p300$^{(+/-)}$) leads to Rubinstein-Taybi syndrome, marked by broad thumbs, first toes, special facial features and learning difficulties[204]. In mouse models heterozygous inactivation of one allele of p300/CBP leads to long-term memory formation impairments[205;206]. Somatic mutations of either protein occur frequently in a number of malignancies. The earliest characterized alliteration were chromosome translocations in acute myeloid leukemia (AML), which disrupt the CBP gene and fused it to another potential Histone acetylase called MOZ[207]. The same kind of fusion has been reported for p300 as well[208]. Additionally several CBP fusions with the Histone-lysine N-methyltransferase 2A (MLL) protein have been reported[209]. In a study with 222 solid tumor cell lines 5.6% carried a truncated variant of p300, with silencing of the other allele[210]. These gene-fusions generally abolish the enzymatic activity or regulation of CBP, therefore removing potential growth inhibition due to activation of the p53 mediated transactivation of pro-apoptotic genes[209]. On the other hand p300/CBP seem to be required for cell proliferation due to their involvement in DNA repair (see section below), which is of uttermost importance for cell division. Additionally they have been found to be essential for transactivation on the Histone-promoter[211].

p300/CBP in DNA repair

Besides the involvement direct involvement in processes leading to chromatin rearrangement the KAT3 family has been found to be directly involved as a regulator in key DNA repair pathways (reviewed in[212]). Both proteins have been found to acetylate PARP-1 (Poly ADP-ribose poly-

merase 1) on multiple lysine residues[213]. This seemingly leads to a stabilization of PARP-1/p53 interaction which is in turn required for NF-κB transcriptional activation[213]. γ-H2AX, another prominent sensor of DNA damage has been found to be acetylated by p300 and CBP in response to DNA damage. The acetylation of residue K36 has been suggested to be required for cell survival, as mutation of this amino acid leads to an increase in sensitivity to ionizing radiation (IR) in mouse embryonic fibroblasts (MEFs)[213]. In general, enzymes required for certain DNA repair pathways have frequently been found to be directly acetylated by a member of the KAT3 family. The human flap endonuclease (FEN1), involved in Okazaki fragment processing[214], was shown to interact with p300 and to be acetylated on four lysines in its C-terminal region[215]. Acetylation was found to reduce the affinity if FEN1 to DNA, affecting its endonuclease activity and thereby reducing its involvement in Base Excision Repair (BER) and Nucleotide Excision Repair (NER). DNA 2 endonuclease/helicase (Dna2), another enzyme involved in Okazaki fragment processing, has been found to interact with and acetylated by p300[216]. In contrast to FEN1, acetylation leads to an increase in DNA binding efficiency. This suggests a mechanism where the inactivation of one of both factors leads to a likewise activation of the other[216]. Additionally several nucleotide specific enzymes in BER are modified by p300/CBP as well:

- Thymine DNA Glycosylase (TDG) is modified while not bound to DNA, while acetylation is prevented directly on DNA[217]

- 8-Oxoguanin DNA glycosylase 1 (OGG1) is acetylated on several lysines, while acetylation is negatively correlated with oxoguanine DNA damage[218]

- Nei-like 2 DNA glycosylases (NEIL1 and NEIL2) are acetylated at several sites, leading to inhibition of glycosylase and lyase activities[219]

- 3-Methyladenine DNA glycosylase is acetylated by p300 *in vitro* and labeling of the enzyme can be enhanced by the presence of Estrogen Receptor α binding[220]. However acetylation of the protein as a result of DNA damage has not been tested.

- AP endonuclease 1 (APE1) has been found to be acetylated in several studies[221;222;223]. APE1 acetylation seems to stimulate DNA repair, rendering tumor cells more resistant to chemotherapeutic drugs.

- DNA polymerase β is acetylated by p300 predominantly on a single residue (K72) with secondary sites acetylated *in vitro* as well. Acetylation at the primary site inhibits the lyase activity of the enzyme and thereby inhibits its activity in BER[224].

Besides the BER pathway several Nucleotide Excision Repair (NER) enzymes have been found to be acetylated by p300/CBP as well. Notably the proteins "DNA repair protein complementing XP-A cells" (XPA) and "DNA repair protein complementing XP-G cells" (XPG), frequently mutated in Xeroderma pigmentosum patients have been found to be targets of p300/CBP[225;226].

XPA is a structural framework factor recruiting other proteins involved in NER around the DNA lesion. p300/CBP acetylation represses this function. Under DNA damage conditions the acetylation is removed by the histone deacetylase Sirtulin-1 (Sirt1), thereby re-enabling NER[225]. In addition to BER and NER proteins several other factors from different DNA repair pathways are modified by p300/CBP. Ku70, a protein involved in Non-Homologous End Joining (NHEJ), is acetylated at several lysines throughout the protein. In a non-acetylated form Ku70 blocks Bax-mediated apoptosis[227]. Two enzymes of the ATP-dependent DNA helicase Q family (RecQ-family) have been found to be targets of p300 acetylation, the Werner protein (WRN) and RecQ4. In case of WRN acetylation of several lysine residues seems to increase the protein stability by blocking ubiquitination[228]. In case of RecQ4 acetylation was found to regulate the cellular localization as acetylation by p300 happens within the NLS of the protein and acetylated protein was found to localize cytoplasmatically[229].

Regulation of p300/CBP activity by post-translational modification

Furthermore the stability and activity of p300/CBP is regulated via phosphorylation of several key residues. S1835 in p300 is phosphorylated by protein kinase B (Akt1) which increases the enzymatic activity by enhancing promoter recruitment of the enzyme[230]. Similar effects have been reported for nuclear Rho kinase 2 (ROCK2)[231]. On the contrary phosphorylation of p300 at S89 by protein kinase C α and δ (PKC) have been reported to repress the activity of p300 by unknown means[232].

In the present work I will show that the lower transactivation potential of TAp73, compared to that of TAp63, is due to a different structural organization of the transactivation domain of both proteins. Additionally I show that TAp63α in its dimeric state is unable to bind transcriptional co-activators, which explains the previously shown inability to transactivate on pro-apoptotic promoters. Lastly I show that the tetramerization of TAp63α follows a two-step kinetic, allowing for additional regulation prior to apoptosis induction.

2 Materials

2.1 Construct List

Table 2.1.1: Constructs used in this study

construct name	construct description	vector
MBP-Taz1	MBP fused to human p300 Taz1 domain (aa 326-424), cleavable by TEV protease	pMAL-c4x
MBP-Taz2	MBP fused to human p300 Taz2 domain (aa 1723-1812, C1738A/C1746A/C1789A/C1790A mutant), cleavable by TEV protease	pMAL-c4x
MBP-Kix	MBP fused to human p300 Kix domain (aa 567-651), cleavable by TEV protease	pMAL-c4x
MBP-IBiD	MBP fused to human p300 IBiD domain (aa 2045-2094), cleavable by TEV protease	pMAL-c4x
MBP-Taz2-p63TAD1	MBP fused to human p300 Taz2 domain (aa 1723-1812, C1738A/C1746A/C1789A/C1790A mutant) fused to p63 TAD (aa 8-35, C28S mutant), cleavable by TEV protease after MBP	pMAL-c4x
MBP-Taz2-p63TAD	MBP fused to human p300 Taz2 domain (aa 1723-1812, C1738A/C1746A/C1789A/C1790A mutant) fused to p63 TAD (aa 8-82, C28S mutant), cleavable by TEV protease after MBP	pMAL-c4x
MBP-Taz2-p73TAD1	MBP fused to human p300 Taz2 domain (aa 1723-1812, C1738A/C1746A/C1789A/C1790A mutant) fused to p73 TAD1 (aa 10-31), cleavable by TEV protease after MBP	pMAL-c4x
MBP-Taz2-p73TAD	MBP fused to human p300 Taz2 domain (aa 1723-1812, C1738A/C1746A/C1789A/C1790A mutant) fused to p73 TAD (aa 10-67), cleavable by TEV protease after MBP	pMAL-c4x
GST-Taz1	GST fused to human p300 Taz1 domain (aa 326-424)	pGEX-6p2

GST-Taz2	MBP fused to human p300 Taz2 domain (aa 326-424)	pGEX-6p2
GST-MED15	MBP fused to human MED15 Kix domain (aa 326-424)	pGEX-6p2
GST-SSRP1	MBP fused to human SSRP1 middle domain (aa 326-424)	pGEX-6p2
GST-HMGB1	MBP fused to human HMGB1 BoxA domain (aa 326-424)	pGEX-6p2
GST-ZZ	GST fused to human p300 ZZ domain (aa 1663-1713), cleavable by TEV protease	pGEX-6p2
GB1-p63TAD1	GB1 fused to p63 TAD (aa 8-35, C28S mutant), cleavable by TEV protease	pET16b
myc-TAp63γ and mutants	myc-tagged TAp63γ and variants, full length	pcDNA3
myc-TAp63α and mutants	myc-tagged TAp63α and variants, full length	pcDNA3
myc-TAp73β and mutants	myc-tagged TAp63β and variants, full length	pcDNA3
myc-TAp73α and mutants	myc-tagged TAp63α and variants, full length	pcDNA3
GB1-PAD and mutants	His-tagged PAD sequence of p63 and mutants with a GB1 expression tag	pET16b(+)
sfGFP-PAD and mutants	His-tagged PAD sequence of p63 and mutants with a sfGFP expression tag	pET21(+)
TAp63α-TEV-PAD-M-TI-His	C-terminally His-tagged TAp63α with TEV site before PAD and an additional methionine after to enable CNBr cleavage	pET16b(+)

2.2 Chemicals and Reagents

All used reagents not mentioned in the list below have been purchased from Carl-Roth GmbH & Co. KG, Germany in 'pure' or higher quality.

^{13}C-Glucose	Cambridge Isotope Laboratories Inc, USA
^{15}N-Ammoniumchloride	Cortecnet, France
Accutase	Sigma-Aldrich Chemie GmbH, Germany
Agarose UltraPure	Thermo Fisher Scientific, Germany
Bovine serum albumin for cell culture	Sigma-Aldrich Chemie GmbH, Germany
cOmplete Mini, EDTA-free protease inhibitor	Roche Diagnostics, Germany
Dulbecco's modified Eagle's medium	Life Technologies GmbH, Germany
Imidazole BioUltra	Sigma-Aldrich Chemie GmbH, Germany
L-Glutamine, 200 mM	Life Technologies GmbH, Germany
Luminol / 3-Aminophtalhydrazide	Sigma-Aldrich Chemie GmbH, Germany
MEM	Life Technologies GmbH, Germany
p-Coumaric acid	Sigma-Aldrich Chemie GmbH, Germany
Penicillin/Streptomycin, 10 kU/ml / 10 mg/ml	Life Technologies GmbH, Germany
TWEEN 20	Sigma-Aldrich Chemie GmbH, Germany

2.3 Laboratory Equipment

96 well microplate, PS, F-bottom non-binding, black	Greiner Bio-One GmbH, Germany
Agar plate incubator	Memmert GmbH & Co. KG, Germany
ÄKTApurifier FPLC system	GE Healthcare Europe GmbH, Germany
ÄKTApure FPLC system	GE Healthcare Europe GmbH, Germany
Amicon centrifugal filter units	Millipore GmbH, Germany
Axiovert 40 CFL microscope	Carl Zeiss AG, Germany
Mini-PROTEAN TGX Precast Gels 4-15%	Bio-Rad Laboratories GmbH, Germany
Mini-PROTEAN Tetra Cell Systems	Bio-Rad Laboratories GmbH, Germany
Cell culture flasks	Greiner Bio-One GmbH, Germany
Cell scraper	Greiner Bio-One GmbH, Germany
Centriprep YM-30 concentrator	Millipore GmbH, Germany
Lumi Imager F1 documentation system	Roche Diagnostics, Germany
Milli-Q Academic ultrapure water system	Millipore GmbH, Germany
NativePAGE NOVEX 3-12% Bis-Tris Gel 1.0 mm	Life Technologies GmbH, Germany
Syringe filter 0.22 μm polysulfone	Carl-Roth GmbH & Co. KG, Germany
Ultrafree Centrif. filters Durapore PVDF 0.65 μm	Millipore GmbH, Germany
XCell II Blot Module	Life Technologies GmbH, Germany
XCell SureLock Mini-Cell SDS-PAGE system	Life Technologies GmbH, Germany

2.3.1 NMR Spectrometers

950 MHz (Bruker Avance III)
5 mm TCI cryo ^{1}H,^{15}N,^{13}C Z-GRD
5 mm TXI ^{1}H,^{15}N,^{13}C XYZ-GRD

900 MHz (Bruker Avance Neo)
5mm TCI cryo ^{1}H,^{15}N,^{13}C Z-GRD
5 mm TXI cryo ^{1}H,^{15}N,^{13}C Z-GRD

800 MHz (Bruker Avance III HD)
5 mm TCI cryo ^{1}H,^{15}N,^{13}C Z-GRD
5 mm TXI ^{1}H,^{15}N,^{13}C XYZ-GRD

700 MHz (Bruker Avance III HD)
5 mm QCI cryo ^{1}H,^{15}N,^{13}C,^{31}P Z-GRD

600 MHz (Bruker Avance III)
5 mm TCI cryo ^{1}H,^{15}N,^{13}C Z-GRD

600 MHz (Bruker Avance II)
5 mm TCI cryo ^{1}H,^{15}N,^{13}C Z-GRD

500 MHz (Bruker Avance II)
5 mm TXI ^{1}H,^{15}N,^{13}C XYZ-GRD

2.3.2 Chromatography

Glutathion Sepharose 4 Fast Flow	GE Healthcare Germany
GSTrap IMAC FF 5 ml prepacked column	GE Healthcare Germany
HiLoad 16/600 Superdex 75	GE Healthcare Germany
HisTrap IMAC FF 5 ml prepacked column	GE Healthcare Germany
Dextrin Sepharose HP	GE Healthcare Germany
OmniFit 25/100 column	Omnifit Diba Industries, USA
HiTrap SP HP 5 ml cation exchange column prepacked	GE Healthcare Germany
HiTrap Q HP 5 ml anion exchange column prepacked	GE Healthcare Germany
Superdex 200 10/300 column	GE Healthcare Germany
Superdex 75 10/300 column	GE Healthcare Germany

2.3.3 Dialysis Membranes

Centriprep YM-3, 10 and 30 concentrators	Millipore GmbH, Germany
Mini Dialysis Kit, 1 kDa cut-off	GE Healthcare Germany
Slide-A-Lyzer Dialysis Cassettes (diff. MWCO)	Pierce / Thermo Scientific, Germany
Spectra/Por 6 dialysis membranes (diff. MWCO)	Spectrum Europe B. V., Netherlands

2.3.4 Kits

Amersham ECL Prime WB Detection System	GE Healthcare Germany
Dual-Glo Luciferase Assay System	Promega GmbH, Germany
Effectene Transfection Reagent	Qiagen GmbH, Germany
EndoFree Plasmid Maxi Kit	Qiagen GmbH, Germany
Gel Filtration Calibration Kit	GE Healthcare Germany
QIAprep Spin Miniprep Kit	Qiagen GmbH, Germany
QIAquick Gel Extraction Kit	Qiagen GmbH, Germany
QIAquick PCR Purification Kit	Qiagen GmbH, Germany
TNT T7 Quick Coupled Transcription/Translation	Promega GmbH, Germany

2.3.5 Antibodies

anti-GAPDH clone 6C5	Millipore GmbH, Germany
anti-Myc tag clone 4A6	Millipore GmbH, Germany
Goat anti-mouse IgG -Fab -HRP conjugated	Sigma-Aldrich Chemie GmbH, Germany

2.3.6 Molecular Weight Markers

GeneRuler 1 kb DNA Ladder	Thermo Scientific, Germany
GeneRuler 100 bp Plus DNA Ladder	Thermo Scientific, Germany
Native Mark Unstained Protein Standard	Life Technologies, Germany
Precision Plus Dual Color (10-250 kDa)	Bio-Rad Laboratories GmbH, Germany

2.3.7 Enzymes

BamHI-HF Restriction Endonuclease	New England Biolabs GmbH, Germany
Benzonase Nuclease (Merck Millopore)	VWR International GmbH, Germany
DNase I from bovine pancreas type IV	Sigma-Aldrich Chemie GmbH, Germanys
DpnI Endonuclease	New England Biolabs GmbH, Germany
Lysozyme from chicken egg white	Sigma-Aldrich Chemie GmbH, Germany
PfuUltra High Fidelity DNA Polymerase	Agilent Technologies, Germany
Pfu-Sso7d DNA Polymerase	self-produced
T4 DNA Ligase	New England Biolabs GmbH, Germany
TEV Protease	self-produced
XhoI Restriction Endonuclease	New England Biolabs GmbH, Germany

2.3.8 Bacterial Strains&Cell Lines

Strain	Supplier
DH5α Competent *E. coli*	New England Biolabs GmbH, Germany
NEB T7 Express (DE3) Competent *E. coli*	New England Biolabs GmbH, Germany
Rosetta (DE3) Competent *E. coli*	Merck Millipore, Germany

Cell line	Description	Supplier
H1299	non-small cell lung cancer	ATCC, USA
Saos2	osteosarcoma	DSMZ GmbH, Germany

2.4 Buffers

2.4.1 Protein Purification

Protease inhibitor cocktail (PIC) 100x 119.7 mg/ml AEBSF

23.8 mg/ml leupeptin

15.4 mg/ml bestatin

9.8 mg/ml aprotinin

8.9 mg/ml E-64

3.4 mg/ml pepstatin

→dissolve in 100 ml 50% (v/v) methanol

→stir overnight, aliquot to 1 ml and evaporate solvent under vacuum

→store at -20°C

MBP-A

25 mM HEPES pH 7.4

1000 mM NaCl

20 mM β-Mercaptoethanol

MBP-B

25 mM HEPES pH 7.4

500 mM NaCl

20 mM β-Mercaptoethanol

20 mM Maltose

Zn-NTA A

25 mM Tris pH 7.8

500 mM NaCl

Zn-NTA B

25 mM Tris pH 7.8

500 mM NaCl

500 mM Imidazole

IEX-A

25 mM HEPES pH 7.0

50 mM NaCl

20 mM β-Mercaptoethanol

IEX-B

25 mM HEPES pH 7.0

1000 mM NaCl

20 mM β-Mercaptoethanol

IEX dilution buffer

25 mM HEPES pH 7.0

20 mM β-Mercaptoethanol

IMAC-A

25 mM Tris pH 8.0

500 mM NaCl

30 mM Imidazole

5% Glycerole

IMAC-B

25 mM Tris pH 8.0

200 mM NaCl

500 mM Imidazole

5% Glycerole

IMAC Stripping buffer

6 mM Guanidium-HCl

100 mM EDTA

GST-A

25 mM Tris pH 7.8

500 mM NaCl

10 mM β-Mercaptoethanol

GST-B

25 mM Tris pH 7.8

500 mM NaCl

10 mM β-Mercaptoethanol

20 mM reduced Glutathione

PAD SEC urea

25 mM Tris pH 8.0

150 mM NaCl

6 M Urea

2.4.2 Assay Buffers

Pull-down buffer

50 mM Tris pH 7.4

100 mM NaCl

10 mM β-Mercaptoethanol

0.05% Tween-20

FP buffer

25 mM HEPES pH 7.5

100 mM NaCl

0.5 mM TCEP

2.4.3 NMR

NMR buffer (Taz2/Taz2-p63)

25 mM MES pH 6.3

200 mM NaCl

0.5 mM TCEP

NMR buffer (Taz2-p73TA/Taz2-p73-TAD1)

25 mM MES pH 6.3

50 mM NaCl

0.5 mM TCEP

kinase NMR buffer

50 mM Bis-Tris pH 6.5

50 mM MgCl$_2$

150 mM NaCl

0.5 mM TCEP

D2O/DSS mix

1 mM 4,4-dimethyl-4-silapentane-1-sulfonic acid (DSS) in 100% D$_2$O

2.4.4 Cell culture

H1299 medium

500 ml RPMI 1640

50 ml fetal bovine serum

5 ml penicillin/streptomycin

5 ml L-glutamine

→store at 4°C

Saos2 medium

500 ml Dulbecco's modified Eagle medium

50 ml FBS

5 ml penicillin/streptomycin

5 ml L-glutamine

→store at 4°C

Cell lysis buffer

50 mM Tris pH 8.0

150 mM NaCl

0.5 mM TCEP

20 mM CHAPS

2.4.5 Ovary culture&staining

Mouse Ovary medium

1x MEM (+ L-glutamine)

10% FBS

1x penicillin/streptomycin

4 mg/ml BSA

70 μM Br-cAMP

CUBIC-2

50% (w/v) sucrose

25% (w/v) urea

10% (w/v) 2,2',2'-nitrilotriethanol

2.4.6 Electrophoresis&Western blot

Agarose gel running buffer

40 mM Tris-Acetate pH 8

20 mM acetic acid (100%)

1 mM EDTA

DNA gel loading dye

10 mM Tris-HCl pH 7.6

0.03% Bromophenol blue

0.03% Xylene Cyanol F

60% Glycerol

60 mM EDTA

SDS PAGE Reducing sample buffer

150 mM Tris (pH 7.0)

12% (w/v) SDS

30% (v/v) Glycerol

6% (v/v) β-Mercaptoethanol

0.05% (w/v) Coomassie Blue

Tris/Tricine Running Buffer, Cathode Buffer (10X)

1 M Tris

1 M Tricine

1% (w/v) SDS

→adjust pH to 8.3

Anode Buffer (10X)

2 M Tris pH 8.8

SDS-PAGE Fixation Buffer

50% Ethanol (v/v)

10% Acetic acid (v/v)

SDS-PAGE Coomassie Staining Buffer

5% Ethanol (v/v)

7.5% Acetic Acid (v/v)

0.001% Coomassie Brilliant Blue R250 (w/v)

Tris-HCl pH 8.5 1 M

1 M Tris (121.14 g)

→adjust pH to 8.5

Coumaric acid stock solution

90 mM Coumaric acid (0.15 g)

→to 10 ml with DMSO, store at -20°C in the dark

Luminol stock solution

250 mM Luminol (0.44 g)

→to 10 ml with DMSO, store at -20°C in the dark

TBS-T

50 ml TBS 20x buffer

0.05% TWEEN 20

Milk Powder solution

50 g milk powder

→to 1 l with TBS-T

ECL solution 1

9 ml Milli-Q H_2O

1 ml Tris-HCl pH 8.5 stock solution

45 μl Coumaric acid stock solution

100 μl Luminol stock solution

ECL solution 2

9 ml Milli-Q H_2O

1 ml Tris-HCl pH 8.5 stock solution

6 μl 30% H_2O_2

2.4.7 Bacterial Growth Media

Vitamins (for 10 ml, 10000x)

100 mg Biotin

100 mg Thiamin

Trace Elements (for 100 ml, 10000x)

8.3 g $FeCl_3$ 6 H_2O

840 mg $ZnCl_2$

130 mg $CuCl_2$ 2 H_2O

100 mg $CoCl_2$ 6 H_2O

100 mg H_3BO_3

16 mg $MnCl_2$ 2 H_2O

$\rightarrow$ to 100 ml with 0,5 M EDTA pH 8

M9 (per liter)

7.52 g Na_2HPO_4

3 g KH_2PO_4

0.5 g NaCl

$\rightarrow$Autoclave

$\rightarrow$afterwards add:

1 ml of 1 M $MgSO_4$ (sterile filtered)

1 ml of 0.1 M $CaSO_4$ (sterile filtered)

4 g of Glucose (2 g if ^{13}C)

1 g of NH_4Cl (equal if ^{15}N)

1 ml of vitamins

100 μl of trace elements

SOC (per liter)

5 g Yeast Extract

20 g Tryptone

0.6 g NaCl

0.2 g KCl

→Autoclave

→afterwards add:

10 mM $MgCl_2$

10 mM $MgSO_4$

20 mM Glucose

2x YT (per liter)

16 g Tryptone

10 g Yeast Extract

5 g NaCl

(optional: adjust to pH 7)

IPTG Stock solution (per liter)

238.3 g IPTG

→solubilize in H_2O, filter sterile and store at -20°C

Ampicillin (1000x)

100 mg/ml

→solubilize in 50% (v/v) Ethanol, filter sterile and store at -20°C

2.5 Web Server

name	description	URL
TALOS+	secondary structure prediction based on ^{13}C CA and CB shifts	`https://spin.niddk.nih.gov/bax/nmrserver/talos/`
9aaTAD	nine amino acid transactivation domain prediction	`http://www.med.muni.cz/9aaTAD/`
Oligocalc	Primer melting point calculation	`http://biotools.nubic.northwestern.edu/OligoCalc.html`
Clustal Omega	Multiple sequence alignment	`https://www.ebi.ac.uk/Tools/msa/clustalo/`
Uniprot	Protein Database	`https://www.uniprot.org/`
PDB	3D Protein Structure Database	`https://www.rcsb.org/`

2.6 Software

Adobe Illustrator CS6	Adobe Systems
Adobe Photoshop CS6	Adobe Systems
Bruker Topspin 3.x	Bruker Corporation
Chromas Lite 2	Technelysium Pty Ltd
Fiji	Under GNU Licence (`https://imagej.net/Fiji`)
NMRFAM Sparky	National Magnetic Resonance Facility at Madison, USA
Office 2013	Microsoft Corporation
Prism 5	GraphPad
Pymol 2	Schrödinger

3 Methods

3.1 Cloning

3.1.1 Polymerase Chain Reaction (PCR)

All types of polymerase chain reaction were performed with a in-house-made variant of the DNA polymerase from *Pyrococcus furiosus* (Pfu polymerase). The Pfu polymerase was fused to the unspecific DNA binding Sso7d protein from *Sulfolobus solfataricus*. The resulting Pfu-Sso7d protein features a dramatically increased processivity as well as large increase in elongation speed. The polymerase was used as a replacement for the commercially available Phusion Polymerase (NEB).

3.1.2 Primer Design

All primers were designed in a way that complementary sequences had a predicted melting point of at least 52°C (non salt adjusted), calculated by the online tool OligoCalc[233]. Additionally primers were terminated on both ends with either a cytosine or guanidine residue. Primers for restriction digest were extended by 4 random nucleotides on the side of the cleavage sequence to ensure proper activity of the enzymes.

3.1.3 Insert PCR

Insert PCR was done according to the instructions for Phusion polymerase (NEB) with the exception that self-prepared polymerase was used. A standard reaction mix is shown in table 3.1.1. A general PCR cycle is described in table 3.1.2.

3.1.4 Restriction Digest of Vector DNA and PCR Products

Vector DNA and PCR products intended for ligation reactions were digested with the respective enzymes according to the instructions of the enzyme producer (New England Biolabs, Frankfurt am Main, Germany). Reactions were performed as a double digest in a total volume of 50 μl at

Table 3.1.1: Composition of a standard Phusion insert PCR reaction mix.

component	volume [μl]
5X Phusion HF buffer	10
dNTPs	1
Pfu-Sso7d polymerase (Phusion)	0.5
DMSO	10
Primer (40 μM)	10
Template (10 ng/μl)	1
H$_2$O	34.5

Table 3.1.2: Standard cycle of an insert PCR

Step	temperature [$^\circ$C]	time [s]
initial DNA denaturation	95	60
DNA denaturation	95	30
Annealing	52	30
Elongation	72	30 per kb
30 cycles		

37°C for 1 h (PCR products) or 4 h (vector DNA) if possible. In case of vector DNA small scale single digests were performed as control experiments to verify enzyme activity. Enzyme quantity was adjusted to the given amount of DNA to be digested. Generally at least a twofold excess over the minimal required enzyme quantity was aimed for.

3.1.5 Ligation

Ligation was done with T4 ligase (NEB) according to the suppliers instructions. The total reaction volume was 10 μl and the molar vector:insert ratio was varied from 1:3 to 1:6, depending on the size difference of vector and insert. Ligation reactions were generally done at room temperature for 1 h. However very small inserts (<100 bp) were subject to ligation at 16°C overnight.

3.1.6 Transformation of Chemo-Competent *E. Coli* Cells

Different chemo-competent *E. coli* cell strains were used for different purposes. For DNA amplification only DH5α cells were used whereas for protein expression either BL21 T7 express cells (NEB Germany, Frankfurt am Main, Germany) or BL21 DE3 Rosetta cells (Merck Millipore, Billerica USA) were used. Independent of the type, 50 μl aliquots of cells were used for each transformation. Cells were thawed from -80°C by incubating them on ice until the cell suspension was completely liquid. Depending on the type of transformation different volumes of DNA were added in the next step. For ligation reactions, QC and RF reactions 10 μl of DNA was added to the cells. For transformations intended for expression 1 μl of DNA was added to the cell suspension. Cells were incubated on ice for 20 min. Subsequently cells were heat shocked

at 42°C for 30 s and returned to the ice for another 60 s. Then 400 μl of SOC medium was added per transformation and the cells were transferred to a shaking incubator and incubated for at least 30 min at 37°C. Finally the cells were plated onto LB agar plates with the correct antibiotic or antibiotics matching the resistance of the transformed plasmids. The plates were then transferred to an incubator for overnight incubation at 37°C.

3.1.7 Overlap Extension (OL) PCR

Generation of artificial protein fusion constructs was done by overlap extension PCR. Primers for OL were designed in a manner that the overlapping complement sequences had a melting point of at least 52°C. Fragment inserts from the first round of PCR were purified by gel extraction to remove any template DNA prior to further processing. In the next step a single insert was generated by using all fragment inserts as template in another round of insert PCR. The forward primer of the first fragment and the reverse primer of the last fragment were used as primer pair. The resulting PCR product was analyzed by preparative DNA gel and the insert with the right size was excised and purified as described before.

3.1.8 Site Directed Mutagenesis

Single or multiple point mutations in the protein coding sequences were introduced with a modified version of the Quikchange-protocol (Agilent, Santa Clara, USA). Two completely complementary primers were designed so that the mutation to be introduces was flanked by sequences complementary to the vector on both sites of the primer with melting points of 52°C or higher on each site. Additionally primers were made to have a 5' and 3' cytosine or guanine base to increase the stability of annealing on the vector. The PCR reaction itself was performed under the buffer conditions as described before. However elongation temperature was dropped to 68°C to increase the processivity of the enzyme. Due to the lower temperature the elongation time was increased to 2 min/kb, therefore yielding 16 min per cycle in most plasmids. If no clones were observed the reaction was repeated with the addition of 2% DMSO or 2 mM $MgSO_4$.

3.1.9 Restriction Free Cloning

Restriction free cloning was performed as a modified variant of the site directed mutagenesis. In this case the mutant primers were replaced by an insert generated via PCR with complementary overlaps to the vector on the 5' and 3' site. Therefore complete expression cassettes or large parts of it can be introduced into a vector with a single PCR reaction[234].

3.1.10 DpnI Digest

DpnI (NEB Germany, Frankfurt am Main, Germany) treatment of PCR products to remove parental, methylated DNA was performed in the PCR reaction mix by addition of 1 μl DpnI per PCR reaction and subsequent incubation at 37°C for 3 h.

3.1.11 Mini/Midi Scale Plasmid DNA Isolation from *E. Coli*

Vector DNA amplification was done by transformation of vector DNA into DH5α cells and subsequent plating to LB agar plates. After overnight incubation at 37°C single clones were used to inoculate either Mini cultures (5 ml in disposable plastic culture tubes) or Midi cultures (250 ml in 500 ml baffled shaking flasks). In both cases 2xYT medium with an additional 10 mM MgSO$_4$ was used as growth medium. Cultures were incubated shaking at 37°C overnight. On the next morning cells were harvested and DNA was purified according to manufacturer's instructions of the kit used (QIAprep Spin Miniprep Kit, Qiagen for Mini cultures and NucleoBond Xtra Midi, Macherey Nagel for Midi cultures). In all cases DNA was resuspended or eluted into MilliQ H$_2$O.

3.1.12 Determination of DNA Concentration

DNA concentration was determined by measurement of the absorption at 260 nm with a Nanodrop 1000 spectrometer (ThermoFisher). Purity of the DNA was assessed by measurement of absorption at 280 nm and the ratio of absorption at 260 nm/280 nm was calculated. For protein-free DNA this ratio must be >1.85.

3.1.13 Sequencing of Vector DNA

Sequencing was done as an overnight service by Microsynth, Göttingen (formerly known as Seqlab Sequence Laboratories). Samples were prepared according to their specifications. Results were analyzed with Chromas Lite 2.

3.2 Protein expression

3.2.1 Rabbit Reticulocyte Lysate (RRL) Expression

Protein expression in RRL was carried out according to the manual provided by the manufacturer (Promega, Fitchburg, USA). Generally, 40 μl of lysate was mixed with 10 μl of a DNA solution, containing a total of 1 μg pDNA3 plasmid of the respective protein. Subsequently the mixture was incubated at 30°C for 90 min in a PCR cycler.

3.2.2 Heterologous Protein Expression in E. Coli

Depending on the target protein, either T7 express cells (NEB) or Rosetta cells (Novagen) were used for protein expression. Rosetta cells harbor an additional pRARE2 plasmid thus enabling expression of less codon-optimized proteins at the expense of a lower growth rate due to the need of an additional antibiotic. Generally, transformation of competent cells was performed the day prior to expression and the cells were cultured on agar plates over-night. On the day of expression, cells were scrapped from the plated and transferred into 500 ml pre-culture flasks containing 200 ml 2xYT medium and supplemented with the corresponding antibiotics. In the pre-culture flask cells were grown at 37 °C up to an OD of 2.

Rich Medium Expression

1 l of 2xYT medium was transferred into 2 l shaking flasks and sterilized by autoclaving. The medium was supplemented with the corresponding antibiotics and tempered to 37°C prior to inoculation with the pre-culture (see section 3.2.2). The main cultures were inoculated with an initial OD of 0.1. Cells were incubated shaking at 180 rpm and a temperature of at 37°C. Growth was monitored and the temperature was reduced to 18°C or 22 °C, depending on the construct, upon reaching an OD of 0.4-0.5. At an OD of 0.7-0.8, 0.5 ml of a 1 M IPTG stock solution was added per liter expression culture to start the expression. Expression was carried out for 16 h overnight. On the next morning cells were harvested by centrifugation.

Minimal Medium Expression

Cells were cultured in 2xYT medium as described in the section above in 2 l expression flasks up to an OD of 0.3. Subsequently the cells were harvested by centrifugation and resuspended in M9 minimal medium containing suitable isotopes for the required labeling scheme. When the cultures reached an OD of 0.4 temperature was reduced to 18-22°C. Protein expression was induced at an OD of 0.55-0.6 with 0.5 ml of a 1 M IPTG stock per liter of expression culture. Expression was carried out for 16 h overnight. On the next morning cells were harvested by centrifugation.

3.3 *E. Coli* Cell Lysis

Cells pellets were resuspended in ice cold lysis buffer (Buffer of subsequent affinity chromatography supplemented with protease inhibitor and self-made DNAse/RNAse mix). Generally, 12 ml of buffer was used per liter of culture, however the amount of buffer was increased if the viscosity of the resulting suspension was deemed too high. Lysis was done via sonicatation with a Sonicator Labsonic U sonicator. Depending on the stability of the protein 30-120 s intervals at 200 W were used for sonication. The procedure was repeated 3-6 times depending on the

turbidity and viscosity of the sample. Between each interval the sample was incubated on ice for at least 2 min. After cell lysis, cell debris and unlysed cells were removed via centrifugation at 18000 rpm (SS34 rotor) for 30 min at 4-8°C.

3.4 Protein Purification

Protein purification was generally performed with the help of FPLC systems (GE ÄKTA basic or GE ÄKTA pure). Affinity chromatography columns were pre-equilibrated with the corresponding Buffer A. Additionally all inlets of the FPLC system were equilibrated to the corresponding buffers as well. The lysate was subsequently loaded onto the column via an external peristaltic pump and subsequently washed for at least 1 column volume (CV) with Buffer A to remove a large portion of cell lysate remaining on the column. Then the column was attached to the FPLC system and washed with a specific buffer scheme, depending on the type of affinity purification. Purification was monitored by absorption at 280 nm or 220 nm, depending on the protein.

3.4.1 Dextrin Sepharose Affinity Chromatography

MBP (Maltose binding protein) fused proteins were purified via a 25 ml dextrin sepharose-column (matrix: GE Healthcare, Chicago, USA; column body: Omnifit Diba Industries, Danbury, USA). Due to the low binding capacity of the dextrose matrix the lysate of ⩽2 l of culture volume was loaded in each round of purification. Loading was done with a flow rate of approximately 3 ml/min. After loading of the cell lysate and washing with at least 1 CV of MBP-A buffer the column was attached to the FPLC system and the column was further washed for an additional 2-3 CV with similar flow rates. Protein was eluted via 1.5 CV of buffer MBP-B. Protein containing fractions were pooled for further processing. Finally the column was regenerated with one CV 6 M guanidine-hydrochloride, followed by 3 CV of buffer MBP-A for re-equilibration. MBP fused constructs were mainly used for expression of Zinc-finger proteins, such as Taz1, Taz2 and derived fusion constructs.

3.4.2 Gluthatione Sepharose Affinity Chromatography

GST (Gluthatione-S-Transferase) fused proteins were purified via a 5 ml gluthatione sephoarose column (GSTrap FF, GE Healthcare, Chicago, USA). Lysate was loaded onto the column with a flow rate ⩽1 ml/min due to the very low on-rate of GST to the immobilized glutathione. After loading the flow rate was increased to 3 ml/min and the column was washed with at least 1 CV of buffer GST-A prior to attachment to the ÄKTA system. Then the column was washed for another 3-5 CV with buffer GST-A, depending on the UV absorbance of the eluate at 280 nm. Subsequently the protein was eluted with freshly prepared buffer GST-B at a flow rate of 1 ml/min. Protein containing fractions were pooled, dialyzed against buffer GST-A to remove free glutathione

and concentrated to at least 1.5 mg/ml. Subsequently the protein was diluted with glycerin to yield a protein/glycerin ratio of 1:1 (v/v). Finally the protein was aliquoted into 1 ml aliquots and flash frozen in liquid nitrogen. The column was regenerated with one CV 6 M guanidine-hydrochloride, followed by 3 CV of buffer GST-A for re-equilibration.

3.4.3 Immobilized Metal Ion Chromatography (IMAC)

5 ml HisTrap FF colums (GE Healthcare) were either loaded with Ni^{2+} or Zn^{2+} ions depending on the type of tag for purification used. His-tagged proteins were purified via nickel based IMAC whereas zinc-finger proteins not containing any tag were purified via zinc based IMAC. Loading of the columns with the respective metal ions was done by washing the column with buffers containing either 100 mM Ni^{2+} or 100 mM Zn^{2+} for 2 CV with a flow rate of 1 ml/min. After that the columns were extensively washed with elution buffer (IMAC-B buffer) to remove metal ions not bound to the column matrix. Finally the columns were equilibrated with washing buffer (IMAC-A buffer). Columns were regenerated after use by extensive washing with IMAC stripping buffer to remove the bound metal ions as well as protein which bound to the column in an unspecific manner.

Nickel-Based IMAC

Cell lysates of His-tagged proteins were loaded onto the columns with a flow rate of 3 ml/min on an external peristaltic pump. After loading the column was washed with 2-3 CV of IMAC-A buffer prior to attachment to the ÄKTA system. The column was washed for another 5 CV prior to protein elution. Elution was done with a linear gradient from 0% buffer B to 100% buffer B linearly increasing the imidazole concentration over 4 CV. This leads to an increased protein purity due to the higher affinity of the His-tagged protein towards the column compared to proteins present in the cell lysates. Therefore the protein of interest tends to elute later in the gradient and can thus easily be separated from the unwanted protein. The elution was monitored via UV absorption at 280 nm and 220 nm and performed at a flow rate of 3 ml/min.

Zinc-Based IMAC

Zinc based IMAC was generally done as a second strep purification to remove TEV protease and the initial purification tag after cleavage in the purification of isolated Taz1 or Taz2 domains. Solution containing the target protein was loaded onto the column with a flow rate of 3 ml/min. After loading of the sample the column was attached to the ÄKTA system without further washing. 2 CV of buffer Zn-NTA A were washed over the column to further remove unwanted proteins. This was followed by elution with 100% buffer Zn NTA B. The elution was monitored via UV absorption at 280 nm and 220 nm and performed at a flow rate of 3 ml/min. Before further processing the eluate was supplemented with Zn^{2+} to a final concentration of 10 mM and TCEP to 1 mM to

ensure proper zinc-loading and reduction state of the zinc-fingers. Supplementing the protein eluate with 10 mM Zn2+ at this point is only feasible in presence of a high concentration of imidazole as a chelating agent due to the low solubility of zinc-ions at the pH of the buffers used.

3.4.4 TEV Cleavage

After affinity purification the tag used in the purification was removed by enzymatic cleavage with TEV protease. For His-tagged proteins a ratio of 1:50 (w/w) TEV to target protein was used. The enzyme features an uncleavable His-tag and can therefore be removed alongside the cleaved tag itself in a subsequent reverse-nickel IMAC purification. The reaction was carried out at 4°C overnight in a dialysis bag to adjust the concentration of imidazole to allow for rebinding of the His tag as well as the protease to a nickel IMAC column. For MBP-tagged proteins a ratio of 1:10 (w/w) was used. In this case a TEV variant with uncleavable MPB-tag was used, allowing for further purification via gel filtration or zinc-IMAC-The reaction was carried out at 16°C overnight.

3.4.5 Reverse Immobilized Metal Ion Chromatograpy (re-IMAC)

After overnight TEV digest and dialyzing the buffer of the protein samples was adjusted to 30 mM imidazole by addition of the right fraction of buffer IMAC-B. Subsequently the protein was loaded onto a nickel column which had previously equilibrated to 30 mM imidazole with a mixture of IMAC-A and IMAC-B. After loading, the column was washed with another 2 CV of buffer containing the same amount of imidazole. The flow through of loading and the subsequent washing step were collected, as it contains the tag-free protein while uncleaved protein, TEV protease and the His tag remained on the column. Finally the column was regenerated as described in section 3.4.3.

3.4.6 Ion Exchange Chromatography (IEX)

Depending on the predicted pI of the protein either anion- or cation-exchange of protein samples was performed. Generally if not stated otherwise the purification was performed at a pH of 7.0. Therefore if the pI of the protein was predicted to be larger than 7 cation-exchange (CEX) was performed (GE Healthcare HiTrap SP HP column) and anion exchange (AEX) was performed for proteins with a pI lower than 7. (GE Healthcare HiTrap Q HP column). Protein samples diluted with IEX dilution buffer to a point where the salt concentration did not exceed 50 mM. The pH of the sample was checked and adjusted to 7.0 if necessary. Then the sample was loaded onto a pre-equilibrated IEX column (IEX-A buffer) by means of an external pump. Alter loading the column was attached to the ÄKTA system. After further washing with buffer IEX-A for 2 CV the protein was eluted with a linear gradient of IEX-B to 40% over 10 CV, leading to an effective concentration of NaCl of 400 mM at the endpoint of the gradient. A steeper gradient to 100% IEX-B over 3 CV was used to remove remaining protein. Protein elution was monitored by UV

absorption at 280 nm. Columns were regenerated with a solution of 6 M guanidine-HCl followed by extensive washing of the column with water.

3.4.7 Size Exclusion Chromatography (SEC)

Size exclusion chromatography was performed at 4°C on ÄKTA purifier or ÄKTA pure systems. All buffers were filtered and degassed, prior to use. Columns were pre-equilibrated with the appropriate buffer before use and cleaned after use according to manufacturer's instructions. Depending on the scale of protein purification either a semi-preparative column (24 ml CV) or a preparative SEC column (120 ml CV) was used. Proteins up to a total amount of 10 mg were applied to a semi-preparative column, while larger quantities were subject to preparative scale SEC.

Semi-Preparative Scale SEC

Proteins for semi-preparative scale SEC were concentrated to a total volume of 500 μl and applied to either to a Superdex 75 HR 10/300 GL or a Superdex 200 10/300 GL (both GE Healthcare) depending on the size of the protein. Flow rates for aqueous buffers were generally 0.5 ml/min thus leading to a run time of approximately 50 min per run. Protein elution was monitored by UV absorption at 280 nm and 220 nm and the eluate was fractionated in 0.5 ml steps.

Preparative Scale SEC

Proteins for preparative scale SEC were concentrated to a total volume of 4 ml or less and applied to either to a Superdex 75 16/600 or a Superdex 200 16/600 (both GE Healthcare) depending on the size of the protein. Flow rates for aqueous buffers were generally 1.0-1.5 ml/min thus leading to a run time of approximately 90-120 min per run. Protein elution was monitored by UV absorption at 280 nm and 220 nm and the eluate was fractionated in 1 ml steps.

3.5 Concentrating of Protein Samples

Protein samples were concentrated either with Amicon Ultra or Centriprep centrifugal filter units (both Merck Millipore). Depending on the molecular weight of the sample 3 kDa or 10 kDa filter cutoff sizes were selected. For less stable samples Centriprep filters were selected, as the concentration is increased homogeneously over the area of the membrane while the V-shaped Amicon Ultra membrane leads to a strong concentration gradient within the sample.

3.6 Peptide Labeling

Peptides designated for fluorescence polarization measurements were labeled in house with fluorescein as a fluorophore. Peptides were designed to feature a single cysteine residue outside of the region important for binding the interaction partner. Prior to labeling the powdered peptide was resuspended in 50 mM Tris pH 8.0. The concentration of the peptide was measured and the pH was checked and adjusted if needed. To ensure a high labeling efficiency TCEP was added in a 2 fold molar excess to reduce all potentially oxidized cysteines. After an incubation period of 1 h freshly dissolved iodamidofluoresceine was added at a molar excess of 10:1. The resulting mixture was incubated at 4°C overnight in the dark. In the next morning the sample was subject to gel filtration to remove unlabeled peptide as well as the dye. Labeling efficiency was checked by MALDI-MS (in house service facility).

3.7 Peptide Spot Membrane

Peptide spot membranes were synthesized Joachim Koch by Fmoc chemistry at activated PEG spacers on cellulose membranes by automated parallel peptide synthesis on a MultiPep RS instrument (Intavis) according to the manufacturer's instructions. The dried membrane was wetted with 100% ethanol in a tray on a shaking platform. In five minutes intervals the liquid was exchanged with mixtures of ethanol/water reducing the ethanol content by 10% in each step. After the last step with pure water, the membrane was incubated in TBS-T for 10 minutes and subsequently blocked with TBS-T containing 5% (w/v) skim milk powder for 1 h at room temperature. Following this, MBP-Taz2 fusion protein was added to a final concentration of 100 nM and the incubation was continued for 2 h at room temperature. Subsequently, the membrane was washed 3x for 10 min with TBS-T, incubated with anti MBP HRP conjugate (1:10000; NEB) in TBS-T containing 5% (w/v) skim milk powder for 1 h and washed again 3x for 10 min. Luminescence was detected via LumiImager F1 (GE Healthcare).

3.8 Peptide Expression and Purification

Isotopically labeled peptides were expressed in *e. coli* as fusion constructs with either GB1 or sfGFP as expression tag and initially purified by standard Ni-IMAC affinity chromatography. Selectively labeled proteins were exclusively produced via cell free protein synthesis. The protein was cleaved by 3C protease overnight at 4°C, while being subject to dialysis in a 1 kDa cutoff membrane to lower the imidazole concentration. On the next day the cleaved protein was subject to reverse-Ni purification to remove the expression tag and the protease. Subsequently the flow through containing the peptide was concentrated with the help of a 3 kDa Amicon Ultra Centrifugal Filter Units and subject to gel filtration over a Superdex 75 10/300 GL column.

3.9 MK2 peptide pre-phosphorylation

Initial phosphorylation with MK2 kinase was performed in standard NMR kinase buffer with 10 mM ATP at kinase peptide ratios of 1:100 at 15°C. After 1 h the reaction mixture was immediately concentrated to 300 μl and subject to gel filtration over a Superdex 75 10/300 GL column to remove the kinase.

3.10 TAp63α purification

The p63 construct used for full length protein kinetic measurement is described in section 2.1.1. Initially the protein was purified by standard Ni-IMAC as described in section 3.4.3. Nickel purification was followed by concentration and gel filtration over a HiLoad Superdex 200 16/600 column.

3.11 MK2 TAp63α pre-phosphorylation

Serine 582 was phosphorylated at 1:100 kinase:protein molar ratio for 30 min at 30°C. Kinase was removed from the protein by gel filtration over a HiLoad Superdex 200 16/600 column.

3.12 Sodium-dodecylsulfate Polyacrylamide-Gelelectrophoresis (SDS-PAGE)

Tris-Tricine SDS PAGE gels were cast and run in the Biorad Mini-Protean Tetra Cell system with a 4% acrylamide stacking and an 11% acrylamide running gel concentration. Gel composition is shown in table 3.12.1. If in-gel fluorescence analysis was desired 37.5 μl 2,2,2-Trichloroethanol was added to the separating gel prior to polymerization. 1x Cathode Buffer was placed between the gels, the remaining running chamber was filled with 1x Anode Buffer. Gels were run at 80 V for 20 min followed by 150 V for 45 min.

Table 3.12.1: Composition of 4%/11% Tris-Tricine SDS-PAGE gels

component	11% separating gel [ml]	4% stacking gel [ml]
water	1.78	1.95
3 M Tris/SDS pH 8.45	2.5	0.775
30% acrylamide	2.5	0.4
glycerol	0.75	
2,2,2-Trichloroethanol (if wanted)	0.0375	
APS 10% (w/v)	0.1	0.05
TEMED	0.01	0.01

3.12.1 In-gel Fluorescence Staining

Protein bands were visualized without prior Coomassie staining by incubating the gel without glass covers on an UV table for 3-4 min. Only proteins having at least one tryptophan can be visualized as the tryptophan chemically reacts with the embedded 2,2,2-trichloroethanol to form a fluorescent dye upon radiation with UV light. Gel fluorescence was documented by photography after completion of the chemical reaction.

3.12.2 Coomassie Blue Gel Staining

After running the gels were removed from the glass slides and submersed in SDS-PAGE fixation buffer shaking for 30 min or until the gel significantly shrank in size. Then the fixation buffer was replaced by staining buffer and continued shaking until the desired staining was achieved. Finally the staining buffer was discarded, the gel was washed twice with H_2O and documented via scanning.

3.13 Western Blot

For western blots pre-casted gradient gels (4-15% Mini-PROTEAN TGX Precast Protein Gels, Biorad) were used. Gels were generally run at 200 V for 20-30 min. Afterwards the gels were subject to semi-dry blotting onto precut PVDF membranes (Biorad) according to the manufacturer's instructions with the preset "Mixed-Molecular-Weight" in the blotting machine (Trans-Blot Turbo Transfer System, Biorad). Subsequently blots were blocked with 5% milk-powder (w/v, Sigma Aldrich) in TBS-T for 1 h at room temperature. Afterwards the blocking buffer was discarded and 10 ml of primary antibody in 5% milk (as above) was added. In most cases primary

antibodies were used in a dilution of 1:1000. The blots were incubated with primary antibody shaking overnight at 4°C. On the next morning the primary antibody was removed, blots were washed 3 times 10 min with TBS-T and the secondary antibody was added. Incubation was continued shaking at room temperature shaking for at least 1 h. Finally the secondary antibody was discarded, the blots were washed for 3 times 10 min with TBS-T and the blots were developed with 10 ml of each ECL-1 and ECL-2 solution. Luminescence was detected with a LumiImager F1 (GE Healthcare). Results were analyzed with ImageJ (NIH).

3.14 Pull-Down Assay

Bait proteins for pull-down experiments were expressed as GST-fusions as described in section 3.4.2. Prey proteins were expressed in rabbit reticulocyte lysate as described in section 3.2.1. Slurry containing 50 μl of GSH-sepharose (GE Healthcare) beads per reaction was washed via centrifugation (500 g for 2 min) and resuspension in 1 ml water per reaction. This process was repeated twice with water and another two times with pull-down buffer. Subsequently 125 μg of bait protein was added per reaction. The protein was allowed to bind to the resin for 2 h on an overhead shaker at 4°C. After the incubation the beads were washed 3 times with pull-down buffer as above. Then the bait protein beads were distributed onto Ultrafree-MC 0.65 μm filter spin columns (Merck Millipore) and spun down (1000 g, 1 min in a table top centrifuge). Washing was repeated once with 400 μl pull-down buffer per spin column. 5 μl of the prey protein expression was mixed with 45 μl SDS loading buffer and kept as input. The remaining 45 μl of the expression was added to the bait protein columns and incubated shaking for 1 h at room temperature. Then the columns were spun down and quickly washed 4 times with 400 μl pull-down buffer. After the final washing step the columns were spun down once more to remove additional fluid. Subsequently the columns were transferred to a new Eppendorf-tube and the pull-down was eluted twice with boiling SDS loading buffer (20 μl per elution). Finally the samples were subject to SDS page and western blot, where 5 μl of input and 10 μl of pull-down were used per lane. Western blot signals were quantified with ImageJ and relative pull-down efficiencies were calculated by compensating the fraction of input against the fraction of pull-down:

$$relative PD = \frac{PD * 4.44}{IP * 100} \tag{3.1}$$

3.15 Fluorescence Polarization (FP)

Fluorescence Polarization (FP)/Anisotropy Fluorescence polarization experiments were either run on a Infinite 200 PRO plate reader (Tecan, Männedorf, Swiss) in black non-binding 96 well plates (Corning) or in cuvettes (Hellma, Müllheim, Germany) on a FP-6500 spectrometer (Jasco, Gross-Umstadt, Germany). In case of 96 well plates a total volume of 50 μl per well was used

and in case of the cuvette 400 μl were used. In both cases the fluorophore-labeled peptide was used in a total concentration of 100 nM for sub-micromolar binders and 500 nM for weaker binders. Dilution series were pipetted such that the concentration of labeled peptide remained constant and the interacting protein was increased from 0 to at least a 3 fold excess over the expected K_D. For manual measurement 11 data points were measured, in case of the 96 well plates at least 24. Measurements were done at room temperature (21°C). For manual cuvette measurement each filter position was independently measured three times. The anisotropy was calculated from the fluorescence read outs in different filter positions as follows:

$$A = \frac{I_{par} - G * I_{ort}}{I_{par} + 2 * G * I_{ort}}$$
(3.2)

Where I_{par} is the fluorescence intensity in parallel filter arrangement, I_{ort} is the fluorescence in orthogonal filter arrangement and G is the correction factor which needs to be introduced due to imperfections of the experimental setup:

$$G = \frac{I_{ort}}{I_{par}}$$
(3.3)

Furthermore a potential decrease in total fluorescence intensity over the titration series due to a change in quantum yield needs to be compensated:

$$Q = \frac{I_{tot}}{I_{freetot}}$$
(3.4)

Where I_{tot} is the sum of parallel and orthogonal filter setting fluorescence intensity of the given sample and $I_{freetot}$ is the sum of both fluorescence intensities (I_{par} and I_{ort}) for free peptide. In case of the 96 well plate a value for the anisotropy was given as readout from the plate reader. The fraction of bound peptide was calculated as follows:

$$fB = \frac{A - A_{free}}{(A - A_{free}) + Q * (A_{bound} - A)}$$
(3.5)

Where fB is the fraction of bound peptide, A is the anisotropy of the given sample, A_{free} is the anisotropy of the free peptide, A_{bound} is the anisotropy of the saturated peptide and Q is the correction factor described above. From the fraction of bound peptide (fB) the K_D was fit in Prism (Graphpad) according to the following formula:

$$fB = \frac{([l]_{tot} + [P]_{tot} + K_D) - \sqrt{([l]_{tot} + [P]_{tot} + K_D)^2 - 4 * [P]_{tot} * [l]_{tot}}}{2 * [l]_{tot}}$$
(3.6)

Where $[l]_{tot}$ is the total concentration of labeled peptide, $[P]_{tot}$ is the total concentration of protein in a given sample and K_D is the dissociation constant.

3.16 Thermal Shift Assay

The thermal shift assay was performed using a iCycler IQ Real Time PCR Detection System (Bio-Rad, Hercules, California, USA). Highly concentrated protein samples were diluted at least 100 fold into the measurement buffer to a final concentration of 20 μM. 36 μl of protein solution was combined with 4 μl of a 1:200 dilution of SYPRO Orange (ThermoFisher). Samples were measured in MicroAmp Optical 96-well plates (ThermoFisher). Temperature was increased a rate of 1°C/min while fluorescence measurements were taken at 0.2°C increments. The resulting data was smoothed by a rolling average over 5 data-points. The first derivative of the result was plotted to obtain the melting point. The experiment was performed in duplicates.

3.17 Kinase kinetics in full length protein

3.17.1 Kinetic reaction

The kinetic reaction was carried out in batch at 303K in a water bath at 1:1000 molar kinase:protein ratio. At each intended time-point, 2.5 mg protein was removed from the mixture and the reaction was quenched by addition of EDTA to a final concentration of 50 mM.

3.17.2 Purification of the peptide/CNBr digest

After inhibition of CK1$\delta$the protein was digested with MBP-TEV protease at 1:10 TEV:protein (w:w) at 4°C for 16 h. Subsequently the protein mixture was denatured with solid urea to a final concentration of 6 M. Next the peptide was purified from the remaining protein and TEV protease by gel filtration over a Superdex 75 10/300 GL column with a running buffer containing 6 M urea (PAD SEC urea buffer). The eluted peptide was concentrated to $\approx$150 μl and acidified with hydrochloric acid to 0.1 M. 10 μl of 5 M CNBr in acetonitrile solution was added. The mixture was then incubated for 36-48 h at room temperature in the dark. Subsequently remaining CNBr was evaporated from the samples by applying a vacuum. The sample was further reduced until urea crystals formed and no obvious residual water was visible. The solidified cleaved peptide/urea mixture was neutralized by the addition of 200 μl 1 M Bis-Tris buffer stock (pH 6.5). Finally the uncleaved fraction of the peptide as well as the C-terminal part of the peptide were removed by Ni-IMAC. The flow-through was concentrated and buffer exchanged to kinase NMR buffer prior to measurement.

3.18 Nuclear Magnetic Resonance (NMR)

All NMR experiments were performed at 303K (30°C) if not otherwise stated. All spectra were recorded at Lamor-frequencies of 500, 600, 700, 800, 900 or 950 Mhz. All spectrometers,

with exception of those with a Lamor-frequency of 500 Mhz, were equipped with cryo-cooled probes. Spectra were acquired and processed with Topspin (Bruker) and analyzed in NMRFAM-Sparky[235]. NMR spectrometers used in this study are listed in section 2.3.1.

3.18.1 Sample Preparation

Generally samples were measured either in 5 mm Shigemi-tubes or Shape-tubes therefore requiring a volume of 350-360 μl. Protein was mixed with 5% of a D_2O/DSS mixture functioning as combined field frequency lock and chemical shift reference. Additionally protease inhibitor as well as antibiotics (Kanamycin and Spectinomycin) were added to avoid proteolysis of the protein as well as bacterial growth within the sample. A typical sample composition is described in table 3.18.1.

Table 3.18.1: General composition of all used NMR samples.

component	volume $[\mu l]$
Protein	max 324.5
D_2O/DSS mix	17.5
Complete Protease Inhibitor mix (50x)	7
Antibiotic mix	1
Buffer	to 350

3.18.2 Pulse calibration

$90°$ ^{1}H hard pulses were calibrated for each sample condition by determining the $360°$ pulse and dividing the pulse length by a factor of 4. ^{1}H pulse length calibration for shaped pulses was done with the help of the "popt" command with a 1D variant of the BEST-TROSY pulse program. ^{15}N and ^{13}C pulse duration calibration was done by 1D variants of SOFAST-HMQC pulse sequences.

3.18.3 ^{15}N BEST-TROSY

2D ^{15}N-BEST-TROSY spectra for sample quality assessment, NMR titrations or assignment were recorded with 256-1024 F1 increments, an inter scan delay D1 of 300 ms and 2-16 scans per increment depending on the concentration of the sample. In most cases spectral width was set to 30-50 ppm depending on the sample. The ^{15}N transmitter frequency offset was set to 121 ppm and adjusted if necessary.

3.18.4 Sequential Backbone Assignment

All assignments were done with a set of standard 3D spectra used for protein backbone and side chain assignment. The initial sequential backbone assignments were done with BEST-TROSY based 3D HNCACB and 3D HN(CO)CACB spectra. A complementary set of 3D HNCO and HN(CA)CO spectra were used to verify the correctness of the assignment, as well as to determine the carbonyl-chemical shifts. Additionally HA chemical shifts were assigned by 3D HNHA spectra.

3.18.5 Aliphatic Side-chain Assignment

Generally aliphatic side chains were assigned with BEST-TROSY based Total Correlation Spectroscopy (TOCSY) spectra. For aliphatic ^{1}H atoms H(CCO)NH spectra were used, ^{13}C side chain atoms were assigned with (H)C(CO)NH spectra. In both cases a given NH chemical shift pair carries the information of the preceding amino acid side chain atoms in the F1 dimension. Sidechains for the Taz2-p73TAD fusion constructs were assigned with the help of a high resolution HCCH-TOCSY recorded at a proton frequency of 950 Mhz to reduce signal overlap. NH based TOCSY spectra were found to be not feasible due to a lack of signal intensity of the sample. Side-chain assignments were validated with the help of aliphatic ^{13}C-HSQCs.

3.18.6 Aromatic Side-chain Assignment

For the assignment of ^{13}C and ^{1}H aromatic ring chemical shifts initially the CB chemical shift was correlated with the HD proton shift of the corresponding amino acid (2D-(HB)CB(CGCD)HD [236]). With the help of CB and HD chemical shifts an aromatic-type TOCSY was used to determine the remaining proton shifts of the aromatic ring. TOCSY spectra were optimized for each type of aromatic side chain. Assignments were verified with aromatic ^{13}C-HSQCs.

3.18.7 Histidine Ring Nitrogen Protonation

Nitrogen protonation within histidine side chains was determined by recording ^{15}N-^{1}H Heteronuclear Multi-Bond Correlation (HMBC) spectra correlating ring nitrogen shifts with carbon bound ring proton shifts. Due to differences is J-coupling between HD2-NE2 (2J coupling) and HD2-ND1 (3J coupling) the nitrogen atoms can be differentiated by their signal intensity. In a second step the chemical shift indicates the protonation state of the nitrogen in question (protonated: ~170 ppm, partially protonated: ~180-200 ppm, deprotonated: ~220 ppm). Determination of nitrogen protonation offers additional restraints for the zinc-finger geometry, as it limits the conformational freedom of the histidine side-chain.

3.18.8 Nuclear Overhauser Effect Distance Restraints (NOESY)

For all structures a minimal set of 3 different 3D NOESY spectra were recorded. In case of the Taz2 p73TAD1 a 4D NOESY spectrum was recorded to validate the structure (see below). In all cases the mixing time for the NOE transfer was set to 70 ms. ^{13}C bound protons were separated into aliphatic and aromatic regions. ^{13}C aromatic chemical shift evolution after NOE transfer was done with the SOFAST-HMQC pulse sequence. In case of ^{13}C-aliphatic protons chemical shift evolution was performed as ^{13}C-HSQC. NOE signals transferred to ^{15}N bound backbone protons were detected with a BEST-TROSY based pulse sequence.

4D ^{13}C SOFAST HMQC-NOESY-^{13}C SOFAST HMQC To validate the peptide structure of the p73TAD1 peptide bound to Taz2 a 4D-NOE experiment was created, probing the distance of aromatic ring protons with those of methyl protons of aliphatic side chains. The mixing time for NOE transfer was set to 70 ms and both chemical shift evolution sequences, prior to NOE transfer and after were done as SOFAST-HMQC. To limit the measurement time the experiment was done with 22% non-uniform sampling (NUS) thus reducing the amount of measurement time needed by a factor of 5 at the expense of signal intensity.

3.18.9 Heteronuclear NOE

To assess the mobility of each residue within the protein sequence, Hetero nuclear NOE (Het-NOE) spectra were recorded. The spectra were recorded in an interleaved manner with and without NOE transfer. Signal intensities of both spectra were analyzed on a residue-by-residue basis and the ratio between both intensities was plotted over the sequence.

3.18.10 D$_2$O Exchange

The buffer of NMR samples was exchanged to buffer containing D$_2$O instead of H$_2$O to assess the long term stability of hydrogen bonds within the protein. Buffer was exchanged by concentrating and dilution until at least 99% of the buffer was exchanged. Then the sample was incubated for 72 h at 303K and subsequently a TROSY spectrum was recorded. All amide signals still present were assumed to participate in hydrogen bonds.

3.18.11 NMR Titration

For NMR titrations two different methods were used: 1) Two NMR samples were generated. Both samples contained exactly the same amount of protein, one did not contain any titrant and one contained an amount of titrant which was thought to saturate the binding to the protein. For both samples spectra were recorded. Subsequently small fractions of both samples were exchanged with one another, thus generating two new concentration of titrant within both samples. These new samples were measured again. This process was repeated 5-10 times until the concentra-

tion of titrant in both samples converged. 2) A single NMR sample without peptide was generated and measurement. Subsequently titrant was added to the sample and it was measured again. This process was repeated until enough data points were available. This method is only possible if the titrant was available in a very high concentration, as otherwise the addition of titrant decreases the concentration too much to allow for K_D approximation.

3.18.12 NMR kinase kinetics at 298K

NMR kinetics at 298K were performed in a total volume of 180 μl in a 3 mm capillary NMR tube. The general composition of all samples is given in table 3.18.2. Kinase was only added after setup of the experiment and the recoding of a reference BEST-TROSY spectrum. This resulted in a general dead time of 60-90 s, prior to acquisition of the first spectrum with kinase. SOFAST-HMQC spectra were recorded with 256 increments in the indirect dimension, a D1 of 300 ms and 2 scans per increment, resulting in a total acquisition time of $\approx$100 s/spectrum. Peak intensities were quantified with a self-written Visual Basic tool, normalized and summed with Microsoft Excel and fitted in Graphpad Prism.

Table 3.18.2: Composition of samples used for acquisition of kinetics at 298K.

component	amount
peptide	250 μM
CK1δ kinase	250 nM
ATP	10 mM
D$_2$O	5%
phosphatase inhibitor mix	1x
protease inhibitor mix	1x
buffer	to 180 μl

3.18.13 NMR kinase kinetics at 303K

NMR kinetics at 303K were performed under similar sample and buffer conditions as compared to the 298K measurements. However to reduce the dead-time after injection a direct injection apparatus as described by Mok *et al.*[237] was employed. In this experiment a 320 μl sample was prepared, including all components of the reaction except for the ATP solution. The ATP solution was loaded into the syringe for direct injection. Next the apparatus was assembled and reference spectra were recorded. Instead of a normal presat-1D experiment 11echo pulse sequences were employed as the apparatus lead to small amounts of air on the height of the

NMR coil and thereby leading to a massive water peak. For the kinetic experiment a 1D variant of the BEST-TROSY pulse sequence was run as a pseudo 2D variant. Spectra were recorded at a proton frequency of 950 Mhz with 16 scans per spectrum and a D1 of 200 ms, leading to 5.2 s/spectrum. The sequence was modified to allow for direct TopSpin controlled injection of the ATP within the experiment itself. Prior to injection 10 reference spectra were recorded, followed by the injection command and immediately followed by 1024 additional spectra. Direct injection of the kinase was not feasible, as the millisecond injection time lead to the destruction of the kinase due to shear forces at the nozzle of the injector.
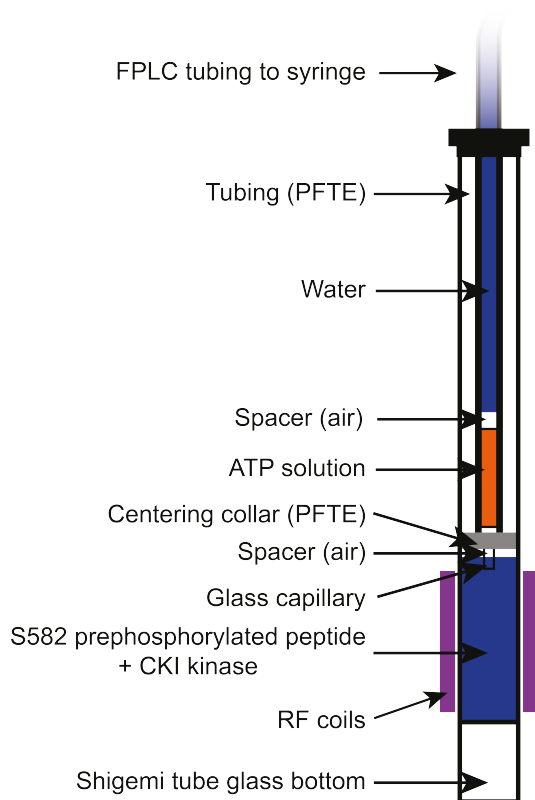
Figure 3.18.1: Injection devices as described by Mok *et al*[237]. The device allows for direct injection of ≈40 μl liquid (orange) directly into the sample (blue) within ≈50 ms. A 5 mm Shigemi tube is shortened and the regular glass insert is replaced by an injector made from a glass capillary at the bottom and PFTE tubing at the top. Additionally PFTE spacers are used to center the injector within the tube. To prevent mixing of either the water/buffer within the tubing with the solution to be injected or the sample and the solution to be injected, two small pockets of air are used as spacer on both sides of the solution to be injected.

The injector is connected to a Hamilton pipette outside of the spectrometer via FPLC tubing filled with H_2O or buffer to circumvent the large compressibility of air which would massively increase the total injection time. The Hamilton pipette is actuated by a piston operated with compressed air in turn controlled by a magnetic valve under control of the NMR console.

3.18.14 Direct determination of phosphorylated residues by 2D/3D ^{31}P NMR

To determine the phosphorylation state of each serine/threonine within the sample a intraHN(CA)P experiment was constructed. This allows for directly overlaying the corresponding HSQC spectrum with a 2D variant (2D HN(CAP)), giving an easy way of directly determining with residue is phosphorylated and which is not, thereby lowering the complexity of spectra evaluation. This pulse sequence (shown below) has been developed by Frank Löhr.

3D [^{15}N,^{1}H]-BEST-TROSY-intraHN(CA)P
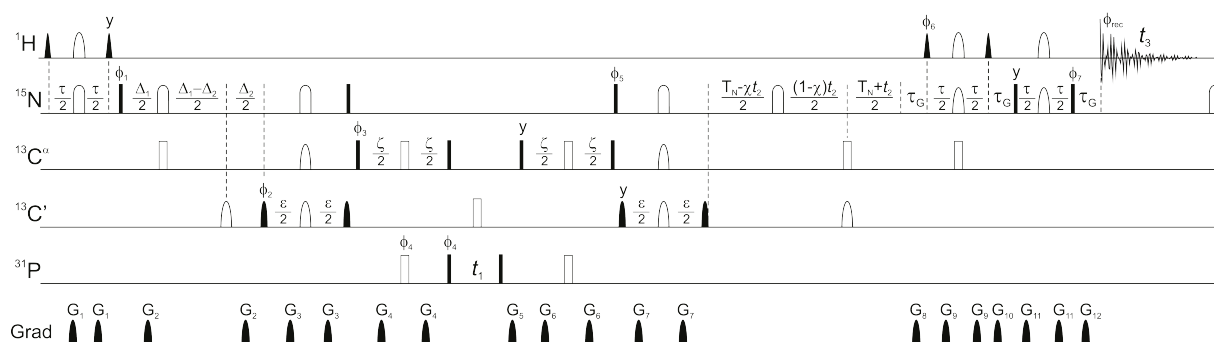
Figure 3.18.2: Pulse sequence of the 3D variant of the intraHN(CA)P. The puslse sequence was developed by Frank Löhr.

3.18.15 Secondary structure prediction with TALOS

Secondary structure of the proteins were predicted after backbone assignment by the chemical shift difference between CA and CB with the help of the TALOS+ algorithm[238]. Chemical shift data was exported from Sparky and reformatted to fit the required input format of TALOS+. The prediction itself was run on a web server (https://spin.niddk.nih.gov/bax/nmrserver/talos/) and the results were analyzed and visualized in Microsoft Excel.

3.18.16 Structure Calculation

Structures were calculated by Sina Kazemi with the automated NOE-peak assignment strategy within CYANA[239]. In addition to these NOE restraints generated from the algorithm, the first helix of Taz2 was defined based on TALOS+ secondary structure prediction, as only a very low number of long range NOEs would be available otherwise. Additionally dihedral angles of glycine residues were restricted to the most favored regions in the Ramachandran plot. Zinc tetrahedral coordination was enforced by construction of a custom CYANA library residue entry. Histidine protonation was taken into account so that the correct ring nitrogen atom points towards the zinc ion. Van der Waals radii for zinc coordination were taken from the Zinc AMBER force field (ZAFF)[240]. The resulting structures were minimized using OPALp[241] employing an AMBER94 force field.

3.19 Mammalian Cell Culture

All experiments were performed with H1299 or Saos2 type cells. Cultivation was done at 37$°$C in a humidified atmosphere containing 5% CO_2. Cells were cultivated in DMEM (with glutamine) containing 10% Fetal Bovine Serum (FBS, Capricorn Scientific) and 100 mg/ml Penicillin/Streptomycin. Depending on the cell type and division rate, cells were sub-cultivated every

2-4 days. Sub-cultivation was done by initially washing the cells with sterile Phosphate Buffered Saline (PBS, Gibco) and subsequent detaching by incubation with Accutase (Sigma-Aldrich) at 37°C for 5 min. After the cells were detached they were counted either with an improved Neubauer counting chamber or with a Cell Scepter (Millipore). Seeding density into new flasks/dishes was dependent on the experiment to be performed.

3.19.1 DNA Transfection

Transient over-expression of proteins in mammalian cells was done by transfection of vector DNA using the lipid-based transfection reagent Effectene (Quiagen) according to the manufacturer's instructions. Generally cells were seeded one day prior to transfection with a titer leading up to a confluence of around 60% on the day of transfection.

3.19.2 Transactivation Assay

Transactivation assays were done with the Dual-Glo Luciferase Reporter Assay Kit (Promega). Cells used for transactivation assays were seeded and transfected as described in section 3.19.1. Cells were transfected with a pcDNA3 derivate containing the transcription factor. Additionally a pGL3 vector containing a firefly luciferase gene under the control of the promoter region of interest and a pRLCMV vector containing firefly luciferase were co-transfected. In total 100 ng of each plasmid were co-transfected in a 12 well dish. The day after transfection cells were harvested with Accutase, pelleted and resuspended in 450 μl cell culture medium. Cells were split into 4x 45 μl in a flat bottom white 96 well plate for assaying. The remaining cells were centrifuged again and the pellet was resuspended into 20 μl SDS loading dye for protein expression quantification by western blot. The assay itself was performed according to the manufacturer's instructions. The detected luminescence of firefly luciferase was normalized by the fluorescence of renilla luciferase. Outliers were detected with Grubb's test and fold induction was quantified by comparison with an empty vector control. If deemed necessary fold induction was further normalized by transcription factor and GAPDH expression level, which were detected via western blot.

3.19.3 Cycloheximide Chase

Cells were seeded in 12 well plates and transfected as described in 3.19.1. Per chase experiment 6 wells were transfected with identical constructs. On the following day the medium was exchanged for medium containing 50 μg/ml cycloheximide. Time points were taken by harvesting single wells at the corresponding time after addition of cycloheximide (generally 0, 1, 2, 4, 8 and 24 h). Protein level was analyzed via western blot and correlated to GAPDH levels to account for cell death due to the toxicity of the cycloheximide.

3.19.4 Blue Native (BN) PAGE

Cells were seeded in 12 well plates and transfected as described previously. After harvesting the cells they were resuspended in 50 μl cold cell lysis buffer with the addition of 1 μl Benzonase and 1x protease inhibitor cocktail. Cells were incubated for 60 min on ice and subsequently cell debris was removed by centrifugation at 13000 rpm for 10 min in a table top centrifuge. 5 μl of supernatant was supplemented with 3x BN-PAGE loading buffer for each sample. Separation was performed with the Novex PN-PAGE system with 3-12% Bis-Tris gradient gels according to the manufacturer's instructions (Thermo Fisher). The cathode buffer was supplemented with 0.002% Coomassie G250. Gels were run at 4°C for 60 min at 150 V and subsequently at 250 V for another 60 min.

3.20 Mouse ovary culture

Ovaries of P8 mice were dissected and cultured in 50 μl of ovary culture medium in a 96 well plate at 37°C in a humidified incubator with a 5% CO2 atmosphere. After overnight incubation ovaries were treated with the respective inhibitors/DNA damaging agents necessary for the experiment. Then incubation was continued for another 6 h. Generally 1 μM of either inhibitor A-485 or mock inhibitor A-486 was used with or without 10 μM DOX.

3.20.1 Ovary Staining

Culture medium was removed from the ovaries and they were washed with PBS twice, followed by fixation with 4% para-formaldehyde (PFA) in PBS (Gibco) overnight. On the following day ovaries were washed with PBS twice and permeabilized with 0.3% Triton X-100 for 30 min at room temperature. Then ovaries were blocked for 2 h at room temperature with blocking buffer (100 μl per ovary in a 96 well plate). Afterwards the ovaries were incubated overnight at 37°C with the primary antibodies as well as DAPI, diluted in blocking buffer (50 μl per ovary). On the next day ovaries were washed tree times with PBS, followed by incubation with the secondary antibodies for 3 h at 37°C in the dark. Antibodies were diluted in blocking buffer (50 μl per ovary). Afterwards the ovaries were washed 3 times and stored in the dark at 4°C until clearing. All steps involving antibody incubation were performed in the dark.

3.20.2 Clearing of Ovaries

Ovaries were cleared with CUBIC-2 solution. 5 droplets of CUBIC-2 were positioned next to one another on a sheet of parafilm per ovary. Initially ovaries were transferred from the 96 well plate into the first droplet and incubated for 5 min. After that the ovaries were transferred to the second droplet and incubated again. This process was repeated until the last droplet was reached. Subsequently the ovaries were extracted from the droplets and mounted into prefabricated capillaries

and submerged in CUBIC-2. The ovaries were left in the dark at room temperature overnight for further clearing prior to imaging.

3.20.3 Imaging of Cleared Ovaries

Imaging was performed by Katharina Hötte (Stelzer group) with a self-constructed light-sheet microscope[242;243]. Picture stacks of oocytes were analyzed with Fiji[244].

4 Results

4.1 Identification of Potential Interaction Partners for TAp63 Isoforms

In contrast to p53 the interaction partners of transactivation domain (TA) containing isoforms of the other two members of the p53 family (p63, p73) are largely undescribed. Most research focuses on the interaction of these proteins with the Mouse Double Minute (MDM) family (MDM2, MDM4). In case of p73 an interaction of the TA domain with the p300/CBP family has also been described. In case of p63 most likely the research has been hampered by the, until recently, poor understanding of the inhibited dimeric state of p63 which seemingly abrogates all interactions of the TA domain with other proteins. Other known interaction partners of p53 were tested in GST-based pull-down assays to get an understanding if interaction with these proteins is possible or not. By researching the Protein Data Bank (PDB) for structures containing parts of the TA domain of p53 four proteins were selected: high-mobility group protein 1 (HMGB1), Structure specific recognition protein 1 (SSRP1), Mediator of RNA polymerase II transcription subunit 15 (MED15) and p300/CBP. The MDM family was excluded as interaction has been reported for all p53 family members. SSRP1 has previously been reported to be a co-activator of p63. In all cases GST-fusion constructs of the potential interacting domain were bacterially expressed and immobilized onto spin columns. Bait protein was expressed in Rabbit Reticulocyte Lysate (RRL). Interaction was then analyzed via western blot. In case of HMGB1 the BoxA domain was selected as it is reported to directly interact with the TA domain of p53[36]. However only very weak interactions with the other family members p63 and p73 were visible (Figure 4.1.1A). The interaction also seemed to be independent of the N-terminal splicing variant (TA or ΔN). In case of p53 the interaction seems to be present in both deletion mutants of parts of the TA domain (ΔTAD1 or ΔTAD2). In case of MED15/ARC105 the Kix domain present in the protein was expressed and tested in a pull-down assay. Only p53 was found to considerably interact with the protein (Figure 4.1.1B). For SSRP1 the so-called "middle domain" was used. Just as in HMGB1's case only p53 and the ΔN isoforms of p63 and p73 were found to be interacting considerably (Figure 4.1.1C).
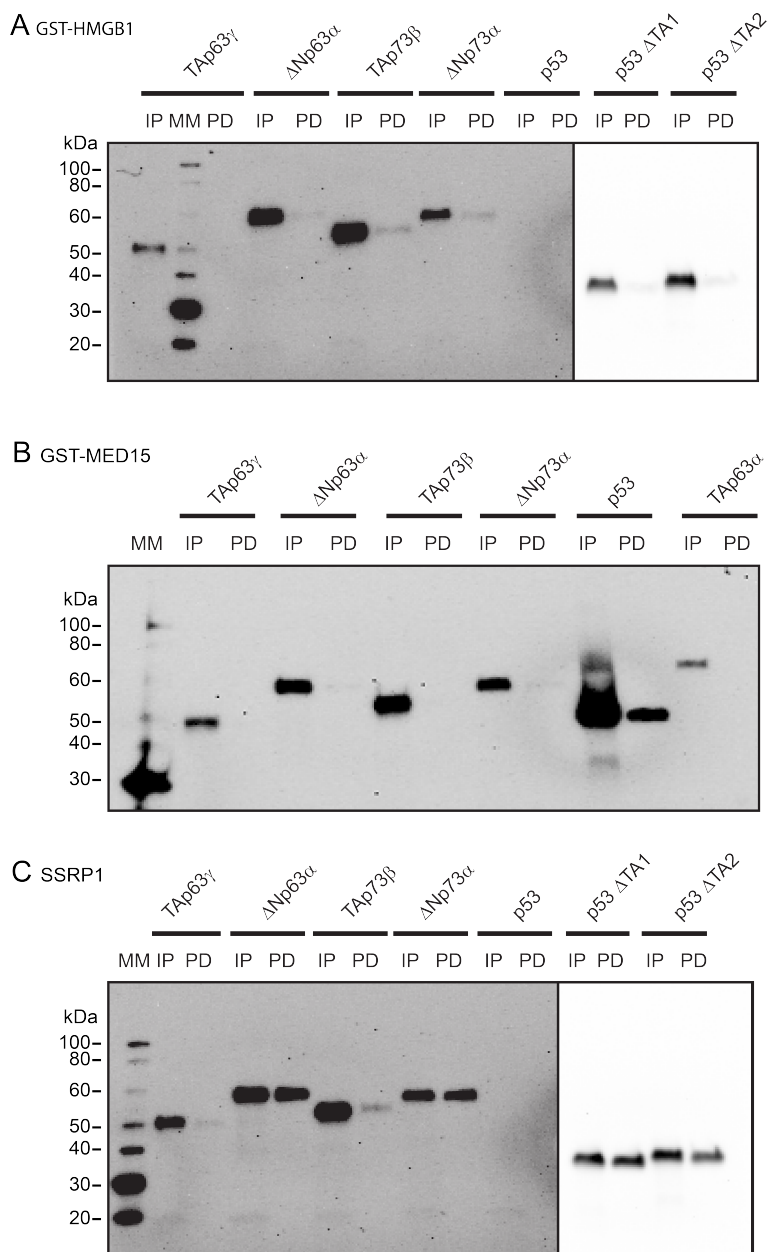
Figure 4.1.1: A pull-down with possible other different interaction partners does not show significant interaction with p63/p73 isoforms containing a transactivation domain. Pull-downs with different potential interaction partners, as described for p53 in the literature, were performed. (A) GST-HMGB1 BoxA does weakly interact with p73 isoforms, independent of whether a transactivation domain is present. (B) GST-MED15 Kix domain only interacts weakly with the positive control p53. (C) GST-SSRP1 middle domain interacts with all tested proteins, however binding to isoforms not containing a transactivation domains (ΔN isoforms) seems to be enhanced. p53 wild type expression was not detectable. Bait proteins were bacterially expressed; prey proteins expression was performed in RRL. The blot shown in (A) and (C) feature different exposure times for the p53 mutants and the rest of the blot, as the expression of those proteins were at least an order of magnitude above the rest. Western blot lane denomination: IN = input, PD = pull-down, MM = Magic Mark XP western blot marker.

Next p300/CBP domains Taz1 and Taz2 were tested concerning their interaction with p63 and p73 isoforms. Additionally to Taz1 and Taz2 the Kix and IBiD domains are contemplatable, however they do generally show much weaker interactions with 9 amino acid transactivation domains containing binding partners and therefore the interaction would most likely not be observable in the pull-down assay. Interaction is clearly visible for both GST-Taz1 and GST-Taz2 for all TA domain containing isoforms, with the exception of TAp63α (Figure 4.1.2). The experiment was repeated in triplicates and subject to quantification via signal intensity integration (Figure 4.1.2 lower panel). The strongest interaction can be observed GST-Taz2 with TAp63γ as a prey protein. In general the interaction with the tetrameric, TAD containing p63 isoform is much stronger

than any of the interactions with TAp73 isoforms. Dimeric TAp63α does not seem to interact with either Taz2 or Taz1 at all, indicating that the TA domain is not accessible in the dimeric state of the protein.
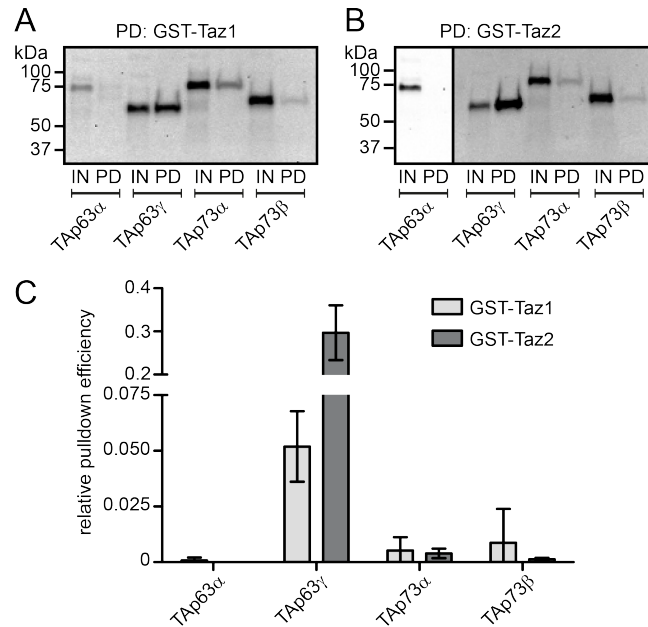
Figure 4.1.2: Tetrameric p53 family members interact with p300 domains whereas dimeric TAp63α does not. GST-pull-down assay with GST-Taz1(A) and GST-Taz2 (B) as bait proteins and TA domain containing isoforms of p63 (TAp63α and TAp63γ) or p73 (TAp73α and TAp73β). (C) Relative pull-down efficiency is normalized on fraction of protein loaded as input on the western blot (1%). Western blot lane denomination: IN = input, PD = pull-down. Bait proteins were bacterially expressed, prey proteins expression was performed in RRL. The figure is modified from Krauskopf, K *et al.* 2018[245].

Furthermore the interaction between tetrameric p63 variants as well as two novel N-terminal variants of p63 (TA* and GTA) with the Taz2 domain were characterized by pull-down. Mutation of the classical MDM2 binding motif (an amphipathic helix with the hydrophobic side composed of an F-W-L motif; F16, W20, L23 in p63) to alanines leads to a disruption of the closed dimeric state into a more open, still dimeric form. The opening of the protein could potentially be sufficient for interaction with Taz2. However almost no interaction is visible (Figure 4.1.3 1st sample) on the western blot for this mutation. This indicates that at least partly the "FWL"-motif is required for Taz2 binding. TAp63γ was used as a positive control as it showed the largest pull-down previously. Additionally a construct with a C-terminal truncation was used (ΔTI). This ensures full tetramerization and removes any potential inhibitory effects of the protein. Interestingly this protein seems to bind Taz2 with less affinity than TAp63γ. Furthermore several variants of the N-terminally elongated TAp63 isoforms (GTA, TA* and GTA* which describes the common sequence between both elongations) were tested. All were able to bind Taz2 to a similar extend in a similar background (ΔTI). However both, deletion of potential TA domain (ΔTAD1) or mutation of the MDM2 binding motif leads to a drastic decrease in binding. Some interaction is still visible on western blot, however this might be a cross linking artifact, as both GTA and TA* have two cysteine residues within the sequence.
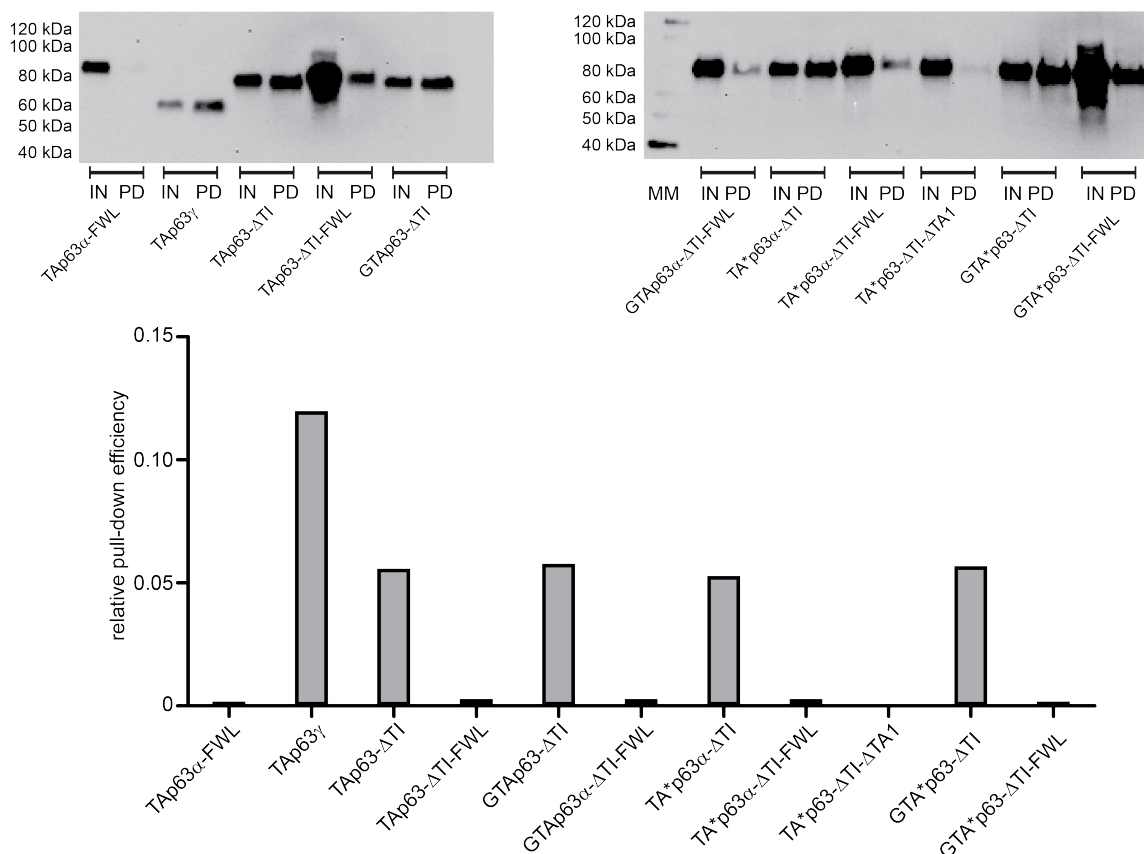
Figure 4.1.3: Tetrameric TAp63 requires a functional complete transactivation domain for p300 interaction. p300 binding capability was tested by GST-pull-down assay with GST-Taz2 as a bait protein and tetrameric mutants/wild type proteins of p63. Several deletion/mutation variants have been used in this experiment: FWL described a triple alanine mutation in the transactivation domain of p63 previously reported to be necessary for the dimeric state of TAp63α as well as required for MDM2 binding[172]. ΔTI indicates that the proteins TI domain has been truncated, ΔTAD1 that the proposed transactivation domain is missing. GTA, TA* and GTA* describe several potential N terminal elongated variants of the TA domain, which are present on mRNA level (TA*) or have been detected on protein level (GTA). GTA* describes a shortened variant of the N-terminal elongation which is common in sequence between the TA* and GTA. Relative pull-down efficiency is normalized on fraction of protein loaded as input on the western blot (1%). Western blot lane denomination: IN = input, PD = pull-down.

To narrow down the sequence of the p63 transactivation domain a peptide spot membrane with the N-termini of p63 as well as the other family members was synthesized. Each spot corresponds to a peptide with the length of 18 amino acids, incremented by one residue per spot. Sequences of interacting peptides are shown and peptide sequences which are present in multiple spots and needed for the interaction with Taz2 are marked in red (Figure 4.1.4). In case of p53 two independent peptides could be detected, as previously described and characterized[32;186]. For p73 (right panel) only one peptide stretch could be detected, although two potential interaction sites have been described[20]. For p63 (center panel) a very long stretch of peptides gave signals on the peptide spot membrane. The signals can be grouped in two different regions; however they share parts of their amino acids. Most spots in the secondary cluster of spots contain a cysteine residue (C28). This might be problematic, as the local concentration of pep-

tide within a spot is extremely high and the Taz2 domain might unspecifically cross-link to those spots.

p53

```
SQAMDDLMLSPDDIEQWF
QAMDDLMLSPDDIEQWFT
AMDDLMLSPDDIEQWFTE
MDDLMLSPDDIEQWFTED
DDLMLSPDDIEQWFTEDP
DLMLSPDDIEQWFTEDPG
LMLSPDDIEQWFTEDPGP
MLSPDDIEQWFTEDPGPD
LSPDDIEQWFTEDPGPDE
SPDDIEQWFTEDPGPDEA

EPPLSQETFSDLWKLLPE
PPLSQETFSDLWKLLPEN
PLSQETFSDLWKLLPENN
LSQETFSDLWKLLPENNV
SQETFSDLWKLLPENNVL
QETFSDLWKLLPENNVLS
ETFSDLWKLLPENNVLSP
```

p63

```
MSQSTQTNEFLSPEVFQH
SQSTQTNEFLSPEVFQHI
QSTQTNEFLSPEVFQHIW
STQTNEFLSPEVFQHIWD
TQTNEFLSPEVFQHIWDF
QTNEFLSPEVFQHIWDFL
TNEFLSPEVFQHIWDFLE
NEFLSPEVFQHIWDFLEQ
EFLSPEVFQHIWDFLEQP
FLSPEVFQHIWDFLEQPI
LSPEVFQHIWDFLEQPIC
SPEVFQHIWDFLEQPICS
PEVFQHIWDFLEQPICSV
EVFQHIWDFLEQPICSVQ
VFQHIWDFLEQPICSVQP

QHINDFLEQPICSVQPID
HIWDFLEQPICSVQPIDL
IWDFLEQPICSVQPIDLN

FLEQPICSVQPIDLNFVD
LEQPICSVQPIDLNFVDE
EQPICSVQPIDLNFVDEP
QPICSVQPIDLNFVDEPS
PICSVQPIDLNFVDEPSE
ICSVQPIDLNFVDEPSED
CSVQPIDLNFVDEPSEDG
SVQPIDLNFVDEPSEDGA
VQPIDLNFVDEPSEDGAT
QPIDLNFVDEPSEDGATH
PIDLNFVDEPSEDGATNK
IDLNFVDEPSEDGATNKI
```

p73

```
ATSPDGGTTFEHLWSSLE
TSPDGGTTFEHLWSSLEP
SPDGGTTFEHLWSSLEPD
PDGGTTFEHLWSSLEPDS
GGTTFEHLWSSLEPDSTY
GTTFEHLWSSLEPDSTYF
TTFEHLWSSLEPDSTYFD
TFEHLWSSLEPDSTYFDL
FEHLWSSLEPDSTYFDLP
EHLWSSLEPDSTYFDLPQ
HLWSSLEPDSTYFDLPQS
LWSSLEPDSTYFDLPQSS
```

Figure 4.1.4: p53 has two distinct p300 interaction peptides whereas p63 and p73 have only one. Peptide spot membrane with N-terminal peptides of all p53 family members were used to determine the peptides sequence responsible for Taz2 binding. Immobilized peptides were 18 amino acids long and shifted by an increment of 1 per spot. Interaction was detected by blocking the membrane with BSA and subsequent incubation with Taz2 fused to MBP. After that the membrane was washed and incubated with an MBP-HRP conjugate antibody and detected by luminescence. Peptides were substantial binding occurs are labeled with their respective sequence. In case binding could be observed in multiple sequential spots the most likely sequence which is responsible for binding is marked in red. The peptide spot membrane was synthesized by Joachim Koch.

4.2 Purification of p300 Taz2

In the next step purification of isolated p300 Taz2 was developed for further interaction studies and potential structure determination in complex with the TA domain of p63. The standard approach of using a simple His-tag purification was not feasible, as the Taz2 domain has three zinc-finger complexes. These complexes generally also have a very high affinity towards nickel

columns, displacing the zinc ions with nickel ions in the process. Elution of the complex is generally then only possible with the use of ethylenediaminetetraacetic acid (EDTA), destroying the protein structure in the process. Therefore a nickel-free process needed to be developed. The expression rate of the GST-constructs used for the pull-down assays was too low for structural studies. Therefore different fusion-proteins/peptides were tested for expression rate. A variant with a maltose binding protein (MBP) at the N-terminus showed a high expression rate, as well as a good solubility, and was therefore selected for all following experiments. Similar constructs have been made for the rest of the interaction domains of p300 (Taz1, Kix, IBiD). Additionally the Taz2 domain has four additional cysteine residues in its sequence (C1738, C1746, C1789, C1790) which do not seem to be structurally relevant or involved in peptide binding.[246] Therefore they were replaced by alanines, to increase the resistance of the protein to oxidation or cross-linking. In general the protein was initially purified via Dextrin Sepharose affinity chromatography, cleaved from Maltose binding protein via TEV protease, subject to zinc-affinity chromatography and finally gel filtration. The purification is described in detail in chapter 3.4. A representative purification of Taz2 is shown in Figure 4.2.1. The Superdex 75 16/600 run is detected at 220 nm instead of 280 nm as Taz2 only has a single tyrosine residue, leading to very low absorption at 280 nm (Figure 4.2.1B). Protein could be produced in high quantity and good purity (Figure 4.2.1C). Generally around 10 mg of isolated Taz2 could be obtained from 1 l of expression culture.
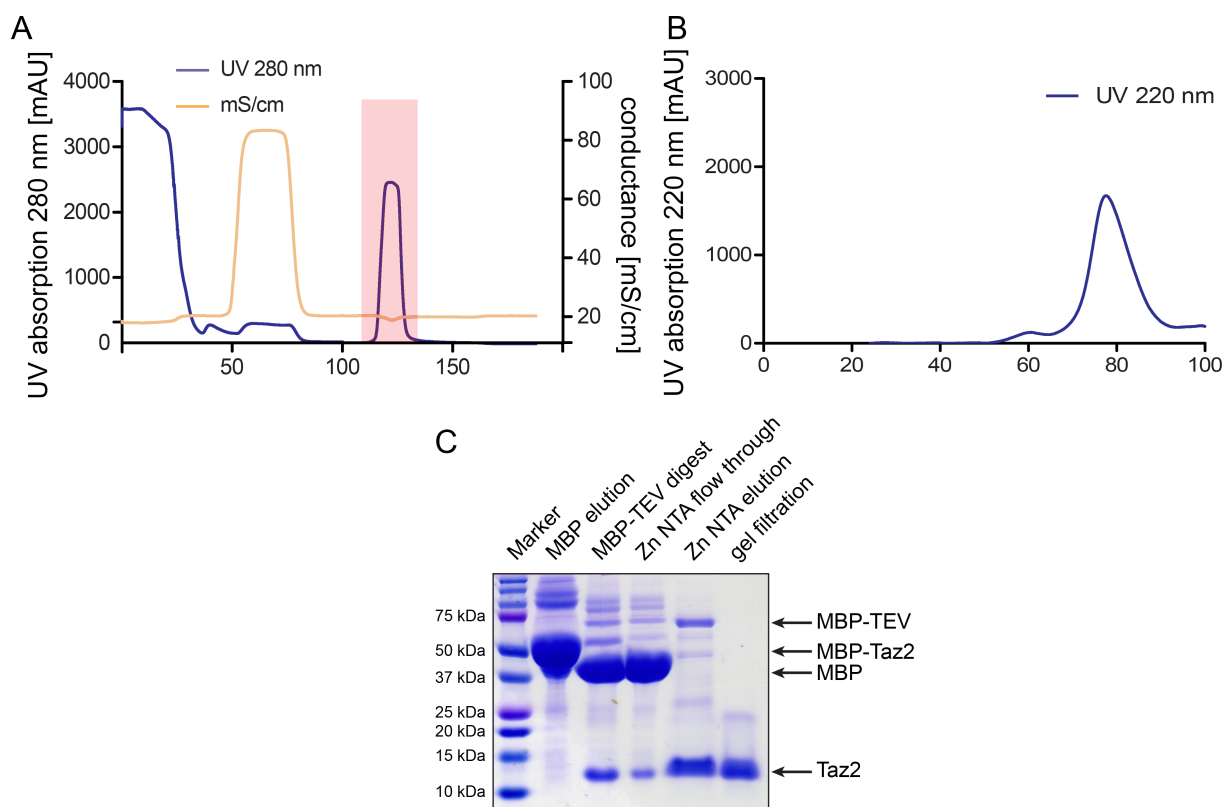
Figure 4.2.1: p300 Taz2 can be purified to high purity as a cleavable MBP fusion. (A) Dextrin Sepharose purification of MBP-Taz2 fusion protein. After an initial wash of the MBP-column a high salt wash was employed to remove unspecifically bound DNA from Taz2 prior to elution. (B) Superdex 75 16/600 gel filtration of cleaved Taz2. 220 nm absorption was detected as Taz2 has almost no absorption at 280 nm. The chromatogram is clipped at 100 ml due to the extremely high absorption at 220 nm due to buffer exchange signals at around 1 column volume. (C) Tris-Tricine SDS page of a typical Taz2 purification.

For further NMR interaction studies, uniformly ^{13}C/^{15}N labeled protein was produced and used for backbone assignment (Figure 4.2.2). A backbone assignment of the analogous domain of CBP has previously been done[185], but due to the low dispersion of the signals and different temperature/pH conditions used it was necessary to repeat the assignment. In the NMR the Taz2 protein seems to be almost mono-disperse and all resonances, except for one could be assigned. For the easy of assignment, all assignments start at alanine 1, which corresponds to alanine 1723 in the protein sequence of p300. The construct sequence features two additional amino acids prior to this alanine for cloning and TEV cleavage reasons. Neither of the signals are visible in the spectrum.
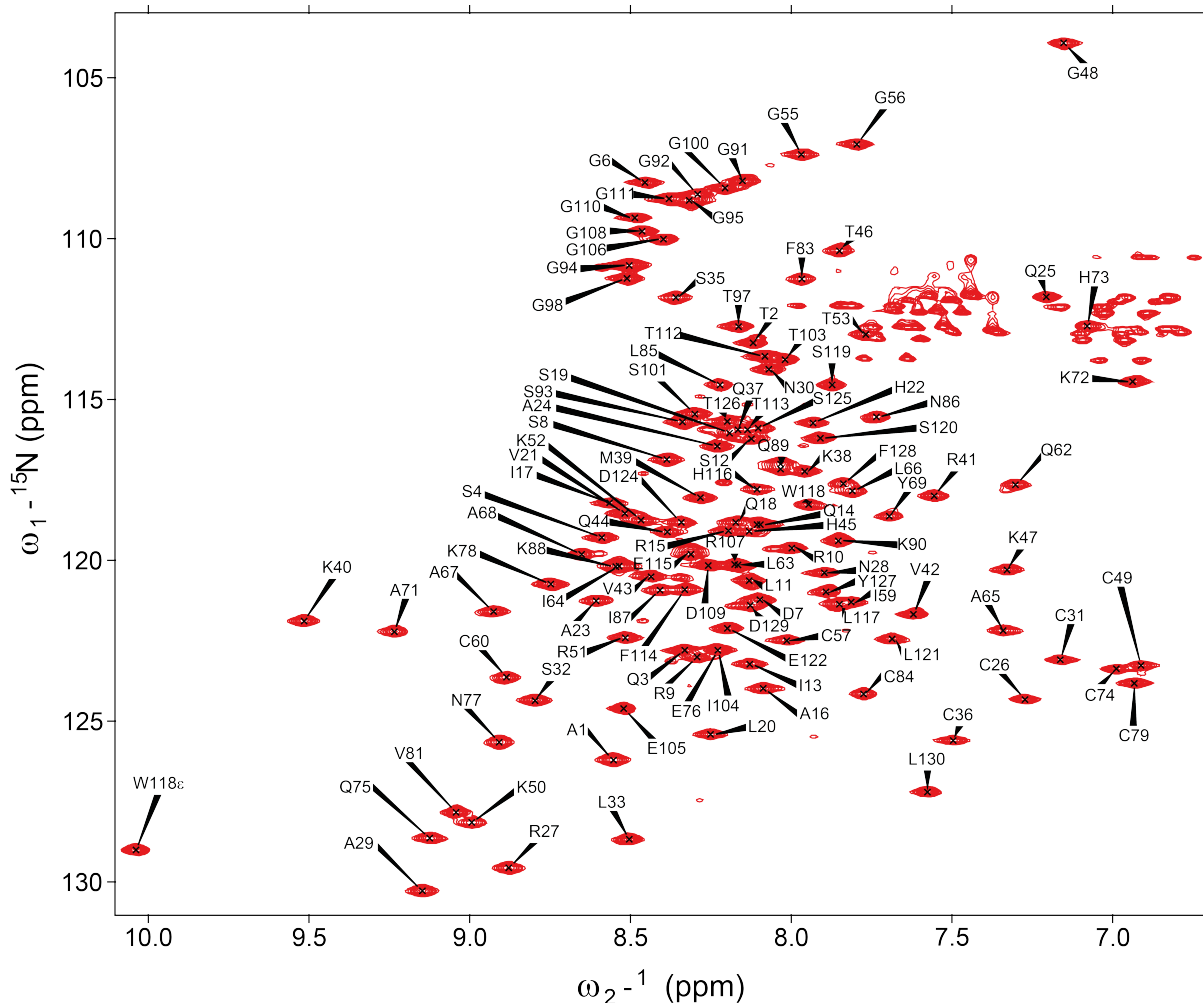
Figure 4.2.2: p300 Taz2 backbone assignment. [^{15}N,^{1}H]-BEST-TROSY of p300 Taz2 showing the backbone assignment of the domain at pH 6.3/303 K. All potentially visible amino acids with the exception of N54 could be assigned.

4.3 Structure Determination of a Complex Between Taz2 and p63TAD

To get a better understanding of the architecture of the Taz2 domain with the transactivation domain of p63 it was decided to try structural characterization of the complex. In a first attempt Taz2 was expressed ^{15}N-labeled and a p63 peptide spanning amino acids 1-34, with a C28A mutation, was expressed unlabeled. The peptide and the protein were purified and an NMR sample with a molar ratio of 1:1.2 Taz2:p63TAD was prepared. A [^{15}N,^{1}H]-BEST-TROSY of the complex (blue) is shown as an overlay with Taz2 (red) in Figure 4.3.1. As expected chemical shift perturbations (CSPs) can be observed. However additionally the linewidth increases drastically, much more than one could expect from the increase of rotational correlation time due to a mass gain of 4 kDa. This most likely indicates an intermediate exchange phenomenon, greatly hampering the possibility of NMR structure determination with this type of sample. Furthermore

it seems like the sample is not in a defined conformational state, as multiple additional peaks appear. This is not expected as the peptide should be invisible, as it is not labeled.
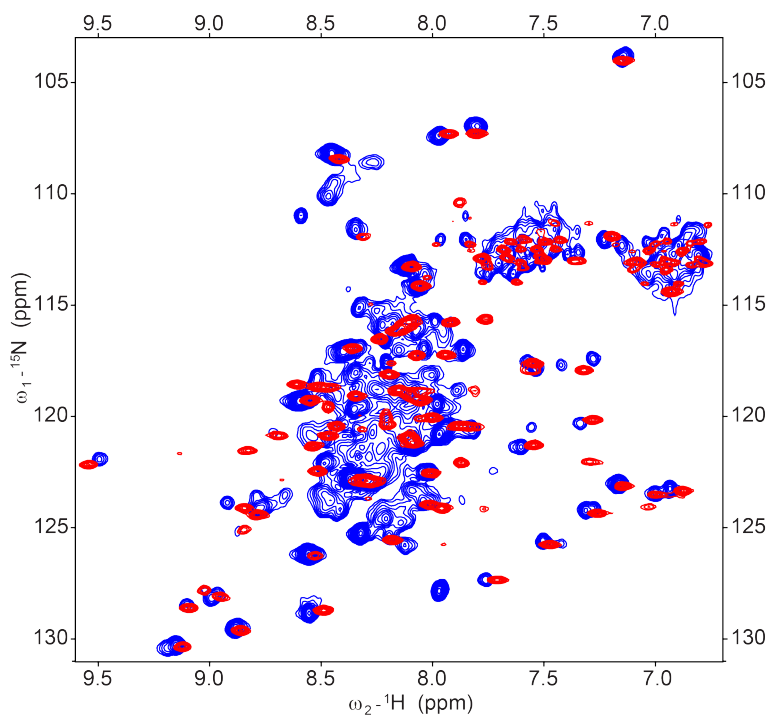
Figure 4.3.1: Comparison of Taz2 in complex with a p63 transactivation domain peptide and Taz2 alone. A p63 peptide spanning amino acids 1-34 was titrated onto ^{15}N-labeled Taz2 at a molar ratio of 1:1.2. The [^{15}N,^{1}H]-BEST-TROSY of the complex (blue) has a greatly increased linewidth compared to that of free Taz2. Additional peaks are visible in the complex spectrum compared to the Taz2 domain alone. Spectra were recorded at pH 6.3/303 K. This data has been modified from Krauskopf K *et al.* 2018[245].

As the peptide spot membrane revealed that the first amino acids of p63 are not crucial for Taz2 binding the peptide length was reduced to amino acids 8-32, to reduce the linewidth of the observed peaks. A full NMR titration of ^{15}N-labeled Taz2 with unmarked peptide is shown in Figure 4.3.2. The titration reveals one set of sites, but higher concentrations of peptide lead to a non-linear behavior of the CSPs indicating multiple binding sites of the peptide on the Taz2 domain. Additionally the Taz2:peptide complex with high ratio of peptide is not stable for extended periods of time, as precipitation of the complex was observed in the NMR tube after several hours.
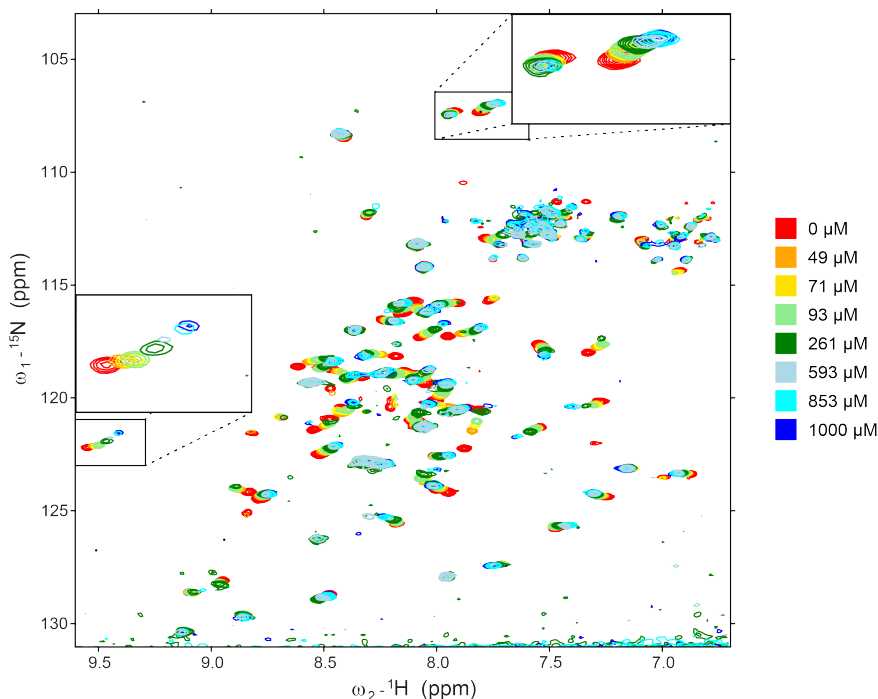
Figure 4.3.2: NMR titration experiments with ^{15}N-labeled Taz2 and a peptide spanning amino acids 8-32 of p63 indicate multiple binding events. [^{15}N,^{1}H]-BEST-TROSY spectra with increasing concentrations of a p63 peptide consisting of amino acids 8-32 of p63. This data has been modified from Krauskopf K *et al.* 2018 [245].

Additionally two fragments of the TA domain of p63 were tested in a one-step NMR titration to get an understanding of the principal organization of the peptide on the Taz2 domain (Figure 4.3.3). One peptide spans amino acids 8-21 while the second peptide contains amino acids 15-25. The first peptide resembles the p53 TAD2. They show high sequence homology especially at the N-terminus featuring a potential helix-inducing sequence with a proline residue (Figure 4.3.3C). The second peptide is the core MDM2 binding motif as reported for p63 and other family members (Figure 4.3.3B) [247].

A p63 8-21 ("TAD2-like")

B p63 15-25 ("TAD1-like")

C

```
p53 TAD2: -LMLSPDDIEQWFTEDP
p63 8-21: NEFLSPEVFQHIWD
```

```
p53 TAD2: LSQETFSDLWKLL
p63 15-24:    EVFQHIWDFLEQ
p73 TAD:   DGGTTFEHLWSSLE
```
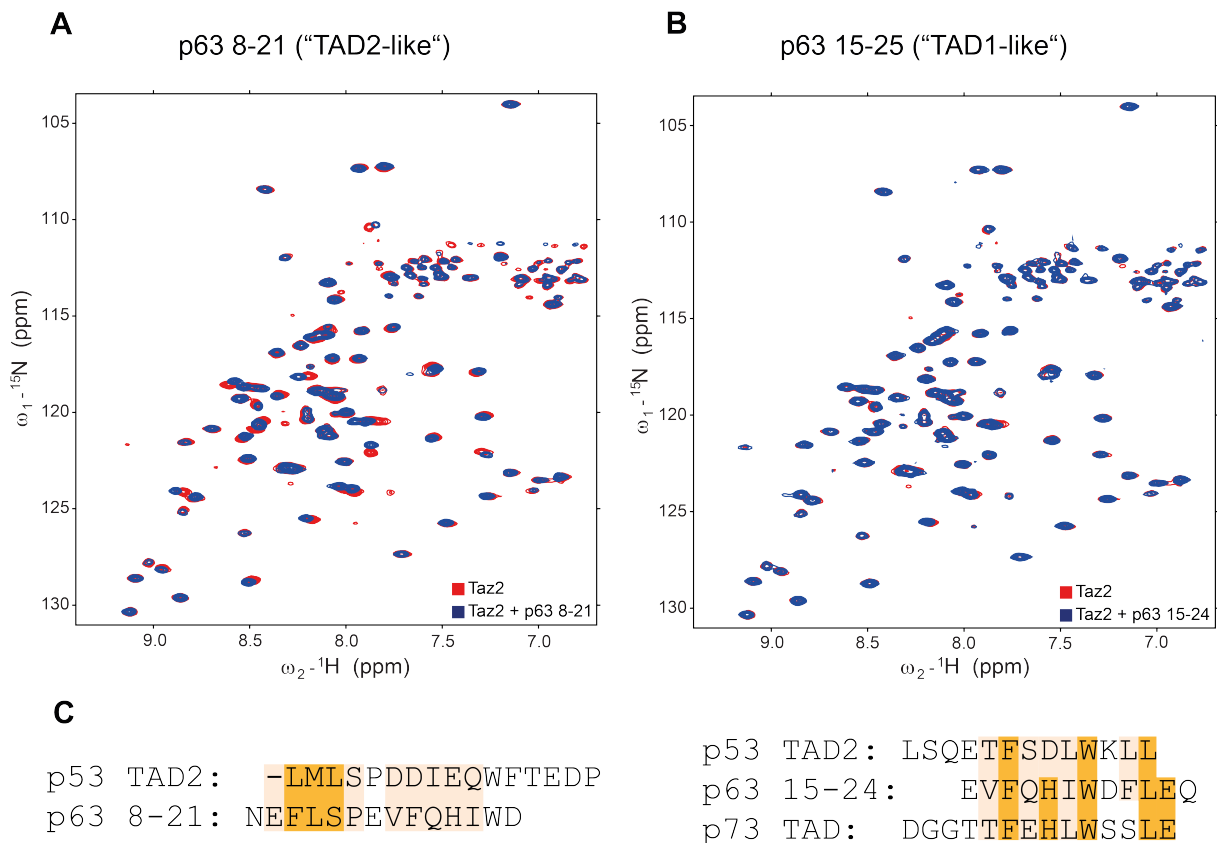
Figure 4.3.3: Two-step NMR titration experiments with ^{15}N-labeled Taz2 and peptides spanning amino acids 8-21 or 15-25 of p63. Both peptide sequences feature almost the full "FWL"-motif within their sequence, but the 8-21 peptide (A) is more alike to the p53 TAD2 sequence, compared to the 15-25 peptide (B) which is highly similar to p53 TAD1 and p73 TAD1. A sequence alignment of the peptides used in the experiment and their comparison to the afore mentioned domains is shown in (C). This data has been modified from Krauskopf K *et al.* 2018[245].

This experiment clearly shows that the importance of the N-terminus is much larger than the C-terminus. CSPs are visible in both cases but they are much more prominent in case of the N-terminal extension of the "FWL"-motif. Therefore it can be assumed that the MDM2 binding motif enhances the interaction between Taz2 and the p63 TA, however it is not necessary for the interaction. To circumvent the problem of stable 1:1 complex formation as well as to get an improvement in line shape a fusion construct between Taz2 and the p63 TA domain was cloned. The peptide was attached via a seven amino acid long flexible linker to the C-terminus of Taz2. The linker length was chosen based on analysis of available Taz2/peptide complex structures to ensure that the peptide is not restricted in its orientation on Taz2 by the linker. The construct was expressed as a MBP-fusion, cleaved with MBP TEV after purification and separated from MBP, MBP-TEV, incomplete/unfolded protein via cation exchange chromatography (CEX). A representative purification is shown in Figure 4.3.4.
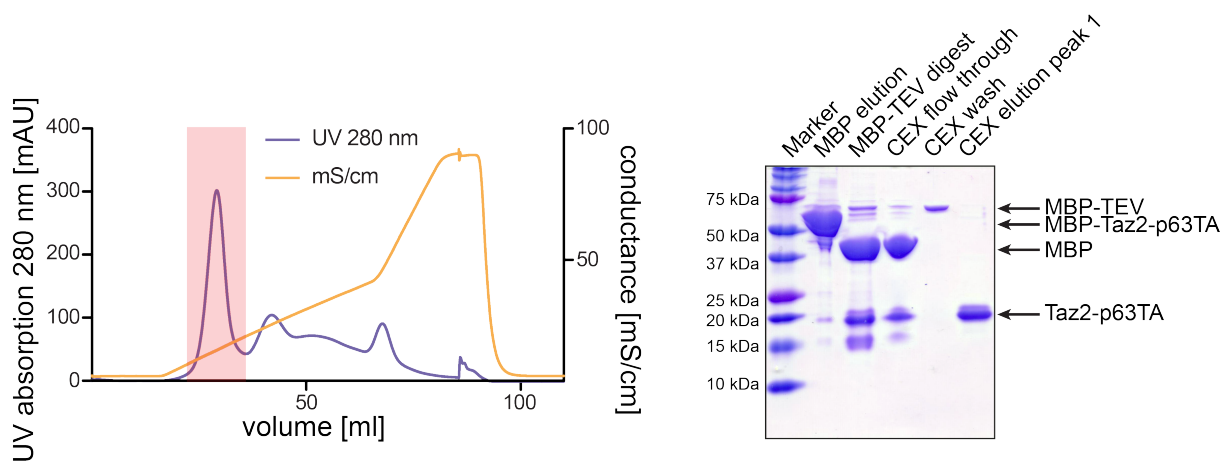
Figure 4.3.4: Purification of p300Taz2-p63TAD fusion protein. p300Taz2-p63TAD was expressed as a MBP fusion protein and purified analogous to Taz2. After TEV cleavage the protein was subject to CEX purification (left panel). Only protein eluting at a defined conductivity was used for further processing (red box). Right panel: Tris-Tricine SDS PAGE of a representative purification.

An initial sample of ^{15}N-labeled material showed good line shape as well as a single set of peaks. Therefore double labeled protein was produced and a backbone assignment was done (Figure 4.3.5). All resonances, again with the exception of N54, could be assigned.
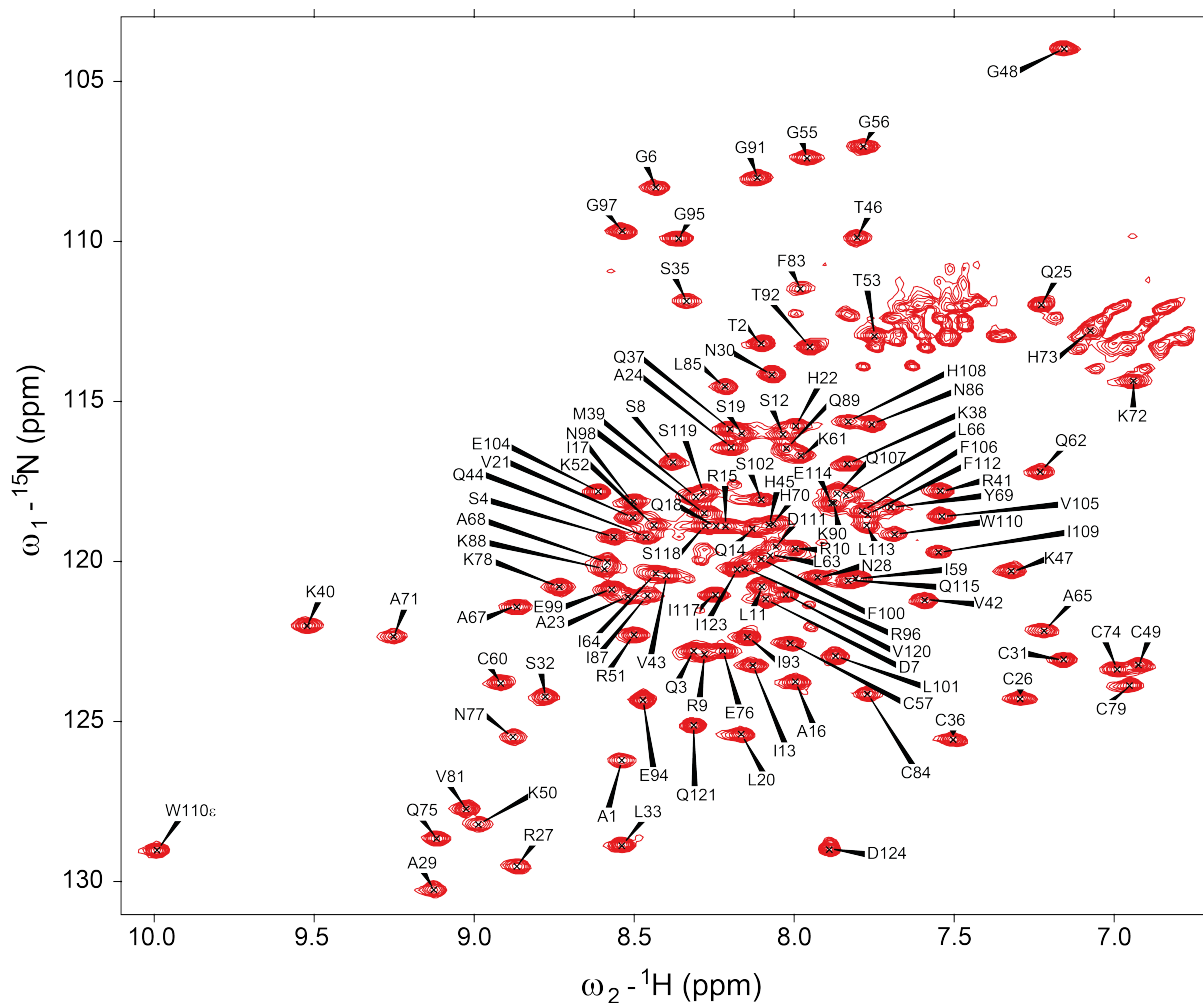
Figure 4.3.5: p300Taz2-p63TAD fusion backbone assignment. [^{15}N,^{1}H]-BEST-TROSY of p300Taz2 p63TAD showing the backbone assignment of the fusion construct at pH 6.3/303 K. All potentially visible amino acids with the exception of N54 could be assigned. Assignment numbers 1-90 refer to the Taz2 domain, amino acids 97-124 to the p63 TAD peptide. The assignment table is shown in the appendix. This data has been published in Krauskopf, K *et al.* 2018[245].

Based on the ^{13}C-Cα/^{13}C-Cβ shifts from the backbone assignment a secondary structure prediction was performed with the TALOS+ web server[238]. The results indicate a possible structure with five helices, four formed by the Taz2 domain and one by the peptide (Figure 4.3.6). Evaluation of the chemical shifts indicates that the linker does not adopt any specific conformation.
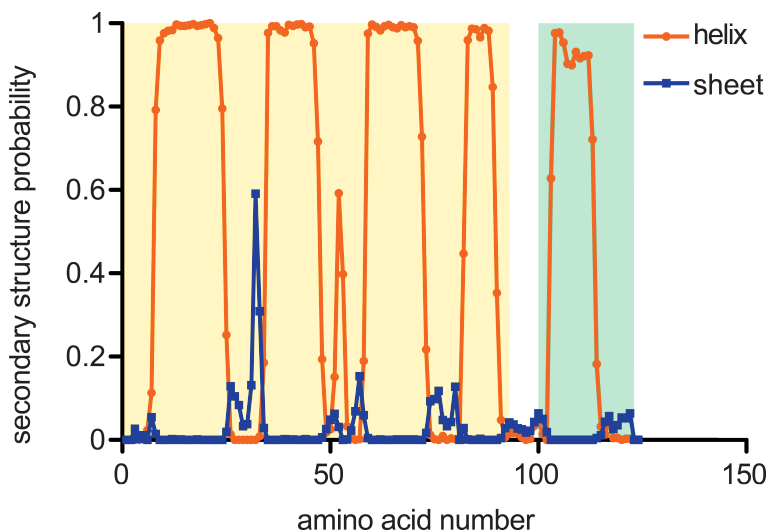
Figure 4.3.6: Chemical shift based secondary structure prediction of p300Taz2-p63TAD. Secondary structure of p300Taz2-p63TAD was predicted with help of the TALOS+ algorithm[238]. Helical probability is shown in orange with solid circles indicating a residue, β-sheet probability is shown in blue with solid squares indicating a residue. The Taz2 domain residues are marked by a yellow background; p63 TAD residues are marked by a green background. This data has been published in Krauskopf, K *et al.* 2018[245].

Additionally the free p63 TAD peptide was expressed and a backbone assignment was done (Figure 4.3.7). Chemical shift evaluation with the TALOS+ algorithm reveals that the potential helix formed by p63 TAD on the Taz2 domain is not present in the free form of the peptide (Figure 4.3.8).
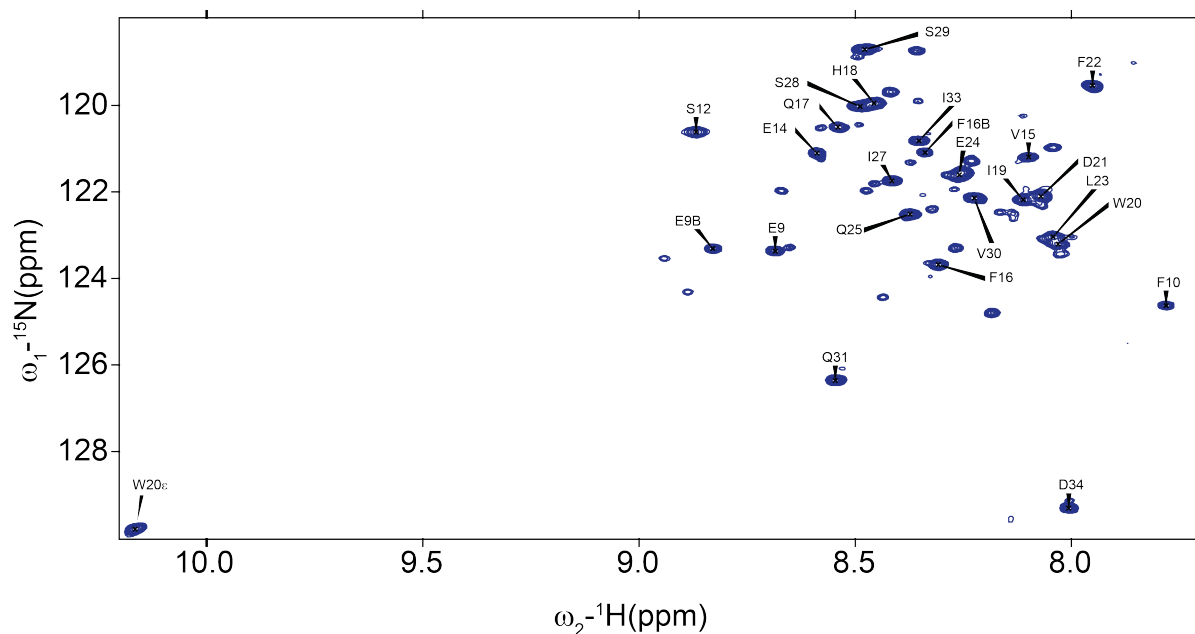
Figure 4.3.7: Backbone assignment of free p63 transactivation domain (amino acids 8-32). [^{15}N,^{1}H]-BEST-TROSY of p300Taz2 p63TAD showing the backbone assignment of free p63 transactivation domain at pH 6.3/303 K. Several residues show conformational instability and are therefore present in two states (one being denoted with a 'B' in the assignment). The numbering of the residues corresponds to the sequence of p63. The assignment table is shown in the appendix.
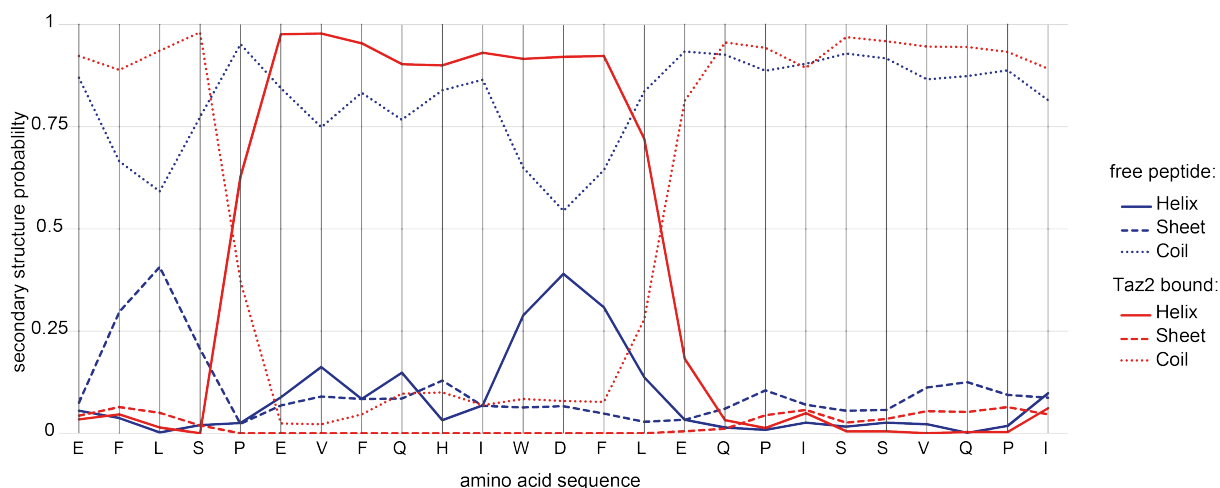
Figure 4.3.8: Chemical shift based secondary structure prediction of free p63 TAD and p63 TAD bound to Taz2 shows a large increase in helicity upon binding. Secondary structure of free p63 peptide (amino acids 8-32; blue) and peptide covalently bound to p300Taz2 (red) was predicted with help of the TALOS+ algorithm[238] and plotted in a sequence-wise manner. Secondary structure probabilities are marked with different styles of lines, where solid lines indicate helix, coarse dotted lines indicated β-sheet and fine dotted lines indicate random coil.

To further asses if the linker between Taz2 and the p63 TAD is indeed flexible a ^{15}N-Heteronuclear NOESY experiment was performed (^{15}N-HetNOE). The result is shown in Figure 4.3.9. The N-terminus as well as the absolute C-terminus of the fusion construct are extremely flexible, leading to negative signals in the HetNOE spectrum. The helices of the Taz2 domain can vaguely be recognized as four regions of higher rigidity compared to the loops in between. The linker region is not as flexible as the N- and C-terminus, but signal intensity drops significantly for the linker, indicating an increased flexibility. The p63 TAD peptide sequence reaches signal values comparable to the helices of Taz2 in the middle of the sequence. This points towards a well-structured helix, which is bound onto the surface of Taz2.
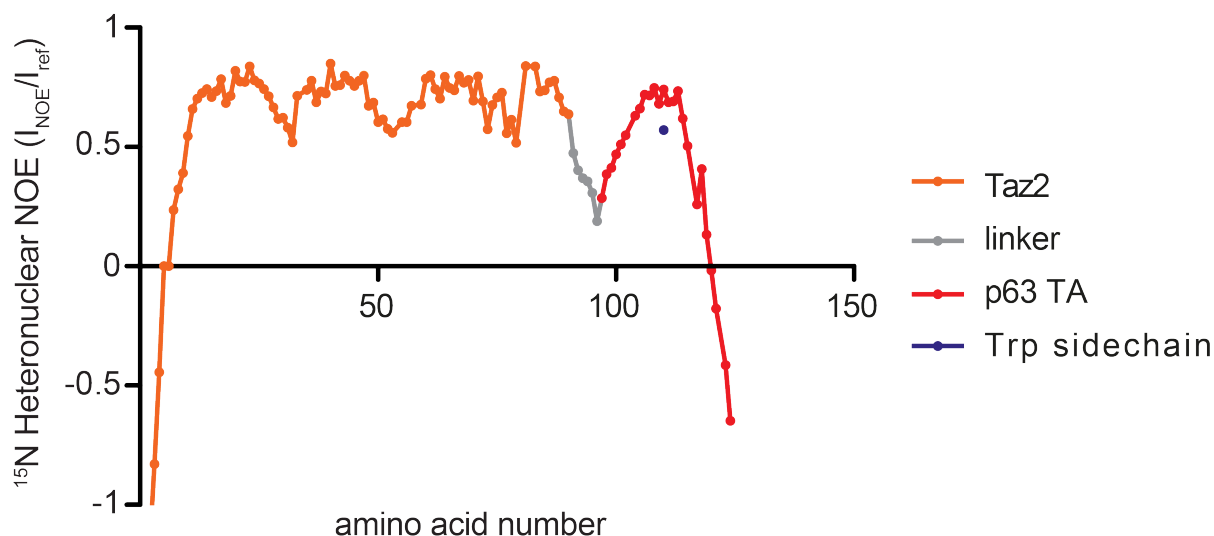
Figure 4.3.9: The ^{15}N-Heteronuclear NOE clearly shows lower rigidity between Taz2 and the p63TAD. The {^{1}H}^{15}N-hetNOE spectrum was recorded with a presaturation of 10 s and otherwise standard experimental conditions. Fragments of the fusion construct are color coded as described in the legend. This data has been published in Krauskopf, K *et al.* 2018 [245].

Next the protonation states of the histidine imidazole ring nitrogen atoms was determined. This is crucial, as in many NMR structures of zinc binding proteins the geometry of the zinc finger is just assumed by looking at NOE restraints or totally omitted and not modeled at all. Determination of the protonation state of the individual histidine residue nitrogen atoms is crucial as to be involved in a complex the respective nitrogen needs to be deprotonated. At physiological pH the imidazole ring of histidine usually carries a net charge of zero. To achieve this, one ring nitrogen has to be protonated and the corresponding other needs to be deprotonated (right panel Figure 4.3.10). In case of a free, non-coordinating histidine the equilibrium lies towards the protonation of $N_{\varepsilon 2}$ at neutral pH [248]. The nitrogen chemical shifts within the imidazole ring generally shift from 170-180 ppm if protonated to 210-220 ppm if deprotonated. With the help of a [^{15}N,^{1}H]-HMBC correlating $N^{\varepsilon 2}/N^{\delta 1}$ with $H^{\varepsilon 1}/H^{\delta 2}$ it was possible to unambiguously assign all nitrogen chemical shifts as well as determine their protonation state. A sample spectrum is shown in Figure 4.3.10. Interestingly all three histidine residues involved in zinc binding (H22, H45 and H70) show a very clear protonation of $N^{\delta 1}$ instead of the more common $N^{\varepsilon 2}$ protonation, indicating a zinc-coordination via the $^{\varepsilon 2}$ atoms. The remaining two histidines are partly protonated at both nitrogen atoms. This can be explained by the slightly acidic buffer conditions.
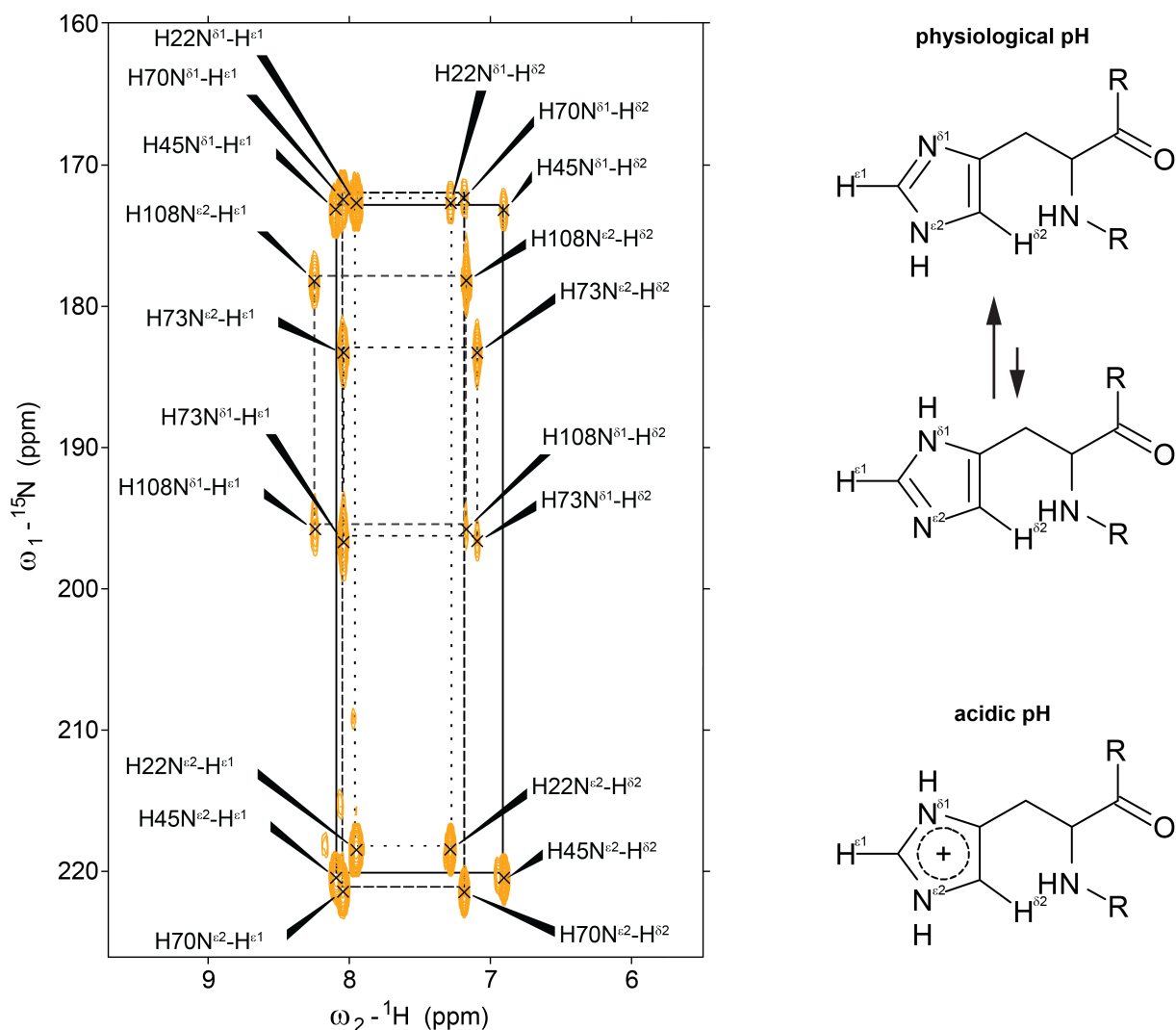
Figure 4.3.10: Histidine-side chain protonation varies depending on the function of the specific histidine within the structure. Right panel: At physiological pH levels, the imidazole ring on histidine side chains carries a net charge of zero. This can either be achieved by a protonation of $N^{\delta1}$ (π-tautomer) or $N^{\varepsilon2}$ (τ-tautomer) while the corresponding other nitrogen is not protonated. The equilibrium slightly lies on the side of $N^{\varepsilon2}$ protonation)[248]. Under more acidic pH conditions both nitrogen atoms become protonated, therefore resulting in a net charge of +1 for the imidazole ring (bottom). Left Panel: To determine the protonation state of histidines in the samples a [^{15}N,^{1}H]-HMBC, correlating protons bound to carbon atoms ($H^{\delta2}$ and $N^{\varepsilon1}$) and nitrogen atoms ($N^{\delta1}$ and $N^{\varepsilon2}$) within the imidazole ring was used. This lead to four signals per histidine in a 2D variant of the spectrum. Nitrogen chemical shift in imidazole rings showed a large dependence on its protonation state. Protonated nitrogen atoms generally showed a chemical shift in the region of around 170-180 ppm while deprotonated nitrogen atoms are located around 210-220 ppm. Intermediate protonation states could be observed in the region between both chemical shifts. Due to larger J-coupling between $H^{\delta2}$ and $N^{\varepsilon2}$ (2J) than $H^{\delta2}$ and $N^{\delta1}$ (3J) signals can be assigned unambiguously. Therefore, the protonation state of both ring nitrogen atoms can be determined by analysis of the chemical shift of these atoms. This data has been used for structure determination for structures published in Krauskopf, K *et al.* 2018[245].

Sidechain assignment was done manually with the help of 3D H(CCCO)NH and (H)CC(CO)NH TOCSY spectra. NOESY peaks were manually picked from three NOESY spectra (3D aromatic ^{13}C resolved NOESY, 3D aliphatic ^{13}C resolved NOESY and 3D ^{15}N resolved NOESY). A total

of 3938 peaks were used for structure calculation. NOESY assignment was done automatically with CYANA[239]. 3019 NOESY cross-peaks could be assigned. From these peaks 1565 were used in the final structure for distance constraints. Structure calculation statistics are shown in Table 4.3.1. After structure calculation the structure was refined with the molecular dynamics simulation program OPALp[241]. A representative Ramachandran plot is shown in Figure 4.3.11. Structure calculation and energy minimization was performed by Sina Kazemi.
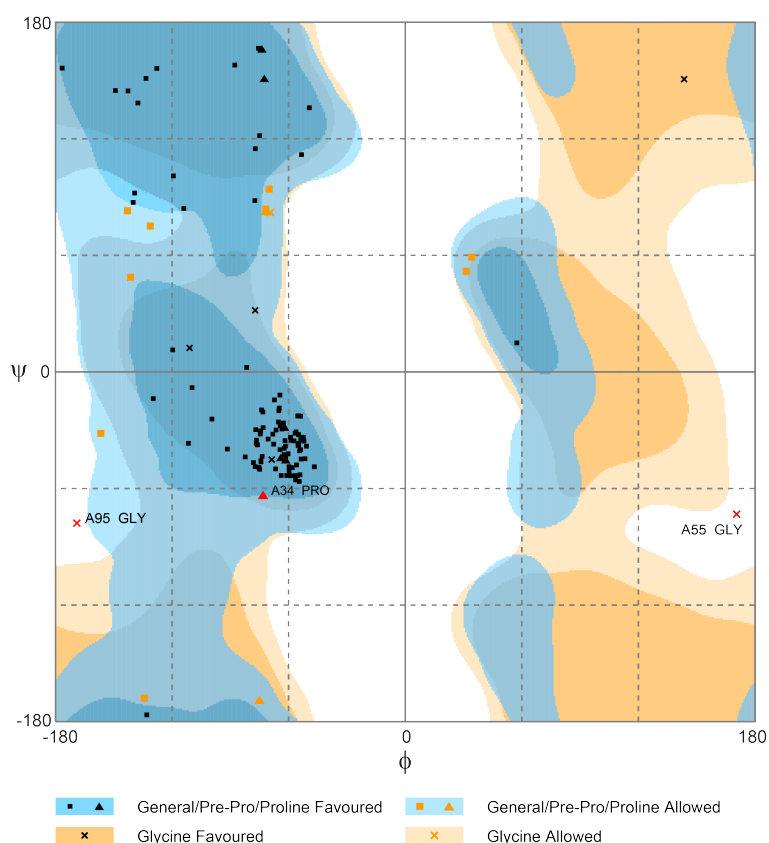
Figure 4.3.11: Ramachandran plot of the fusion construct of p300Taz2-p63TAD structure. 98% of backbone residues were found in allowed regions and 2% were found to be outliers. The Ramachandran plot was created with RAMPAGE[249].

The resulting structure confirmed the TALOS+ prediction of a single helix formed by the p63 peptide, although ranging from amino acid P13 to P26 and therefore two amino acids longer than predicted. The bundle is shown in Figure 4.3.12. The peptide is bound to Taz2 by a hydrophobic surface patch formed by helices one to three. This is consistent with the structures of Taz2 with p53 TAD2[43;45]. Electrostatic surface charge for the peptide as well as Taz2 was calculated with the Adaptive Poisson-Boltzmann Solver (APBS)[250;251]. The result is shown in Figure 4.3.13. Uncharged hydrophobic stretches of Taz2 are completely buried by the peptide. Therefore the surface of the complex is highly charged, positive in case of Taz2 and negative in case of the peptide. This indicated that the binding is at least partly driven by electrostatic interactions. This has also been reported for p53 TAD peptides binding to Taz2 before[43].

Table 4.3.1: Structure calculation statistics p300Taz2-p63TAD

NOE assignment (a)	CYANA result	energy minimized (b)
^{15}N-resolved NOESY cross peaks	1283	
^{13}C-resolved NOESY cross peaks	2227	
^{13}C-resolved aromatic NOESY cross peaks	428	
Total number of NOESY cross peaks (d)	3938 (100%)	
Assigned cross peaks (d)	3019 (76.7%)	
Unassigned cross peaks (d)	919 (23.3%)	
Structural restraints		
Assigned NOE distance restraints (e)	1565 (100%)	
Short range |i-j|≤1	899 (57.4%)	
Medium range 1<|i-j|<5	385 (24.6%)	
Long range |i-j|≥5	281 (18.0%)	
Dihedral angle restraints (ϕ/ψ)	182	
Restraints for zinc coordination (upl/lol)	48	
Structure statistics		
Average CYANA target function value (Å^2)	1.90 ± 0.16	1.88 ± 0.38
Average AMBER Energies (kcal/mol)	3859.73 ± 133.03	4818.54 ± 109.39
Restraint violations (c)		
Max. distance restraint violation (Å)	0.50	0.12
Number of violated distance restraints > 0.2 Å	0	0
Max. dihedral angle restraint violations (°)	5.96	4.71
Number of violated dihedral angle constraints > 5°	0	0
Ramachandran plot		
Residues in most favored regions	80.5%	84.3%
Residues in additionally allowed regions	19.5%	15.2%
Residues in generously allowed regions	0.0%	0.5%
Residues in disallowed regions	0.0%	0.0%
RMSD (residues 7..48, 59..91, 101..114)		
Average backbone RMSD to mean (Å)	0.52 ± 0.06	0.58 ± 0.07
Average heavy atom RMSD to mean (Å)	0.96 ± 0.08	1.02 ± 0.09

(a) using automated NOE assignment and structure calculation functionalities of CYANA

(b) after restrained energy minimization with OPALp

(c) after energy minimization, calculated with CYANA

(d) in parenthesis the percentage of the total cross peaks

(e) in parenthesis the percentage of the total distance restraints from the peak assignment
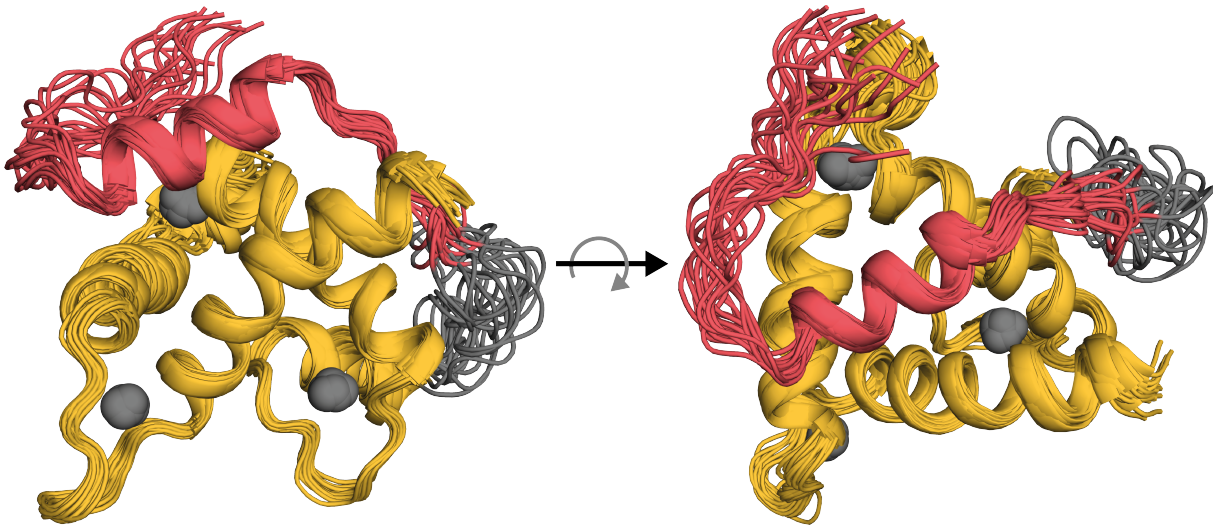
Figure 4.3.12: Bundle representation of the NMR structure of p300Taz2-p63TAD. The bundle of 20 lowest energy structures is shown as a cartoon representation in two different angles. Zinc ions are shown as spheres. Color code: Orange: Taz2, Red: p63TA, Grey: linker and zinc ions. The structure was published in Krauskopf, K *et al.* 2018 [245].
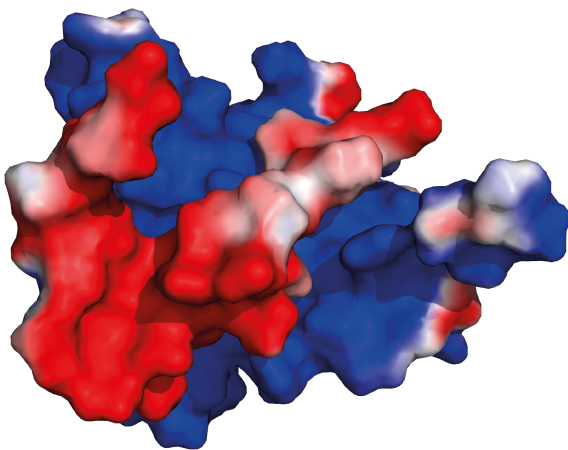
Figure 4.3.13: Surface charge distribution of the Taz2 domain and the attached p63 peptide. Surface electrostatic potential of the Taz2 domain and the p63TAD peptide as calculated by APBS [250;251]. Positive net potential is displayed as blue surface, negative net potential as red surface with the intensity of the color correlating to the absolute potential.

Detailed analysis of the structure indicate that the key residues within p63 for Taz2 binding are F10, F16, I19, W20, F22, L23. All residues, except for F10 are located within the formed helix. A more detailed view of the peptide bound to Taz2 is depicted in Figure 4.3.14. W20 is deeply buried within a pocket of Taz2. I19 is situated in the same pocket (not shown). Interestingly the complete "FWL"-motif contributes to binding, although it is not the driving force of the binding itself. Additionally the structure resembles p53 TAD2/Taz2 structures in the respect that residues N-terminal to the induced helix already make contact with the Taz2 domain surface.
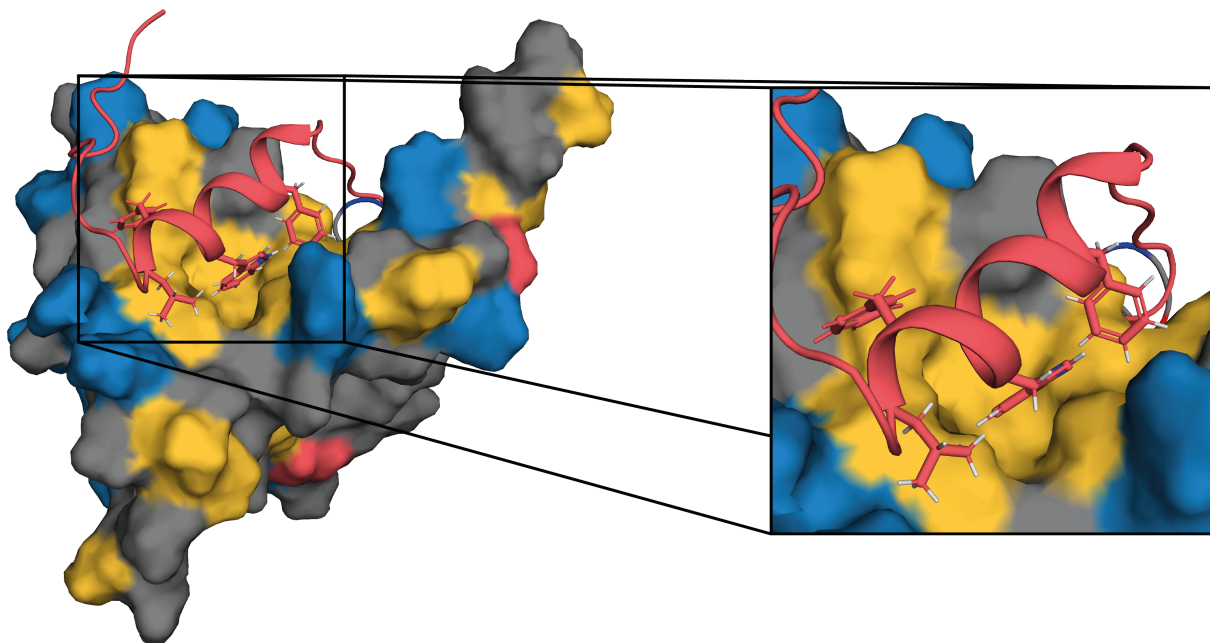
Figure 4.3.14: The surface of Taz2 mainly consists of a hydrophobic belt surrounding the protein and positive charges, binding amphipathic helices with negative charges on their outward facing side. The surface of the Taz2 domain is color coded according to the properties of the respective amino acids. Blue spots represent positively charged side chains, red spots represent negatively charged side chains, and orange spots represent hydrophobic/aromatic side chains. The remaining amino acids have been colored in grey. The p63TAD peptide is shown as red cartoon with key interacting residues depicted as sticks. The structure was published in Krauskopf, K *et al.* 2018 [245].

To determine if the TAp63 N-terminus could potentially harbor a secondary transactivation domain, a longer fusion construct of p300 Taz2 and the N-terminus of p63 was expressed and a backbone assignment was attempted. Only parts of the peptide sequence could be assigned, due to massive spectral overlap or conformational instability. A TALOS+ prediction of the secondary structure of the peptide is shown in 4.3.15. The corresponding HSQC for the assignment is shown in the appendix (8.0.1).
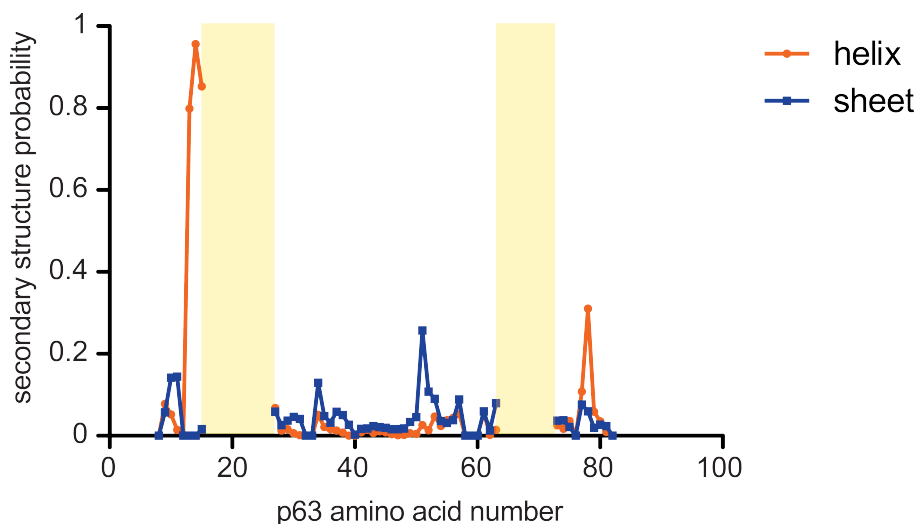
Figure 4.3.15: TALOS+ secondary structure prediction of a p63 peptide fused to the p300 Taz2 domain. Only parts of the peptide sequence could be assigned. Yellow boxes correspond to regions where no assignment was possible. The first region which could not be assigned has α-helical structure in the shorter fusion construct. The assignment table and a HSQC are shown in the appendix. This data has been published in Krauskopf, K *et al.* 2018 [245].

4.4 Structure Determination of a Complex Between Taz2 and p73TAD

To get a better understanding of the very low intrinsic transactivation potential of p73[81] it was decided to try and solve a Taz2-p73TAD structure. The transactivation domain of p73 features two separate peptides involved in Taz2 binding[20]. The N-terminal interacting peptide spans amino acids 10-31 while the C-terminal peptide spans amino acids 40-67. The N-terminal peptide contributes the majority of the binding affinity[20]. As a peptide containing the complete p73 TA domain (amino acids 10-70) lies in the intermediate exchange regime within the NMR[20] a similar fusion construct strategy to the Taz2-p63TAD construct was employed. The linker length between Taz2 and p73TAD was increased from seven residues to 17 residues as the binding mode of the peptide was totally unknown. Two different constructs were made, one stopping at amino acid 31 of p73 (dubbed p73 TAD1 hereafter) or stopping at amino acid 67 (dubbed p73 TAD hereafter).

4.4.1 Structure determination of Taz2-p73TAD1

The shorter construct leads to mono-disperse spectra with good line shape (Figure 4.4.1).
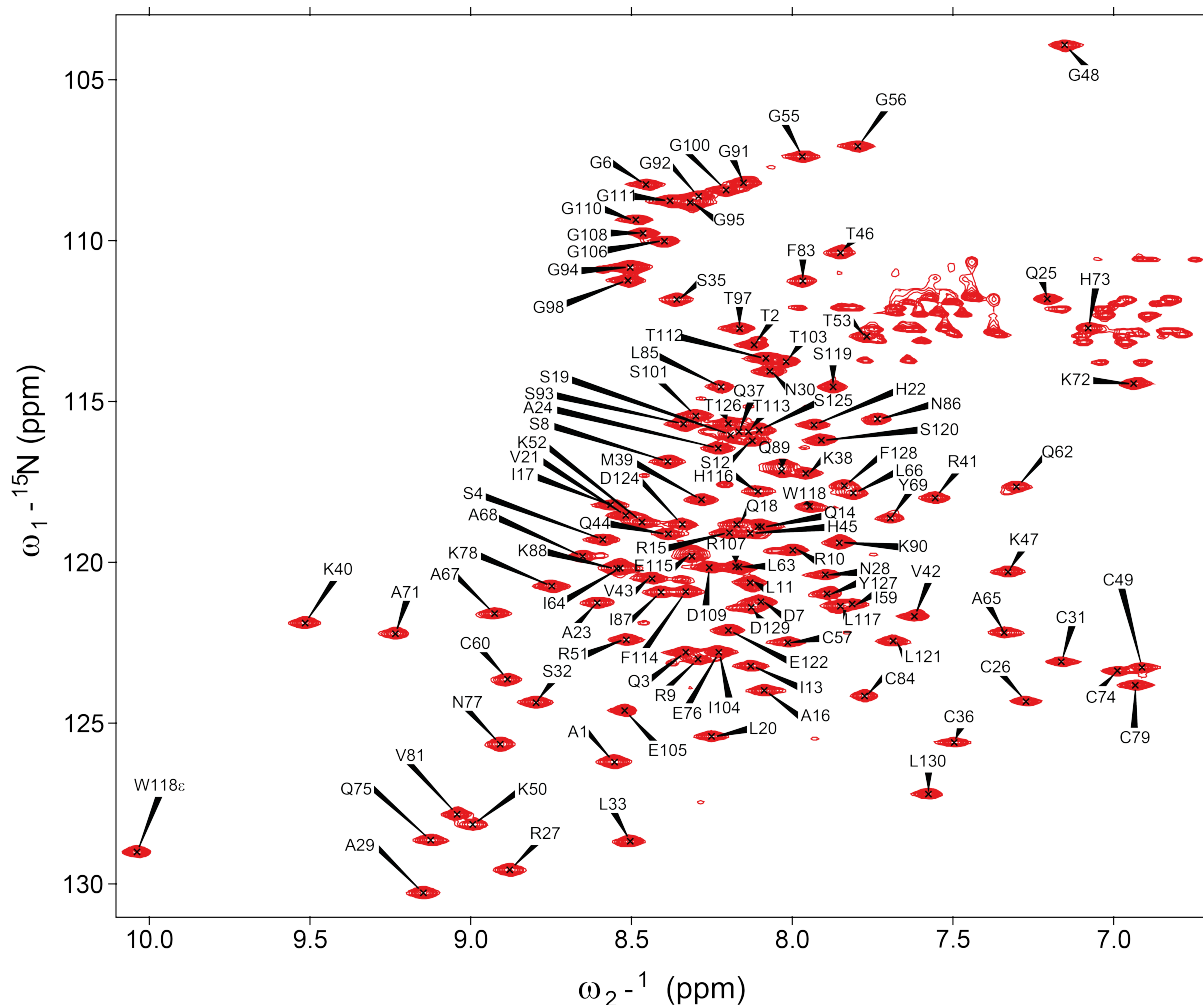
Figure 4.4.1: p300Taz2-p73TAD1 fusion backbone assignment. [^{15}N,^{1}H]-BEST-TROSY of p300Taz2-p73TAD1 showing the backbone assignment of the fusion construct at pH 6.3/303 K. All potentially visible amino acids could be assigned. The assignment table is shown in the appendix. This data has been published in Krauskopf, K *et al.* 2018[245].

Backbone assignment was performed and the results were used for secondary structure prediction with TALOS+[238]. The result indicate that, as for p63, the TAD1 of p73 forms at least one helix (Figure 4.4.2). However another potential structural element emerges from the data, as the prediction for Y28 (p73 nomenclature; Y127 in the assignment) indicates a potential helical structure.
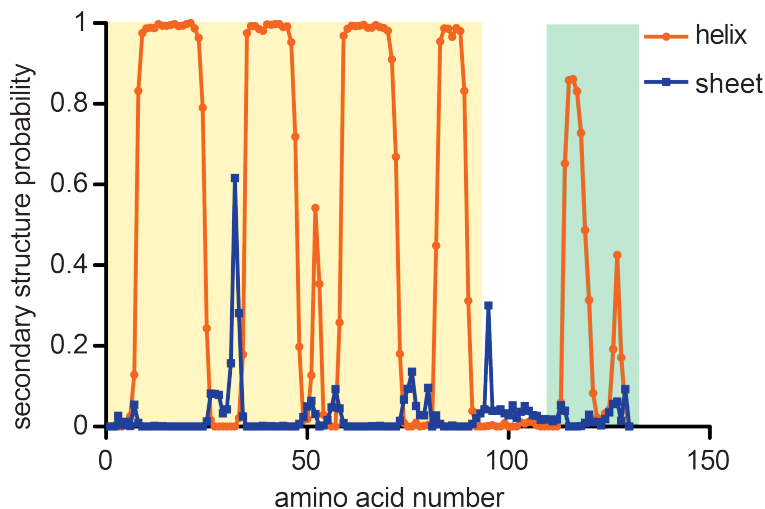
Figure 4.4.2: Chemical shift based secondary structure prediction of p300Taz2-p73TAD1. Secondary structure of p300Taz2-p73TAD1 was predicted with help of the TALOS+ algorithm[238]. Helical probability is shown in orange with solid circles indicating a residue, β-sheet probability is shown in blue with solid squares indicating a residue. The Taz2 domain residues are marked by a yellow background; p63 TAD residues are marked by a green background. This data has been published in Krauskopf, K *et al.* 2018[245].

Linker flexibility was verified with a ^{15}N-HetNOE experiment (Figure 3.4.4). As expected the linker is more flexible than either Taz2 or the peptide, indicating that the linker is not restraining the p73 peptide in its position on the Taz2 domain. Rigidity increases in the peptide sequence again, therefore making it likely that the peptide is indeed bound to the surface of the domain.
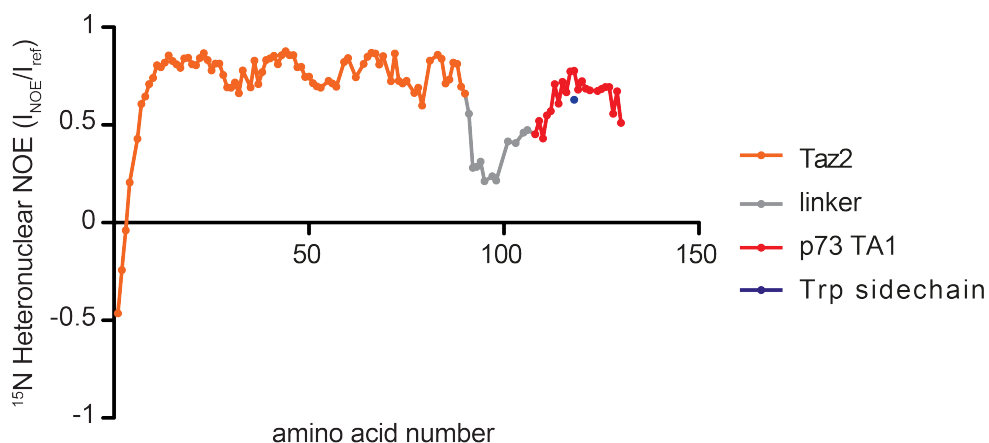
Figure 4.4.3: The ^{15}N-Heteronuclear NOE clearly shows lower rigidity between Taz2 and the p73TAD1. The $\{^1H\}^{15}$N-hetNOE spectrum was recorded with a presaturation of 8 s and otherwise standard experimental conditions. Fragments of the fusion construct are color coded as described in the legend. This data has been published in Krauskopf, K *et al.* 2018[245].

Next side chain assignments were done with 3D-H(CCCO)NH and (H)CC(CO)NH TOCSY spectra. Zinc coordination by histidines was measured analogous to the p63 structure above. As expected, identical protonation states in the histidine side chains could be detected. Four different NOESY spectra were recorded (3D aromatic ^{13}C resolved NOESY, 3D aliphatic ^{13}C resolved NOESY, 3D ^{15}N-resolved NOESY and 4D aromatic ^{13}C resolved/aliphatic ^{13}C resolved

NOESY). A 4D NOESY was required to gain enough certainty of the position of the aromatic residues within the peptide, especially F16 and F29. NOESY peaks were picked by hand and assigned by CYANA. Of 4565 NOESY cross-peaks 3031 could be assigned by CYANA and 1563 were used for the final structure. Structure calculation statistics are shown in Table 4.4.1. A Ramachandran plot is shown in Figure 4.4.4. After structure calculation the structure was minimized by OPALp. The structure was calculated and minimized by Sina Kazemi.
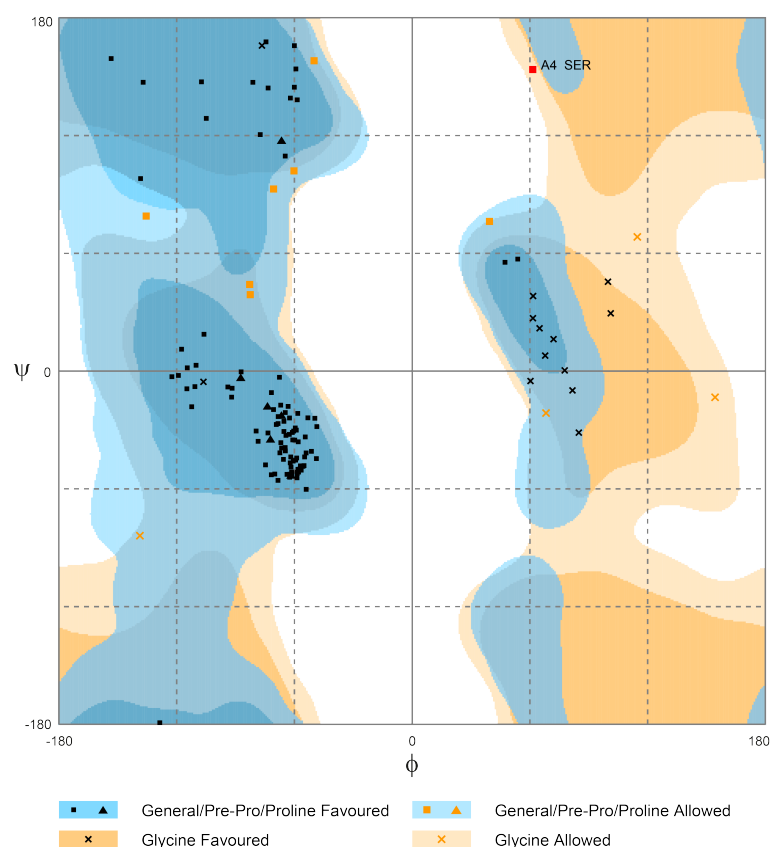
Figure 4.4.4: Ramachandran plot of the short fusion construct of p300Taz2-p73TAD1 structure.
99% of all residues are found in allowed regions and 1% are considered to be outliers. The Ramachandran plot was created with RAMPAGE [249].

The resulting structure reveals a peptide structure consisting of a single helix of roughly two turns, with an elongated region C-terminal to the helix. Indeed as predicted by TALOS+ [238], the C-terminal aromatic residue Y127 (construct nomenclature) is involved in this secondary predicted helical structural element. A bundle representation is shown in figure 4.4.5.

Table 4.4.1: Structure calculation statistics p300Taz2-p73TAD1

NOE assignment (a)	CYANA result	energy minimized (b)
[15]N-resolved NOESY cross peaks	1278	
[13]C-resolved NOESY cross peaks	2719	
[13]C-resolved aromatic NOESY cross peaks	409	
[13]C-^{13}C-resolved NOESY 4D	159	
Total number of NOESY cross peaks	4565 (100%)	
Assigned cross peaks (d)	3031 (66.4%)	
Unassigned cross peaks (d)	1534 (33.6%)	
Structural restraints		
Assigned NOE distance restraints (e)	1563 (100%)	
Short range |i-j|≤1	881 (56.4%)	
Medium range 1<|i-j|<5	387 (24.8%)	
Long range |i-j|≥5	295 (18.9%)	
Dihedral angle restraints (ϕ/ψ)	174	
Restraints for zinc coordination (upl/lol)	46	
Structure statistics		
Average CYANA target function value (Å^2)	1.45 ± 0.16	2.36 ± 0.45
Average AMBER Energies (kcal/mol)	-3933.45 ± 99.80	-4964.04 ± 92.86
Restraint violations (c)		
Max. distance restraint violation (Å)	0.28	0.15
Number of violated distance restraints > 0.2 Å	0	0
Max. dihedral angle restraint violations (°)	7.81	3.48
Number of violated dihedral angle constraints > 5°	0	0
Ramachandran plot		
Residues in most favored regions	81.9%	84.3%
Residues in additionally allowed regions	18.0%	15.1%
Residues in generously allowed regions	0.1%	0.0%
Residues in disallowed regions	0.0%	0.0%
RMSD (residues 7..91, 113..130)		
Average backbone RMSD to mean (Å)	0.67 ± 0.17	0.72 ± 0.16
Average heavy atom RMSD to mean (Å)	1.07 ± 0.15	1.14 ± 0.14

(a) using automated NOE assignment and structure calculation functionalities of CYANA

(b) after restrained energy minimization with OPALp

(c) after energy minimization, calculated with CYANA

(d) in parenthesis the percentage of the total cross peaks

(e) in parenthesis the percentage of the total distance restraints from the peak assignment
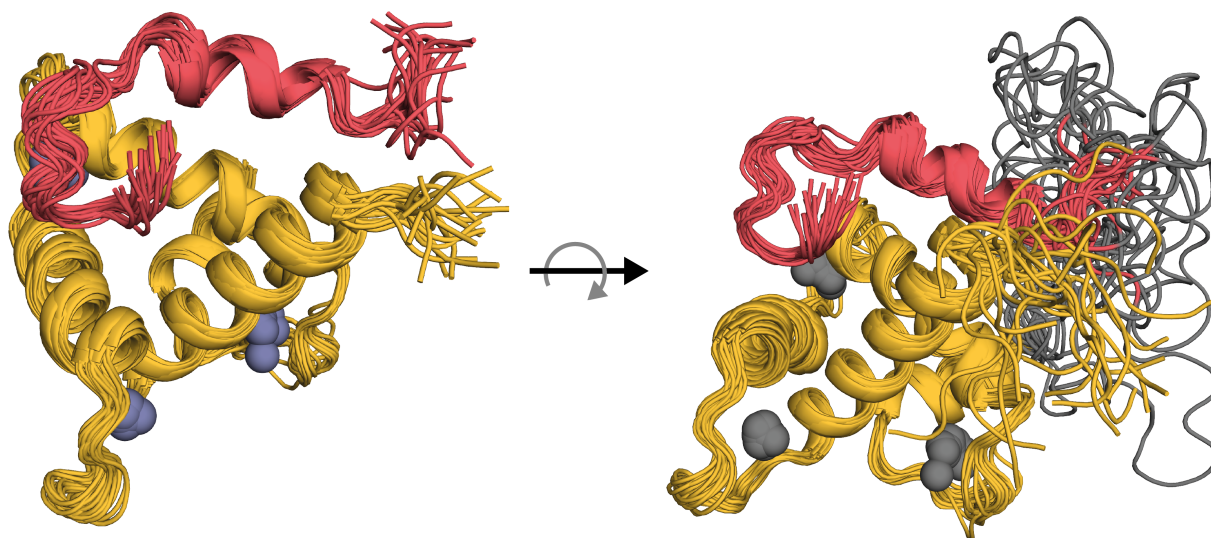
Figure 4.4.5: Bundle representation of the NMR structure of p300Taz2-p73TAD1. The bundle of 20 lowest energy structures is shown as a cartoon representation in two different angles. Zinc ions are shown as spheres. In the left panel the linker between Taz2 and the peptide has been omitted for clarity reasons. Color code: Orange: Taz2, Red: p63TA, Grey: linker and zinc ions. The structure was published in Krauskopf, K *et al.* 2018[245].

Furthermore, geometry of the linker region varies greatly between individual structures. This indicates that the orientation of the peptide is not restrained by linker length. Structural analysis of the residues most likely contributing to the binding affinity reveals that the binding mode significantly differs between the transactivation domains of p63 and p73. While p63 has a single structured helix, p73 has an additional extended interaction motif C-terminal to the helix. In case of p73 the most important interacting residues consist mainly of the MDM2 binding "FWL"-motif (F15, W19, L22) and the additional aromatic residues Y28 and F29 on the C-terminal side of the helix (Figure 4.4.6).
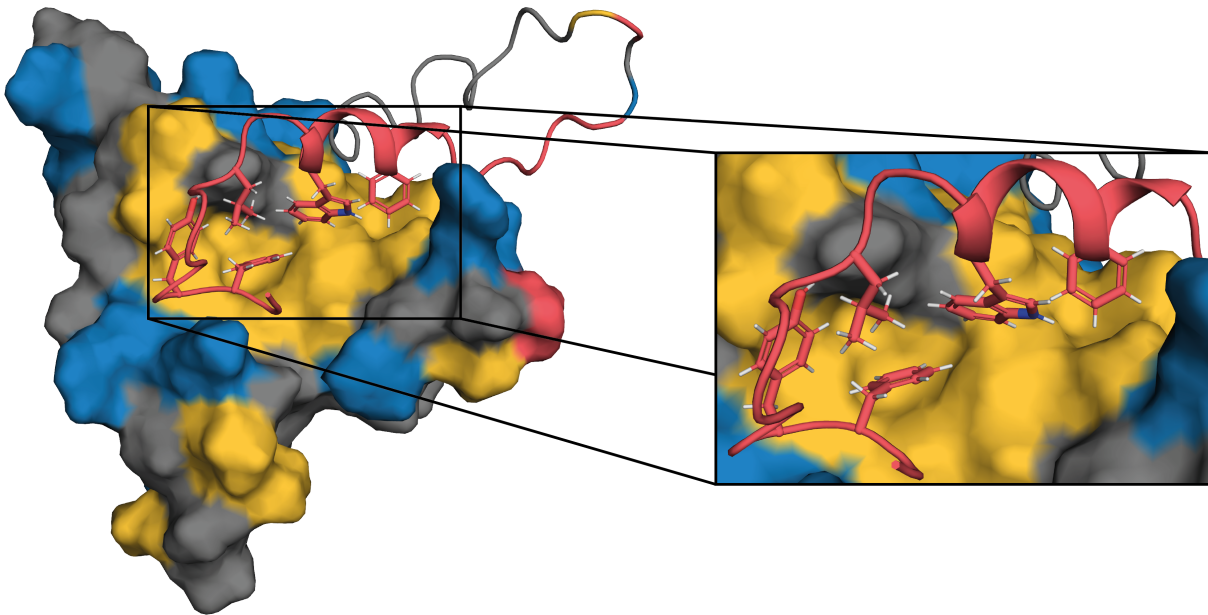
Figure 4.4.6: The surface of Taz2 mainly consists of a hydrophobic belt surrounding the protein and positive charges, binding amphipathic helices with negative charges on their outward facing side. The surface of the Taz2 domain is color coded according to the properties of the respective amino acids. Blue spots represent positively charged side chains, red spots represent negatively charged side chains, and orange spots represent hydrophobic/aromatic side chains. The remaining amino acids have been colored in grey. The p73TAD1 peptide is shown as red cartoon with key interacting residues depicted as sticks. The structure was published in Krauskopf, K *et al.* 2018[245].

As for p63, the p73 peptide covers large parts of the hydrophobic surface of Taz2. Additionally the p73 peptide shows a strong negative charge potential (Figure 4.4.7).
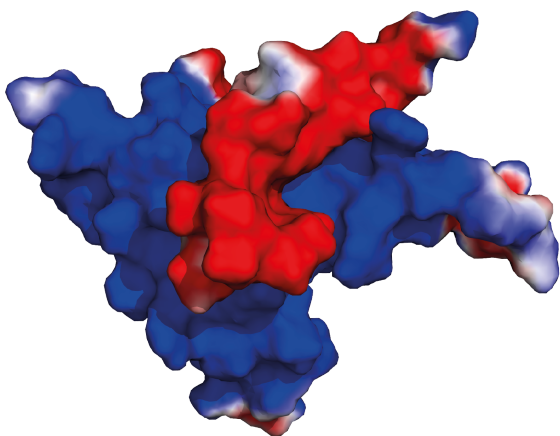
Figure 4.4.7: Surface electrostatic potential of the Taz2 domain and the p63TAD peptide as calculated by APBS[250;251]. Positive net potential is displayed as blue surface, negative net potential as red surface with the intensity of the color correlating to the absolute potential. The structure was published in Krauskopf, K *et al.* 2018[245].

4.4.2 Structure determination of Taz2-p73TA

To get a better understanding if the elongation of the p73 TAD peptide leads to significant changes in the structure a backbone assignment of the longer construct (Taz2 with amino acids 10-67 of p73) was done (Figure 4.4.8). A large change in structure could be expected as the C-terminal region of p73 TAD does show interaction with Taz2[20]. Additionally it has been shown for p53 that the TAD1 and TA2 domains can occupy the same surface of the Taz2 domain in a

mutually exclusive manner[42]. A newer structure including both TA domains at the same time, revealed another binding interface on the surface of Taz2, enabling the peptide to be bound with both transactivation domains at the same time[45].
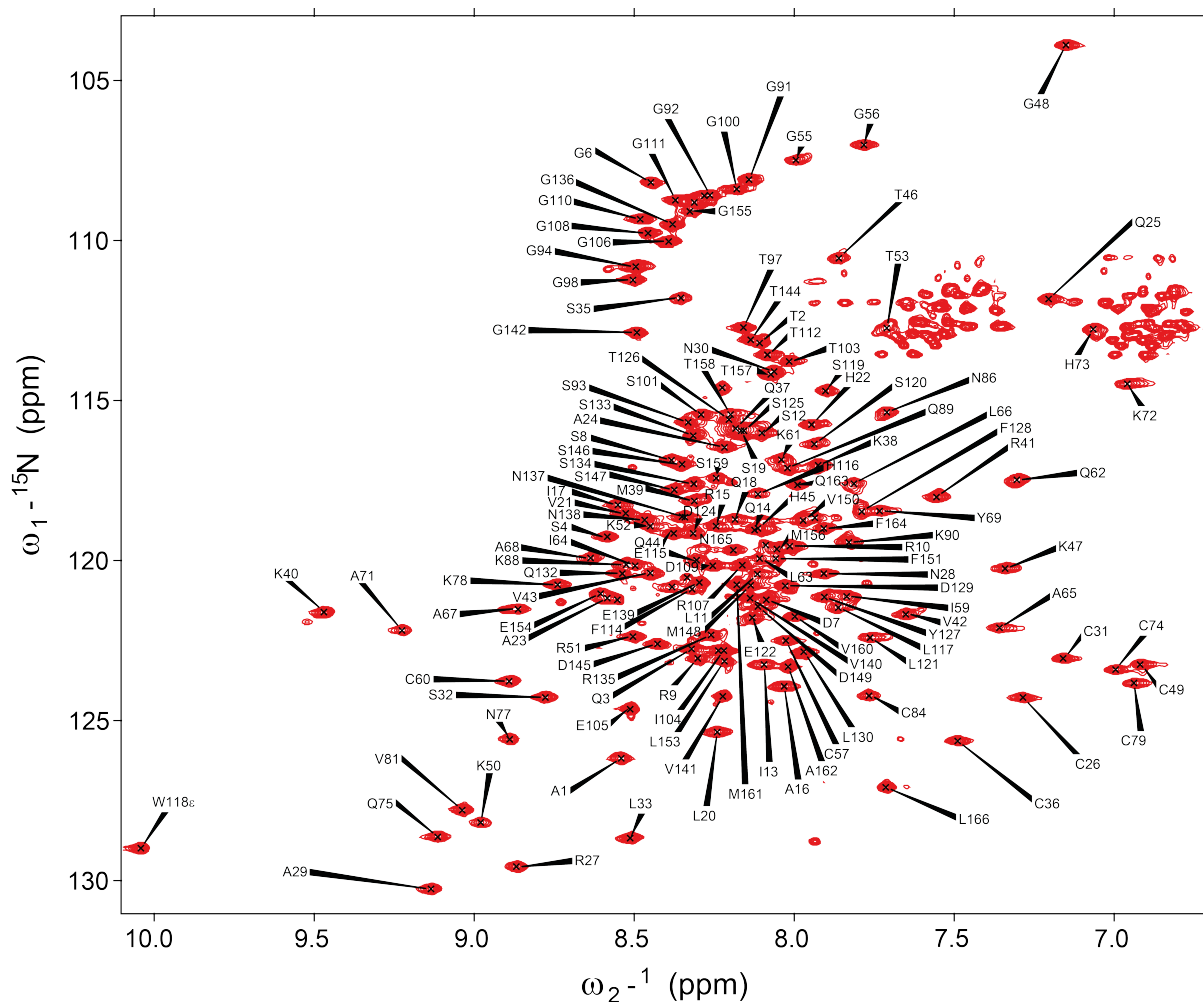
Figure 4.4.8: Backbone assignment of an extended construct of p300Taz2-p73TAD spanning the first 67 amino acids of p73. The construct shown is identical to the p300Taz2-p73TAD1 construct shown above. However the p73 transactivation domain peptide length has been increased to include another potential interacting sequence as determined in[20]. Most residues could be assigned, however some assignments of the linker between Taz2 and the peptide are missing. The assignment table is shown in the appendix. This data has been published in Krauskopf, K *et al.* 2018[245].

The resulting TALOS+ secondary structure prediction reveals another potential short helix in the very C-terminus of the peptide sequence (Figure 4.4.9). This agrees nicely with results that have been previously found by another group[20].
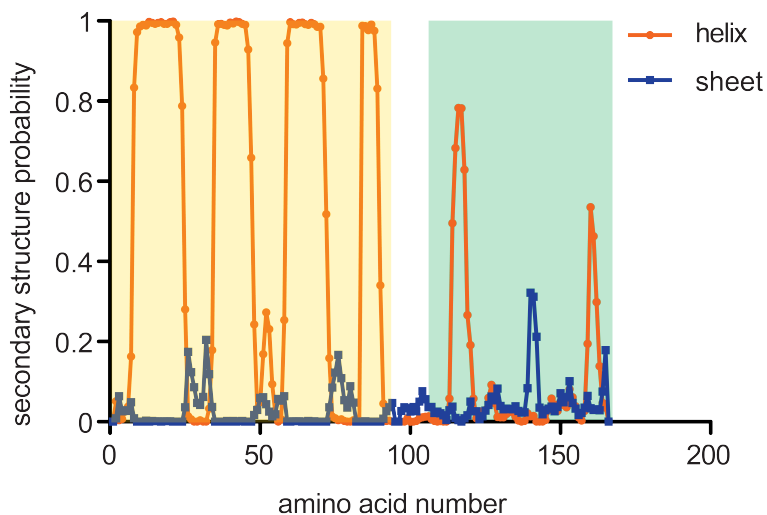
Figure 4.4.9: Chemical shift based secondary structure prediction of p300Taz2-p73TAD. Secondary structure of p300Taz2-p73TAD was predicted with help of the TALOS+ algorithm. Helical probability is shown in orange with solid circles indicating a residue, β-sheet probability is shown in blue with solid squares indicating a residue. This data has been published in Krauskopf, K *et al.* 2018[245].

Additionally ^{15}N-HetNOE spectra revealed that two stretches that are more rigid could be found within the long p73 TAD peptide(Figure 4.4.10). The rigidity correlates with the predicted secondary structure elements found by the TALOS+ prediction. Both of these results indicate that the C-terminus of the long p73 peptide does, at least transiently, interact with the Taz2 domain.
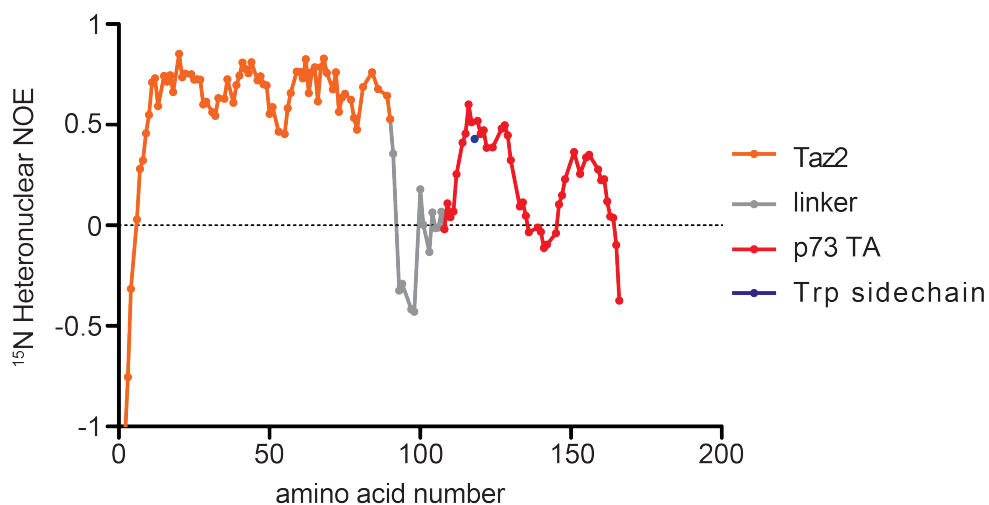
Figure 4.4.10: The ^{15}N-Heteronuclear NOE clearly shows lower rigidity between Taz2 and the p73TAD. The $\{^1H\}^{15}$N-hetNOE spectrum was recorded with a presaturation of 8 s and otherwise standard experimental conditions. Fragments of the fusion construct are color coded as described in the legend. This data has been published in Krauskopf, K *et al.* 2018[245].

Unfortunately, structure calculation was not possible to a satisfactory degree, partly due to the very low sequence complexity of the C-terminal part of the transactivation domain and partly to the lack of unambiguous NOE restraints. The sequence at the C-terminus of the peptide, defined as somewhat rigid by evaluation of the HetNOE spectrum, consists of 21 amino acids: **SSMDVFHLEGMTTSVMAQFNL**. Unfortunately this peptide contains multiple pairs of identical amino acids, thereby hampering the unambiguous assignment of NOE restraints.

In this sequence the most promising residues for assignable NOE contacts are three methionines, due to their methyl group. This should in principle enable manual NOE assignment due

to their specific chemical shift in a [^{13}C,^{1}H]-HSQC. Unfortunately the chemical shift of all three methyl groups is virtually degenerated in the ^{13}C, as well as, the ^{1}H dimension. Figure 4.4.11 shows an overlay of the Taz2-p73TAD construct and the Taz2-p73TAD1 construct with a cut-out of the methionine methyl region of the long construct.
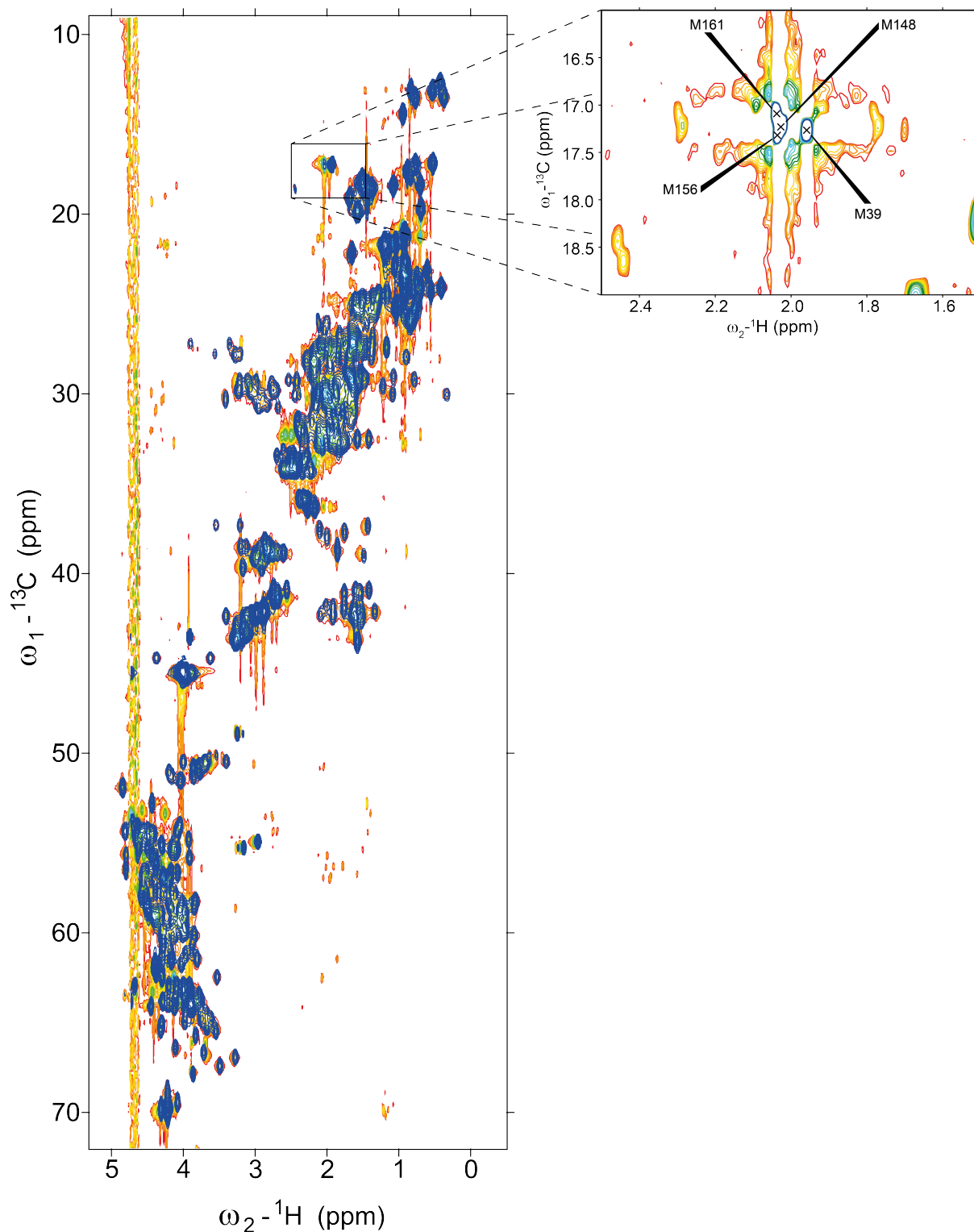
Figure 4.4.11: **[^{13}C,^{1}H]-HSQC overlay of p300Taz2-p73TAD1 and p300Taz2-p73TAD.** p300Taz2-p73TAD1 (blue) and p300Taz2-p73TAD (rainbow) show an almost identical [^{13}C,^{1}H]-HSQC, the major difference being additional resonances for the longer construct. The second part of the p73 transactivation domain features three additional, almost completely degenerate, methionines within ten amino acids (cutout, right).

Additionally the four phenylalanines within the sequence of the p73 TAD make analysis of aromatic ^{13}C-NOESY spectra virtually impossible in this region due to their massive spectral overlap

and the relatively low intrinsic resolution of such spectra. A structure, calculated from all gathered but partly ambiguous data, is shown in figure 4.4.12. The Taz2 domain, as well as the p73 TAD1 region is well defined and very close to the structure observed with the shorter construct. However, the second party of the peptide structure is not bound to the surface of Taz2 in any way. Short range and sequential NOEs define a short helix, ranging from V61 to F65 (p73 nomenclature). This indicates that at least transient interactions to the Taz2 domain exist, as it is very likely that a helical secondary structure does not exist in the free form of the peptide. Additionally interaction with Taz2 in this region of the peptides has been observed before[20].
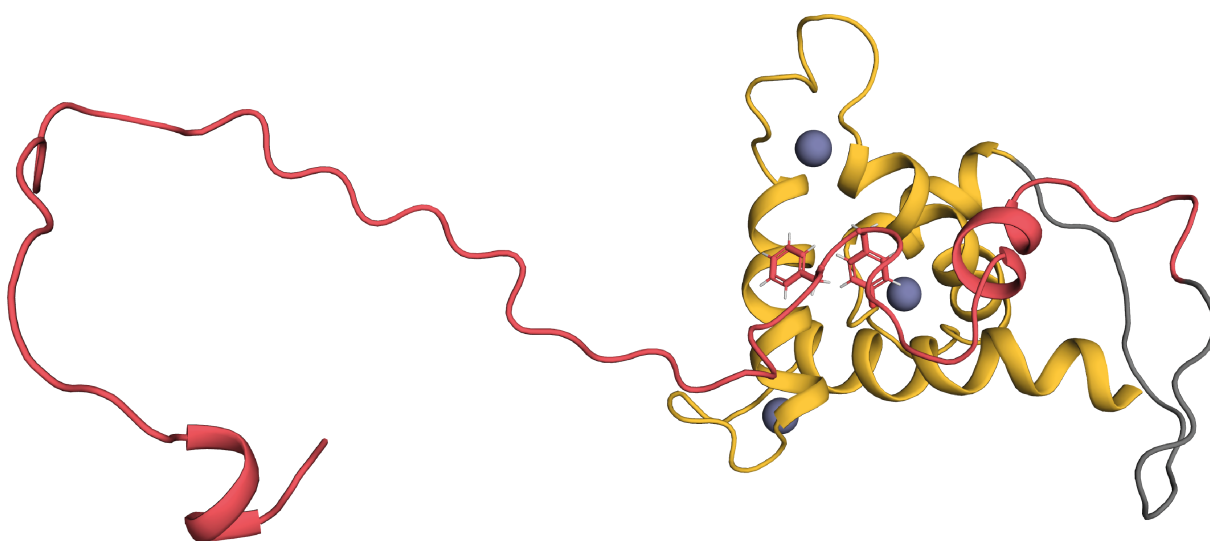
Figure 4.4.12: Cartoon representation of p300Taz2-p73TAD. The Taz2 domain is shown in orange, the linker between the domain and peptide in grey and the p73TAD peptide in red. Additionally zinc ions are shown as grey spheres. Both key aromatic residues of p73 (Y28 and F29) are shown as sticks.

An overlay of ^{15}N-HSQC spectra of both Taz-p73 fusion proteins shows only very little visible CSPs (Figure 4.4.13). The strongest CSP observable on the Taz2 domain can be attributed to K40 (construct nomenclature), however this residue is also the most sensitive to buffer inconsistencies. The CSPs of all Taz2 residues between both the long and the short construct were quantified in hope to get an idea where the second part of the peptide might bind onto the surface of Taz2. Quantified CSPs were color-coded and mapped onto a surface representation of Taz2 (Figure 4.4.14).
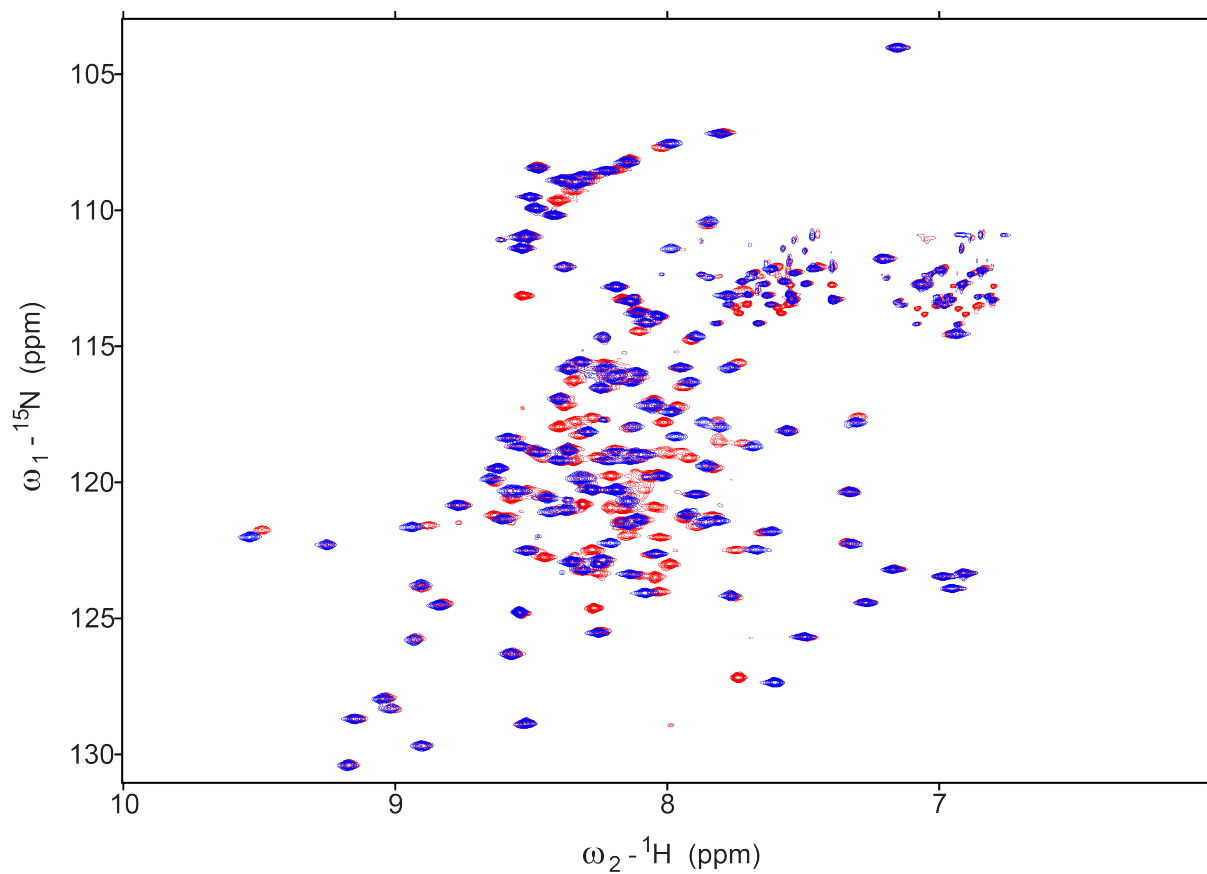
Figure 4.4.13: The overlay both p300Taz2-p73 fusion constructs shows only very little variance. [^{15}N,^{1}H]-BEST-TROSY spectra of p300Taz2-p73TAD1 (blue) and p300Taz2-p73TAD (red) are shown. Besides additional peaks in the spectrum of the longer construct only a few chemical shift perturbations can be observed.
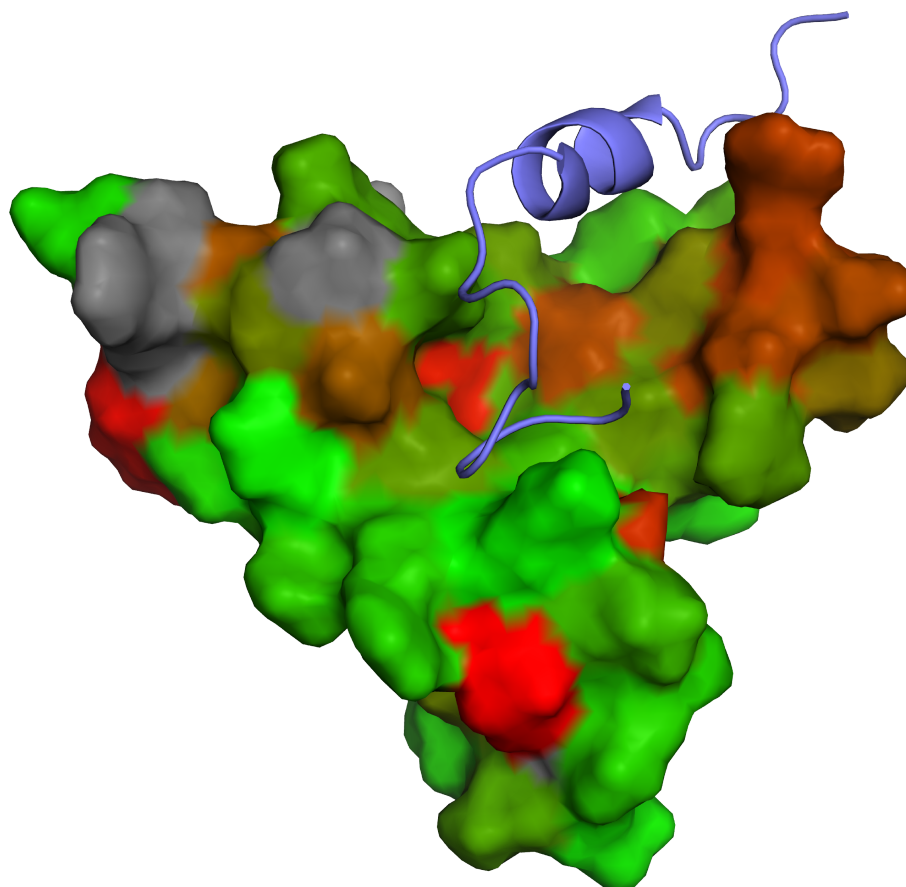
Figure 4.4.14: CSPs of the Taz2 domain upon binding of the p73TAD2 peptide are limited. Differences of CSPs between the constructs Taz2-p73TAD1 and Taz2-p73TAD are shown on the surface of Taz2. The residues are color-coded, green indicating no CSP between both constructs and red indicating the largest observed CSPs. The position of the p73TAD1 peptide is shown as a cartoon (purple).

Unfortunately, no clear secondary binding site could be observed. Most of the larger CSPs seem to be limited to the p73TAD1 binding region. This could either indicate that there is an exchange between the TAD1 and TAD2 peptide in the same binding site or that elongation of the peptide after the TAD1 changes the dynamics of TAD1 binding to the binding site. This seems more likely, as the calculated structure of Taz2-p73TAD displays the same binding site for the TAD1 peptide on the surface of Taz2.

Several other strategies were employed to acquire additional restraints for structure calculation of the longer construct:

- Addition of a cysteine residue at the C-terminus of the fusion construct for S-(1-oxyl-2,2,5,5-tetramethyl-2,5-dihydro-1H-pyrrol-3-yl)methyl methanesulfonothioate (MTSL) labeling and subsequent paramagnetic relaxation enhancement (PRE) measurement. Several labeling conditions were tested. Unfortunately the protein precipitates completely within several minutes after MTSL addition. This is most likely due to unspecific labeling of cysteines within the zinc-fingers of the Taz2 domain, although selective labeling of cysteines

in presence of other metal shielded cysteines within the same protein has successfully been done before[252].

- Similarly attachment of a lanthanide binding tag to the C-terminus of the protein seemed to be feasible. Protein expression and labeling with a lanthanide ion did work. However the resulting PRE line broadening effects were too strong, making evaluation of the resulting spectra impossible.

- Mutation of either phenylalanine of the peptide sequence to a tyrosine to increase spectral dispersion in aromatic side chain signals leads to instability and subsequent precipitation of the resulting protein.

- Fusion of separately expressed and labeled protein and peptide by means of a SortaseA enzyme was explored as well. In this case either Taz2 or the p73 TAD peptide could be labeled while the other part is expressed in an unlabeled manner. This would enable filter-NOE experiments, therefore greatly reducing the number of NOE cross peaks to evaluate. Unfortunately, the expression of the isolated p73 TAD peptide in large quantities was not possible due to a rather low intrinsic solubility of the expressed p73 TAD peptide as well as a low intrinsic expression rate of the tested peptide constructs. The expression of unlabeled p73 TAD peptide with a C-terminal cysteine residue did not lead to any significant soluble expression, therefore making external MTSL labeling prior to linking impossible.

4.5 Determination of Affinities of p300 Domains and p63/p73 Derived Peptides

For the transactivation domains of p53 and p73 the affinity towards p300/CBP domains has been frequently reported before[32;42;20;187;43]. For p63 initially Isothermal Titration Calorimetry (ITC) was tested. However this lead to the problem that multisite binding of the p63 TAD peptide had to be considered and that the association of the peptide towards the tested domains showed only little enthalpic contribution. To circumvent both of these problems a fluorescence polarization (FP) assay was employed. The peptides used for FP were chemically labeled with fluorescein, while the interacting domain was not modified in any way. The fluorescence polarization of serial dilutions of the corresponding domain with constant peptide concentration were measured. Final peptide concentration generally were 100 nM or 500 nM, while the protein concentration was varied from 0 up to 160 μM in case of the IBiD domain. In all cases the peptide concentration is at least an order of magnitude lower than the highest protein concentration, therefore guaranteeing that only the binding site with the highest affinity towards the peptide is occupied. Binding curves of all four TAD peptide binding p300 domains (Taz2, Kix, Taz2, IBiD) are shown in figure 4.5.1A and the resulting K_D values are given in table 4.5.1B. As expected the p63 peptide shows its highest affinity towards the Taz2 domain with a sub-micro molar affinity of $\approx$200 nM. All other

interaction domains (Taz1, Kix, IBiD) show low micro molar binding. The measured affinities are well within the plausible range, as predicted from literature values for p53 and p73 peptides.

A

B

p300 domain	p63 TA (amino acid 8-32) K_D [µM]
Taz2	0.20±0.02
Taz1	2.13±0.20
Kix	7.55±0.10
Ibid	5.04±1.17
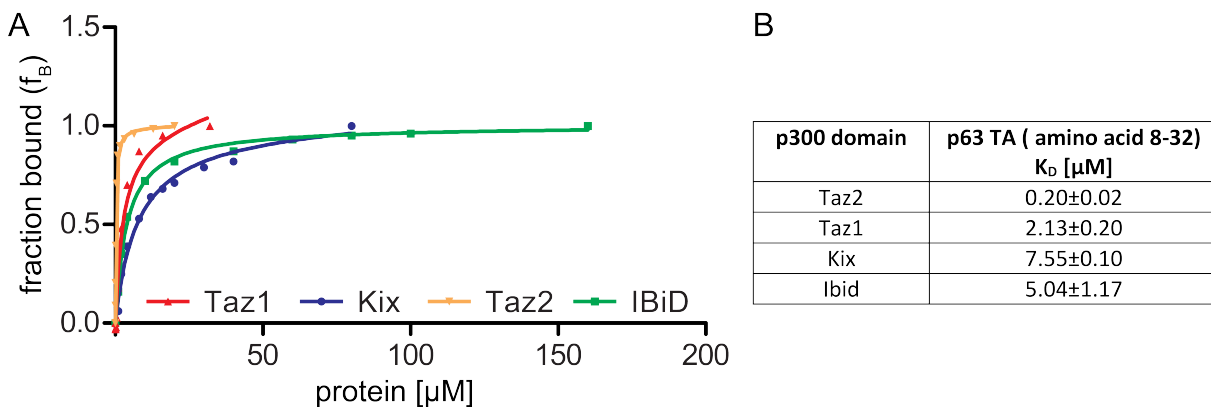
Figure 4.5.1: The Taz2 domain is the strongest binder of the p63 TAD by an order of magnitude. (A) Binding curves from measurement of fluorescence polarization of a p63 TA domain peptide (amino acid 8-32) with all p300 domains, known to be binding transactivation domains, are shown. Fraction of bound protein is plotted against the total concentration of the domain under test. (B) Table of dissociation constants of all tested p300 domains with the p63 TAD peptide.

Next several p73 derived mutant and phosphor peptides were tested for Taz2 affinity. As expected the p73 wild type peptide is the weakest binder with ≈ 1 μM. Phosphorylation of two residues which are situated in close proximity to positive side chains on the Taz2-p73TAD structure lead to a four-fold increase in affinity. Furthermore, a hybrid peptide consisting of the amino acids 8-15 of p63 and amino acids 15-31 of p73 showed another minor increase of affinity compared to the phosphorylated peptide, reaching an affinity that is slightly higher than that of p63 wild type peptide. Interestingly removing both aromatic side chains in the p73 TAD1 peptide (Y28A, F29A) does not completely abolish Taz2 binding, but severely affects the binding affinity. The resulting binding curves are shown in figure 4.5.2A and summed up in table 4.5.1. The K_D was estimated by an NMR titration experiment to be ≥ 50 μM (Figure 4.5.2B).
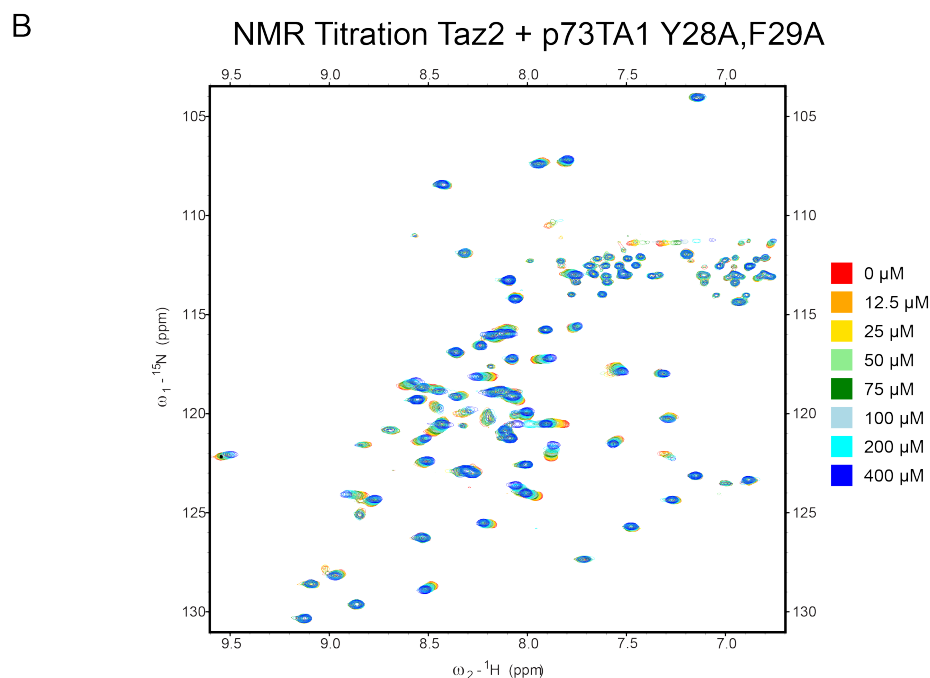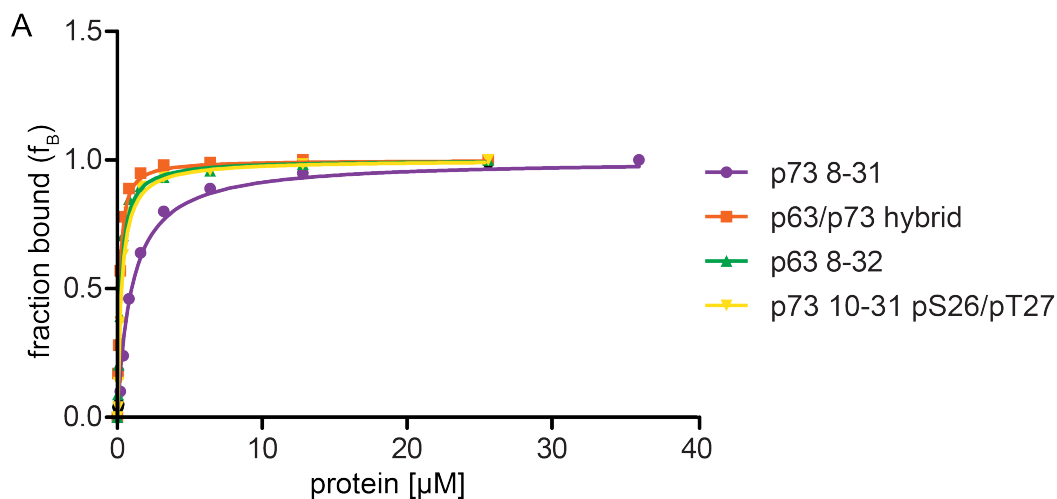
Figure 4.5.2: Exchange of 8 amino acids in the p73 transactivation domain peptide leads to an almost ten-fold increase in affinity to Taz2. (A) Wild type p73 TAD peptide (amino acids 8-31), wild type p63 TAD peptide (8-32) and several mutants/phosphorylated peptides were tested for Taz2 affinity. The hybrid between p63 and p73 was tested as it showed a greatly enhanced transactivation potential in a transactivation assay. The phosphorylated peptide was tested as analysis of the p300Taz2-p73TAD1 structure pointed towards a possibility for electrostatic enhancement of the binding by phosphorylation. (B) [^{15}N,^{1}H]-BEST-TROSY spectra with increasing concentrations of a p73 peptide consisting of amino acids 8-31 of p73 with the mutations Y28A and F29A. Interaction is still visible but largely impaired in comparison to wild type peptide. The estimated K_D is around 50 μM. This data has partly been published in Krauskopf, K *et al.* 2018[245]

Table 4.5.1: Summary of fluorescence polarization measurements with Taz2 and different p63/p73 peptides and mutants. Measurement was performed at room temperature (21°C). All domains were tested at least twice in independent measurements. Results were averaged and the error represents the standard deviation (SD) between measurements. The results have partly been published in Krauskopf, K *et al.* 2018[245].

peptide	p300 Taz2 K_D [μM]
p63 8-32	0.20±0.02
p73 8-31	0.94±0.06
p63(8-15)/p73(18-31) hybrid	0.12±0.01
p73 10-31 S26pS/T27pT	0.25±0.03
p73 8-31 Y28A/F29A	>50

The influence of exchanging the amino acids 8-15 of p73 towards those of p63 was tested in a transactivation assay in Saos2 cells as well (Figure 4.5.3). The experiments were performed by Katharina Krauskopf. The result clearly coincides with the observation of an almost an order of magnitude enhancement of Taz2 binding of p73 by exchange of these amino acids. p63 as well as p73 were used in naturally occurring isoforms, carrying a transactivation domain but lacking the negative regulatory transcription inhibition domain. The low intrinsic transactivation potential of TAp73β on the P21 promoter was completely restored to TAp63γ levels by exchanging either amino acids 1-15 or 8-15 to the p63 sequence.
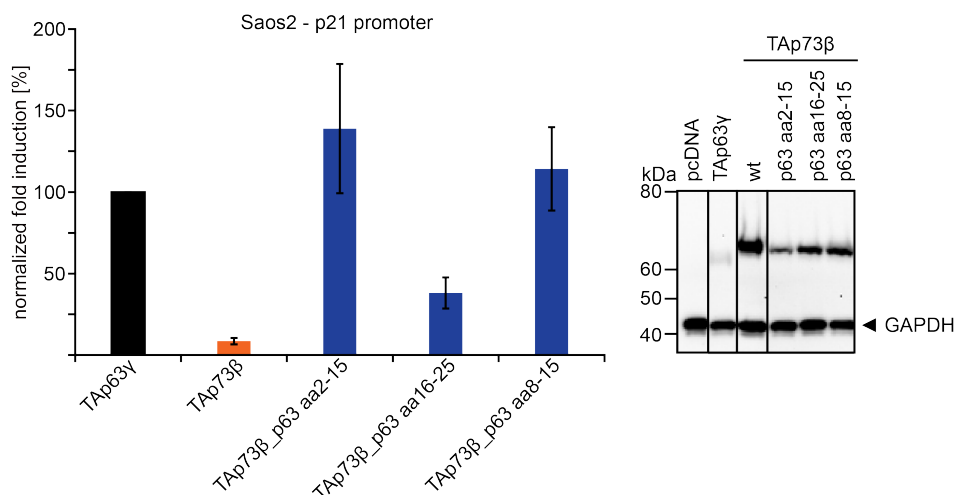
Figure 4.5.3: Exchanging the amino acids 8-15 in p73 to the equivalent amino acids of p63 is sufficient to restore the transactivation potential of p63 onto p73. A transactivation assay in Saos2 cells on the p21 promoter was performed with TAp63γ as a control and normalization factor. Several hybrids based on TAp73β, exchanging parts of the transactivation domain to that of p63, were tested for transactivation potential. Fold induction was normalized to GAPDH expression level and to TAp63γ. Experiments were performed in triplicates. Error is represented as standard deviation (SD). The experiments were performed by Katharina Krauskopf. Modified from Krauskopf, K *et al.* 2018[245].

4.6 Inhibition of p300 in Ovaries Under DNA Damaging Conditions

p300/CBP plays an important role in the process of transactivation, as it enables the reading of the DNA sequence of interest by removing histones via acetylation. Without removal of histones from the DNA via acetylation/methylation it remains decorated with them, greatly hampering the readout by the RNA Polymerase II complex. Therefore inhibition of p300/CBP within cells should reduce proapoptotic protein production upon DNA damage. This was tested via 3D staining of mouse ovaries for Y-box-box-binding protein 2 (MSY-2) under different cellular conditions. MSY-2 is a protein exclusively expressed in oocytes of different stages and is therefore ideal for selective staining of these cells. Ovaries were cultured and treated with doxorubicin to induce DNA damage. Additionally a novel, selective p300/CBP HAT inhibitor (A-485) was added[253]. Additionally different ovaries were treated in the same manner; however an inactive control inhibitor (A-486)[253] was added. The results are shown in figure 4.6.1. Both compounds are structurally virtually identical, except for the positioning of a single urea group bound to an aromatic ring.
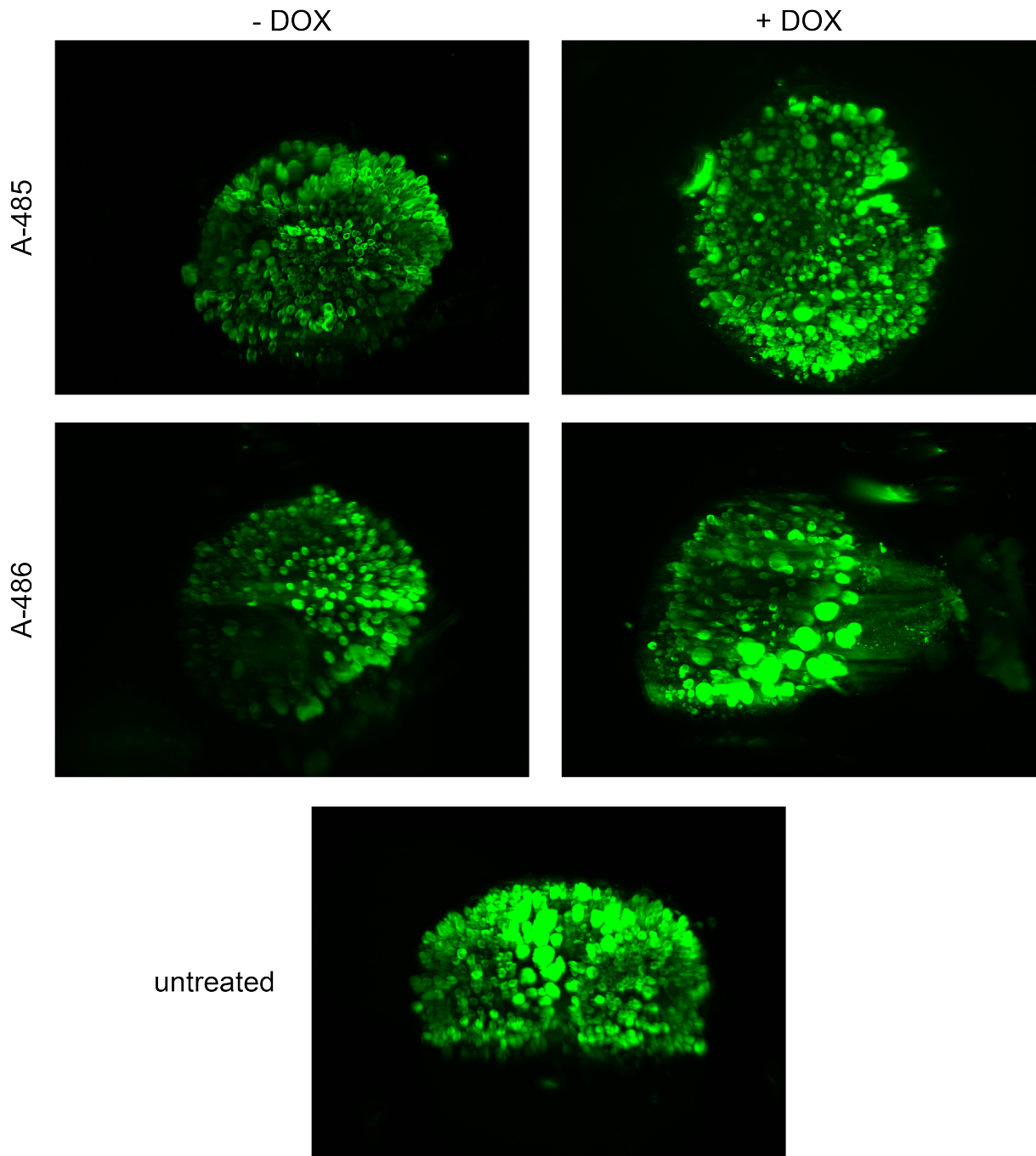
Figure 4.6.1: Intensity Z-projections of mouse ovary 3D stainings under DNA damaging conditions with a p300 inhibitor or an inactive derivative of the inhibitor. Mouse ovaries were harvested from P8 mice and cultured under different conditions: Ovaries were treated with DOX to induce DNA damage while p300 was inhibited by the novel inhibitor A-485[253] or the structurally virtual identical mock control A-486[253]. Untreated control ovaries were cultured in parallel without addition of inhibitors or doxorubicin. After cultivation the ovaries were fixed, stained for MSY and imaged with a light sheet microscope[242;243]. Images were processed in Fiji[244] and a Z-stack based on the intensity of the fluorescence signal was generated. Ovary preparation and staining have been performed in co-operation with Katharina Krauskopf, imaging has been performed by Katharina Hötte.

As expected the treatment of ovaries with doxorubicin and A-486 leads to a loss of primary oocytes (smaller oocytes) while secondary oocytes (larger oocytes) are not sensitive to DNA

damage. In contrast to this doxorubicin treatment in addition with A-485 seems have a oocyte preserving effect. This indicates that the p300/CBP family plays an important role in the pathway leading to apoptosis in oocytes under DNA damage. Control experiments with A-485 or A-486 do not indicate a toxic effect of the inhibitors themselves. This experiment would have to be repeated with another mouse strain, expressing Green Fluorescent Protein (GFP) directly in the oocytes, to remove background staining and enable counting of individual oocytes.

4.7 Acetylation of TAp63 under DNA Damaging Conditions

H1299 cells, stably expressing TAp63α, were treated with doxorubicin to trigger phosphorylation and activation of the protein. Protein was immonoprecipitated and digested for mass spectrometry. Primarily this dataset of phosphorylated residues within TAp63α was generated to determine the kinases relevant for TAp63α activation[1]. Additionally the dataset was evaluated for acetylated residues. The result is shown in figure 4.7.1. This dataset might be incomplete, as the experimental conditions favored enrichment of phosphorylated peptides and therefore some acetylated peptides might not be represented. Several of the found acetylations might be a result of PCAF, Tip60 or other acetyl transferases. These experiments were performed by Marcel Tuppi.
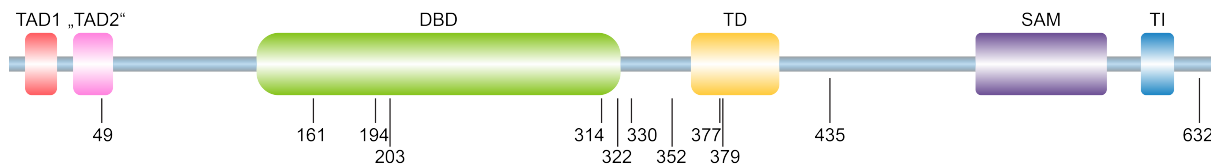
Figure 4.7.1: Mass spectrometry reveals multiple acetylation events on p63 in vitro. Mass spectrometry data generated for a different project was reevaluated for acetylation events within p63. A cell line stably expressing TAp63α under an inducible promoter was induced for expression and subsequently treated with doxorubicin to induce DNA damage. p63 was then purified from the cells and digested for mass spectrometry. Several acetylation events could be found, clustering mainly into the area between the C-terminus of the DBD and the TD.

In total twelve acetylation sites were found, mostly clustering in the region between the C-terminus of the DBD and the TD. Six of the acetylation sites are located within folded domains (161, 194, 203, 377 and 379) the rest is situated within intrinsically unfolded regions. For functional testing of the acetylation sites, all lysine residues were mutated to either arginine, thus preventing acetylation, or glutamine, therefore mimicking acetylation. Glutamine is frequently used to mimic acetylation although it is considerably smaller than acetyl-lysine[254]. As K377 and K379 are situated within the tetramerization domain, the effect on dimer formation was tested via native page. Neither an acetylation-mimicking mutation nor an acetylation-preventing mutation had an impact on the native dimeric state of the proteins. This was also independent on single or double mutations (Figure 4.7.2).
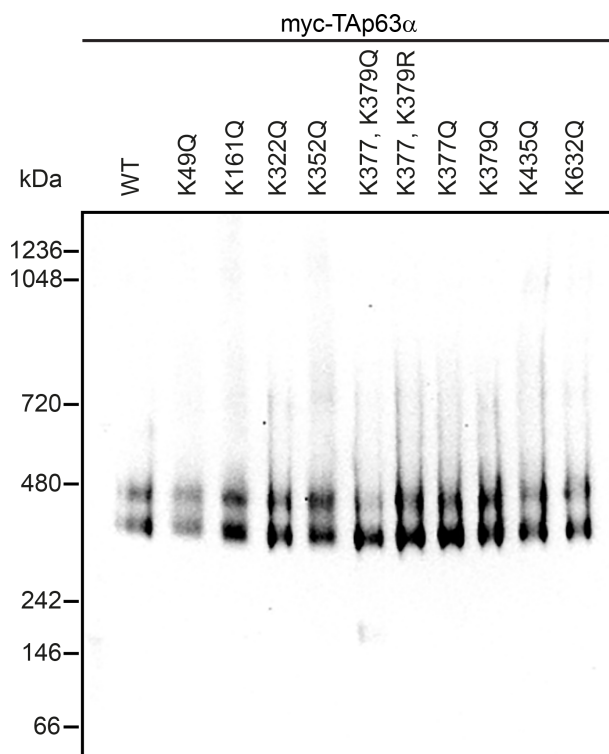
Figure 4.7.2: All TAp63α acetylation mimics are dimeric in vitro. H1299 cells were transfected with WT or acetylation mutants of TAp63α and subsequently checked for oligomeric state via native page/western blot. In all cases a double band at around 480 kDa can be observed, indicating a dimeric state.

Although the mutations in the tetramerization domain do not seem to have a disrupting effect on the oligomeric state of the protein in cell culture based assays, the thermal stability of the isolated tetramerization domains was severely compromised. In a thermal shift assay (TSA) (Figure 4.7.3), the melting point of both tetramerization domains, carrying either the K377Q or K379Q mutation was lowered by approximately 30°C. Additionally a double melting event was observed for the K377Q mutation, potentially indicating a stable dimeric conformation, prior to unfolding completely at higher temperatures. The values for melting points are given in table 4.7.1.

Table 4.7.1: Summary of thermal shift assay melting points of WT and acetylation mimicking mutations.

Construct	Melting point 1 [$^\circ$C]	Melting point 2 [$^\circ$C]
WT	82.5	-
K377Q	53.7	76.5
K379Q	56.1	-
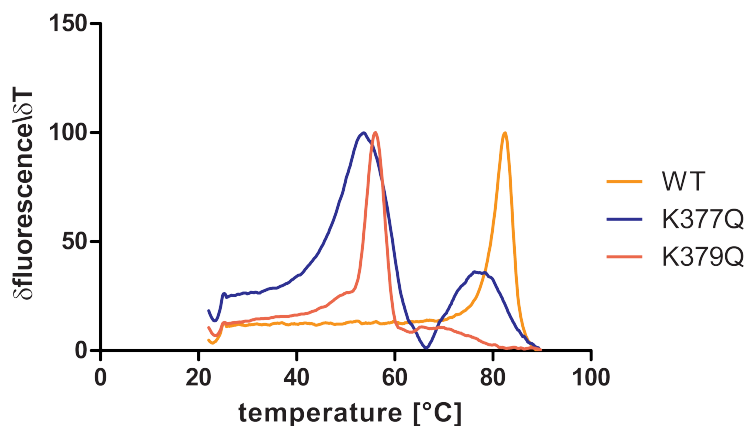
Figure 4.7.3: Acetylation mimic mutants within the tetramerization domain display a large thermal destabilization. Thermal stability of mutants of the isolated tetramerization domain of p63, mimicking acetylated residues found in mass spectrometry, were tested for thermal stability in a thermal shift assay (TSA). Due to the extraordinary stability of the domain itself the experiments were performed at pH 4.5 close to the pI of the wild type protein. The melting points obtained therefore do not represent the actual melting temperatures under physiological relevant conditions. The experiment was performed in triplicates.

Lysine residues are important amino acids for other post-translational modifications via isopeptide bond formation. These modifications can have a big influence on protein stability or localization. To test protein stability of TAp63 variants a cycloheximide (CHX) chase experiment was performed. In this case all mutations were introduced in TAp63γ, as it is an intrinsic tetramer. This leads to much shorter half-life times of the synthesized protein, making the read out of the experiment more independent on general cellular status upon inhibition of the ribosomes due to cycloheximide. The total expression level of protein prior to addition of CHX differed substantially. This indicates that different mutants have either substantially different synthesis rates, turnover rates or protein stability. Exemplary western blots are shown in figure 4.7.4.
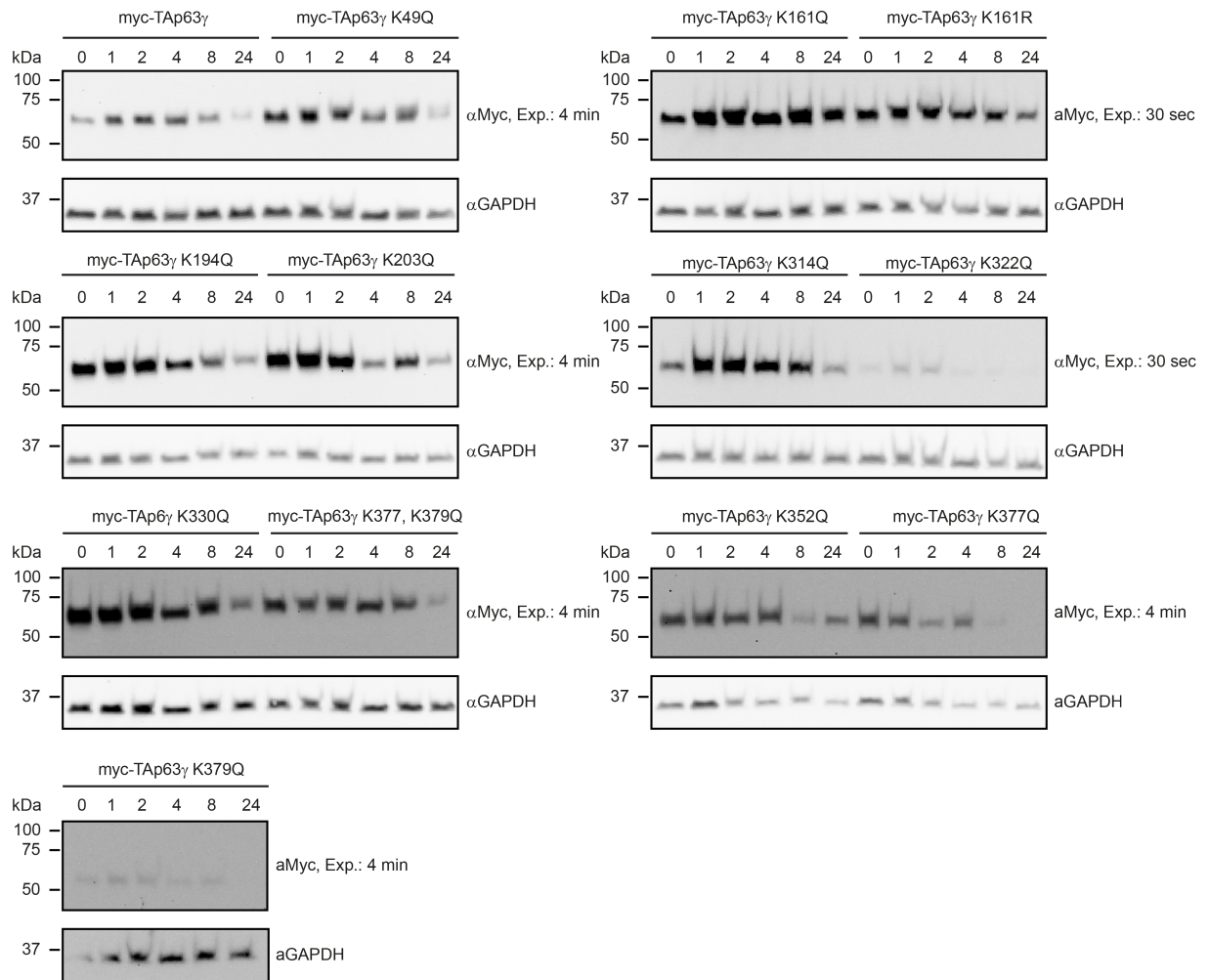
Figure 4.7.4: Protein half life time is largely reduced for acetyl-mimic mutations in the TD of p63. H1299 cells were transfected with different constructs containing K to Q mutations on the background of TAp63γ. After 24 h the medium was exchanged for fresh medium containing 50 μg/l CHX. Samples were harvested at indicated time points and subject to western blot for protein level quantification.

To get a quantitative result expression levels of the mutants after one and 24 h were compared (Figure 4.7.5). The one-hour time point was used as the reference because for some samples the visible protein expression is higher one hour past CHX treatment compared to the initial sample.
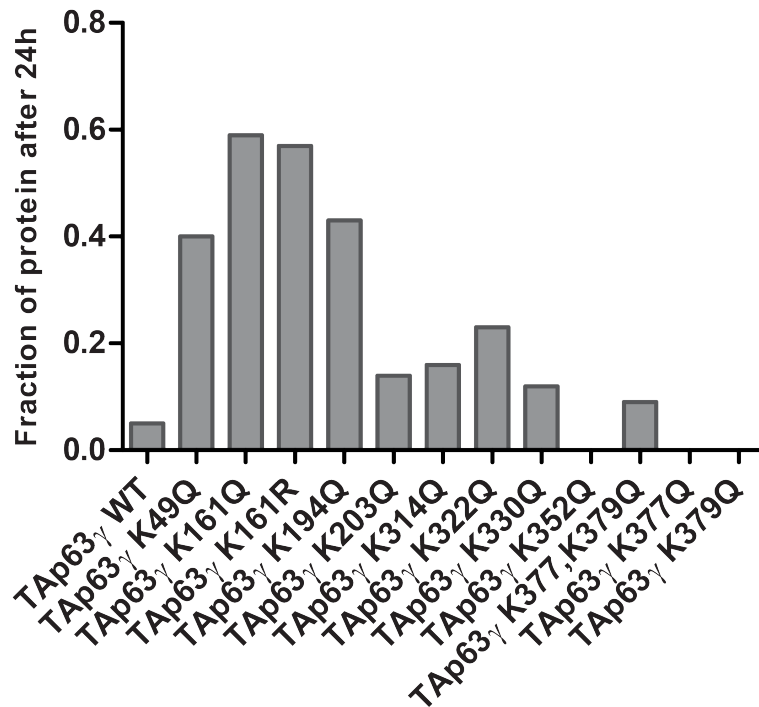
Figure 4.7.5: Protein turnover rates are highly dependent on the acetylation mimic. Protein levels of TAp63γ mutants after 24 h of CHX treatment were normalized with their expression level after one hour of treatment.

While wild type protein abundance drops to 5% after 24 h compared to the level measured at one hour, several other mutations are significantly more stable. Especially the mutation of K161 leads to a drastic increase in stability, independent of the type of mutation (K161R or K161Q). This suggests a K161 as a potential residue for direct post-translational modification by Ubiquitin. Mutation of K49 or K194 also leads to a stabilization of the protein. However in this case the K→R mutants were not tested, therefore it is not known if they could potentially be a direct target for modification as well. Mutation of either residue in the TD (K377Q or K379Q) lead to a loss of the complete protein after 24 h. Interestingly the double mutation (K377Q and K379Q) has a higher intrinsic expression and retains some protein even after 24 h. Finally, the transactivation potential of acetylation mimics and acetylation dead mutants on the background of TAp63γ was tested. No significant differences in transactivation potential could be detected across any of the mutants (Figure 4.7.6A).
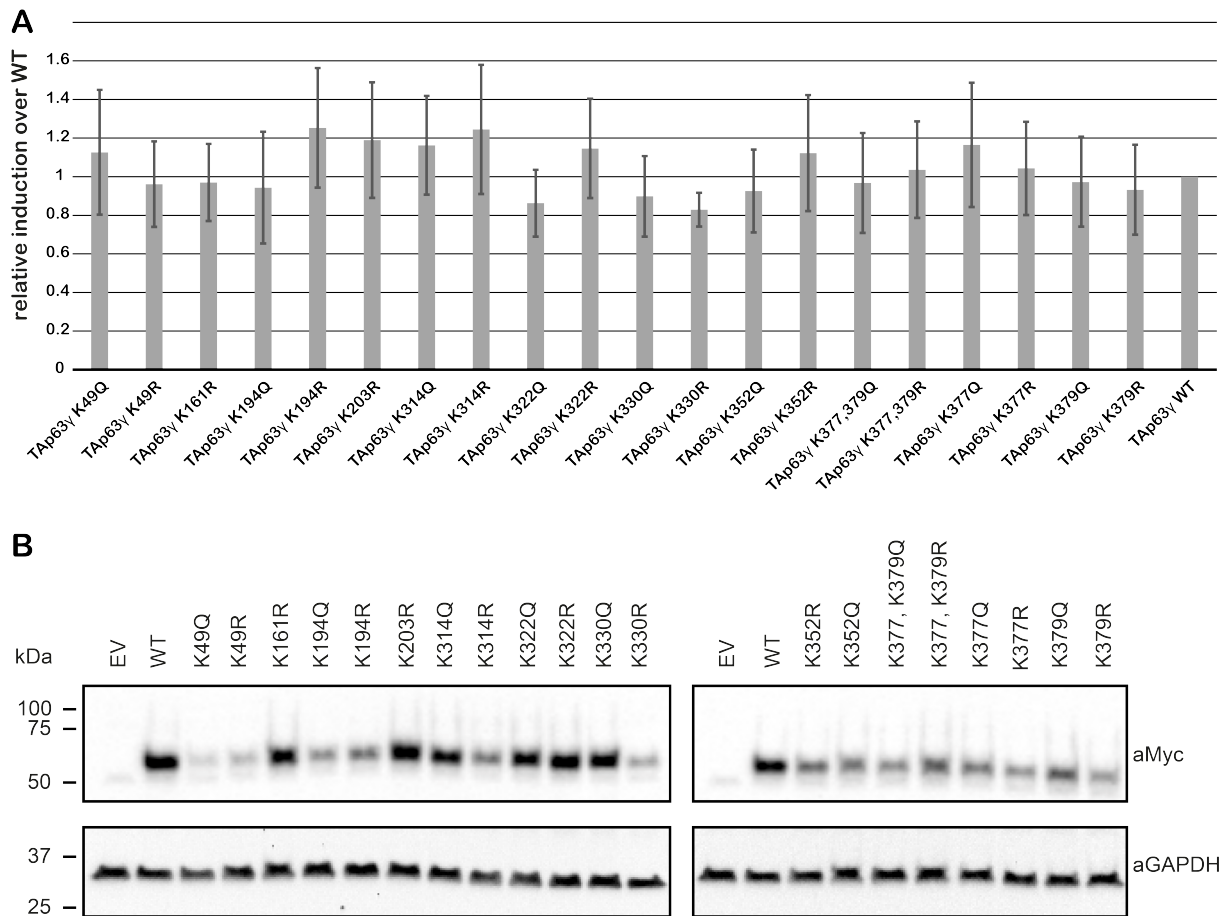
Figure 4.7.6: The transactivation potential of TAp63γ acetylation mimics is nearly identical on the p21 promoter despite significant differences in expression level. (A) The transactivation potential of acetylation mimics (K→Q) as well as acetylation dead mutants (K→R) of TAp63γ was tested in H1299 cells on the p21 promoter. Transactivation was normalized on WT protein level. (B) Protein expression of proteins tested in the transactivation assay and loading control (GAPDH).

4.8 Phosphorylation kinetics of TAp63α

To get an understanding of the in-vitro phosphorylation kinetics of CK1δ kinase on p63, the p63 Phosphorylation Activation Domain (PAD) peptide was pre-phosphorylated at S582 by MK2 kinase, as a surrogate for Chk2 kinase. Then the kinase was separated from the peptide by gel filtration. For both states a backbone assignment was performed (Figure 4.8.1).
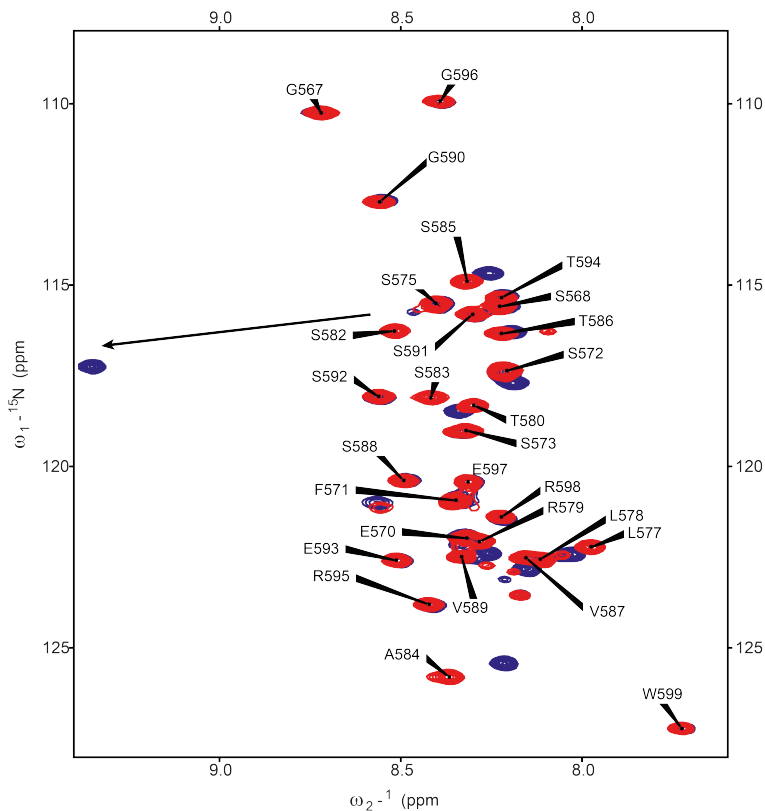
Figure 4.8.1: Assignment of the unphosphorylated variant of the PAD peptide and overlay of the S582 mono-phosphorylated peptide. The dispersion of the ^{15}N HSQC peaks indicates a non-folded state of the peptide sequence. Shift differences between the unphosphorylated peptide and the mono-phosphorylated variant are limited to S582 and neighboring amino acids.

Then a kinetic measurement of CK1δ phosphorylation was performed at different temperatures and the end-state of the phosphorylation was assigned as well (Figure 4.8.2). Furthermore the direct phosphorylation state of all residues was determined by a 2D variant of the HN(CAP) experiment (Figure 4.8.3).
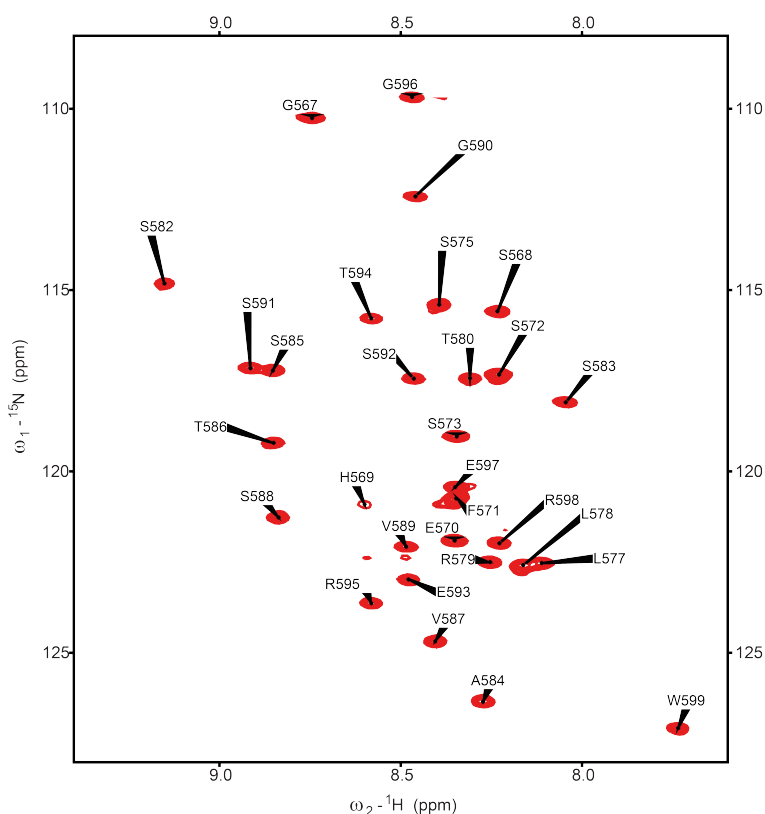
Figure 4.8.2: Assignment of the PAD peptide after phosphorylation with MK2 and CK1δ. The ^{15}N HSQC looks completely different in comparison to the MK2 phosphorylated or the completely unphosphorylated state. The observed chemical shifts might indicate a folded structure but analysis of the CA/CB chemical shifts indicate a complete disorder of this peptide.
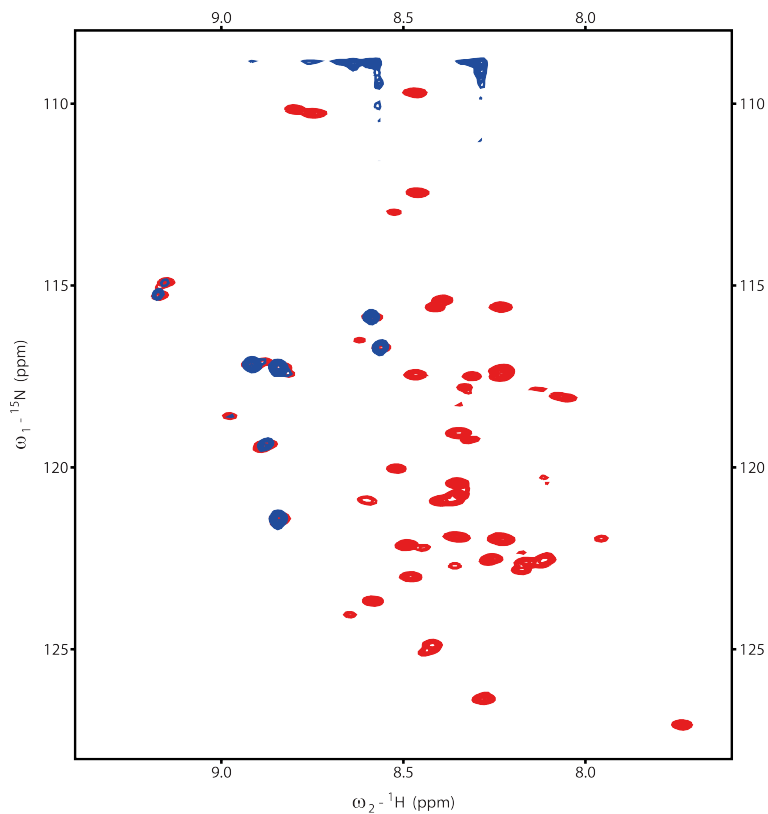
Figure 4.8.3: Overlay of a fully CK1δphosphorylated PAD sequence (red) with a 2D variant of the iHN(CA)P experiment (blue). All residues present in iHN(CA)P are phosphorylated serine or threonine residues.

The observed phosphorylations are shown in figure 4.8.4. Interestingly both kinases show an additional phosphorylation besides their consensus sequence. In case of MK2 the expected S582 and additionally S585 will get phosphorylated. The phosphorylation of S585 is very slow for MK2, thereby the reaction can easily be stopped at the S582 phosphorylated states, if incubation times are kept under two hours. In case of CK1δ, T586 is phosphorylated in addition to the expected S585, S588, S591 and T594.
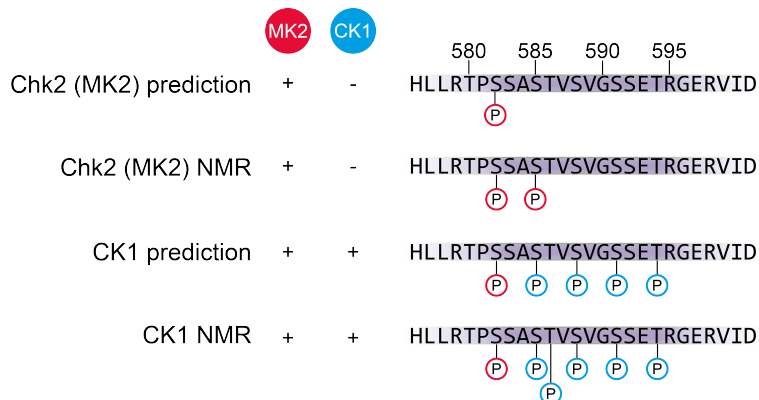
Figure 4.8.4: Expected versus found phosphorylated residues by MK2 and CK1δ kinases. The Chk2 surrogate kinase is expected to phosphorylate only at residue S582 but was found to additionally phosphorylate S585 after extensive incubation. The unique consensus sequence of CK1δ, phosphorylating a serine/threonine residue when a phosphorylated serine or threonine in position i +3 is present, should lead to four additional phosphorylated residues. However in the experiment an additional phosphorylation at T586 could be detected.

Next S582 pre-phosphorylated peptide was used to determine the kinetics of CK1δ phosphorylation. Initially the experiment was run at 298K and 1:1000 kinase:peptide ratios. The resulting kinetics are shown in figure 4.8.5. Interestingly the result shows a potential processivity for S585 and S588 whereas the phosphorylation was ≈30 fold slower for S591 and T594.
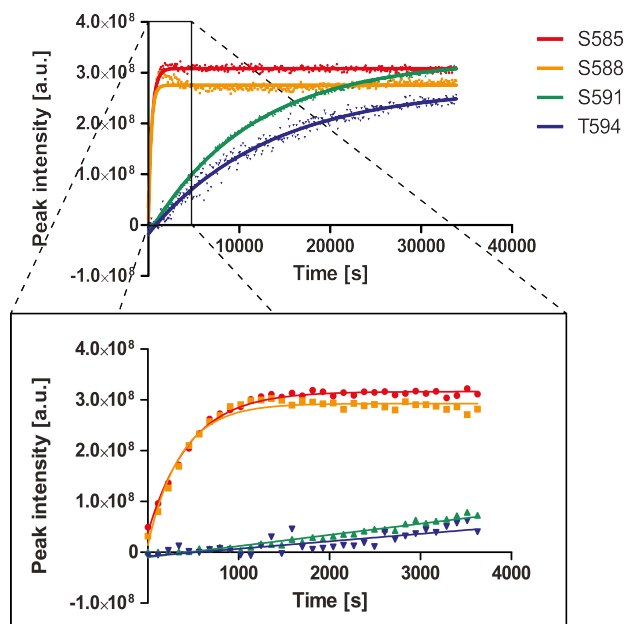
Figure 4.8.5: Phosphorylation kinetics at 298K and 1:1000 kinase:peptide molar ratio. The four phosphorylation events predicted, according to the consensus sequence, can be observed in the NMR experiment. The first two reactions (S585 and S88) are much faster than the third and fourth phosphorylation (S591 and T594).

To understand if the difference between the two "fast" phosphorylations and the two slow phosphorylation (kinetic "breakpoint") is a feature of the kinase or a result of the peptide sequence, several mutations were introduced into the peptide sequence. The mutants were designed to better match the peptide sequence to the reported consensus sequence of CK1δ, or inhibit off-

sequence phosphorylation (T586A). None of the tested mutants had a significant effect except for a mutation of two amino acids between the third and fourth phosphorylation (S592V, E593G). This mutation leads to drastic reduction in the difference between the "fast" and "slow" process of phosphorylation to a factor of $\approx$2 (Figure 4.8.6).
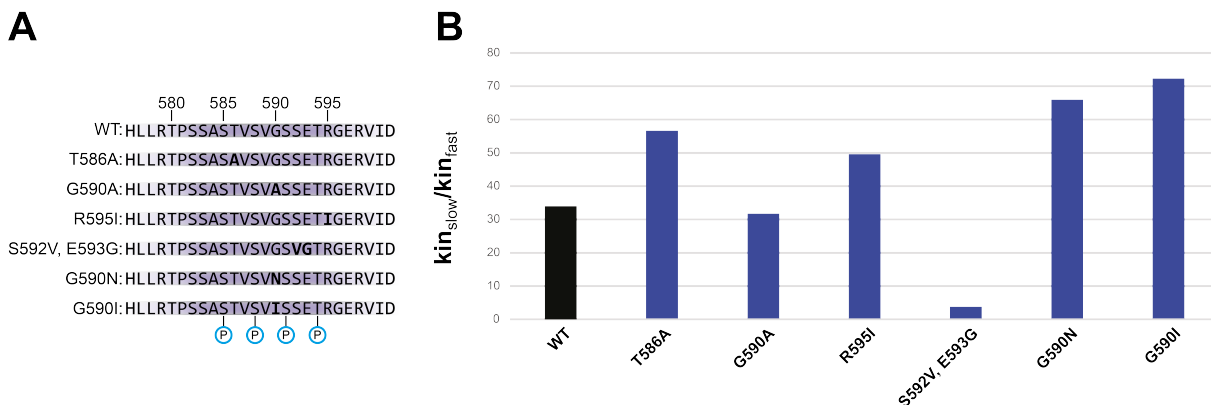
Figure 4.8.6: Influence of the specific peptide sequence on the phosphorylation kinetic of the 3rd and 4th phosphorylation. Mutants of the PAD peptide sequence were tested for phosphorylation kinetic analogous the wild type sequence Figure 3.8.3). The tested peptides are shown in (A), the resulting relative kinetics of the slow/fast phosphorylation are shown in (B).

Additionally the temperature dependence of the break point was tested by increasing the temperature to 303K. This resulted in a much faster overall kinetics therefore the normal procedure of external kinase/peptide mixing was replaced by direct injection of ATP into a mixture of peptide (apparatus shown in figure 3.18.1) and kinase within the magnet (Figure 4.8.7). Direct injection of kinase into a sample of peptide and ATP was tested as well but lead to significantly lower rates, most likely due to sheer forces leading to unfolding of the kinase.
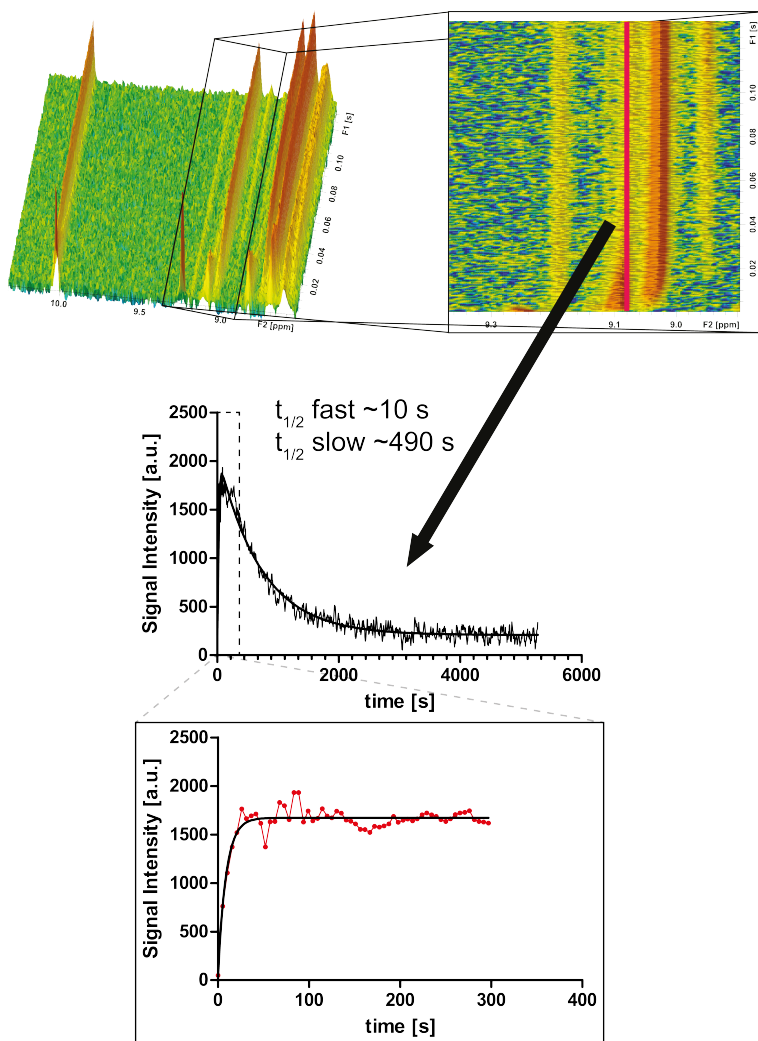
Figure 4.8.7: Direct injection kinetic at 303K and 1:100 kinase:peptide ratio. ATP was directly injected into a Shigemi tube within the magnet and a pseudo 2D spectrum with 5.2 s/increment was recorded. The fast and the slow process was quantified by extraction of a single column of the pseudo 2D and subsequently used for fitting.

Furthermore a crystal structure of CK1δ with a triple phosphorylated PAD peptide was obtained in cooperation with Apirat Chaikuad (Knapp group) and Marcel Tuppi. Interestingly the structure shows a product bound state of the peptide, therefore the 3rd phosphorylated residue is located within the active site and the phosphate group of pS588 is pointing towards the ATP binding cleft. The resulting structure is shown in figure 4.8.8 and 4.8.9.
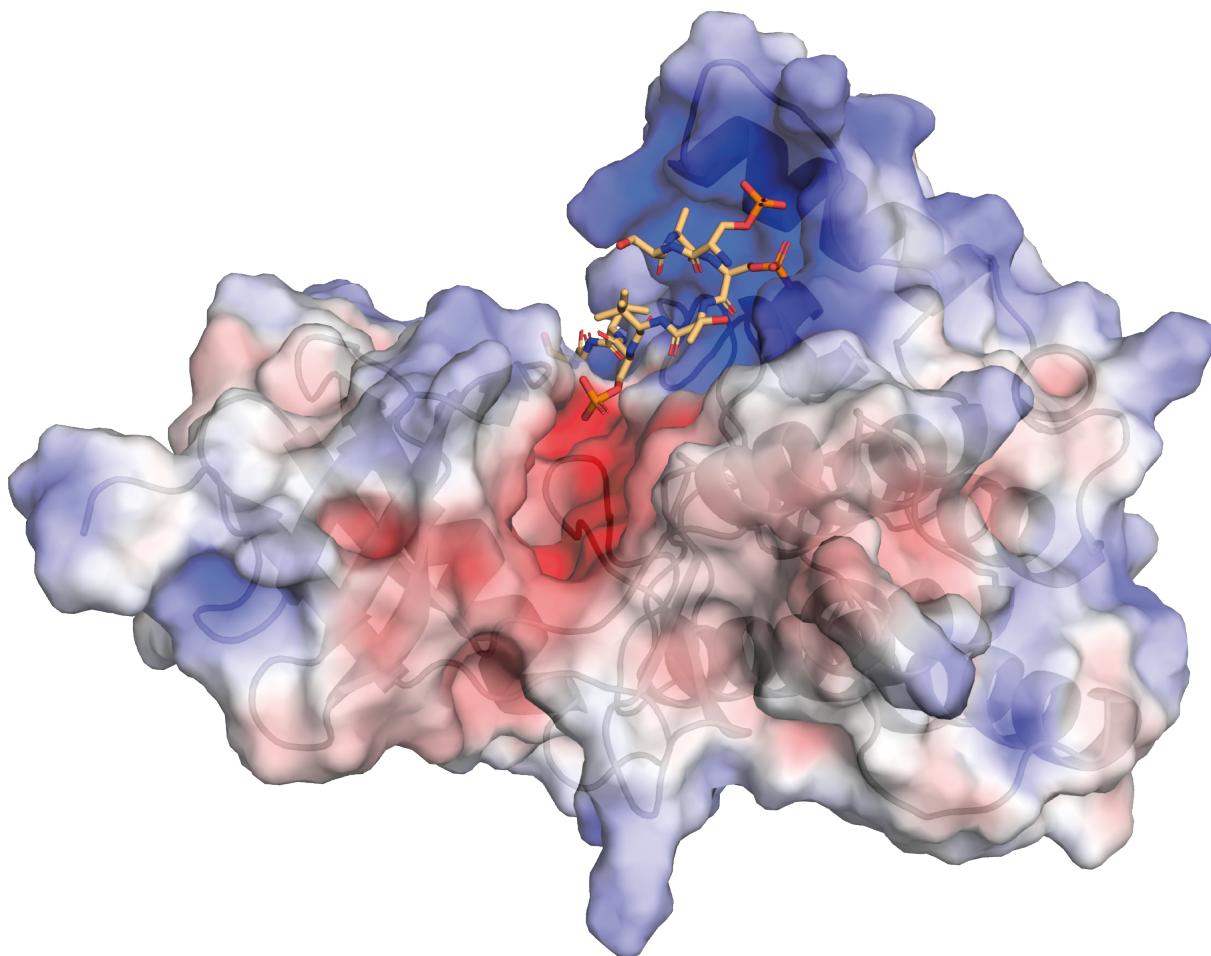
Figure 4.8.8: Structure of the triple-phosphorylated p63 PAD peptide bound to CK1d at 2 Å resolution. The surface of CK1δ is displayed in a semi-translucent manner with underlying cartoon representation. The surface is colored based on the electrostatic potential as calculated by APBS.
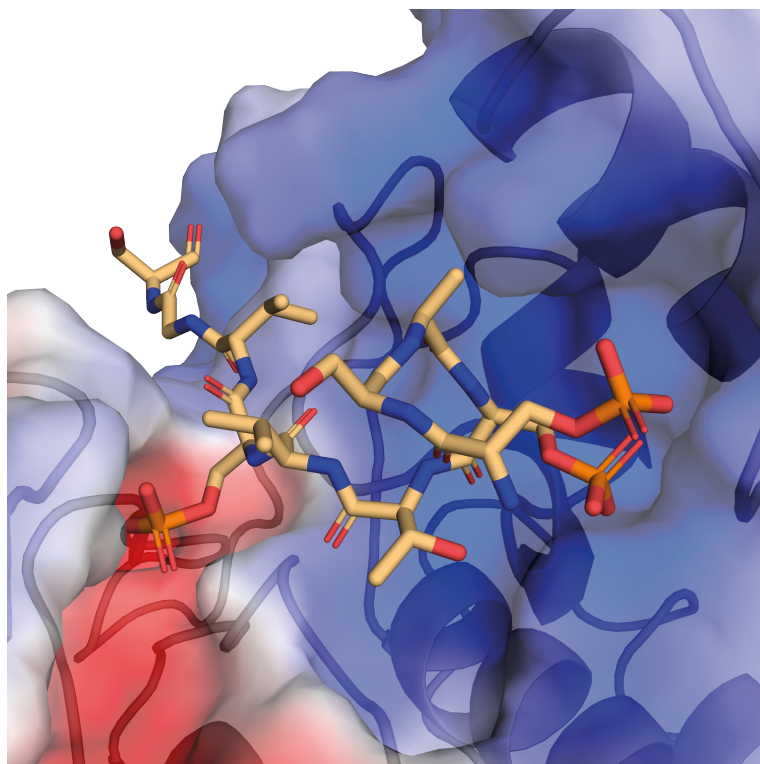
Figure 4.8.9: Close-up of the binding interface between CK1δand the triple-phospho peptide. The color code is analogous to Figure 3.8.7. Two of the three phosphate groups are bound to a basic surface patch, while the third phosphate is pointing into the ATP binding cleft (colored in red due to negative surface potential), thereby binding in a product-bound configuration.

A LigPlot interaction map of the kinase with the peptide reveals that the interaction is mainly mediated by charge-charge interactions of positively charged side chains K130 and R178 in CK1δ and the phosphorylated serines within the peptide (Figure 4.8.10). Additional interactions stem from hydrogen bonds and van-der-Waals interactions. Interestingly the phosphate group attached to the first serine (S582) does not seem to make any direct contact towards a specific side chain of the protein.
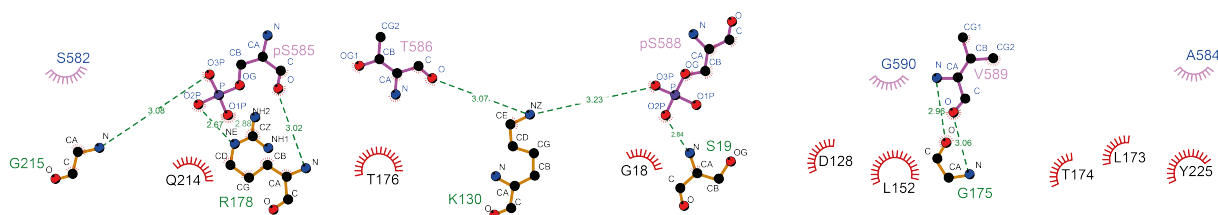
Figure 4.8.10: Interaction map of CK1δwith the triple-phosphorylated peptide. The interaction is mainly mediated by hydrogen bonds of the phosphorylated residues S582 and S585 with basic side chains of CK1δR178 and K130. Additionally the backbone amides of S19, G175 and G21 are involved in peptide binding as well. G175 forms a double hydrogen bond with V589 of p63 where the amide of CK1δG175 functions as a proton donor and CO of V589 as an acceptor and vice versa. Additionally several van-der-Waals contacts can be observed as well.

To get an idea if the CK1δ phosphorylation kinetic is similar in full length protein, modified TAp63α was expressed ^{15}N-labeled, purified and MK2 pre-phosphorylated. After a second round of gel filtration the protein was incubated with 1:100 molar ratio of CK1δ kinase. The reaction was stopped after 4 h by addition of EDTA. Then the peptide sequence of interest was purified from the protein (described in detail in section 3.17.2). Figure 4.8.11 shows two

^{15}N-HSQC spectra of peptides obtained from full-length TAp63α. MK2 phosphorylation of p63 generates a single phosphorylation (Figure 4.8.11A), as observed with the isolated PAD peptide (Figure 4.8.3). Therefore almost the complete assignment could be transferred from the peptide sequence. In contrast to this the CK1δ phosphorylation of TAp63α leads to a much more chaotic spectrum (Figure 4.8.11B), making a transfer of the assignment from the isolated peptide impossible (Figure 4.8.2).
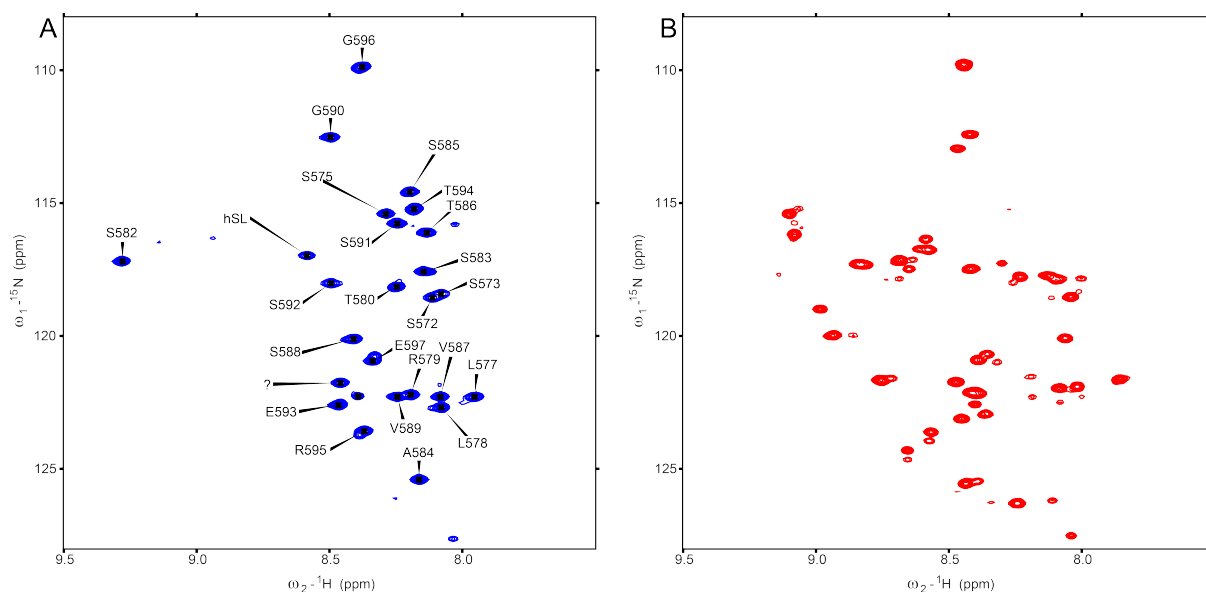
Figure 4.8.11: ^{15}**N-TROSY-HSQC spectra of peptides cleaved from TAp63α. The protein was pre-phosphorylated with MK2 kinase (A). S582 phosphorylation can be identified easily. The assignment from the isolated peptide can be adopted for the MK2 sample purified from TAp63α. In case of additional CK1δ incubation the spectrum substantially differs from the isolated peptide, therefore adopting the assignment is not possible (B).**

5 Discussion

5.1 Interaction of p53 family isoforms with reported co-activators of p53

p53 is in itself a protein of tremendous interest in the scientific community, due to its importance in tumor suppression and the observation that tumor cells frequently harbor mutations that give rise either to abrogated transcripts, aggregating protein variants or loss of DNA binding. This lead to a massive investigation of potential interaction partners. As a result, several structures of the p53 TAD with several different interaction partners were obtained (Figure 1.1.2). In contrast to p53 only very few interaction partners of the TADs of p73 and p63 are known. This prompted us to determine whether known interaction partners of p53 also interact with these known interaction partners. Unfortunately neither HMGB1 nor MED15 showed any significant interaction with the tetrameric, TAD containing isoforms of p63 or p73 (TAp63γ or TAp73β). HMGB1 seems to interact weakly with both ΔNp73α as well as TAp73β indicating that the interaction is not exclusively dependent on the TAD but might be the result of unspecific interactions with the C-terminal sequence of both proteins. The Kix domain of MED15 only shows a significant interaction with p53 and a very weak signal for the ΔN-isoforms of p63 and p73. It can be assumed that these interactions are the result of unspecific interactions with the hydrophobic C-terminus of the α-isoform containing the TI domains. The middle domain of SSRP1 has been reported to interact with p63 before[255]. However the interaction seemed to strongly depend on the availability of a free TI domain, as the interaction was mainly visible in ΔNp63α/ΔNp73α but only barely visible in C-terminally shorter isoforms which contained a TAD (TAp63γ and TAp73β). In case of p53 interaction was detectable independent whether the TA1 or TA2 domain were deleted. This suggests an unspecific interaction with the CTD of p53 and SSRP1 similar to the observed interactions with p63 and p73. Next p300/CBP domains were tested for potential interaction with p63 and p73. It is well known that four domains of these protein family are able to bind to the TADs of p53 (Taz1, Taz2, Kix and IBiD). The interaction has been characterized in depth in vitro and in vivo as well as structurally[32;44;43;45;256]. Additionally the interaction of the TAD of p73 with CBP domains has been characterized before. p300 has been reported to interact with TAp63γ as well but the interaction was never characterized any further[20]. Two domains of p300 were tested for interaction with TAD-containing isoforms of p63 and p73. Both Taz-domains were selected as they showed the strongest interaction with the p53 TADs as well as p73 TADs. An

interaction could be detected for all tested bait/prey combinations with the exception of TAp63α, which did not show any interaction with neither bait protein. This pull-down enables two independent statements: 1) The dimeric TAp63α TAD is not available for transcriptional co-factor binding. It has been reported by Coutandin *et al.*[129] that the TAD of p63 is involved in formation of the autoinhibitory complex that keeps TAp63α in a dimeric state prior to activation. 2) The unmodified TAD of p63 is binding to Taz1 and Taz2 of p300 much more strongly than any TAp73 isoform. This is expected as it has been shown by Luh *et al.*[81] that TAp73 is intrinsically much less transcriptionally active than any tetrameric TAp63 isoform. Additionally several N-terminally elongated TAp63-variants were tested (TA* and GTA). Both elongations show strong binding to the p300 Taz2 domain. However using a transcriptionally dead mutant of tetrameric TAp63 ("FWL"-mutant) lead to no remaining detectable binding. This indicates that either the N-terminal extensions of the protein harbor no secondary TAD or that the binding is too unstable to be detected by a pull-down assay. To further localize the p63 TAD sequence a peptide spot membrane was synthesized and tested with the p300 Taz2 domain. The necessary interaction motif was determined to range from amino acid 15-22 (VFQHIWD) with the strongest binding for a sequence from amino acid 9-25 (EFLSPEVFQHIWDFLE). The longer motif is in itself interesting as it does only harbor a single amino acid which can be post-translationally modified (S12). This indicates that regulation of transcriptional activity by modulation of TAD modification as reported in p53 is very limited[187].

5.2 Comparison of Structures of p53/p63/p73 TADs with Taz2 domains

The creation of a fusion construct of p300 Taz2 and the TADs of p63 and p73 allowed the determination of the TAD structures bound to the Taz2 domain. In both cases this circumvented the problem of intermediate exchange, and in case of p63 binding of multiple peptide molecules to a single Taz2 molecule. By NMR titration it could be revealed that the N-terminal part of the transactivation domain of p63 as mapped by the peptide spot membrane is more relevant for Taz2 binding compared to the C-terminal part of the sequence (Figure 4.3.3). Nevertheless the resulting structure of Taz2-p63TAD revealed that both parts of the sequence form one single helix, starting at P13 and stopping at P26. This indicates that P13 could work as a helix inducer, reducing the entropic penalty by pre-forming a helix prior to binding. However a pre-formed helix structure could not be observed in the free peptide (Figure 4.3.8). Only in the middle of the peptide sequence a small tendency for a pre-formed helix could be found by chemical shift analysis (amino acids I19-L23). Overall the p63 structure is highly similar to the p53 TAD2 structure. The major difference is a slightly shifted angle of the single α-helix formed by the sequence, as well as an increase in the length of the helix by one turn. Interestingly the comparison of the interaction surface of both structures with that of CBP p53 TAD2 (PDB 5HP0) revealed that the

TAD of p63 exclusively binds via van-der-Waals interactions while the p53 TAD2 binds via salt-bridging as well (Figure 5.2.1). This is conspicuous, as a massive difference in pI between the binding p300/CBP domains (pI>9) and the transactivation domains (pI<4.5) can be observed. This suggests a primarily hydrogen bond/salt bridge driven initial binding mode. Nevertheless van-der-Waals interactions seem to be the most relevant interaction in this case as well, as an increase in the salt concentration has a positive effect on the affinity of the peptide to the Taz2 domain in case of p53[43]. The hydrophobic binding mode of the p63 TAD might also be the result of an evolutionary pressure to generate an amphipathic helix with a hydrophobicity as high as possible on one side to ensure a high stability of the autoinhibitory complex with the equally hydrophobic TID. The stability of this complex will be subject to high evolutionary pressure as females, where the complex is instable, will be sterile. Probably the sequence of the p63 TAD is a compromise between transactivation potential on one side and stability of the repressive dimeric complex of TAp63α on the other side.

In case of p73 a fusion construct was used to circumvent intermediate exchange as well. As literature reported two independent binding sites for Taz2[20] two different construct length were cloned and assigned. Structure calculation was found to be unsatisfactory for the long construct due to a very low amino acid complexity region within the 2nd interacting region of p73. This resulted in unsolvable peak-overlap and therefore no unambiguous NOE restraints in the C-terminus of the structure. However it could be determined that the shorter structure is correct, as similar NOE restraints for the position of TAD1 could be found in both construct length. To further reduce the ambiguity of the structure a 4D-NOE experiment was performed to directly correlate aromatic side chains with methyl groups. The resulting structure shows a very surprising secondary structure. While a short helix spanning the "FWL"-motif is present, its position is very far off the center of the interaction surface formed by helices 1-3 of the Taz2 domain. Instead the center of this surface is occupied by the two aromatic residues F28 and Y29 of p73. They are buried within the binding pocket and in a stretched conformation. Mutation of these residues to alanine leads to a massive reduction in binding affinity (Figure 4.5.2). In contrast to p63 the binding of the p73 TAD1 includes two hydrogen bonds besides van-der-Waals interactions (Figure 5.2.1). Unfortunately a satisfactory structure with the full p73 TAD1-TAD2 peptide could not be obtained for reasons discussed in section 4.4.2. It is most likely that the p73 TAD2 binds to a similar surface on Taz2 as reported for the Taz2-p53TAD1-TAD2 structure[45].
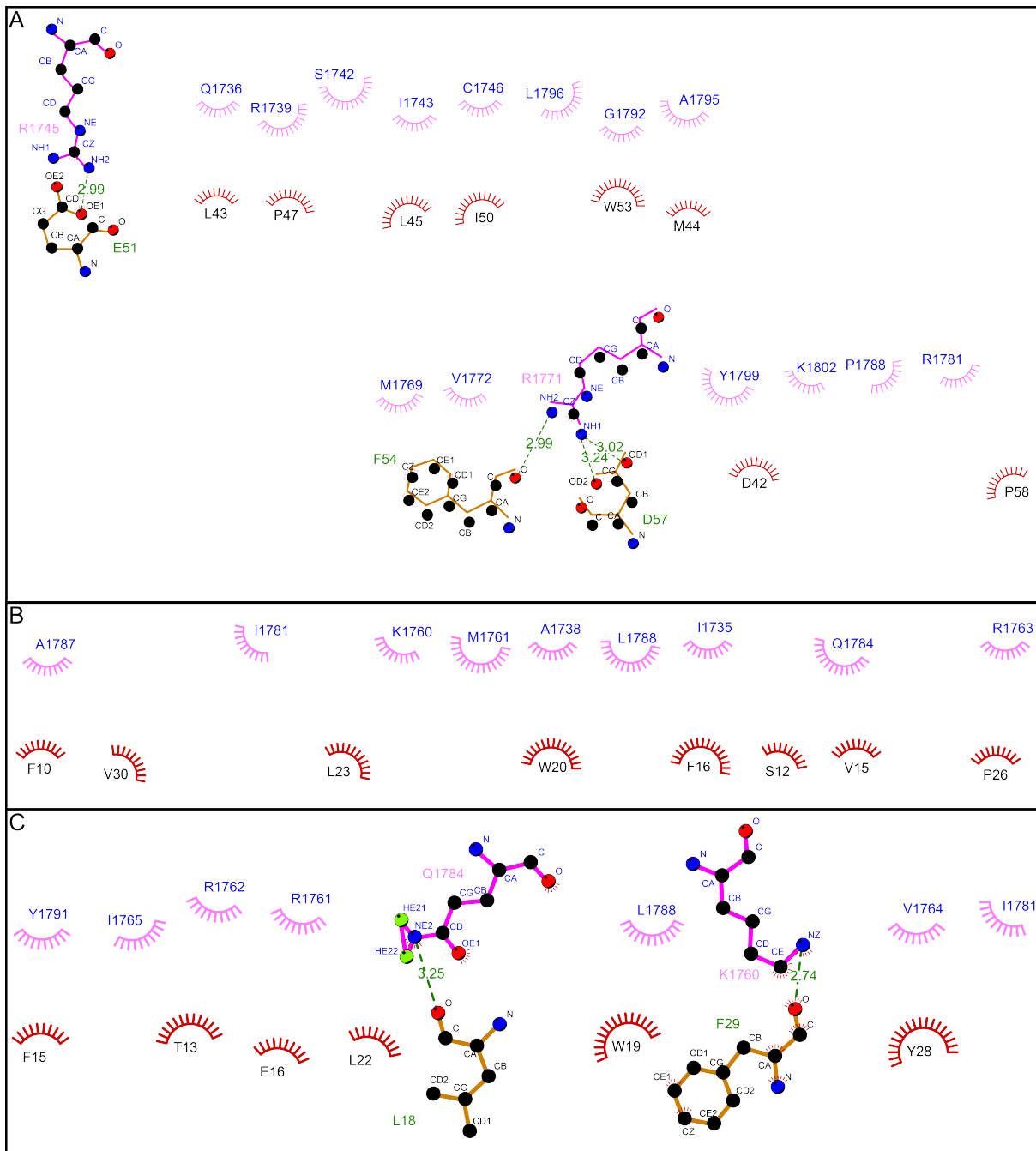
Figure 5.2.1: Binding interfaces in structures of p53 TAD2 (PDB: 5HP0, A), p63 TAD (B) and p73 TAD1 (C) with Taz2. The binding interfaces between the Taz2 domain and the corresponding peptides are conserved on the Taz2 domain side, while differing on the peptide side. (A) The p53 interface is formed by a single amphipathic helix which consists of ≈2 helix turns. The hydrophobic side of the helix is closely bound to the hydrophobic surface of Taz2, formed by helices 1-3. On both sides of the helix two negatively charged residues participate in a hydrogen bond with arginine residues of Taz2. (B) In contrast to p53 the p63 helix is longer by one complete helix turn and is bound exclusively by hydrophobic interactions. Although the p63 TAD sequence features negatively charged residues as well as hydrophilic residues none of these residues seems to come close enough for a contact. (C) The p73 TAD1 structure mainly consists of hydrophobic interactions as well. Additionally it features two unusual side chain-backbone hydrogen bonds. The Taz2-p53 structure taken from Krois et.al[45] (PDB: 5HP0) was solved with the CBP Taz2. Therefore the residue numbering is shifted by eight amino acids, compared to the other two. Diagrams were generated with LigPlot+[257].

5.3 Affinities of p63 TAD to p300 domains

The p63 TAD peptide shows affinities to all four p300 domains in question in a comparable manner as the reported interactions with p53 TAD1/TAD2 and p73 TAD1/TAD2[44;43]. The highest affinity was found for the Taz2 domain at $\approx$200 nM, followed by the Taz1 domain with an affinity an order of magnitude weaker. Kix and IBiD domains affinities are even weaker. An identical affinity gradient could be observed for p53 and p73 as well. In case of the Kix domain the real affinity is highly dependent on a potential secondary co-factor, as it has been shown to be able to bind two independent proteins at the same time in a cooperative manner[183]. In striking contrast to both family members the p63 TAD only has a single residue which is available for post-translational modification (S12). Phosphorylation at S12 and N-terminal to the TAD at S4 has been implicated to occur by the kinase IκB, leading to a small reduction in transcriptional activity of Tap63γ on the p21 promoter[50]. From a structural standpoint this makes sense as the S12 side chain is pointing towards the surface of Taz2. Phosphorylation at this point will most likely lead to structural hindrances, leading to a reduction of Taz2 binding affinity. Besides this no further post-translational modifications are possible. This emphasizes the idea that TAp63α is a constitutively active protein, controlled in its activity by keeping the protein in a dimeric state without accessible transactivation domains and a reduced DNA binding affinity.

5.4 Modulation of p73 TAD1 affinities to p300 Taz2

Part of this project was focused on determining the reason for the low intrinsic transcriptional activity of TAp73 compared to tetrameric forms of TAp63 and p53. By mutational analysis Katharina Krauskopf could derive that an exchange of amino acids 8-15 of the TAD1 of p73 to those of p63 are sufficient for increasing the transcriptional activity of TAp73β to TAp63γ like levels (Figure 4.5.3). These amino acids are exactly the same that show strong binding to the Taz2 domain in a NMR titration (Figure 4.3.3). Most likely the exchange of these eight amino acids leads to a structural re-organization of the TAD1 of p73, removing the flexibility introduced by G11 and G12, thereby stabilizing the formation of a longer helix. Additionally P10 of p63 is introduced as a helix-inducer, thereby leading to a further stabilization of the helix. This is also reflected in an almost 10-fold increase in Taz2 affinity over the wild-type p73 peptide (Figure 4.5.2).

In contrast to p63 the p73 TAD1 features seven amino acids which can potentially be modified by phosphorylation. Additionally the linker region between TAD1 and TAD2 offers several additional residues which can be post-translationally modified. For example S47 was implicated in a 2003 study to be modified by Chk1, promoting the pro-apoptotic function of p73[258]. However this study has been retracted since then due to proven image manipulation. Nevertheless it could be shown that modification within the complete TAD of p73 by Chk1/Chk2 functions as a promoter of the transcriptional activity of p73[259]. Besides the modification by Chk1/Chk2 modification of Y28 by Hck[260] and T27 by Polo-like kinase 1 (Plk1)[261] were reported. Both phosphorylation

events were reported to be repressive for the transcriptional activity. However in our hands phosphorylation of S26 and T27 leads to a massive increase in binding affinity of a p73 TAD1 peptide towards the Taz2 domain, leading to comparable affinities to the p63 TAD peptide as well as the hybrid peptide (Figure 4.5.2). The phosphorylation of Y28 having a negative effect on the transactivation potential is in agreement with the structure obtained. Y28 is partly oriented towards the surface of Taz2 and phosphorylation in this place would need to severely change the binding orientation to avoid steric clashes between the peptide and the Taz2 domain. Additionally in another study a T14 phosphorylated peptide was tested[20]. The authors observed a 10-fold increase in affinity towards the interacting domains of p300/CBP. Structurally this makes sense in case of Taz2 as T14 is in close proximity to several positively charged side chains, and thereby might contribute additional salt bridges.

5.5 Inhibition of p300/CBP under DNA stress in ovaries

The novel inhibitor A-485 of p300/CBP was tested on mice ovaries to determine whether it reduces the lethality of DOX treatment. The inhibitor was developed as a replacement of the older inhibitor C646[262] which has increasingly been dismissed as too low affinity and additionally shows thiol-reactive properties[263]. The novel inhibitor has been tested for its specificity and additionally a structural virtually identical but inactive analog has been synthesized as well, thereby enabling comparative studies to pinpoint exactly whether the observed effect is due to the inhibitor or an effect based on the chemical itself[253]. The inhibitor has been developed as a therapeutic agent in p300 addicted, CBP[(-/-)] cancer types such as some castration-resistant prostate cancers. Lowering the effective p300 level in these cells leads to a significant growth retardation due to lower levels of histone acetylation and thereby less availability of DNA for transcription[253]. As p300/CBP are one of the primary binding partners to proteins of the p53 family and essential for transcriptional activity the effect of inhibiting p300/CBP was tested in vivo. Indeed a reduction of oocyte death under simultaneous DOX/A-485 treatment could be observed. This effect was lost when A-485 was replaced by A-486, therefore indicating a specific effect of the inhibition of the Histone acetylases. This seems to indicate that inhibition of p300/CBP is indeed sufficient to block the transactivation potential of TAp63α, at least to the point that oocytes survive the treatment with DOX over the timeframe of the experiment. Nevertheless using a p300/CBP to inhibit cell death to conserve female fertility during chemotherapy might severely compromise the desired therapeutic effect of the chemotherapy or radiation therapy. In types of cancer expressing wild type p53 or a TAp73 isoform the therapeutic effect is mainly driven by induction of apoptosis due to the inability of the cells to repair the induced DNA damage. As the expression of target genes is dependent on Histone acetylation mediated by p300/CBP the resulting effective reduction of enzymatic activity in both proteins would result in an increased resistance to therapy of these cancer types. Furthermore p300/CBP has been implicated in several DNA repair pathways, most likely functioning as a switch to regulate the different pathways,

ensuring that always the adequate pathway is switched on and all other pathways remain silent (reviewed in[212]). Inhibiting this gearwheel of DNA repair could have unwanted side-effects such as aberrant DNA repair, leading to faulty DNA-repair. This will in turn have unwanted consequences to potential descendants, as these mutations will persist in the germline. It has been shown that TAp63α KO mice are fertile and have healthy offsprings, demonstrating that oocytes are able to efficiently repair DNA damage[128]. Overall the inhibition of activation of TAp63α might be a more suitable way to preserve fertility without compromising cancer therapy.

5.6 Acetylation of p63 under stress conditions

Investigations of post-translational modifications in TAp63α under DNA damaging conditions also identified lysine acetylation sites, which were then tested for potential function. In total twelve acetylation events could be found, the majority of them clustering in a region within the last helix of the DBD and the first helix of the TD. Additionally three acetylation events could be found within the DBD and three in unfolded regions throughout the protein. As a first step several acetylated lysine residues were mutated to glutamines one by one in TAp63α. Glutamine is the standard acetyl-lysine mimic used in the evaluation of acetylated protein function[264]. They were expressed in H1299 cells and the oligomeric state was evaluated via native page (Figure 4.7.2). Interestingly all tested constructs are clearly dimeric, although several of the tested mutants could destabilize the tetramerization domain in the dimer (K377Q, K379Q and the double mutants). It is assumed that the first helix of the tetramerization domain is essential for the stabilization of the closed dimeric state of TAp63α[129] and removal of two charges within the charge network of the dimer could potentially lead to a disruption of the closed state. However this does not seem to be the case. Furthermore we found that K379 is participating in an essential salt-bridge in stabilizing the tetramerization domain in its tetrameric state[24]. To assess the stability of the tetramerization domain itself the identical mutations (K377Q and K379Q) were introduced to isolated TDs. They were subject to a thermal shift assay (TSA) and the melting point was evaluated (Figure 4.7.3 and Table 4.7.1). As expected a huge drop in the melting points of both mutated TDs, by about 30°C, could be observed for both mutants. Interestingly the K377Q mutation shows a bi<phasic melting behavior. This might be due to the fact that K377 is involved in an inter-dimer contact thereby stabilizing the tetramer whereas K379 seems to be more relevant for the stabilization of a single dimer. Both mutations lead to a significant destabilization but the K377Q mutation seemingly enables the existence of a dimeric state of the protein prior to melting at even higher temperatures. Next overall protein stability was examined with the help of a CHX chase experiment on TAp63γ. This isoform was chosen, as it is a transcriptionally active tetrameric form, and therefore undergoes rapid turnover within cells. The results show striking differences between several of the tested mutations (Figure 4.7.4). The amount of protein remaining after 24 h compared to 1 h after medium exchange was very low in the wild type protein and all tetramerization domain mutants. In contrast mutations of amino

acids K49, K161 and K194 show a strong stabilization effect compared to the wild type. In case of K161 two mutations (K161Q and K161R) were used, to assess whether the stabilization is due to an acetylation-mimicking or inhibition of degradation by blocking ubiquitination. It was found that mutation K161 to either amino acid induces a stabilization of the protein level. This implies that K161 is indeed relevant for the degradation of the protein, independent of the exact type of the amino acid. Furthermore it strongly suggests a direct modification by ubiquitin during the degradation of the protein. K194 is conserved in p53 and this lysine has been reported to be acetylated by p300/CBP as well as ubiquitinated. Alike the effect observed in TAp63 it has been reported that acetylation at this lysine stabilizes the protein[265]. However as this experiment has only been conducted once and repetitions are needed to confirm the stabilizing effect of these mutations. Additionally a limitation of this assay is the the fact that the protein expression is not stopped instantaneously after addition of CHX as protein levels are significantly higher after 1 h compared to the beginning of the experiment in some cases. In a next step more experiments are needed to confirm the effecting acetyl-transferase responsible for acetylation of the found lysine residues. In case of p53 Tip60 (K120 of p53) and PCAF (K320 of p53) have been reported to acetylate those lysine residues. K120 acetylated in p53 is conserved in p63 (K149) but was not found to be acetylated in the experiment. Either the acetylated peptide was not found for experimental reasons, or the acetylation of this residue is dependent on a biological state not present under these conditions. In case of p53, Tip60 mediated K120 acetylation leads to the execution of a pro-apoptotic program instead of cellular senescence[266]. K352 of p63 corresponds roughly to K320 of p53 and was found to be acetylated. It is one of the lysines located in the Nuclear Localization Signal (NLS) of the protein, and might therefore have an influence on the cellular localization. In p53 this residue is acetylated by PCAF[83], thereby making it plausible that PCAF is responsible for this event in p63 as well. In combination with the acetylation of K377 and K379 the acetylation of K320 offers an interesting opportunity for the cell to regulate the content of tetrameric p63. Disruption of the tetramer by acetylation of the tetramerization domain exposes the Nuclear Export Sequence (NES) buried within the TD. Therefore K320/K377/K379 acetylated p63 will be much less likely to translocate to the nucleus due to the partly disrupted NLS while the likelihood of export rises due to the availability of the NES. Lastly the transactivation potential of the acetyl-mutants, as well as the acetyl-dead mutants was tested. Surprisingly the transactivation potential on the p21 promoter did not differ in a significant manner for any of the tested mutants, although they have vastly different protein stability and resulting from that apparent expression levels. The overall protein level in the cells was determined to be an order of magnitude different compared to the wild type protein, even though the total luciferase activity in the transactivation assay was similar. This was especially surprising for the TD mutants, because p53 family proteins are active as tetramers and bind to DNA in a cooperative manner. By massively weakening the TD in its structure the resulting protein should be degraded almost instantaneously, thereby being unable to function as a transcription factor.

5.7 Kinetics of TAp63α activation

To understand a potential therapeutic window preserving oocytes under a chemotherapeutic regime it is necessary to understand which kinases activate TAp63α. TAp63α was found to be activated by a consecutive action of the checkpoint kinase Chk2 and the so called executioner kinase CK1[1]. To get a better understanding of the kinetic process of the action of the executioner kinase CK1δ in vitro phosphorylation reactions were performed at different temperatures. The NMR experiments showed that CK1δ is able to phosphorylate T594, which has not been previously observed. Additionally CK1δ is not processive over the whole substrate. Phosphorylation of the first two residues (S585 and S588) seem to follow exactly the same kinetic, indicating a potential processive reaction. However phosphorylation of S591 and T594 is $\approx$30 fold slower within the wild type peptide at 25°C, excluding a processive reaction. This difference in the kinetic is even more pronounced at 30°C ($\approx$50 fold). Due to these results the question arose whether this distinct kinetic difference is a property of the kinase or a property of the peptide sequence. To tackle this question several peptide mutants were tested. A double mutation of S592V/E593G leads to a massive matching of both processes reducing the differences from a factor of $\approx$30 to only a factor of $\approx$2. This mutation essentially doubles an identical sequence within the peptide (V589/G590 in the wild type), thereby indicating that the difference in the observed kinetics might very well be substrate specific and not a property of the kinase. Simultaneously the crystal structure of CK1δ with a triple phospho-peptide was solved. The structure shows a very interesting product-bound state of the peptide within the active site of the kinase. This indicates that the kinase:peptide product complex of the triple phosphorylated peptide might be thermodynamically favored over the kinase:educt complex. This complex should be possible as well, as the peptide used for structure determination is long enough to accommodate this complex. However this structure does not contain bound ADP which would be required to further solidify the idea of a post-catalytic product complex observed here. As of the time of writing of this thesis we were able to obtain a low resolution dataset, containing both, a peptide and ADP within the crystal. The peptide was present in a product complex as seen in the high resolution structure. Unfortunately the resolution of the dataset was not deemed sufficient, therefore more crystals will have to be tested. To finally assess whether the observed complex kinetics is a definitive property of the kinase or the peptide sequence, another known CK1δ substrate will have to be analyses under identical conditions as the p63 PAD peptide. Furthermore the kinetic of phosphorylation of an isolated peptide must be compared to the phosphorylation kinetic of full-length protein to determine the influence of potential steric hindrances on the availability of the PAD sequence. Generally Marcel Tuppi has observed that TAp63α gets tetramerized after phosphorylation of all residues up to S591, while T594 seems to be not relevant for formation of the tetramer. Interestingly S591 is the first of the two residues belonging to the "slow" kinetic, thereby indicating that the effective tetramerization is regulated by a process that is $\approx$30 fold slower than it could potentially be if the kinase reaction would be fully processive. The PAD

sequence itself is evolutionary highly conserved with only very little variation between species. Amino acids C-terminal to S588 are completely conserved, making it likely that this sequence is relevant for the slowing of the kinase activity at this point. This indicates that the process might be "artificially" slowed down to allow for DNA repair which might in turn lead to dephosphorylation in the PAD sequence. Removal of a single phosphate group prior to phosphorylation of S591 is sufficient to shut down the activation of TAp63α as the number of phosphorylations within the PAD sequence will not be sufficient any longer to disrupt the inhibitory complex. Additionally simultaneous activity of CK1δ and a phosphatase will most likely lead to complete dephosphorylation after a certain time, as CK1δ is only able to attach new phosphate groups in +3 position to a prior phosphorylation. Any N-terminal phosphorylation removed by a phosphatase cannot be restored by CK1δ and is therefore lost.

5.8 Model of p63 activity regulation

During the last years our group could show that TAp63α, unlike all other isoforms or members of the p53 protein family is a dimer and transcriptionally completely inactive[267]. It could be shown that the DNA binding affinity is reduced in the dimeric state but still possible. Additionally it could be shown that activation of p63 is mediated by two independent kinases Chk2 and CKI in vitro and in vivo[1]. Here I show that in its dimeric form TAp63α is incapable of binding transcriptional co-activators, especially the crucial Histone-acetylase family KAT3 (Figure 4.1.2). However tetrameric isoforms of TAp63 are capable of binding to Taz1 and Taz2 at high affinity in the pull down experiment. Additionally the transactivation domain of p63, as mapped by a peptide spot membrane, interacts with similar affinity with p300 domains compared to the p53 TAD2. By solving the NMR solution structures of Taz2 with p63TAD or p73TAD1 I could show that the fundamental organization of the transactivation domains differs between both proteins. While the TAD of p63 only has a single residue within its sequence which can be modified by phosphorylation the TAD1 of p73 has seven phosphorylatable residues within 20 amino acids. Further studies are needed to determine which of these sites have positive impacts on the transactivation potential and which are repressive. Additionally the p73 TAD1 shows a very unusual fold, as the domain consists of a short helix with a C-terminal extended stretch, compared to a single α-helix normally found in these domains. Additionally I could show that the TAD2 of p73 forms an additional helix, binding to Taz2 simultaneously with TAD1. Unfortunately the interaction is too transient to obtain restrains for a complete structure calculation. Additionally we could show that a specific inhibitor of p300/CBP protects oocytes from p63 dependent apoptosis upon DNA damage. Furthermore direct acetylation of p63 under DNA damaging conditions does not affect the overall transcriptional activity of the protein, however has a big influence on general protein stability and expression level.
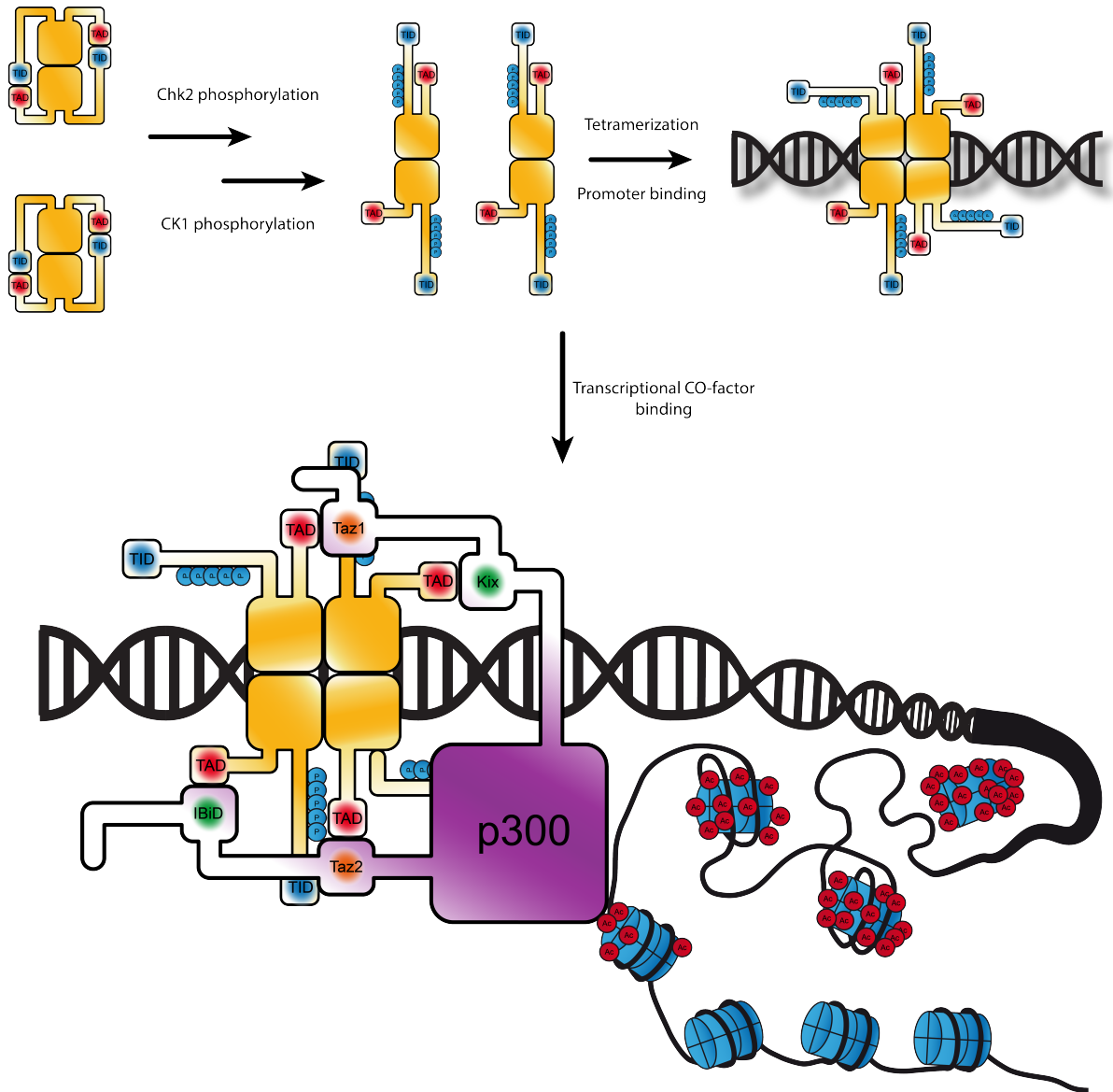
Figure 5.8.1: Model of the activation of TAp63α.

6 References

[1] Tuppi, M., Kehrloesser, S., Coutandin, D. W., *et al.* Oocyte DNA damage quality control requires consecutive interplay of CHK2 and CK1 to activate p63. *Nature Structural and Molecular Biology*, **25**(3), 261–269 (2018). doi:10.1038/s41594-018-0035-7.

[2] Chen, P. L., Chen, Y. M., Bookstein, R., and Lee, W. H. Genetic mechanisms of tumor suppression by the human p53 gene. *Science (New York, N.Y.)*, **250**(4987), 1576–80 (1990).

[3] Kaghad, M., Bonnet, H., Yang, A., *et al.* Monoallelically expressed gene related to p53 at 1p36, a region frequently deleted in neuroblastoma and other human cancers. *Cell*, **90**(4), 809–19 (1997). doi:10.1016/S0092-8674(00)80540-1.

[4] Schmale, H. and Bamberger, C. A novel protein with strong homology to the tumor suppressor p53. *Oncogene*, **15**(11), 1363–1367 (1997). doi:10.1038/sj.onc.1201500.

[5] Yang, A., Kaghad, M., Wang, Y., *et al.* P63, a P53 Homolog At 3Q27-29, Encodes Multiple Products With Transactivating, Death-Inducing, and Dominant-Negative Activities. *Molecular Cell*, **2**(3), 305–316 (1998). doi:10.1016/S1097-2765(00)80275-0.

[6] Dötsch, V., Bernassola, F., Coutandin, D., Candi, E., and Melino, G. P63 and P73, the Ancestors of P53. *Cold Spring Harbor Perspectives in Biology*, **2**(9), 1–15 (2010). doi:10.1101/cshperspect.a004887.

[7] Joerger, A. C., Wilcken, R., and Andreeva, A. Tracing the Evolution of the p53 Tetramerization Domain. *Structure (London, England : 1993)*, **22**(9), 1301–10 (2014). doi:10.1016/j.str.2014.07.010.

[8] Belyi, V. A., Ak, P., Markert, E., *et al.* The origins and evolution of the p53 family of genes. *Cold Spring Harb Perspect Biol*, **2**(6), a001198 (2010). doi:10.1101/cshperspect.a001198.

[9] De Laurenzi, V., Costanzo, A., Barcaroli, D., *et al.* Two New p73 Splice Variants, γ and δ, with Different Transcriptional Activity. *The Journal of Experimental Medicine*, **188**(9), 1763–1768 (1998). doi:10.1084/jem.188.9.1763.

[10] Bamberger, C. and Schmale, H. Identification and tissue distribution of novel KET/p63 splice variants. *FEBS Letters*, **501**(1-3), 121–126 (2001). doi:10.1016/S0014-5793(01)02643-6.

[11] Hofstetter, G., Berger, A., Fiegl, H., *et al.* Alternative splicing of p53 and p73: The novel p53 splice variant p53 is an independent prognostic marker in ovarian cancer. *Oncogene*, **29**(13), 1997–2004 (2010). doi:10.1038/onc.2009.482.

[12] Surget, S., Khoury, M. P., and Bourdon, J. C. Uncovering the role of p53 splice variants in human malignancy: A clinical perspective. *OncoTargets and Therapy*, **7**, 57–67 (2013). doi:10.2147/OTT.S53876.

[13] Osada, M., Ohba, M., Kawahara, C., *et al.* Cloning and functional analysis of human p51, which structurally and functionally resembles p53. *Nature Medicine*, **4**, 839–843 (1998). doi:10.1038/nm0798-822.

[14] Yang, A., Walker, N., Bronson, R., *et al.* Pheromonal and Inflammatory Defectsbutlack-spontaneoustumours. *Nature*, **25**(1997), 99–103 (2000).

[15] Beyer, U. and Dobbelstein, M. Non-hominid TP63 lacks retroviral LTRs but contains a novel conserved upstream exon. *Cell Cycle*, **10**(12), 1905–1911 (2011). doi:10.4161/cc.10.12.15838.

[16] Beyer, U., Moll-Rocek, J., Moll, U. M., and Dobbelstein, M. Endogenous retrovirus drives hitherto unknown proapoptotic p63 isoforms in the male germ line of humans and great apes. *Proceedings of the National Academy of Sciences*, **108**(9), 3624–3629 (2011). doi:10.1073/pnas.1016201108.

[17] Piskacek, S., Gregor, M., Nemethova, M., Grabner, M., Kovarik, P., and Piskacek, M. Nine-amino-acid transactivation domain: Establishment and prediction utilities. *Genomics*, **89**(6), 756–768 (2007). doi:10.1016/j.ygeno.2007.02.003.

[18] Bourdon, J. C. P53 and Its Isoforms in Cancer. *British Journal of Cancer*, **97**(3), 277–282 (2007). doi:10.1038/sj.bjc.6603886.

[19] Candau, R., Scolnick, D. M., Darpino, P., Ying, C. Y., Halazonetis, T. D., and Berger, S. L. Two tandem and independent sub-activation domains in the amino terminus of p53 require the adaptor complex for activity. *Oncogene*, **15**(7), 807–816 (1997). doi:10.1038/sj.onc.1201244.

[20] Burge, S., Teufel, D. P., Townsley, F. M., Freund, S. M. V., Bycroft, M., and Fersht, A. R. Molecular basis of the interactions between the p73 N terminus and p300: effects on transactivation and modulation by phosphorylation. *Proceedings of the National Academy of Sciences*, **106**(9), 3142–7 (2009). doi:10.1073/pnas.0900383106.

[21] Zhao, K., Chai, X., Johnston, K., Clements, A., and Marmorstein, R. Crystal Structure of the Mouse p53 Core DNA-binding Domain at 2.7 Å Resolution. *Journal of Biological Chemistry*, **276**(15), 12120–12127 (2001). doi:10.1074/jbc.M011644200.

[22] Coutandin, D., Löhr, F., Niesen, F. H., *et al.* Conformational stability and activity of p73 require a second helix in the tetramerization domain. *Cell death and differentiation*, **16**(12), 1582–9 (2009). doi:10.1038/cdd.2009.139.

[23] Joerger, A. C., Rajagopalan, S., Natan, E., Veprintsev, D. B., Robinson, C. V., and Fersht, A. R. Structural evolution of p53, p63, and p73: Implication for heterotetramer formation. *Proceedings of the National Academy of Sciences*, **106**(42), 17705–17710 (2009). doi: 10.1073/pnas.0905867106.

[24] Gebel, J., Luh, L. M., Coutandin, D., *et al.* Mechanism of TAp73 inhibition by Δnp63 and structural basis of p63/p73 hetero-tetramerization. *Cell Death and Differentiation*, **23**(12), 1930–1940 (2016). doi:10.1038/cdd.2016.83.

[25] Weinberg, R. L., Freund, S. M., Veprintsev, D. B., Bycroft, M., and Fersht, A. R. Regulation of DNA binding of p53 by its C-terminal domain. *Journal of Molecular Biology*, **342**(3), 801–811 (2004). doi:10.1016/j.jmb.2004.07.042.

[26] Hamard, P. J., Lukin, D. J., and Manfredi, J. J. p53 basic C terminus regulates p53 functions through DNA binding modulation of subset of target genes. *Journal of Biological Chemistry*, **287**(26), 22397–22407 (2012). doi:10.1074/jbc.M111.331298.

[27] Serber, Z., Lai, H. C., Yang, A., *et al.* A C-terminal inhibitory domain controls the activity of p63 by an intramolecular mechanism. *Molecular and cellular biology*, **22**(24), 8601–8611 (2002). doi:10.1128/MCB.22.24.8601-8611.2002.

[28] Liu, G. and Chen, X. The C-terminal sterile alpha motif and the extreme C terminus regulate the transcriptional activity of the alpha isoform of p73. *Journal of Biological Chemistry*, **280**(20), 20111–20119 (2005). doi:10.1074/jbc.M413889200.

[29] Piskacek, M., Havelka, M., Rezacova, M., and Knight, A. The 9aaTAD transactivation domains: From Gal4 to p53. *PLoS ONE*, **11**(9), 1–16 (2016). doi:10.1371/journal.pone.0162842.

[30] Okuda, M. and Nishimura, Y. Extended string binding mode of the phosphorylated transactivation domain of tumor suppressor p53. *Journal of the American Chemical Society*, **136**(40), 14143–14152 (2014). doi:10.1021/ja506351f.

[31] Lill, N. L., Grossman, S. R., Ginsberg, D., Decaprio, J., and Livingston, D. M. Binding and modulation of p53 by p300 / CBP coactivators. *Nature*, **387**(June), 1354–1357 (1997).

[32] Teufel, D. P., Freund, S. M., Bycroft, M., and Fersht, A. R. Four domains of p300 each bind tightly to a sequence spanning both transactivation subdomains of p53. *Proceedings of the National Academy of Sciences of the United States of America*, **104**(17), 7009–14 (2007). doi:10.1073/pnas.0702010104.

[33] Léveillard, T., Andera, L., Bissonnette, N., *et al.* Functional interactions between p53 and the TFIIH complex are affected by tumour-associated mutations. *The EMBO journal*, **15**(7), 1615–24 (1996).

[34] Di Lello, P., Jenkins, L. M., Jones, T. N., *et al.* Structure of the Tfb1/p53 Complex: Insights into the Interaction between the p62/Tfb1 Subunit of TFIIH and the Activation Domain of p53. *Molecular Cell*, **22**(6), 731–740 (2006). doi:10.1016/j.molcel.2006.05.007.

[35] Nakatsubo, T., Nishitani, S., Kikuchi, Y., *et al.* Human mediator subunit MED15 promotes transcriptional activation. *Drug discoveries & therapeutics*, **8**(5), 212–217 (2014). doi: 10.5582/ddt.2014.01036.

[36] Rowell, J. P., Simpson, K. L., Stott, K., Watson, M., and Thomas, J. O. HMGB1-facilitated p53 DNA binding occurs via HMG-Box/p53 transactivation domain interaction, regulated by the acidic tail. *Structure*, **20**(12), 2014–2024 (2012). doi:10.1016/j.str.2012.09.004.

[37] Liu, X., Miller, C. W., Koeffler, P. H., and Berk, A. J. The p53 activation domain binds the TATA box-binding polypeptide in Holo-TFIID, and a neighboring p53 domain inhibits transcription. *Molecular and cellular biology*, **13**(6), 3291–300 (1993). doi:10.1128/MCB. 13.6.3291.Updated.

[38] Bochkareva, E., Kaustov, L., Ayed, A., *et al.* Single-stranded DNA mimicry in the p53 transactivation domain interaction with replication protein A. *Proceedings of the National Academy of Sciences*, **102**(43), 15412–15417 (2005). doi:10.1073/pnas.0504614102.

[39] Chen, J., Marechal, V., and Levine, a. J. Mapping of the p53 and mdm-2 interaction domains. *Molecular and cellular biology*, **13**(7), 4107–4114 (1993). doi:10.1128/MCB.13. 7.4107.Updated.

[40] Böttger, A., Böttger, V., Garcia-Echeverria, C., *et al.* Molecular characterization of the hdm2-p53 interaction. *Journal of molecular biology*, **269**(5), 744–56 (1997). doi:10.1006/ jmbi.1997.1078.

[41] Shin, J.-S., Ha, J.-H., Lee, D.-H., *et al.* Structural convergence of unstructured p53 family transactivation domains in MDM2 recognition. *Cell cycle (Georgetown, Tex.)*, **14**(4), 533–43 (2015). doi:10.1080/15384101.2014.998056.

[42] Feng, H., Jenkins, L. M., Durell, S. R., *et al.* Structural Basis for p300 Taz2-p53 TAD1 Binding and Modulation by Phosphorylation. *Structure*, **17**(2), 202–210 (2009). doi:10. 1016/j.str.2008.12.009.

[43] Miller Jenkins, L. M., Feng, H., Durell, S. R., *et al.* Characterization of the p300 Taz2-p53 TAD2 Complex and Comparison with the p300 Taz2-p53 TAD1 Complex. *Biochemistry*, **54**(11), 2001–2010 (2015). doi:10.1021/acs.biochem.5b00044.

160

[44] Teufel, D. P., Bycroft, M., and Fersht, A. R. Regulation by phosphorylation of the relative affinities of the N-terminal transactivation domains of p53 for p300 domains and Mdm2. *Oncogene*, **28**(20), 2112–2118 (2009). doi:10.1038/onc.2009.71.

[45] Krois, A. S., Ferreon, J. C., Martinez-Yamout, M. A., Dyson, H. J., and Wright, P. E. Recognition of the disordered p53 transactivation domain by the transcriptional adapter zinc finger domains of CREB-binding protein. *Proceedings of the National Academy of Sciences*, **113**(13), E1853–E1862 (2016). doi:10.1073/pnas.1602487113.

[46] Grossman, S. R., Perez, M., Kung, A. L., *et al.* p300/MDM2 complexes participate in MDM2-mediated p53 degradation. *Molecular Cell*, **2**(4), 405–415 (1998). doi:10.1016/S1097-2765(00)80140-9.

[47] Kobet, E., Zeng, X., Zhu, Y., Keller, D., and Lu, H. MDM2 inhibits p300-mediated p53 acetylation and activation by forming a ternary complex with the two proteins. *Proceedings of the National Academy of Sciences of the United States of America*, **97**, 12547–12552 (2000). doi:10.1073/pnas.97.23.12547.

[48] Zeng, X., Li, X., Miller, A., *et al.* The N-Terminal Domain of p73 Interacts with the CH1 Domain of p300/CREB Binding Protein and Mediates Transcriptional Activation and Apoptosis. *Molecular and Cellular Biology*, **20**(4), 1299–1310 (2000). doi:10.1128/MCB.20.4.1299-1310.2000.

[49] MacPartlin, M., Zeng, S., Lee, H., *et al.* P300 Regulates P63 Transcriptional Activity. *Journal of Biological Chemistry*, **280**(34), 30604–30610 (2005). doi:10.1074/jbc.M503352200.

[50] Liao, J. M., Zhang, Y., Liao, W., *et al.* IkB kinase β (IKKβ) inhibits p63 Isoform γ (TAp63γ) transcriptional activity. *Journal of Biological Chemistry*, **288**(25), 18184–18193 (2013). doi:10.1074/jbc.M113.466540.

[51] Ortt, K. and Sinha, S. Derivation of the consensus DNA-binding sequence for p63 reveals unique requirements that are distinct from p53. *FEBS Letters*, **580**(18), 4544–4550 (2006). doi:10.1016/j.febslet.2006.07.004.

[52] El-Deiry, W. S., Kern, S. E., Pietenpol, J. A., Kinzler, K. W., and Vogelstein, B. Definition of a consensus binding site for p53. *Nature Genetics*, **1**(1), 45–49 (1992). doi:10.1038/ng0492-45.

[53] Wang, Y., Schwedes, J. F., Parks, D., Mann, K., and Tegtmeyer, P. Interaction of p53 with its consensus DNA-binding site. *Molecular and Cellular Biology*, **15**(4), 2157–2165 (1995). doi:10.1128/MCB.15.4.2157.

[54] Kearns, S., Lurz, R., Orlova, E. V., and Okorokov, A. L. Two p53 tetramers bind one consensus DNA response element. *Nucleic Acids Research*, **44**(13), 6185–6199 (2016). doi:10.1093/nar/gkw215.

[55] Bork, P., Holm, L., and Sander, C. The immunoglobulin fold. Structural classification, sequence patterns and common core. *Journal of molecular biology*, **242**(4), 309–20 (1994). doi:10.1006/jmbi.1994.1582.

[56] Enthart, A., Klein, C., Dehner, A., *et al.* Solution structure and binding specificity of the p63 DNA binding domain. *Scientific Reports*, **6**, 1–11 (2016). doi:10.1038/srep26707.

[57] Chen, C., Gorlatova, N., Kelman, Z., and Herzberg, O. Structures of p63 DNA binding domain in complexes with half-site and with spacer-containing full response elements. *Proceedings of the National Academy of Sciences*, **108**(16), 6456–6461 (2011). doi:10.1073/pnas.1013657108.

[58] Perez, C. A., Ott, J., Mays, D. J., and Pietenpol, J. A. p63 consensus DNA-binding site: Identification, analysis and application into a p63MH algorithm. *Oncogene*, **26**(52), 7363–7370 (2007). doi:10.1038/sj.onc.1210561.

[59] Patel, S., Bui, T. T., Drake, A. F., Fraternali, F., and Nikolova, P. V. The p73 DNA binding domain displays enhanced stability relative to its homologue, the tumor suppressor p53, and exhibits cooperative DNA binding. *Biochemistry*, **47**(10), 3235–3244 (2008). doi:10.1021/bi7023207.

[60] Bullock, A. N., Henckel, J., and Fersht, A. R. Quantitative analysis of residual folding and DNA binding in mutant p53 core domain: Definition of mutant states for rescue in cancer therapy. *Oncogene*, **19**(10), 1245–1256 (2000). doi:10.1038/sj.onc.1203434.

[61] Baugh, E. H., Ke, H., Levine, A. J., Bonneau, R. A., and Chan, C. S. Why are there hotspot mutations in the TP53 gene in human cancers? *Cell Death and Differentiation*, **25**(1), 154–160 (2018). doi:10.1038/cdd.2017.180.

[62] Zhang, Y., Coillie, S. V., Fang, J. Y., and Xu, J. Gain of function of mutant p53: R282W on the peak? *Oncogenesis*, **5**(October 2015), 2–5 (2016). doi:10.1038/oncsis.2016.8.

[63] Huqun, A., Endo, Y., Xin, H., Takahashi, M., Nukiwa, T., and Hagiwara, K. A naturally occurring p73 mutation in a p73-p53 double-mutant lung cancer cell line encodes p73α protein with a dominant-negative function. *Cancer Science*, **94**(8), 718–724 (2003). doi:10.1111/j.1349-7006.2003.tb01508.x.

[64] Heering, J., Jonker, H. R., Löhr, F., Schwalbe, H., and Dötsch, V. Structural investigations of the p53/p73 homologs from the tunicate species Ciona intestinalis reveal the sequence

requirements for the formation of a tetramerization domain. *Protein Science*, **25**(2), 410–422 (2016). doi:10.1002/pro.2830.

[65] Natan, E. and Joerger, A. C. Structure and kinetic stability of the p63 tetramerization domain. *Journal of Molecular Biology*, **415**(3), 503–513 (2012). doi:10.1016/j.jmb.2011.11.007.

[66] Rajagopalan, S., Huang, F., and Fersht, A. R. Single-molecule characterization of oligomerization kinetics and equilibria of the tumor suppressor p53. *Nucleic Acids Research*, **39**(6), 2294–2303 (2011). doi:10.1093/nar/gkq800.

[67] Ano Bom, A. P., Rangel, L. P., Costa, D. C., *et al.* Mutant p53 aggregates into prion-like amyloid oligomers and fibrils: Implications for cancer. *Journal of Biological Chemistry*, **287**(33), 28152–28162 (2012). doi:10.1074/jbc.M112.340638.

[68] Santini, S., Di Agostino, S., Coppari, E., Bizzarri, A. R., Blandino, G., and Cannistraro, S. Interaction of mutant p53 with p73: A Surface Plasmon Resonance and Atomic Force Spectroscopy study. *Biochimica et Biophysica Acta - General Subjects*, **1840**(6), 1958–1964 (2014). doi:10.1016/j.bbagen.2014.02.014.

[69] Kamiya, M., Takeuchi, Y., Katho, M., Yokoo, H., Sasaki, A., and Nakazato, Y. Expression of p73 in normal skin and proliferative skin lesions. *Pathology International*, **54**(12), 890–895 (2004). doi:10.1111/j.1440-1827.2004.01777.x.

[70] Noszczyk, B. H. and Majewski, S. T. p63 Expression during Normal Cutaneous Wound Healing in Humans. *Plastic and Reconstructive Surgery*, **108**(5), 1242–1247 (2001).

[71] Rocco, J. W., Leong, C.-O., Kuperwasser, N., DeYoung, M. P., and Ellisen, L. W. P63 Mediates Survival in Squamous Cell Carcinoma By Suppression of P73-Dependent Apoptosis. *Cancer Cell*, **9**(1), 45–56 (2006). doi:10.1016/j.ccr.2005.12.013.

[72] Lomax, M. E., Barnes, D. M., Hupp, T. R., Picksley, S. M., and Camplejohn, R. S. Characterization of p53 oligomerization domain mutations isolated from Li-Fraumeni and Li-Fraumeni like family members. *Oncogene*, **17**(5), 643–649 (1998). doi:10.1038/sj.onc.1201974.

[73] Stapleton, D., Balan, I., Pawson, T., and Sicheri, F. The crystal structure of an Eph receptor SAM domain reveals a mechanism for modular dimerization. *Nature Structural Biology*, **6**(1), 44–49 (1999). doi:10.1038/4917.

[74] Peterson, A. J., Kyba, M., Bornemann, D., Morgan, K., Brock, H. W., and Simon, J. A domain shared by the Polycomb group proteins Scm and ph mediates heterotypic and homotypic interactions. *Molecular and cellular biology*, **17**(11), 6683–92 (1997). doi:10.1128/MCB.17.11.6683.

[75] Aviv, T., Lin, Z., Lau, S., Rendl, L. M., Sicheri, F., and Smibert, C. A. The RNA-binding SAM domain of Smaug defines a new family of post-transcriptional regulators. *Nature Structural Biology*, **10**(8), 614–621 (2003). doi:10.1038/nsb956.

[76] Barrera, F. N., Poveda, J. A., González-Ros, J. M., and Neira, J. L. Binding of the C-terminal Sterile α Motif (SAM) Domain of Human p73 to Lipid Membranes. *Journal of Biological Chemistry*, **278**(47), 46878–46885 (2003). doi:10.1074/jbc.M307846200.

[77] Cheng, C., Feng, S., Jiao, J., *et al.* DLC2 inhibits development of glioma through regulating the expression ratio of TAp73α/TAp73β. *American journal of cancer research*, **8**(7), 1200–1213 (2018).

[78] Russo, C., Osterburg, C., Sirico, A., *et al.* Protein aggregation of the p63 transcription factor underlies severe skin fragility in AEC syndrome. *Proceedings of the National Academy of Sciences of the United States of America*, **115**(5), E906–E915 (2018). doi:10.1073/pnas.1713773115.

[79] Serber, Z., Lai, H. C., Yang, A., *et al.* A C-terminal inhibitory domain controls the activity of p63 by an intramolecular mechanism. *Molecular and cellular biology*, **22**(24), 8601–8611 (2002). doi:10.1128/MCB.22.24.8601-8611.2002.

[80] Straub, W. E., Weber, T. A., Schäfer, B., *et al.* The C-terminus of p63 contains multiple regulatory elements with different functions. *Cell Death and Disease*, **1**, e5 (2010). doi:10.1038/cddis.2009.1.

[81] Luh, L. M., Kehrloesser, S., Deutsch, G. B., *et al.* Analysis of the oligomeric state and transactivation potential of TAp73α. *Cell death and differentiation*, **20**(8), 1008–16 (2013). doi:10.1038/cdd.2013.23.

[82] Deutsch, G. B., Zielonka, E. M., Coutandin, D., *et al.* DNA damage in oocytes induces a switch of the quality control factor TAp63α from dimer to tetramer. *Cell*, **144**(4), 566–576 (2011). doi:10.1016/j.cell.2011.01.013.

[83] Liu, L., Scolnick, D. M., Trievel, R. C., *et al.* p53 Sites Acetylated In Vitro by PCAF and p300 Are Acetylated In Vivo in Response to DNA Damage. *Molecular and Cellular Biology*, **19**(2), 1202–1209 (1999). doi:10.1128/MCB.19.2.1202.

[84] Laptenko, O., Shiff, I., Freed-Pastor, W., *et al.* The p53 C Terminus Controls Site-Specific DNA Binding and Promotes Structural Changes within the Central DNA Binding Domain. *Molecular Cell*, **57**(6), 1034–1046 (2015). doi:10.1016/j.molcel.2015.02.015.

[85] Hamard, P. J., Barthelery, N., Hogstad, B., *et al.* The C terminus of p53 regulates gene expression by multiple mechanisms in a target- and tissue-specific manner in vivo. *Genes and Development*, **27**(17), 1868–1885 (2013). doi:10.1101/gad.224386.113.

[86] Momand, J., Zambetti, G. P., Olson, D. C., George, D., and Levine, A. J. The mdm-2 oncogene product forms a complex with the p53 protein and inhibits p53-mediated trans-activation. *Cell*, **69**(7), 1237–1245 (1992). doi:10.1016/0092-8674(92)90644-R.

[87] Barak, Y., Gottlieb, E., Juven-Gershon, T., and Oren, M. Regulation of mdm2 expression by p53: Alternative promoters produce transcripts with nonidentical translation potential. *Genes and Development*, **8**(15), 1739–1749 (1994). doi:10.1101/gad.8.15.1739.

[88] Jones, S. N., Roe, A. E., Donehower, L. A., and Bradley, A. Rescue of embryonic lethality in Mdm2-deficient mice by absence of p53. *Nature*, **378**(6553), 206–8 (1995). doi:10.1038/378206a0.

[89] Meek, D. W. and Anderson, C. W. Posttranslational modification of p53: cooperative integrators of function. *Cold Spring Harbor perspectives in biology*, **1**(6), 1–17 (2009). doi:10.1101/cshperspect.a000950.

[90] Dai, C. and Gu, W. P53 post-translational modification: Deregulated in tumorigenesis. *Trends in Molecular Medicine*, **16**(11), 528–536 (2010). doi:10.1016/j.molmed.2010.09.002.

[91] Li, M., Luo, J., Brooks, C. L., and Gu, W. Acetylation of p53 inhibits its ubiquitination by Mdm2. *Journal of Biological Chemistry*, **277**(52), 50607–50611 (2002). doi:10.1074/jbc.C200578200.

[92] Nie, L., Sasaki, M., and Maki, C. G. Regulation of p53 nuclear export through sequential changes in conformation and ubiquitination. *Journal of Biological Chemistry*, **282**(19), 14616–14625 (2007). doi:10.1074/jbc.M610515200.

[93] Merrick, B. A., He, C., Witcher, L. L., *et al.* HSP binding and mitochondrial localization of p53 protein in human HT1080 and mouse C3H10T1/2 cell lines. *Biochimica et Biophysica Acta - Protein Structure and Molecular Enzymology*, **1297**(1), 57–68 (1996). doi:10.1016/0167-4838(96)00089-1.

[94] Marchenko, N. D., Zaika, A., and Moll, U. M. Death signal-induced localization of p53 protein to mitochondria. A potential role in apoptotic signaling. *The Journal of biological chemistry*, **275**(21), 16202–12 (2000).

[95] Fogal, V., Gostissa, M., Sandy, P., *et al.* Regulation of p53 activity in nuclear bodies by a specific PML isoform. *The EMBO journal*, **19**(22), 6185–95 (2000). doi:10.1093/emboj/19.22.6185.

[96] Gonfloni, S., Di Tella, L., Caldarola, S., *et al.* Inhibition of the c-Abl-TAp63 pathway protects mouse oocytes from chemotherapy-induced death. *Nature Medicine*, **15**(10), 1179–1185 (2009). doi:10.1038/nm.2033.

[97] Rossi, M., Aqeilan, R. I., Neale, M., *et al.* The E3 ubiquitin ligase Itch controls the protein stability of p63. *Proceedings of the National Academy of Sciences*, **103**(34), 12753–12758 (2006). doi:10.1073/pnas.0603449103.

[98] Ranieri, M., Vivo, M., De Simone, M., *et al.* Sumoylation and ubiquitylation crosstalk in the control of ΔNp63α protein stability. *Gene*, **645**, 34–40 (2018). doi:10.1016/j.gene.2017.12.018.

[99] Munarriz, E., Barcaroli, D., Stephanou, A., *et al.* PIAS-1 is a checkpoint regulator which affects exit from G1 and G2 by sumoylation of p73. *Molecular and cellular biology*, **24**(24), 10593–610 (2004). doi:10.1128/MCB.24.24.10593-10610.2004.

[100] Ghioni, P., D'Alessandra, Y., Mansueto, G., *et al.* The protein stability and transcriptional activity of p63alpha are regulated by SUMO-1 conjugation. *Cell cycle*, **4**(1), 183–190 (2005). doi:1359[pii].

[101] Zeng, X., Chen, L., Jost, C. A., *et al.* MDM2 suppresses p73 function without promoting p73 degradation. *Mol Cell Biol*, **19**(5), 3257–3266 (1999). doi:10.1128/MCB.19.5.3257.

[102] Bálint, E., Bates, S., and Vousden, K. H. Mdm2 binds p73α without targeting degradation. *Oncogene*, **18**(27), 3923–3929 (1999). doi:10.1038/sj.onc.1202781.

[103] Wu, H., Abou, Z. R., Flores, E. R., and Leng, R. P. Pirh2, a Ubiquitin E3 Ligase, Inhibits p73 Transcriptional Activity by Promoting Its Ubiquitination. *Molecular Cancer Research*, **9**(12), 1780–1790 (2011). doi:10.1158/1541-7786.MCR-11-0157.

[104] Jung, Y. S., Qian, Y., and Chen, X. The p73 tumor suppressor is targeted by Pirh2 RING finger E3 ubiquitin ligase for the proteasome-dependent degradation. *Journal of Biological Chemistry*, **286**(41), 35388–35395 (2011). doi:10.1074/jbc.M111.261537.

[105] Rossi, M., De Laurenzi, V., Munarriz, E., *et al.* The ubiquitin-protein ligase Itch regulates p73 stability. *EMBO Journal*, **24**(4), 836–848 (2005). doi:10.1038/sj.emboj.7600444.

[106] Gonzalez-Cano, L., Hillje, A. L., Fuertes-Alvarez, S., *et al.* Regulatory feedback loop between TP73 and TRIM32. *Cell Death and Disease*, **4**(7) (2013). doi:10.1038/cddis.2013.224.

[107] Conforti, F., Sayan, a. E., Sreekumar, R., and Sayan, B. S. Regulation of p73 activity by post-translational modifications. *Cell Death and Disease*, **3**(3), e285 (2012). doi:10.1038/cddis.2012.27.

[108] Gebel, J., Tuppi, M., Krauskopf, K., *et al.* Control mechanisms in germ cells mediated by p53 family proteins. *Journal of Cell Science*, **130**(16), 2663–2671 (2017). doi:10.1242/jcs.204859.

[109] DeLeo, A. B., Jay, G., Appella, E., Dubois, G. C., Law, L. W., and Old, L. J. Detection of a transformation-related antigen in chemically induced sarcomas and other transformed cells of the mouse. *Proceedings of the National Academy of Sciences of the United States of America*, **76**(5), 2420–4 (1979). doi:10.1073/pnas.76.5.2420.

[110] Mowat, M., Cheng, A., Kimura, N., Bernstein, A., and Benchimol, S. Rearrangements of the cellular p53 gene in erythroleukaemic cells transformed by Friend virus. *Nature*, **314**(6012), 633–636 (1985). doi:10.1038/314633a0.

[111] Srivastava, S., Zou, Z., Pirollo, K., Blattner, W., and Chang, E. H. Germ-line transmission of a mutated p53 gene in a cancer-prone family with Li-Fraumeni syndrome (1990). doi: 10.1038/348747a0.

[112] Sameshima, Y., Akiyama, T., Mori, N., *et al.* Point mutation of the p53 gene resulting in splicing inhibition in small cell lung carcinoma. *Biochemical and Biophysical Research Communications*, **173**(2), 697–703 (1990). doi:10.1016/S0006-291X(05)80091-9.

[113] Yonish-Rouach, E., Resnftzky, D., Lotem, J., Sachs, L., Kimchi, A., and Oren, M. Wild-type p53 induces apoptosis of myeloid leukaemic cells that is inhibited by interleukin-6. *Nature*, **352**(6333), 345–347 (1991). doi:10.1038/352345a0.

[114] Shaw, P., Bovey, R., Tardy, S., Sahlit, R., Sordat, B., and Costa, J. Induction of apoptosis by wild-type p53 in a human colon tumor-derived cell line. *Biochemistry*, **89**(May), 4495–4499 (1992). doi:10.1073/pnas.89.10.4495.

[115] Zhan, Q., Carrier, F., and Fornace Jr., A. J. Induction of cellular p53 activity by DNA-damaging agents and growth arrest. *Molecular and Cellular Biology*, **13**(7), 4242–4250 (1993).

[116] Linke, S. P., Clarkin, K. C., Di Leonardo, A., Tsou, A., and Wahl, G. M. A reversible, p53-dependent Go/G1 cell cycle arrest induced by ribonucleotide deplenon in the absence of detectable DNA damage. *Genes and Development*, **10**, 934–937 (1996). doi:10.1101/gad.10.8.934.

[117] Graeber, T. G., Peterson, J. F., Tsai, M., Monica, K., Fornace, A. J., and Giaccia, A. J. Hypoxia induces accumulation of p53 protein, but activation of a G1-phase checkpoint by low-oxygen conditions is independent of p53 status. *Molecular and Cellular Biology*, **14**(9), 6264–6277 (1994). doi:10.1128/MCB.14.9.6264.

[118] Tishler, R. B., Calderwood, S. K., Coleman, C. N., and Price, B. D. Increases in sequence specific DNA binding by p53 following treatment with chemotherapeutic and DNA damaging agents. *Cancer research*, **53**(10 Suppl), 2212–6 (1993).

[119] Kaiser, A. M. and Attardi, L. D. Deconstructing networks of p53-mediated tumor suppression in vivo. *Cell Death and Differentiation*, **25**(1), 93–103 (2017). doi:10.1038/cdd.2017.171.

[120] Atadja, P., Wong, H., Garkavtsev, I., Veillette, C., and Riabowol, K. Increased activity of p53 in senescing fibroblasts. *Proceedings of the National Academy of Sciences of the United States of America*, **92**(18), 8348–52 (1995). doi:10.1073/pnas.92.18.8348.

[121] Medrano, E. E., Ini, S., Yang, F., and Abdel-malek, Z. A. Ultraviolet B Light Induces G , Arrest in Human Melanocytes by Prolonged Inhibition of Retinoblastoma Protein Phosphorylation Associated with Long-Term Expression of the p2lWaf-I / SDM / ciP-1Protein1. *Cancer Research*, **55**, 4047–52 (1995).

[122] Toshiyuki, M. and Reed, J. C. Tumor suppressor p53 is a direct transcriptional activator of the human bax gene. *Cell*, **80**(2), 293–299 (1995). doi:10.1016/0092-8674(95)90412-3.

[123] Oda, E., Ohki, R., Murasawa, H., *et al.* Noxa, a BH3-only member of the Bcl-2 family and candidate mediator of p53-induced apoptosis. *Science*, **288**(5468), 1053–1058 (2000). doi:10.1126/science.288.5468.1053.

[124] Nakano, K., Vousden, K. H., Ashcroft, M., *et al.* PUMA, a novel proapoptotic gene, is induced by p53. *Molecular cell*, **7**(3), 683–94 (2001). doi:10.1016/S1097-2765(01)00214-3.

[125] Shi, Y., Chen, J., Weng, C., *et al.* Identification of the protein-protein contact site and interaction mode of human VDAC1 with Bcl-2 family proteins. *Biochemical and Biophysical Research Communications*, **305**(4), 989–996 (2003). doi:10.1016/S0006-291X(03)00871-4.

[126] McArthur, K., Whitehead, L. W., Heddleston, J. M., *et al.* BAK/BAX macropores facilitate mitochondrial herniation and mtDNA efflux during apoptosis. *Science*, **359**(6378) (2018). doi:10.1126/science.aao6047.

[127] Donehower, L. A. The p53-deficient mouse: A model for basic and applied cancer studies. *Seminars in Cancer Biology*, **7**(5), 269–278 (1996). doi:10.1006/scbi.1996.0035.

[128] Suh, E. K., Yang, A., Kettenbach, A., *et al.* P63 Protects the Female Germ Line During Meiotic Arrest. *Nature*, **444**(7119), 624–628 (2006). doi:10.1038/nature05337.

[129] Coutandin, D., Osterburg, C., Srivastav, R. K., *et al.* Quality control in oocytes by p63 is based on a spring-loaded activation mechanism on the molecular and cellular level. *eLife*, **5**(MARCH2016), 1–22 (2016). doi:10.7554/eLife.13909.

[130] Bolcun-Filas, E., Rinaldi, V. D., White, M. E., and Schimenti, J. C. Reversal of female infertility by Chk2 ablation reveals the oocyte DNA damage checkpoint pathway. *Science*, **343**(6170), 533–536 (2014). doi:10.1126/science.1247671.

[131] Livera, G., Petre-Lazar, B., Guerquin, M. J., Trautmann, E., Coffigny, H., and Habert, R. P63 Null Mutation Protects Mouse Oocytes From Radio-Induced Apoptosis. *Reproduction*, **135**(1), 3–12 (2008). doi:10.1530/REP-07-0054.

[132] Romano, R.-A., Smalley, K., Magraw, C., *et al.* Â Np63 knockout mice reveal its indispensable role as a master regulator of epithelial development and differentiation. *Development*, **139**(4), 772–782 (2012). doi:10.1242/dev.071191.

[133] Romano, R. A., Birkaya, B., and Sinha, S. Defining the regulatory elements in the proximal promoter of Δnp63 in keratinocytes: Potential roles for Sp1/Sp3, NF-Y, and p63. *Journal of Investigative Dermatology*, **126**(7), 1469–1479 (2006). doi:10.1038/sj.jid.5700297.

[134] van Bokhoven, H., Hamel, B. C., Bamshad, M., *et al.* p63 Gene mutations in eec syndrome, limb-mammary syndrome, and isolated split hand-split foot malformation suggest a genotype-phenotype correlation. *American journal of human genetics*, **69**(3), 481–92 (2001). doi:10.1086/323123.

[135] McGrath, J. a., Duijf, P. H., Doetsch, V., *et al.* Hay-Wells syndrome is caused by heterozygous missense mutations in the SAM domain of p63. *Human molecular genetics*, **10**(3), 221–229 (2001). doi:10.1093/hmg/10.3.221.

[136] Soares, E. and Zhou, H. Master regulatory role of p63 in epidermal development and disease. *Cellular and Molecular Life Sciences*, **75**(7), 1179–1190 (2018). doi:10.1007/s00018-017-2701-z.

[137] Wilhelm, M. T., Rufini, A., Wetzel, M. K., *et al.* Isoform-specific p73 knockout mice reveal a novel role for DNp73 in the DNA damage response pathway. *Genes and Development*, pages 549–560 (2010). doi:10.1101/gad.1873910.ing.

[138] Talos, F., Abraham, A., Vaseva, A. V., *et al.* P73 is an essential regulator of neural stem cell maintenance in embryonal and adult CNS neurogenesis. *Cell Death and Differentiation*, **17**(12), 1816–1829 (2010). doi:10.1038/cdd.2010.131.

[139] Tomasini, R., Tsuchihara, K., Wilhelm, M., *et al.* TAp73 knockout shows genomic instability with infertility and tumor suppressor functions. *Genes and Development*, **22**(19), 2677–2691 (2008). doi:10.1101/gad.1695308.

[140] Baird, D. T., Collins, J., Egozcue, J., *et al.* Fertility and ageing. *Human Reproduction Update*, **11**(3), 261–276 (2005). doi:10.1093/humupd/dmi006.

[141] Tomasini, R., Tsuchihara, K., Tsuda, C., *et al.* TAp73 regulates the spindle assembly checkpoint by modulating BubR1 activity. *Proceedings of the National Academy of Sciences*, **106**(3), 797–802 (2009). doi:10.1073/pnas.0812096106.

[142] Niikura, Y., Ogi, H., Kikuchi, K., and Kitagawa, K. BUB3 that dissociates from BUB1 activates caspase-independent mitotic death (CIMD). *Cell Death and Differentiation*, **17**(6), 1011–24 (2010). doi:10.1038/cdd.2009.207.

[143] Vernole, P., Neale, M. H., Barcaroli, D., *et al.* TAp73α binds the kinetochore proteins Bub1 and Bub3 resulting in polyploidy. *Cell Cycle*, **8**(3), 421–429 (2009). doi:10.4161/cc.8.3.7623.

[144] Holembowski, L., Kramer, D., Riedel, D., *et al.* Tap73 is essential for germ cell adhesion and maturation in testis. *Journal of Cell Biology*, **204**(7), 1173–1190 (2014). doi:10.1083/jcb.201306066.

[145] Nemajerova, A., Kramer, D., Siller, S. S., *et al.* TAp73 is a central transcriptional regulator of airway multiciliogenesis. *Genes and Development*, **30**(11), 1300–1312 (2016). doi:10.1101/gad.279836.116.

[146] Marshall, C. B., Mays, D. J., Beeler, J. S., *et al.* P73 Is Required for Multiciliogenesis and Regulates the Foxj1-Associated Gene Network. *Cell Reports*, **14**(10), 2289–2300 (2016). doi:10.1016/j.celrep.2016.02.035.

[147] Rufini, A., Niklison-Chirou, M. V., Inoue, S., *et al.* TAp73 depletion accelerates aging through metabolic dysregulation. *Genes and Development*, **26**(18), 2009–2014 (2012). doi:10.1101/gad.197640.112.

[148] Agostini, M., Annicchiarico-Petruzzelli, M., Melino, G., and Rufini, A. Metabolic pathways regulated by TAp73 in response to oxidative stress. *Oncotarget*, **7**(21) (2016). doi:10.18632/oncotarget.8935.

[149] Hodawadekar, S. C. and Marmorstein, R. Chemistry of acetyl transfer by histone modifying enzymes: Structure, mechanism and implications for effector design. *Oncogene*, **26**(37), 5528–5540 (2007). doi:10.1038/sj.onc.1210619.

[150] Drazic, A., Myklebust, L. M., Ree, R., and Arnesen, T. The world of protein acetylation. *Biochimica et Biophysica Acta - Proteins and Proteomics*, **1864**(10), 1372–1401 (2016). doi:10.1016/j.bbapap.2016.06.007.

[151] Vetting, M. W., Luiz, L. P., Yu, M., *et al.* Structure and functions of the GNAT superfamily of acetyltransferases. *Archives of Biochemistry and Biophysics*, **433**(1), 212–226 (2005). doi:10.1016/j.abb.2004.09.003.

[152] Zhang, X., Ouyang, S., Kong, X., *et al.* Catalytic mechanism of histone acetyltransferase p300: From the proton transfer to acetylation reaction. *Journal of Physical Chemistry B*, **118**(8), 2009–2019 (2014). doi:10.1021/jp409778e.

[153] Yan, Y., Harper, S., Speicher, D. W., and Marmorstein, R. The catalytic mechanism of the ESA1 histone acetyltransferase involves a self-acetylated intermediate. *Nature Structural Biology*, **9**(11), 862–869 (2002). doi:10.1038/nsb849.

[154] Berndsen, C. E., Albaugh, B. N., Tan, S., and Denu, J. M. Catalytic mechanism of a MYST family histone acetyltransferase. *Biochemistry*, **46**(3), 623–9 (2007). doi:10.1021/bi602513x.

[155] Ogryzko, V. V., Schiltz, R. L., Russanova, V., Howard, B. H., and Nakatani, Y. The transcriptional coactivators p300 and CBP are histone acetyltransferases. *Cell*, **87**(5), 953–959 (1996). doi:10.1016/S0092-8674(00)82001-2.

[156] Chrivia, J. C., Kwok, R. P., Lamb, N., Hagiwara, M., Montminy, M. R., and Goodman, R. H. Phosphorylated CREB binds specifically to the nuclear protein CBP. *Nature*, **365**(6449), 855–859 (1993). doi:10.1038/365855a0.

[157] Sebé-Pedrós, A., De Mendoza, A., Lang, B. F., Degnan, B. M., and Ruiz-Trillo, I. Unexpected repertoire of metazoan transcription factors in the unicellular holozoan capsaspora owczarzaki. *Molecular Biology and Evolution*, **28**(3), 1241–1254 (2011). doi:10.1093/molbev/msq309.

[158] Bordoli, L., Netsch, M., Lüthi, U., Lutz, W., and Eckner, R. Plant orthologs of p300/CBP: conservation of a core domain in metazoan p300/CBP acetyltransferase-related proteins. *Nucleic acids research*, **29**(3), 589–97 (2001). doi:10.1093/nar/29.3.589.

[159] D'Arcy, S. and Luger, K. Understanding histone acetyltransferase Rtt109 structure and function: How many chaperones does it take? *Current Opinion in Structural Biology*, **21**(6), 728–734 (2011). doi:10.1016/j.sbi.2011.09.005.

[160] Giebler, H. A., Lemasson, I., and Nyborg, J. K. p53 recruitment of CREB binding protein mediated through phosphorylated CREB: a novel pathway of tumor suppressor regulation. *Molecular and cellular biology*, **20**(13), 4849–58 (2000). doi:10.1128/MCB.20.13.4849-4858.2000.Updated.

[161] Gillotin, S. and Lu, X. The ASPP proteins complex and cooperate with p300 to modulate the transcriptional activity of p53. *FEBS Letters*, **585**(12), 1778–1782 (2011). doi:10.1016/j.febslet.2011.04.012.

[162] Hosoda, H., Kato, K., Asano, H., *et al.* CBP/p300 is a cell type-specific modulator of CLOCK/BMAL1-mediated transcription. *Molecular Brain*, **2**(1), 1–18 (2009). doi:10.1186/1756-6606-2-34.

[163] Petrif, F., Giles, R., Dauwerse, H., *et al.* Rubinstein-Taybi syndrome caused by mutations in the transcriptional co-activator CBP. *Nature*, **376**(6538), 348–351 (1995). doi:10.1038/376348a0.

[164] Yao, T. P., Oh, S. P., Fuchs, M., *et al.* Gene dosage-dependent embryonic development and proliferation defects in mice lacking the transcriptional integrator p300. *Cell*, **93**(3), 361–372 (1998). doi:10.1016/S0092-8674(00)81165-4.

[165] Reizer, J., Reizer, A., Saier, M. H., Bork, P., and Sander, C. Exopolyphosphate phosphatase and guanosine pentaphosphate phosphatase belong to the sugar kinase/actin/hsp 70 superfamily. *Trends in biochemical sciences*, **18**(7), 247–8 (1993).

[166] Parker, D., Ferreri, K., Nakajima, T., *et al.* Phosphorylation of CREB at Ser-133 induces complex formation with CREB-binding protein via a direct mechanism. *Molecular and cellular biology*, **16**(2), 694–703 (1996). doi:10.1128/MCB.16.2.694.

[167] Lin, C. H., Hare, B. J., Wagner, G., Harrison, S. C., Maniatis, T., and Fraenkel, E. A small domain of CBP/p300 binds diverse proteins: Solution structure and functional studies. *Molecular Cell*, **8**(3), 581–590 (2001). doi:10.1016/S1097-2765(01)00333-1.

[168] Delvecchio, M., Gaucher, J., Aguilar-Gurrieri, C., Ortega, E., and Panne, D. Structure of the p300 catalytic core and implications for chromatin targeting and HAT regulation. *Nature Structural and Molecular Biology*, **20**(9), 1040–1046 (2013). doi:10.1038/nsmb.2642.

[169] Bandobashi, K., Maeda, A., Teramoto, N., *et al.* Intranuclear localization of the transcription coadaptor CBP/p300 and the transcription factor RBP-Jk in relation to EBNA-2 and -5 in B lymphocytes. *Virology*, **288**(2), 275–282 (2001). doi:10.1006/viro.2001.1103.

[170] Bordoli, L., Hüsser, S., Lüthi, U., Netsch, M., Osmani, H., and Eckner, R. Functional analysis of the p300 acetyltransferase domain: the PHD finger of p300 but not of CBP is dispensable for enzymatic activity. *Nucleic acids research*, **29**(21), 4462–71 (2001). doi:10.1093/nar/29.21.4462.

[171] Uesugi, M. Induced Helix in the VP16 Activation Domain upon Binding to a Human TAF. *Science*, **277**(5330), 1310–1313 (1997). doi:10.1126/science.277.5330.1310.

[172] Kussie, P. H., Gorina, S., Marechal, V., *et al.* Structure of the MSM2 Oncoprotein Bound to the p53 Tumor Suppressor Transactivation Domain. *Science*, **274**(5289), 948–953 (1996).

[173] Ali, M. and Ivarsson, Y. High-throughput discovery of functional disordered regions. *Molecular systems biology*, **14**(5), e8377 (2018).

[174] Uesugi, M. and Verdine, G. L. The alpha -helical FXXPhi Phi motif in p53: TAF interaction and discrimination by MDM2. *Proceedings of the National Academy of Sciences*, **96**(26), 14801–14806 (1999). doi:10.1073/pnas.96.26.14801.

[175] De Guzman, R. N., Wojciak, J. M., Martinez-Yamout, M. A., Dyson, H. J., and Wright, P. E. CBP/p300 TAZ1 domain forms a structured scaffold for ligand binding. *Biochemistry*, **44**(2), 490–497 (2005). doi:10.1021/bi048161t.

[176] Dial, R., Sun, Z. Y. J., and Freedman, S. J. Three conformational states of the p300 CH1 domain define its functional properties. *Biochemistry*, **42**(33), 9937–9945 (2003). doi:10.1021/bi034989o.

[177] Dames, S. A., Martinez-Yamout, M., De Guzman, R. N., Dyson, H. J., and Wright, P. E. Structural basis for Hif-1Â /CBP recognition in the cellular hypoxic response. *Proceedings of the National Academy of Sciences*, **99**(8), 5271–5276 (2002). doi: 10.1073/pnas.082121399.

[178] De Guzman, R. N., Martinez-Yamout, M. A., Dyson, H. J., and Wright, P. E. Interaction of the TAZ1 domain of the CREB-binding protein with the activation domain of CITED2: Regulation by competition between intrinsically unstructured ligands for non-identical binding sites. *Journal of Biological Chemistry*, **279**(4), 3042–3049 (2004). doi: 10.1074/jbc.M310348200.

[179] Radhakrishnan, I., Pérez-Alvarado, G. C., Parker, D., Dyson, H. J., Montminy, M. R., and Wright, P. E. Solution structure of the KIX domain of CBP bound to the transactivation domain of CREB: a model for activator:coactivator interactions. *Cell*, **91**(6), 741–52 (1997). doi:10.1016/S0092-8674(00)80463-8.

[180] Kjaergaard, M., Teilum, K., and Poulsen, F. M. Conformational selection in the molten globule state of the nuclear coactivator binding domain of CBP. *Proceedings of the National Academy of Sciences*, **107**(28), 12535–12540 (2010). doi:10.1073/pnas.1001693107.

[181] Dahal, L., Kwan, T. O., Shammas, S. L., and Clarke, J. pKID Binds to KIX via an Unstructured Transition State with Nonnative Interactions. *Biophysical Journal*, **113**(12), 2713–2722 (2017). doi:10.1016/j.bpj.2017.10.016.

[182] Thakur, J. K., Arthanari, H., Yang, F., *et al.* A nuclear receptor-like pathway regulating multidrug resistance in fungi. *Nature*, **452**(7187), 604–609 (2008). doi:10.1038/nature06836.

[183] Brüschweiler, S., Konrat, R., and Tollinger, M. Allosteric communication in the KIX domain proceeds through dynamic repacking of the hydrophobic core. *ACS Chemical Biology*, **8**(7), 1600–1610 (2013). doi:10.1021/cb4002188.

[184] Wojciak, J. M., Martinez-Yamout, M. A., Dyson, H. J., and Wright, P. E. Structural basis for recruitment of CBP/p300 coactivators by STAT1 and STAT2 transactivation domains. *EMBO Journal*, **28**(7), 948–958 (2009). doi:10.1038/emboj.2009.30.

[185] De Guzman, R. N., Liu, H. Y., Martinez-Yamout, M., Dyson, H. J., and Wright, P. E. Solution structure of the TAZ2 (CH3) domain of the transcriptional adaptor protein CBP. *Journal of Molecular Biology*, **303**(2), 243–253 (2000). doi:10.1006/jmbi.2000.4141.

[186] Jenkins, L. M., Yamaguchi, H., Hayashi, R., *et al.* Two distinct motifs within the p53 trans-activation domain bind to the taz2 domain of p300 and are differentially affected by phosphorylation. *Biochemistry*, **48**(6), 1244–1255 (2009). doi:10.1021/bi801716h.

[187] Lee, C. W., Ferreon, J. C., Ferreon, A. C. M., Arai, M., and Wright, P. E. Graded enhancement of p53 binding to CREB-binding protein (CBP) by multisite phosphorylation. *Proceedings of the National Academy of Sciences of the United States of America*, **107**(45), 19290–5 (2010). doi:10.1073/pnas.1013078107.

[188] Khodarev, N. N., Roizman, B., and Weichselbaum, R. R. Molecular pathways: Interferon/Stat1 pathway: Role in the tumor resistance to genotoxic stress and aggressive growth. *Clinical Cancer Research*, **18**(11), 3015–3021 (2012). doi:10.1158/1078-0432.CCR-11-3225.

[189] Schwaiger, M., Schönauer, A., Rendeiro, A. F., *et al.* Evolutionary conservation of the eumetazoan gene regulatory landscape. *Genome Research*, **24**(4), 639–650 (2014). doi:10.1101/gr.162529.113.

[190] Finlan, L. and Hupp, T. R. The N-terminal interferon-binding domain (IBiD) homology domain of p300 binds to peptides with homology to the p53 transactivation domain. *Journal of Biological Chemistry*, **279**(47), 49395–49405 (2004). doi:10.1074/jbc.M405974200.

[191] Qin, B. Y., Liu, C., Srinath, H., *et al.* Crystal structure of IRF-3 in complex with CBP. *Structure*, **13**(9), 1269–1277 (2005). doi:10.1016/j.str.2005.06.011.

[192] Sheppard, H. M., Harries, J. C., Hussain, S., Bevan, C., and Heery, D. M. Analysis of the steroid receptor coactivator 1 (SRC1)-CREB binding protein interaction interface and its importance for the function of SRC1. *Molecular and cellular biology*, **21**(1), 39–50 (2001). doi:10.1128/MCB.21.1.39-50.2001.

[193] Dhalluin, C., Carlson, J. E., Zeng, L., He, C., Aggarwal, A. K., and Zhou, M. M. Structure and ligand of a histone acetyltransferase bromodomain. *Nature*, **399**(6735), 491–496 (1999). doi:10.1038/20974.

[194] Park, S., Martinez-Yamout, M. A., Dyson, H. J., and Wright, P. E. The CH2 domain of CBP/p300 is a novel zinc finger. *FEBS Letters*, **587**(16), 2506–2511 (2013). doi:10.1016/j.febslet.2013.06.051.

[195] Park, S., Stanfield, R. L., Martinez-Yamout, M. A., Dyson, H. J., Wilson, I. A., and Wright, P. E. Role of the CBP catalytic core in intramolecular SUMOylation and control of histone

H3 acetylation. *Proceedings of the National Academy of Sciences*, **114**(27), E5335–E5342 (2017). doi:10.1073/pnas.1703105114.

[196] Diehl, C., Akke, M., Bekker-Jensen, S., Mailand, N., Streicher, W., and Wikström, M. Structural analysis of a complex between small ubiquitin-like modifier 1 (SUMO1) and the ZZ domain of CREB-binding protein (CBP/p300) reveals a new interaction surface on SUMO. *Journal of Biological Chemistry*, **291**(24), 12658–12672 (2016). doi:10.1074/jbc. M115.711325.

[197] Henry, R. A., Kuo, Y. M., and Andrews, A. J. Differences in specificity and selectivity between CBP and p300 acetylation of histone H3 and H3/H4. *Biochemistry*, **52**(34), 5746–5759 (2013). doi:10.1021/bi400684q.

[198] Schindler, U., Beckmann, H., and Cashmore, A. R. HAT3.1, a novel Arabidopsis homeodomain protein containing a conserved cysteine-rich region (1993). doi:10.1046/j.1365-313X.1993.04010137.x.

[199] Sanchez, R. and Zhou, M. M. The PHD finger: A versatile epigenome reader. *Trends in Biochemical Sciences*, **36**(7), 364–372 (2011). doi:10.1016/j.tibs.2011.03.005.

[200] Bedford, D. C. and Brindle, P. K. Is histone acetylation the most important physiological function for CBP and p300? *Aging*, **4**(4), 247–255 (2012). doi:10.18632/aging.100453.

[201] McManus, K. J. and Hendzel, M. J. Quantitative Analysis of CBP- and P300-Induced Histone Acetylations In Vivo Using Native Chromatin Quantitative Analysis of CBP- and P300-Induced Histone Acetylations In Vivo Using Native Chromatin. *Molecular and cellular biology*, **23**(21), 7611–7627 (2003). doi:10.1128/MCB.23.21.7611.

[202] Jin, Q., Yu, L. R., Wang, L., *et al.* Distinct roles of GCN5/PCAF-mediated H3K9ac and CBP/p300-mediated H3K18/27ac in nuclear receptor transactivation. *EMBO Journal*, **30**(2), 249–262 (2011). doi:10.1038/emboj.2010.318.

[203] Kouzarides, T. Chromatin Modifications and Their Function. *Cell*, **128**(4), 693–705 (2007). doi:10.1016/j.cell.2007.02.005.

[204] Petrij, F., Dauwerse, H. G., Blough, R. I., *et al.* Diagnostic analysis of the Rubinstein-Taybi syndrome: five cosmids should be used for microdeletion detection and low number of protein truncating mutations. *Journal of medical genetics*, **37**(3), 168–76 (2000). doi:10.1136/jmg.37.3.168.

[205] Oliveira, A. M. M., Estévez, M. A., Hawk, J. D., Grimes, S., Brindle, P. K., and Abel, T. Subregion-specific p300 conditional knock-out mice exhibit long-term memory impairments. *Learning and Memory*, **18**(3), 161–9 (2011). doi:10.1101/lm.1939811.

[206] Alarcón, J. M., Malleret, G., Touzani, K., *et al.* Chromatin acetylation, memory, and LTP are impaired in CBP+/-mice: A model for the cognitive deficit in Rubinstein-Taybi syndrome and its amelioration. *Neuron*, **42**(6), 947–959 (2004). doi:10.1016/j.neuron.2004.05.021.

[207] Borrow, J., Stanton, V. P., Andresen, J. M., *et al.* The translocation t(8;16)(p11;p13) of acute myeloid leukaemia fuses a putative acetyltransferase to the CREB-binding protein. *Nature Genetics*, **14**(1), 33–41 (1996). doi:10.1038/ng0996-33.

[208] Ida, K., Kitabayashi, I., Taki, T., *et al.* Adenoviral E1A-associated protein p300 is involved in acute myeloid leukemia with t(11;22)(q23;q13). *Blood*, **90**(12), 4699–704 (1997).

[209] Sobulo, O. M., Borrow, J., Tomek, R., *et al.* MLL is fused to CBP, a histone acetyltransferase, in therapy-related acute myeloid leukemia with a t(11;16)(q23;p13.3). *Proceedings of the National Academy of Sciences of the United States of America*, **94**(16), 8732–7 (1997). doi:10.1073/pnas.94.16.8732.

[210] Gayther, S., Russell, P., Ponder, B., Kouzarides, T., and Caldas, C. Truncating mutations of the EP300 acetylase in human cancers. *Nature genetics*, **24**(3), 300–303 (2000).

[211] He, H., Yu, F. X., Sun, C., and Luo, Y. CBP/p300 and SIRT1 are involved in transcriptional regulation of S-Phase specific histone genes. *PLoS ONE*, **6**(7) (2011). doi:10.1371/journal.pone.0022088.

[212] Dutto, I., Scalera, C., and Prosperi, E. CREBBP and p300 lysine acetyl transferases in the DNA damage response. *Cellular and Molecular Life Sciences*, **75**(8), 1325–1338 (2018). doi:10.1007/s00018-017-2717-4.

[213] Hassa, P. O., Haenni, S. S., Buerki, C., *et al.* Acetylation of poly(ADP-ribose) polymerase-1 by p300/CREB-binding protein regulates coactivation of NF-κB-dependent transcription. *Journal of Biological Chemistry*, **280**(49), 40450–40464 (2005). doi:10.1074/jbc.M507553200.

[214] Chai, Q., Zheng, L., Zhou, M., Turchi, J. J., and Shen, B. Interaction and Stimulation of Human FEN-1 Nuclease Activities by Heterogeneous Nuclear Ribonucleoprotein A1 in ??-Segment Processing during Okazaki Fragment Maturation. *Biochemistry*, **42**(51), 15045–15052 (2003). doi:10.1021/bi035364t.

[215] Hasan, S., Stucki, M., Hassa, P. O., *et al.* Regulation of human flap endonuclease-1 activity by acetylation through the transcriptional coactivator p300. *Molecular Cell*, **7**(6), 1221–1231 (2001). doi:10.1016/S1097-2765(01)00272-6.

[216] Balakrishnan, L., Stewart, J., Polaczek, P., Campbell, J. L., and Bambara, R. A. Acetylation of Dna2 endonuclease/helicase and flap endonuclease 1 by p300 promotes DNA stability

by creating long flap intermediates. *Journal of Biological Chemistry*, **285**(7), 4398–4404 (2010). doi:10.1074/jbc.M109.086397.

[217] Tini, M., Benecke, A., Um, S. J., Torchia, J., Evans, R. M., and Chambon, P. Association of CBP/p300 acetylase and thymine DNA glycosylase links DNA repair and transcription. *Molecular Cell*, **9**(2), 265–277 (2002). doi:10.1016/S1097-2765(02)00453-7.

[218] Bhakat, K. K., Mokkapati, S. K., Boldogh, I., Hazra, T. K., and Mitra, S. Acetylation of Human 8-Oxoguanine-DNA Glycosylase by p300 and Its Role in 8-Oxoguanine Repair In Vivo. *Molecular and Cellular Biology*, **26**(5), 1654–1665 (2006). doi:10.1128/MCB.26.5. 1654-1665.2006.

[219] Bhakat, K. K., Hazra, T. K., and Mitra, S. Acetylation of the human DNA glycosylase NEIL2 and inhibition of its activity. *Nucleic Acids Research*, **32**(10), 3033–3039 (2004). doi:10.1093/nar/gkh632.

[220] Likhite, V. S., Cass, E. I., Anderson, S. D., Yates, J. R., and Nardulli, A. M. Interaction of Estrogen Receptor α with 3-Methyladenine DNA Glycosylase Modulates Transcription and DNA Repair. *Journal of Biological Chemistry*, **279**(16), 16875–16882 (2004). doi: 10.1074/jbc.M313155200.

[221] Sengupta, S., Mantha, A. K., Mitra, S., and Bhakat, K. K. Human AP endonuclease (APE1/Ref-1) and its acetylation regulate YB-1-p300 recruitment and RNA polymerase II loading in the drug-induced activation of multidrug resistance gene MDR1. *Oncogene*, **30**(4), 482–493 (2011). doi:10.1038/onc.2010.435.

[222] Bhakat, K. K., Izumi, T., Yang, S. H., Hazra, T. K., and Mitra, S. Role of acetylated human AP-endonuclease (APE1/Ref-1) in regulation of the parathyroid hormone gene. *EMBO Journal*, **22**(23), 6299–6309 (2003). doi:10.1093/emboj/cdg595.

[223] Fantini, D., Vascotto, C., Marasco, D., *et al.* Critical lysine residues within the overlooked N-terminal domain of human APE1 regulate its biological functions. *Nucleic Acids Research*, **38**(22), 8239–8256 (2010). doi:10.1093/nar/gkq691.

[224] Balliano, A., Hao, F., Njeri, C., Balakrishnan, L., and Hayes, J. J. HMGB1 stimulates activity of polymerase β on nucleosome substrates. *Biochemistry*, **56**(4), 647–656 (2017). doi: 10.1021/acs.biochem.6b00569.

[225] Fan, W. and Luo, J. SIRT1 regulates UV-induced DNA repair through deacetylating XPA. *Molecular Cell*, **39**(2), 247–258 (2010). doi:10.1016/j.molcel.2010.07.006.

[226] Tillhon, M., Cazzalini, O., Nardo, T., *et al.* P300/CBP acetyl transferases interact with and acetylate the nucleotide excision repair factor XPG. *DNA Repair*, **11**(10), 844–852 (2012). doi:10.1016/j.dnarep.2012.08.001.

[227] Cohen, H. Y., Lavu, S., Bitterman, K. J., *et al.* Acetylation of the C terminus of Ku70 by CBP and PCAF controls Bax-mediated apoptosis. *Molecular Cell*, **13**(5), 627–638 (2004). doi:10.1016/S1097-2765(04)00094-2.

[228] Li, K., Wang, R., Lozada, E., Fan, W., Orren, D. K., and Luo, J. Acetylation of WRN protein regulates its stability by inhibiting ubiquitination. *PLoS ONE*, **5**(4) (2010). doi:10.1371/journal.pone.0010341.

[229] Dietschy, T., Shevelev, I., Pena-Diaz, J., *et al.* p300-mediated acetylation of the Rothmund-Thomson-syndrome gene product RECQL4 regulates its subcellular localization. *Journal of Cell Science*, **122**(10), 1701–1701 (2009). doi:10.1242/jcs.052944.

[230] Huang, W.-c. and Chen, C.-c. Akt phosphorylation of p300 at Ser-1834 is essential for its histone acetyltransferase and transcriptional activity. *Molecular and cellular biology*, **25**(15), 6592–602 (2005). doi:10.1128/MCB.25.15.6592-6602.2005.

[231] Tanaka, T., Nishimura, D., Wu, R. C., *et al.* Nuclear Rho kinase, ROCK2, targets p300 acetyltransferase. *Journal of Biological Chemistry*, **281**(22), 15320–15329 (2006). doi:10.1074/jbc.M510954200.

[232] Yuan, L. W. and Gambee, J. E. Phosphorylation of p300 at serine 89 by protein kinase C. *Journal of Biological Chemistry*, **275**(52), 40946–40951 (2000). doi:10.1074/jbc.M007832200.

[233] Kibbe, W. A. OligoCalc: an online oligonucleotide properties calculator. *Nucleic acids research*, **35**(Web Server issue), W43–6 (2007). doi:10.1093/nar/gkm234.

[234] Van Den Ent, F. and Löwe, J. RF cloning: A restriction-free method for inserting target genes into plasmids. *Journal of Biochemical and Biophysical Methods*, **67**(1), 67–74 (2006). doi:10.1016/j.jbbm.2005.12.008.

[235] Lee, W., Tonelli, M., and Markley, J. L. NMRFAM-SPARKY: Enhanced software for biomolecular NMR spectroscopy. *Bioinformatics*, **31**(8), 1325–1327 (2015). doi:10.1093/bioinformatics/btu830.

[236] Prompers, J. J., Groenewegen, A., Hilbers, C. W., and Pepermans, H. A. M. Two-dimensional NMR experiments for the assignment of aromatic side chains in C-13-labeled proteins. *Journal of Magnetic Resonance*, **130**(1), 68–75 (1998).

[237] Mok, K. H., Nagashima, T., Day, I. J., *et al.* Rapid sample-mixing technique for transient NMR and photo-CIDNP spectroscopy: Applications to real-time protein folding. *Journal of the American Chemical Society*, **125**(41), 12484–12492 (2003). doi:10.1021/ja036357v.

[238] Shen, Y., Delaglio, F., Cornilescu, G., and Bax, A. TALOS+: A hybrid method for predicting protein backbone torsion angles from NMR chemical shifts. *Journal of Biomolecular NMR*, **44**(4), 213–223 (2009). doi:10.1007/s10858-009-9333-z.

[239] Güntert, P. and Buchner, L. Combined automated NOE assignment and structure calculation with CYANA. *Journal of Biomolecular NMR*, **62**(4), 453–471 (2015). doi: 10.1007/s10858-015-9924-9.

[240] Peters, M. B., Yang, Y., Wang, B., Füsti-Molnár, L., Weaver, M. N., and Merz, K. M. Structural aurvey of zinc containing proteins and the development of the Zinc AMBER Force Field (ZAFF). *Journal of Chemical Theory and Computation*, **6**(9), 2935–2947 (2010). doi:10.1021/ct1002626.

[241] Koradi, R., Billeter, M., and Güntert, P. Point-centered domain decomposition for parallel molecular dynamics simulation. *Computer Physics Communications*, **124**(2-3), 139–147 (2000). doi:10.1016/S0010-4655(99)00436-1.

[242] Huisken, J., Swoger, J., Del Bene, F., Wittbrodt, J., and Stelzer, E. H. Optical sectioning deep inside live embryos by selective plane illumination microscopy. *Science*, **305**(5686), 1007–1009 (2004). doi:10.1126/science.1100035.

[243] Verveer, P. J., Swoger, J., Pampaloni, F., Greger, K., Marcello, M., and Stelzer, E. H. K. High-resolution three-dimensional imaging of large specimens with light sheet-based microscopy. *Nature Methods*, **4**(4), 311–313 (2007). doi:10.1038/nmeth1017.

[244] Schindelin, J., Arganda-Carreras, I., Frise, E., *et al.* Fiji: An open-source platform for biological-image analysis. *Nature Methods*, **9**(7), 676–682 (2012). doi:10.1038/nmeth. 2019.

[245] Krauskopf, K., Gebel, J., Kazemi, S., *et al.* Regulation of the Activity in the p53 Family Depends on the Organization of the Transactivation Domain. *Structure*, **26**(8), 1091–1100.e4 (2018). doi:10.1016/j.str.2018.05.013.

[246] Miller, M., Dauter, Z., Cherry, S., Tropea, J. E., and Wlodawer, A. Structure of the Taz2 domain of p300: Insights into ligand binding. *Acta Crystallographica Section D: Biological Crystallography*, **65**(12), 1301–1308 (2009). doi:10.1107/S0907444909040153.

[247] Fuchs, S. Y., Adler, V., Buschmann, T., Wu, X., and Ronai, Z. Mdm2 association with p53 targets its ubiquitination. *Oncogene*, **17**(19), 2543–2547 (1998). doi:10.1038/sj.onc. 1202200.

[248] Li, S. and Hong, M. Protonation, tautomerization, and rotameric structure of histidine: A comprehensive study by magic-angle-spinning solid-state NMR. *Journal of the American Chemical Society*, **133**(5), 1534–1544 (2011). doi:10.1021/ja108943n.

[249] Lovell, S. C., Davis, I. W., Arendall, W. B., *et al.* Structure validation by Calpha geometry: phi,psi and Cbeta deviation. *Proteins*, **50**(3), 437–50 (2003). doi:10.1002/prot.10286.

[250] Baker, N. A., Sept, D., Joseph, S., Holst, M. J., and McCammon, J. A. Electrostatics of nanosystems: Application to microtubules and the ribosome. *Proceedings of the National Academy of Sciences*, **98**(18), 10037–10041 (2001). doi:10.1073/pnas.181342398.

[251] Jurrus, E., Engel, D., Star, K., *et al.* Improvements to the APBS biomolecular solvation software suite. *Protein Science*, **27**(1), 112–128 (2018). doi:10.1002/pro.3280.

[252] Puljung, M. C. and Zagotta, W. N. Labeling of specific cysteines in proteins using reversible metal protection. *Biophysical Journal*, **100**(10), 2513–2521 (2011). doi:10.1016/j.bpj. 2011.03.063.

[253] Lasko, L. M., Jakob, C. G., Edalji, R. P., *et al.* Discovery of a selective catalytic p300/CBP inhibitor that targets lineage-specific tumours. *Nature*, **550**(7674), 128–132 (2017). doi: 10.1038/nature24028.

[254] Wang, X. and Hayes, J. J. Acetylation Mimics within Individual Core Histone Tail Domains Indicate Distinct Roles in Regulating the Stability of Higher-Order Chromatin Structure. *Molecular and Cellular Biology*, **28**(1), 227–236 (2008). doi:10.1128/MCB.01245-07.

[255] Zeng, S. X., Dai, M. S., Keller, D. M., and Lu, H. SSRP1 functions as a co-activator of the transcriptional activator p63. *EMBO Journal*, **21**(20), 5487–5497 (2002). doi:10.1093/ emboj/cdf540.

[256] Lee, C. W., Martinez-Yamout, M. a., Dyson, H. J., and Wright, P. E. Structure of the p53 transactivation domain in complex with the nuclear receptor coactivator binding domain of CREB binding protein. *Biochemistry*, **49**(46), 9964–71 (2010). doi:10.1021/bi1012996.

[257] Laskowski, R. A. and Swindells, M. B. LigPlot+: multiple ligand-protein interaction diagrams for drug discovery. *Journal of chemical information and modeling*, **51**(10), 2778–86 (2011). doi:10.1021/ci200227u.

[258] Gonzalez, S., Prives, C., and Cordon-Cardo, C. P73$lpha Regulation by Chk1 in Response to DNA Damage. *Mol. Cell. Biol.*, **23**(22), 8161–8171 (2003). doi:10.1128/MCB. 23.22.8161.

[259] Urist, M., Tanaka, T., Poyurovsky, M. V., and Prives, C. p73 induction after DNA damage is regulated by checkpoint kinases Chk1 and Chk2. *Genes and Development*, **18**(24), 3041–3054 (2004). doi:10.1101/gad.1221004.

[260] Paliwal, P., Radha, V., and Swarup, G. Regulation of p73 by Hck through kinase-dependent and independent mechanisms. *BMC Molecular Biology*, **8**, 1–18 (2007). doi:10.1186/ 1471-2199-8-45.

[261] Soond, S. M., Barry, S. P., Melino, G., Knight, R. A., Latchman, D. S., and Stephanou, A. P73-Mediated Transcriptional Activity Is Negatively Regulated By Polo-Like Kinase. *Cell Cycle*, **7**(9), 1214–1223 (2008). doi:10.4161/cc.7.9.5777.

[262] Bowers, E. M., Yan, G., Mukherjee, C., *et al.* Virtual ligand screening of the p300/CBP histone acetyltransferase: Identification of a selective small molecule inhibitor. *Chemistry and Biology*, **17**(5), 471–482 (2010). doi:10.1016/j.chembiol.2010.03.006.

[263] Dahlin, J. L., Nelson, K. M., Strasser, J. M., *et al.* Assay interference and off-target liabilities of reported histone acetyltransferase inhibitors. *Nature Communications*, **8**(1) (2017). doi:10.1038/s41467-017-01657-3.

[264] Kamieniarz, K. and Schneider, R. Tools to Tackle Protein Acetylation. *Chemistry and Biology*, **16**(10), 1027–1029 (2009). doi:10.1016/j.chembiol.2009.10.002.

[265] Tang, Y., Zhao, W., Chen, Y., Zhao, Y., and Gu, W. Acetylation Is Indispensable for p53 Activation. *Cell*, **133**(4), 612–626 (2008). doi:10.1016/j.cell.2008.03.025.

[266] Tang, Y., Luo, J., Zhang, W., and Gu, W. Tip60-Dependent Acetylation of p53 Modulates the Decision between Cell-Cycle Arrest and Apoptosis. *Molecular Cell*, **24**(6), 827–839 (2006). doi:10.1016/j.molcel.2006.11.021.

[267] Deutsch, G. B., Zielonka, E. M., Coutandin, D., *et al.* DNA damage in oocytes induces a switch of the quality control factor TAp63α from dimer to tetramer. *Cell*, **144**(4), 566–76 (2011). doi:10.1016/j.cell.2011.01.013.

7 List of Figures/Tables

List of Figures

List of Tables

8 Contributions

Cloning and Expression

All constructs used in this study were designed and cloned by me, with the exception of wild type p63/p73 isoforms in cell culture vectors which have been cloned previously in the lab. Labeled and unlabeled expression and purification of *E. coli* constructs was done by me.

Identification of new interaction partners for p63

All pulldown assays were performed by me. The peptide spot membrane has been synthesized by Joachim Koch, the experiment itself was performed by me.

Structure determination of Taz2 complex structures

2D/3D/4D NMR spectra for assignment and restraint generation were setup by Frank Löhr. Spectra evaluation, assignment and NOE peak picking was done by me. Structure calculation and minimization was done by Sina Kazemi. Parts of the backbone assignment of p300Taz2-p73TAD were done by my bachelor student Matthias Bretscheider. 2D NMR spectroscopy for interaction studies were done by me. Additional data evaluation, such as TALOS predictions or HetNOE spectra evaluation were done by me.

Fluorescence anisotropy

Various peptides used for FA assays were synthesized commercially and fluorophore labeled by me. FA assays to determine the affinities of TAD peptide variants to Taz2 were done by me with help of Katharina Krauskopf. FA assays for the affinity determination of various p300 domains towards the p63 TAD were done by me.

Transactivation Assays of p73 TA mutants

These transactivation assays have been done by Katharina Krauskopf and are reproduced in this work for completeness reason.

p300 Inhibition in mouse ovaries

Mice were mainly finalized and ovaries were prepared by Katharina Krauskopf with some help from me. Ovary culture and inhibitor treatment was done by Katharina Krauskopf. Ovary staining and clearing was done in cooperation with Katharina Krauskopf. Imaging of the ovaries was performed by Katharina Hötte. The resulting 3D image stacks were evaluated by me.

Acetylation of p63 under DNA damaging conditions MS data of acetylation sites in p63 was provided by Marcel Tuppi. All experiments were performed by me or my practical student (Kim Wendrich) of that time.

Phosphorylation kinetics

All peptide related experiments have been done by me. In several instances Frank Löhr helped

with the setup of the experiments, especially for the setup of direct injection experiments. Additionally he developed the HN(CA)P pulse sequence for direct detection of phosphorylated serine/threonine residues. ^{15}N-labeled TAp63α for the CNBr digest was expressed by me and purified and pre-phosphorylated by Marcel Tuppi and Franziska Finke. CNBr peptide cleavage from full-length protein was done by me with help of Marcel Tuppi. CK1δ/peptide complex crystallography has been done by Apirat Chaikuad.

Appendix

Table 8.0.1: Backbone chemical shifts of p63 amino acids 9-34. Amino acids 7-8 represent TEV protease cleavage remnants.

amino acid	CA	CB	H	N
G7	43.39			
S8	58.35	63.77	8.743	115.7
E9	56.97	30.18	8.686	123.4
E9B			8.829	123.3
F10	58.92	40.31	7.783	124.6
L11	54.51	42.70		
S12	56.60	63.20	8.870	120.6
P13	63.51	32.09		
E14	56.97	30.01	8.590	121.1
V15	62.50	32.71	8.099	121.2
F16	57.74	39.55	8.308	123.7
F16B			8.339	121.1
Q17	55.37	29.27	8.535	120.5
H18	55.36	29.16	8.456	120.0
I19	61.76	38.45	8.113	122.2
W20	56.95	29.26	8.030	123.2
D21	54.52	40.95	8.072	122.1
F22	58.06	39.23	7.951	119.5
L23	55.09	42.47	8.047	123.0
E24	56.40	30.25	8.260	121.6
Q25	53.48	28.98	8.374	122.5
P26	62.94	32.10		
I27	61.33	38.75	8.415	121.7
S28	58.12	63.85	8.492	120.0
S29	58.24	63.86	8.480	118.7
V30	62.23	32.68	8.227	122.1
Q31	53.46	28.95	8.547	126.3
P32	63.02	32.25		
I33	61.19	39.15	8.355	120.8
D34	55.78	42.16	8.007	129.3

Table 8.0.2: Chemical shifts of the fusion construct of Taz2 with the TAD of p63

amino acid	C	CA	CB	CE3	CD2	CD	CD1	CE	CE1	CE2	CG	CG2	CG1	CH2	CZ	H	HA	HA2	HA3	HB	HB2	HB3	HD1	HD2	HD3	HE1	HE2	HE3	HG	HG12	HG13	HG2	HG3	HH2	HZ	N	ND1	NE1	NE2	QA	QB	QD	QD1	QD2	QE	QG	QG1	QG2	QGD	QOG	QZ
A1	178.0	52.82	19.31													8.535	4.431																			126.2					1.439										
T2	174.5	61.87	69.80									21.70				8.099	4.330			3.975																113.2												1.208			
Q3	175.7	55.69	29.85								33.93					8.312	4.435				2.110	1.998										2.064	1.984			122.8									2.400						
S4		56.37	63.41													8.561																				119.2					2.333										
P5		63.41	32.06			50.85					27.58						4.449							3.835	3.807																										
G6	174.6	45.73														8.430	4.627																			108.3				3.947	2.745										
D7	177.3	55.17	41.37													8.087	4.325																			121.2					3.971										
S8	176.2	60.30	63.23													8.376	4.174																			116.9					2.745										
R9	177.5	58.39	30.00			43.46					27.62					8.283	4.058				1.640			3.222	3.109				1.627			1.708	1.542			122.9					1.863	3.225									
R10	178.0	58.58	30.27			43.42					27.62					7.997	4.058				1.708	1.573														119.6					1.884										
L11	178.5	57.08	41.90		23.90		24.67				27.18					8.100	4.197																			120.8					1.697		0.8850	0.8415							
S12	176.8	60.88	63.23													8.032	4.299			4.065			3.931													116.0															
I13	177.2	64.97	37.72				13.21				29.22	17.17				8.128	3.594			1.759																123.2							0.5305					0.5360			
Q14	179.1	59.46	28.26								33.93					8.130	4.009				2.516											2.452				119.0					2.171	3.233			1.688			1.494			
R15	179.2	59.26	30.18			43.46					27.63					8.213	4.133				1.957	1.860														118.9					1.434							1.263			
A16	179.9	55.46	18.49													7.995	4.152																			123.7						0.9230						1.063			
I17	177.8	64.96	37.30				13.99				34.20	18.39				8.502	3.689			2.132												2.190				118.1															
Q18	179.6	59.34	28.13													8.246	4.083				2.296	2.190										2.628	2.510			116.0															
S19	176.2	61.88	62.94								27.43					8.162	4.397				2.074	1.691							1.534							125.4							0.8470	0.9075							
L20	177.1	58.71	42.31		23.64		25.92									8.163	4.055			2.100				7.281												124.6															
V21	177.8	66.98	31.78						139.4							7.993	4.281				2.153	1.988														115.7	172.7										0.9257				
H22	179.1	60.23	27.86					129.2								7.993	4.192				2.524	2.055				7.949										121.1															
A23	179.1	55.17	19.76								33.56					8.518	4.144				2.976	2.850														116.4					2.141	3.179									
A24	177.6	54.02	18.56								26.91					8.196	4.054															2.464	2.278			112.0															
Q25	174.4	54.67	30.75													7.225	4.474				2.947	2.601										1.682	1.630			124.3					1.433										
C26	176.2	60.91	29.25													7.293	3.881				3.017	2.974														120.5															
R27	175.2	54.64	30.11			43.25										7.925	4.837				2.976	2.850														130.2															
N28	176.2	60.91	29.25													9.125	4.091				2.947	2.601														114.1							0.5540	0.5980							
A29	178.0	54.38	18.47													9.068	4.848				3.017	2.974														123.0															
N30	174.1	51.92	38.87													7.156	4.022				4.112	3.871														124.2															
C31	176.8	61.77	30.03													7.774	4.585																			128.8										2.180						
S32	174.8	51.92	38.87													8.536	4.481				1.595															111.8						3.768									
L33	178.3	65.43	40.82	51.03							27.77					8.335	4.238				1.433	1.987	3.981													125.6															
P34	174.2	63.02	31.98								34.17					8.197	4.223				4.079	3.871														125.8					1.866										
S35	176.6	64.05	29.70								25.43					7.833	4.207				3.190	2.760														116.9					1.843	3.285			1.706						
C36	176.9	60.44	63.02	42.08							33.52					8.308	3.962				2.160	2.105										2.528	2.459			118.0										1.451						
Q37	179.4	56.81	28.20								27.43					9.519	4.019				2.341	1.897										2.713	2.566			122.0					2.871	3.279			1.378			1.182			
K38	179.0	59.57	32.66	29.41					42.91		27.79					7.541	4.183				2.127	1.971		1.842	1.669											117.8							1.391	1.776							
M39	179.7	58.49	30.02	43.71							22.98					7.592	3.725				2.154	2.001														121.2					2.504										
K40	179.8	61.46	31.51								23.15	21.52				8.396	3.493									8.093						3.876	3.356			120.4	173.2			220.4		4.017	0.4370				1.125	0.9635			
R41	177.5	66.65	31.52								33.81					8.459	3.968				2.944	2.660														119.2					2.871				2.883			0.9480	0.8560			
V42	179.0	67.39	28.12													8.079	4.289				2.279	1.804														109.9									3.057	1.423						
V43	177.9	59.95	27.26								25.37					7.798	3.828			4.185	1.624	1.570		6.905												120.5									3.154	1.706						
Q44	179.9	65.67	69.55			29.17			44.24							7.320	4.067				2.694	2.047		1.624	1.570							1.571	1.540			123.8										1.378						
H45	175.8	44.72						128.0								7.152					2.061	1.838		1.724	1.616											104.0															
T46	173.8	58.66	32.13						42.29		25.09					6.921	3.968				2.694	2.047														123.2															
K47	176.8	61.19	29.76						42.71		25.74					8.985	4.504				2.297	2.053		1.775	1.610											128.2											3.285					
G48	174.6	45.66	31.64	43.75							24.87					8.500	4.400																			122.3													1.648			
Q49	177.6	56.66	32.88	29.75							27.58					7.742	4.130			4.221																118.8	172.4			221.5												
K50	176.9	57.64	32.25													7.959	4.725																			112.9									6.839						
R51	177.2	57.81	68.82						42.10		24.48					7.783	3.509				3.410	2.904		7.183									1.255	1.151			120.3				3.976	1.581	1.558						1.182			
K52		63.87					121.0									8.011					2.453	1.755		7.089		8.033										122.1	196.7				1.420				2.870						
T53	176.0	53.77									24.95					6.937	3.817				3.237	3.157										2.389	2.333			117.9							0.3655								
N54	175.2	45.85	38.37													7.072	4.812				3.548	3.224														117.4			183.3		1.503										
G55	173.2	45.55	18.05								33.92					6.988	4.115				2.024	1.996														107.0					1.675										
G56		55.58	30.75								35.85					9.115	4.665																			122.5															
C57	175.8	65.06	32.53	51.53			12.89				27.38	18.26				7.802	3.686			1.521													2.059				123.8					1.497	4.017						1.379			
P58	175.5	64.74	38.92								25.47					8.914	4.081				2.963	2.763														126.7					1.837				2.858	1.305			0.6810			
I59	175.7	66.51	29.20				131.1		41.94	133.1	25.47					7.979	3.832				1.812	1.684	1.584													116.7					2.825										
C60	177.5	60.07	32.60	29.48						129.6	33.85					7.232	4.124				1.902	1.923			1.479											117.2					1.913										
K61	179.0	58.40	28.43								27.58					8.081	4.133			1.405						8.044										119.8										1.305						
Q62	176.8	65.58	41.75		23.10								0.2560			8.434	3.509																			120.3					2.871					2.315						
L63	179.1	57.79	37.39		13.50						26.86	17.18				7.224	4.095				2.059			7.089		8.033								1.042		122.1													1.005			
I64	180.3	53.24	18.37					24.95								7.826	4.095				1.770	1.645														117.9														0.7460		
A65	178.9	57.97	44.42								25.81					8.863	3.919																			121.4															
L66	179.7	55.56	19.08				133.1		118.2		25.56					7.697	4.087																			121.0															
A67	179.4	56.76	18.05				129.6			140.1	38.57					8.063	4.170				3.237	3.157														118.3	172.4				1.675										
A68	176.8	54.82	38.57								27.85					9.249	4.396				3.548	3.224														123.3															
Y69	178.9	79.79	27.85								24.48					6.937	3.817				3.410	2.904		7.183												114.3		196.7			1.581										
H70	176.8	66.58	63.77					121.0	42.12		33.77					6.988	4.115				2.453	1.755		7.089		8.033										112.8	196.7				1.420	1.558			2.870						
A71	179.9	54.82	19.79								24.48					9.249	3.007				3.817															123.3															
K72	176.6	58.30	29.03		137.4			137.4			24.48					6.937	3.817				3.410	2.904		7.183									1.255	1.151			114.3					1.581										
H73	173.6	54.35	30.33								33.92					7.072	4.812				2.453	1.755		7.089		8.033							2.389	2.333			112.8	196.7				1.420					2.324						
C74	176.1	66.11	30.12		121.0											6.988	4.115				2.024	1.996														124.3					1.837										
Q75	175.5	54.65	29.36						42.12		33.92					9.115	4.665																			126.8															
E76	175.8	55.83	30.45								35.85					8.219	4.391				2.024	1.996														122.8										2.981	1.336					
N77	175.8	54.62	38.54								24.74					8.876	4.502				2.949	2.837														125.5					2.825				2.981						
K78	174.9	55.17	31.01	29.17					44.20		30.69					8.732	4.423				2.094	2.038														120.8					1.913	1.653						1.663			
C79	57.78	30.69									26.59	18.30	24.12			6.950	4.303							4.144												123.9															
P80	176.8	62.95	32.11	51.37												9.023	3.625			2.192					3.855																	1.901							0.6815	0.6815	
V81	62.49	31.55									28.34					3.880																				127.7													0.4070			
P62	174.7	64.20	31.64	50.51																																																

193

Table 8.0.3: Chemical shifts of the fusion construct of Taz2 with the TAD of p63 (continued)

amino acid	C	CA	CB	CD	CD1	CD2	CE	CE1	CE2	CE3	CG	CG1	CG2	CH2	CZ	CZ2	CZ3	H	HA	HA2	HA3	HB	HB2	HB3	HD1	HD2	HD3	HE1	HE2	HE3	HG	HG12	HG13	HG2	HG3	HH2	HZ	HZ2	HZ3	N	ND1	NE1	NE2	QA	QB	QD	QD1	QD2	QE	QG	QG1	QG2	QQD	QQG	QZ
R83	175.2	60.94	37.33		131.8	131.8		131.0	131.0						129.1			7.977	4.219				3.546	3.220																111.4						7.077			7.339						7.403
C84	176.9	65.02	29.87															7.768	3.978				3.235	2.762																124.1					1.762										
L85	179.3	58.40	41.10		24.78						27.22							8.215	4.023												1.552									114.5					2.881								0.9520		
N86	177.7	56.67	38.86															7.756	4.394																					115.7					2.171										
I87	179.4	64.58	37.82		13.53							28.99	17.82					8.457	3.700			2.018																		121.0											1.678	0.8555			0.7815
K88	179.1	60.33	32.59	30.63			41.94				26.18							8.589	3.991				2.007	1.950		1.815	1.689													120.2															
Q89	177.3	57.61	28.95								34.27							8.024	4.196															2.605	2.433					116.4															
K90	177.6	57.13	32.91	29.07			42.23				25.08							7.871	4.298				1.954			1.556	1.694							1.556	1.505					118.2									3.003						
G91	174.2	45.61																8.116																						108.0															
G91	174.2	45.61																		4.116	3.945																			113.3															
T92	174.5	61.78	69.75										21.62					7.947	4.351																					122.3							0.8215								
I93	176.2	61.40	38.84		13.27							27.44	17.80					8.144	4.157			1.839									1.444	1.145								124.3										1.154	0.8520			
E94	176.9	57.05	30.15								36.35							8.469	4.239				2.028	1.939																109.9										2.251					
G95	177.4	45.54																8.359																						108.9				3.941											
R96	176.9	56.25	30.79	43.46							27.15							8.156	4.360				1.899	1.758																120.2						3.161				1.620					
G97	174.2	45.58																8.535																						109.6				3.967											
N98	175.5	53.51	38.90															8.280	4.670																					118.5					2.753										
E99	176.2	57.27	29.88								36.20							8.568	4.184				1.902	1.850								2.119	2.078							120.9										2.251					
F100	175.2	57.66	39.57		131.9	131.9		131.3	131.3						129.6			8.102	4.613				3.120	3.001																119.9						7.208			7.281						
L101	175.9	54.57	42.75		25.27	24.17					26.93							7.869	4.348												1.505									122.9					1.466								0.7960		
S102		55.86	63.61															8.101																						118.0															
P103	177.9	64.98	32.01	50.79							27.76								4.168				3.893	4.053																117.8					1.978				1.971						
E104	177.8	58.74	29.19								36.56							8.610	4.116				2.278	2.122																117.8									2.276						
V105	177.2	64.56	31.97									21.77	21.08					7.539	3.824			2.017																		118.6											0.8765	0.7275			
F106	176.5	59.74	38.72		131.7	131.7		131.0	131.0						129.4			7.785	4.245				2.911	2.966														7.064		118.4						7.105			7.149						
Q107	176.7	57.90	28.66								34.17							7.867	4.006				3.170	3.060																117.8					2.061					2.307					
H108	176.6	56.79	29.17			120.3		137.4										7.829	4.525								7.166		8.237											115.6	195.8		178.2												
I109	176.2	63.87	37.99		13.82							28.29	17.36					7.549	3.802			1.679																		119.7											0.9490	0.5595			0.6525
W110	177.7	58.47	28.88		127.4					120.7				124.2		114.4	121.7	7.685	4.504				3.288	3.132	7.150			9.991		7.482						7.083		7.342	7.028	119.1		129.0						0.6525						
D111	177.9	56.54	40.32															8.053	4.445				2.661	2.614																119.5															
F112	176.6	59.33	39.04		131.8	131.8		131.2	131.2						129.6			7.769	4.416				3.196	3.096																118.5						7.215			7.229						
L113	177.4	55.97	42.32		25.95						23.58							7.768	4.087				1.750	1.687							1.521									118.9													0.8320		
E114	176.4	56.55	30.27								36.33							7.880	4.232				2.091	1.923																118.2															
Q115		53.82	28.90															7.838	4.572				2.072	1.951										2.253	2.179		7.224			120.6															
P116	177.1	63.21	32.01	50.59							27.50								4.454							3.647	3.771							2.009	1.900										2.259										
I117	176.4	61.48	38.83		13.30							27.60	17.71					8.244	4.152			1.861										1.504	1.198							121.0						0.8605					1.504	0.9170			
S118	174.6	58.31	63.87															8.274	4.491				3.894	3.855																118.9															
S119	174.3	58.47	63.99															8.276	4.510				4.161																	117.8															
V120	175.8	62.24	32.68										20.96					8.026	4.161			2.086																		121.0													0.9170		
Q121		53.50	29.13															8.312	4.653				2.092	1.954		3.809	3.685													125.1															
P122	176.7	63.14	32.21	50.79							27.48								4.481				2.295	1.996																120.2									1.984						
I123	175.1	61.23	39.23		13.43							27.13	17.81					8.178	4.213			1.896									1.479	1.175							120.2						0.8625							0.9300		
D124		55.76	42.42															7.888																						129.0															

194

Table 8.0.4: Chemical shifts of the fusion construct of Taz2 with the TAD1 of p73

amino acid	CA	CB	CD	CD1	CD2	CE	CE1	CG	CG1	CG2	H	HA	HB2	HB3	N
A1	52.80	19.29									8.552	4.436			126.2
T2	61.86	69.82								21.65	8.118	4.329			113.2
Q3	55.66	29.93						33.88			8.330	4.438	2.124	2.000	122.8
S4	56.42	63.40									8.588				119.3
P5	64.09	32.04	50.82					27.50				4.450			
G6	45.76										8.453	3.949			108.2
G6															
D7	55.20	41.33									8.097	4.624			121.2
S8	60.40	63.24									8.386	4.285			116.9
P9	58.32	29.99	43.28					27.38				4.192			123.0
R10	58.70	30.21	43.33					27.64			8.293	4.041			119.6
L11	57.16	41.92		24.74	23.68			27.11			7.998	4.207			120.6
S12	61.08	63.16									8.131	4.283			120.2
I13	64.88	37.67		13.10					29.19	17.12	8.128	4.170			123.2
Q14	59.48	28.26						34.08			8.097	3.990			118.9
R15	59.37	30.22	43.53					27.96			8.195	4.125			119.1
A16	55.48	18.57									8.088	4.155			124.0
I17	65.21	37.52		14.38					29.57	18.41	8.565	3.670			118.2
Q18	59.30	28.13						34.16			8.172	4.077			118.8
S19	61.93	62.99									8.191	4.381			116.0
L20	58.65	42.27		25.98	23.47			27.29		21.02	8.250	4.027			125.4
V21	66.91	31.77							23.34	21.02	8.519	3.277			118.5
H22	60.18	27.80			129.6		139.5				8.607	4.197			116.7
A23	55.15	19.81									8.230	4.150			121.3
A24	53.99	18.55									8.207	4.047			116.5
Q25	54.51	30.77						33.46			7.207	4.481			111.8
C26	60.86	29.21									7.274	3.867			124.3
R27	54.65	30.10	43.21					26.93			8.878	4.593			129.6
N28	51.84	39.07									7.897	4.840			120.4
A29	54.44	18.46									9.147	4.085			130.4
N30	51.89	38.86									8.070	4.847			114.1
C31	61.74	30.00									7.162	4.588			123.1
S32	57.94	64.05									8.797				124.3
L33	54.28	40.92						27.82			8.506	4.588			128.7
P34	65.37	31.90	51.03									4.317			
S35	60.46	63.04						34.12			8.358	4.263			111.8
C36	63.94	29.77						32.29			7.495	3.964			125.6
Q37	59.88	28.17						33.44			8.172	4.045			115.9
K38	59.61	32.70	29.55			42.20		27.41			7.957	4.557			117.2
M39	56.70	31.78				17.24		27.94			8.283	3.808			118.1
K40	61.44	32.77	30.11			42.95			22.85	21.45	9.517	4.167			121.9
R41	59.62	29.99	43.68					33.71	23.15		7.555	3.720			118.0
V42	66.66	31.45									7.619	3.490			120.7
V43	67.36	32.09						25.31		22.15	8.407	3.972			119.1
Q44	58.89	28.09									8.386	4.251			119.1
H45	59.90	27.19			129.0						8.131	3.830			110.4
T46	65.72	69.53									7.850	4.064			120.3
K47	58.67	32.12	29.17			42.27	140.1	25.04			7.329				103.9
G48	44.68										7.152	3.969			123.3
C49	61.15	29.81						24.84			6.912	4.506			128.2
K50	56.59	32.84	28.88			42.33					8.994	4.383			122.4
R51	57.67	31.66	43.72								8.517	4.517			118.8
K52	57.72	32.28	29.75			42.71					8.468				113.0
T53	63.88	68.82									7.766	4.714			
N54	53.81	38.29													
G55	45.81										7.968				107.4
G66	46.55										7.795				107.1
C57	55.63	30.73						27.36			8.012	4.300			122.5
P58	65.03	32.46	51.53									3.740			
I59	64.85	39.01		12.70				25.48	27.93	18.34	7.811	3.848			121.3
C60	66.37	29.28						34.26			8.887	4.151			123.6
K61	60.13	32.65	29.50			41.95		27.54			7.303				117.6
Q62	58.64	28.85									8.169	3.549			120.1
L63	58.02	41.83		25.16	13.49						8.533	4.111			112.7
I64	65.46	37.35		13.49					30.02	17.21	7.340	4.113			122.2
A65	55.22	18.24									7.809	3.916			117.8
L66	57.92	42.35		25.52	24.41			26.58			8.232	4.108			121.6
A67	55.85	19.09									8.907				119.8
A68	55.50	18.11									8.747	4.379			118.6
Y69	61.44	38.48		133.2		42.22	118.2/140.2	24.71			6.933	3.924			
H70	65.03	32.46		129.3								3.831			122.2
A71	58.84	27.60						26.48			9.235	4.811			114.4
K72	58.21	32.52	29.00			42.12		24.48			6.937	2.892			112.7
H73	54.32	30.32		121.2			137.5				7.060	4.811			123.4
C74	60.10	30.13									6.990	4.112			
Q75	54.63	29.36						33.76			9.125	4.662			128.6
E76	55.86	30.40						35.80			8.232	4.384			122.8
N77	55.19	38.49									8.907	4.498			125.7
K78	54.57	30.98	29.15	24.41		42.22		24.71			8.652	4.424			120.7
C79	57.84	30.71									7.693	4.108			123.8
P80	62.90	32.07	51.38					26.48	24.09	19.70		4.676			
V81	62.50	31.58									9.044	3.527			
P82	64.19	31.55	50.47					28.45				3.982			127.8

195

Table 8.0.5: Chemical shifts of the fusion construct of Taz2 with the TAD1 of p73 (continued)

amino acid	CA	CB	CD	CD1	CD2	CE	CE1	CE2	CE3	CG	CG1	CG2	CH2	CZ	CZ2	CZ3	H	HA	HB	HB2	HB3	HD1	HD2	HD3	HE1	HE3	HG	HG12	HG13	HG2	HG3	HH2	HZ	HZ2	HZ3	N	ND1	NE1	NE2	QA	QB	QD	QD1	QD2	QE	QG	QG2	QOD
F83	60.91	37.27		131.9	131.9		131.1	131.1						129.2			7.966	4.199		3.545	3.213												7.388			111.2						7.096			7.353			
C84	64.95	29.85															7.774	3.979		3.240	2.766															124.2												
L85	58.34	41.07		24.92	24.11					27.12							8.221	4.020									1.540									114.5							0.9430					
N86	56.54	38.81															7.734	4.385																		115.5					2.831							
I87	64.60	38.01		13.52								17.77					8.408	4.218																		120.9											0.8345	
K88	60.05	32.64	30.54			42.34				26.00							8.539	4.008																		120.1					1.991	1.683	0.7663		2.988	1.446		
Q89	57.32	28.85															8.032	4.214		2.575										2.436						117.1					2.178					2.436		
K90	56.94	32.54	29.06			42.27				24.84							7.853	4.297																		119.4					1.928				2.988	1.508		
G91	45.65																8.151																			108.2				4.026								
G92	45.32																8.289																			108.6												
S93	58.67	63.87															8.337	4.486																		115.7					3.901							
G94	45.45																8.503																			110.8				3.998								
G95	45.34																8.316																			108.8												
G96	45.34																																							4.049								
T97	61.95	69.82										21.58					8.165	4.396	4.313																	112.8											1.201	
G98	45.53																8.511																			111.2												
G99	45.66																																															
G100	45.43																																															
S101	58.55	63.94																																		108.4												
G102	45.46																																			115.5												
T103	61.81	70.09										21.64					8.018	4.398	4.216																	113.8											1.176	
I104	61.44	38.72		13.04							27.42	17.60					8.226	4.165	1.853									1.464	1.171							122.8							0.8340				0.8880	
E105	56.98	30.21															8.521	4.266		2.039	1.966															124.6										2.271		
G106	45.51																8.396																			110.0				3.959								
R107	56.17	30.98	43.43							36.31							8.168	4.383		1.909	1.781															120.1						3.189				1.638		
G108	45.47																8.463																			109.8				3.980								
D109	54.18	41.39								27.17							8.256	4.637		2.732	2.703															120.2												
G110	45.75																8.485																			109.3				3.971								
G111	45.55																8.380																			108.7				4.003								
T112	62.17	69.81										21.66					8.082	4.379	4.210																	113.7											1.146	
T113	62.41	69.81										21.76					8.154	4.277																		115.9											1.147	
F114	59.23	39.10		131.9	131.9		131.2	131.2						129.6			8.330	4.389															7.079			120.9					3.003	7.133			7.192			
E115	58.48	29.64															8.312	3.854																		119.8										2.172		
H116	57.03	29.65			119.6		138.0			36.36							8.105	4.455					7.027		8.050											117.8	176.5		209.3									
L117	55.69	42.09		25.07	23.99					26.80							7.850	4.060									1.358									121.4							0.7570	0.7180				
W118	58.09	29.24		127.2					120.7				124.3		114.4	124.4	7.944	4.512		3.210	3.117	7.099			10.04	7.429						7.047		7.330	6.984	118.3		129.0										
S119	59.69	63.54															7.873	4.300		3.895	3.777															114.5												
S120	58.96	63.77															7.909	4.425		3.886	3.849															116.2												
L121	55.08	42.56		25.32	23.78					26.72							7.685	4.304									1.521									122.4					1.608							0.7750
E122	54.40	29.76															8.198																			122.1												
P123	63.80	32.00	50.53							27.45								4.285		2.128			3.780	3.694						1.944	1.874																	
D124	54.13	41.10															8.342	4.636		2.947	2.716															118.8												
S125	59.14	63.79															8.102	4.348																		115.9												
T126	62.97	69.38										21.59					8.199	4.202	4.082																	115.7											1.044	
Y127	59.90	38.82		133.0	132.9		118.2	118.3									7.891	4.310		2.740	2.693															121.0						6.829			6.694			
F128	57.24	39.64		132.0	132.0		131.2	131.2						129.3			7.838	4.556		3.175	2.912												7.140			117.6						7.227			7.282			
D129	54.26	40.89															8.127	4.656		2.744	2.561															121.4												
L130	56.65	43.78															7.575																			127.2												

Table 8.0.6: Chemical shifts of the fusion construct of Taz2 with the complete TAD of p73

amino acid	C	CA	CB	CD	CG	H	HA	HB	N
A1	178.0	52.79	19.32			8.543	4.444		126.2
T2	174.5	61.85	69.84			8.110	4.337		113.2
Q3	175.7	55.70	29.92		33.90	8.322	4.450	2.008	122.8
S4	173.2	56.46	63.42			8.585	4.457		119.3
P5	178.0	64.13	32.05	50.82	27.52		4.457		
Q6	174.6		55.25			8.449	4.640	1.989	108.2
D7	177.1		41.34			8.098	4.291	3.555	121.2
S8	176.3	60.48	63.20			8.386	4.044		116.9
R9	176.6	58.45	29.97	43.35	27.44	8.304	4.188		123.0
R10	178.1	58.73	30.20	43.39	27.53	8.015	4.044	1.638	119.6
L11	178.8	57.26	41.89		27.21	8.118	4.204	1.878	120.5
S12	177.0	61.20	63.11			8.103	4.281		116.0
I13	177.2	64.98	37.73	13.21	29.24	8.094	3.640		123.3
Q14	179.1	59.76	28.30			8.122	3.999		119.0
R15	179.3	59.36	30.20	43.58	27.92	8.243	4.128		119.0
A16	180.0	55.44	18.64			8.035	4.117		123.9
I17	177.7	65.29	37.59	14.44	34.18	8.553	3.670		118.3
Q18	179.6	59.32	28.17			8.187	4.079	2.292	118.7
S19	177.6	62.00	63.12			8.169	4.376		115.9
L20	177.1	58.68	42.31	23.54	26.02	8.243	4.047		125.4
V21	178.4	66.94	31.77			8.528	3.293	2.105	118.5
H22	178.0	60.23	27.81			7.945	4.202		115.7
A23	179.2	55.18	19.75		27.92	8.028	4.157		121.0
A24	177.5	53.99	18.60			8.220	4.051		116.5
Q25	177.5	54.60	30.75		33.51	7.208	4.485	2.000	111.8
C26	176.2	60.88	29.20		26.91	7.287	3.894	2.066	124.3
R27	175.2	54.66	30.14	43.23		8.870	4.606	1.636	129.6
N28	175.7	51.92	39.08			7.910	4.853		120.4
A29	178.0	54.39	18.49			9.135	4.097		130.3
N30	174.1	51.93	38.89			8.064	4.853	2.612	114.1
C31	176.8	61.76	30.04			7.161	4.035	2.989	123.1
S32	174.8	58.00	64.07			8.778	4.589		124.3
L33	176.8	54.29	40.92	24.31	27.36	8.514	4.498	1.429	128.7
R34	178.3	65.40	31.95	51.01	27.76	1.995	4.322	1.995	
S35	174.4	60.52	63.07			8.354	4.274		111.8
C36	176.6	63.99	29.78		34.15	7.491	4.220	2.764	126.6
G37	179.4	45.89		23.18	25.42	8.184	3.977	2.140	115.9
K38	179.0	59.60	32.75	29.61	33.46	7.928	4.050		117.0
M39	179.3	56.79	31.74	42.96	27.43	8.312	4.534	1.890	118.1
K40	179.8	61.46	32.79	30.18	27.84	9.473	3.817	1.844	121.6
R41		59.50	29.99	43.66		7.556	4.168	1.986	118.0
W42	177.6	66.79	31.42			7.652	3.689	2.439	121.7
V43	178.9	67.41	31.56			8.450	3.497	2.215	120.4
Q44	178.9	60.95	28.11	129.0	33.72	8.380	3.976		119.2
H45	177.9	59.81	27.22			8.116	4.270		119.0
T46	175.9	66.74	69.55			7.863	3.853	4.210	110.5
K47	177.7	58.72	32.15	29.18	25.38	7.342	4.066		120.3
Q48	173.8	44.70				7.154	2.715	4.383	103.9
C49	176.7	61.21	29.83		25.05	6.921	3.978	2.049	123.2
K50	178.6	56.63	32.89	28.99	27.73	8.979	4.513	1.806	128.2
R51	177.6	57.70	31.58	43.71	24.84	8.507	4.394	2.048	122.4
K52	177.1	57.64	32.29	29.74		8.453	4.499		118.9
N53	175.7	63.74	68.89		26.79	7.717	4.152	1.748	112.8
N54	180.3	55.27	18.29			7.360	4.107		121.1
G55	179.0	57.96	42.38	25.52		7.815	4.144	1.604	117.6
G56	179.9	55.83	19.06			8.869	3.924		121.5
C57	179.9	55.53	18.07			8.636	4.113		119.9
I58	173.2	45.53				7.732	4.178	3.162	118.4
I59	174.6	55.64	30.82	51.54	27.40	8.028	4.824		
K60	178.7	65.08	32.56			7.838	4.325	2.680	121.1
K61	178.3	64.81	34.88	12.73	28.05	8.041	3.769	1.947	123.8
C62	177.6	66.40	29.31	29.54	25.50	8.893	4.111	2.781	116.9
L63	178.6	60.16	32.71		34.50	8.979	3.867	1.769	117.5
I64	178.1	58.72	29.02		27.65	7.308	4.170	2.139	110.9
A65	179.0	58.02	41.81	25.15		8.497	4.163	1.916	120.2
L66	176.9	65.40	37.37	13.52		7.815	3.555		122.1
A67	180.3	55.27	18.29			7.360	4.107		117.6
A68	179.9	55.83	19.06			8.869	3.924		121.5
Y69	178.7	61.46	38.48	133.2	26.79	7.732	4.178		118.4
H70	174.6	55.64	30.82			8.028	4.824		122.2
A71	178.9	59.85	47.83	18.07		9.226	4.389		114.5
K72	176.6	59.21	32.53	29.00	24.50	6.960	3.848	1.442	112.8
H73	173.7	54.37	30.31	121.1		7.073	4.821	2.904	183.2
C74	176.9	60.15	30.01			6.999	4.125	1.777	123.4
Q75	175.5	54.69	29.33		33.82	9.116	4.676	1.845	128.6
E76		55.71	30.39			7.994	4.395		
N77	175.8	55.13	38.48		24.72	8.890	4.506	2.812	125.6
K78	174.9	54.57	30.98	29.18		8.740	4.430	1.628	120.8
C79	176.0	57.85	30.73			6.940	4.308	2.842	123.8
P80	176.9	62.86	32.13			9.040	3.540		127.8
V81	174.2	62.46	31.54		28.42	3.960		2.206	
R82	174.2	64.24	31.55	50.48		9.040	3.540	4.001	127.8

Table 8.0.7: Chemical shifts of the fusion construct of Taz2 with the complete TAD of p73 (continued)

amino acid	C	CA	CB	CD	CD1	CD2	CE	CE1	CE2	CE3	CG	CG1	CG2	CH2	CZ	CZ2	CZ3	H	HA	HA2	HA3	HB	HB2	HB3	HD1	HD2	HD3	HE	HE1	HE2	HG	HG12	HG13	HG2	HG3	HH2	HZ	HZ2	HZ3	N	ND1	NE1	NE2	QA	QB	QD	QD1	QD2	QE	QG	QG1	QG2	QQD	QQG

(Full numerical data table — an extensive grid of chemical shift values for residues F83 through L166 follows. Due to the density of the tabulated data, individual cell values are not reproduced here.)

Table 8.0.8: Backbone chemical shifts of a longer variant of p63 TAD fused to the Taz2 domain of p300

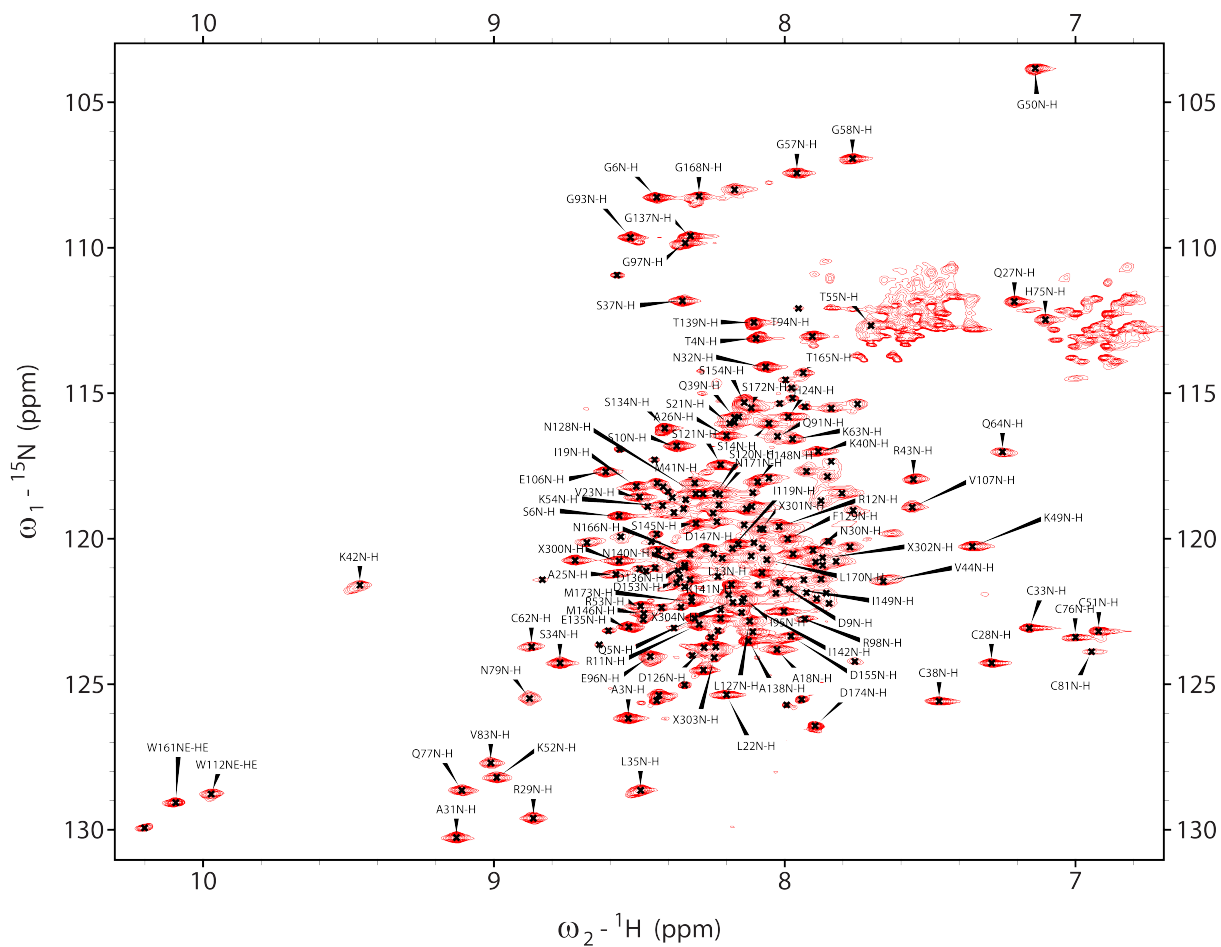| amino acid	CA	CB	H	HE	N	NE
S2	58.36	64.04				
A3	52.80	19.32	8.539		126.2	
T4	61.85	69.80	8.099		113.1	
P5	64.09	32.03				
Q5	55.69	29.87	8.310		122.7	
G6	45.75		8.442		108.3	
S6	56.43	63.41	8.570		119.2	
D9	55.22	41.33	8.080		121.2	
S10	60.31	63.21	8.372		116.8	
R11	58.36	30.01	8.298		122.9	
R12	58.52	30.26	8.020		119.6	
L13	57.13	41.94	8.116		120.6	
S14	60.95	63.28	8.057		116.0	
R17	59.32	30.19				
A18	55.46	18.57	8.028		123.8	
I9	65.11	37.46	8.515		118.2	
Q20	59.27	28.16				
S21	61.97	63.00	8.181		116.0	
L22	58.67	42.27	8.206		125.4	
V23	66.96	31.77	8.501		118.6	
H24	60.21	27.82	7.988		115.8	
A25	55.14	19.73	8.581		121.2	
A26	53.95	18.65	8.201		116.5	
Q27	54.55	30.76	7.213		111.8	
C28	60.88	29.21	7.290		124.3	
R29	54.61	30.05	8.866		129.6	
N30	51.87	39.08	7.905		120.4	
A31	54.35	18.47	9.130		130.3	
N32	51.91	38.87	8.066		114.1	
C33	61.76	29.99	7.161		123.1	
S34	57.99	64.06	8.774		124.3	
L35	54.24	40.90	8.497		128.6	
P36	65.34	31.81				
S37	60.47	63.01	8.351		111.8	
C38	64.00	29.73	7.470		125.6	
Q39	59.87	28.17	8.169		115.8	
K40	59.64	32.71	7.886		117.0	
M41	56.84	31.83	8.310		118.1	
K42	61.50	32.70	9.461		121.6	
R43	59.45	30.01	7.558		118.0	
V44	66.73		7.665		121.5	
T48	65.78	69.58				
K49	58.75	32.17	7.356		120.3	
G50	44.70		7.142		91.36	
C51	61.18	29.86	6.923		123.2	
K52	56.63	32.83	8.991		128.2	
R53	57.68	31.59	8.497		122.3	
K54	57.72	32.16	8.419		118.9	
T55	63.91	68.76	7.692		112.7	
N56	53.65	38.34				
G57	45.86		7.958		107.4	
G58	45.55		7.770		106.9	
I61	51.66					
C62	66.44	29.24	8.873		123.7	
K63	60.17	32.60	7.976		116.6	
Q64	58.70		7.249		117.0	
K74		32.43				
H75	54.24	30.05	7.104		112.5	
C76	60.07	29.97	7.006		123.4	
K76	58.11					
Q77			9.111		128.7	
E78	43.03					
N79	55.20		8.875		125.5	
C81	61.00	38.95	6.945		123.9	
P82	62.93	32.18				
V83	62.59	31.66	9.011		127.7	
Q91	57.34	29.03	8.028		116.5	
G93	45.60		8.531		109.6	
T94	61.78	69.96	7.906		113.0	
I95	61.44	38.78	8.141		122.1	
E96	57.06	30.14	8.463		124.1	
G97	45.51		8.345		109.8	
R98	55.59	30.84	8.004		122.5	
P105	65.00	31.96				
E106	58.93	29.22	8.617		117.7	
V107	64.83	31.85	7.562		118.9	
W112				9.972		128.0
P118	63.26	31.95				
I119	61.55	38.79	8.218		120.7	
S120	58.35	63.89	8.242		118.4	
S121	58.52	63.90	8.220		117.5	
I125	61.21	39.16				
D126	54.01	41.41	8.279		123.8	
L127	55.11	42.02	8.123		122.8	
N128	53.50	38.94	8.300		118.5	
F129	57.82	39.46	7.991		120.0	
P133	63.35	32.15				
S134	58.20	64.12	8.412		116.2	
E135	56.77	30.25	8.536		123.0	
D136	54.62	41.25	8.345		121.0	
G137	45.65		8.325		109.6	
A138	52.83	19.38	8.125		123.5	
T139	62.11	69.74	8.107		112.6	
N140	53.32	38.94	8.346		120.9	
K141	56.44	33.12	8.183		121.6	
I142	61.22	38.78	8.147		122.2	
I144	61.00	38.95				
S145	58.18	63.95	8.306		119.5	
M146	55.83	32.80	8.485		122.6	
D147	55.03	41.08	8.272		120.3	
C148	59.03	28.04	8.096		118.1	
I149	61.64	38.42	7.986		121.7	
D153	54.83	41.09	8.371		121.5	
S154	58.72	63.95	8.140		115.3	
D155	52.30	41.78	7.980		123.4	
W161				10.09		129.1
Y164	57.89	38.67				
T165	62.26	69.92	7.938		114.3	
N166	53.45	38.63	8.326		120.5	
L167	55.85	42.13				
G168	45.83		8.297		108.2	
L169	55.55	42.36				
L170	55.49	42.22	8.064		120.8	
N171	53.41	39.09	8.223		118.5	
S172	58.59	63.90	8.120		115.5	
M173	55.51	33.15	8.320		122.2	
D174	55.88	42.27	7.896		126.4	
X300	57.26	29.82	8.571		120.8	
X301	57.80	39.43	8.086		119.7	
X302	62.08	33.13	7.872		120.7	
X303	54.16	41.47	8.243		124.1	
X304	54.18	30.11	8.179		122.2	

Figure 8.0.1: p300Taz2-p63TAD long fusion backbone assignment. [^{15}N,^{1}H]-BEST-TROSY of p300Taz2 with an elongated p63 peptide showing the backbone assignment of the fusion construct at pH 6.3/303 K. Parts of the sequence could not be assigned due to spectral overlap and conformational instability of the protein as visualized by three independent tryptophan side chain signals, despite the construct having only two tryptophan residues.

Acknowledgments

First, I want to thank my supervisor Volker Dötsch for giving me the opportunity to work in his lab and on such an interesting project. He has given me the great opportunity to look left and right beside the core of the project thereby leading to additional interesting findings.

Secondly, I have to thank Frank "Murph" Löhr for tremendous help with the NMR, recording all kinds of spectra and generally showing me around in this method. After a long time doing NMR I still feel like I barely scratched the surface, and therefore my questions are probably almost as stupid as in the very beginning.

Sina Kazemi has also been an integral part of this project, doing structure calculations over and over again until the very last zinc ion has its correct geometry.

I also would like to thank my in-group cooperation partners Katharina Krauskopf and Marcel Tuppi for the great collaboration and in extension also Franziska Finke who gets to do all the work that neither Marcel nor me are inclined to do.

I also want to thank my students, that I supervised in the last couple of years. Especially Kim Wendrich has been a tremendous help in the later stages of my thesis, as she was a very capable and independent practical student, where also independently performed complex experiments would lead to very good results. In addition, I want to thank Lisa Pietrek for doing one assignment after another when the phosphorylation kinetic project was still in the very beginning and nobody could really see if it was worth pursuing it after all. Furthermore my bachelor students Matthias Bretschneider and Michael Gecht who worked on various parts of the p300 project. Eike Laube was another great bachelor student, who did great work in demonstrating that previously published work by other groups is most likely not specific interaction but co-aggregation.

Many thanks also to all members of the p63 project, Christian Osterburg, Susanne Pitzius, Alexander Strubel and Niklas Gutfreund as well as Jessica Huber for helpful discussion and input.

Erik Henrich and Juljia Mezhyrova deserve massive credit for being the "cell-free expression team", having always time for the expression of selectively labeled peptides or the random "let's try if this construct expresses cell-free" in general. In extension I want to thank Aisha Laguerre, formerly a member of the cell-free group, for sometimes helpful discussions but mostly for belay-

Curriculum Vitae

Jakob Gebel

born in Solingen on September 27, 1987

Address: Antoninusstr. 64, 60439 Frankfurt, Germany

Phone: +49 176 20950604

Email: JakobGebel@gmail.com

Nationality: German

Education

since 01/2014	**PhD student** in Biochemistry, Institute of Biophysical Chemistry at the Goethe University, Frankfurt/Main, Germany
	PhD thesis: "Structural investigations on the interaction of and phosphorylation of TAp63" (Supervisor: Prof. Dr. Volker Dötsch)
03/2013-10/2013	**Diploma thesis**, Dötsch group, Institute of Biophysical Chemistry, Goethe University Frankfurt, Germany
	"Structural and functional characterization of the novel isoform of p63, GTAp63α and NMR solution structure of the p63/p73 hetero tetramerization complex"
	grade: 1.0 (magna cum laude)
10/2008-11/2013	**Studies in Biochemistry** at the Goethe University, Frankfurt/Main, Germany
	Focus subjects: biochemistry (1.0), biophysical chemistry (1.0) and organic chemistry (1.0)
08/1998-07/2007	**Secondary school**, Gymnasium Schwertstraße, Solingen
	Bilingual Abitur (German/English, grade 1.9)
08/2004-06/2005	Ilmajoen lukio, High school
	Ilmajoki, Finland

Professional experience

since 12/2013   **Instructor**, Introduction into NMR spectra evaluation and assignment

03/2013-10/2013   **Diploma thesis**, Dötsch group, Institute of Biophysical Chemistry, Goethe University Frankfurt, Germany

"Structural and functional characterization of the novel isoform of p63, GTAp63α and NMR solution structure of the p63/p73 hetero tetramerization complex"

05/2012-08/2012   **Internship**, Kühlbrandt group, Max-Planck-institute for biophysics Frankfurt

"Expression, purification and crystallisation of archeal NhaP transporters"

Expression, solubilisation and purification of a membrane transporter. Crystallization using screens and subsequently fine-screens.

05/2011-08/2011   **Internship**, Schwalbe group, Institute of Chemical Biology, Goethe University Frankfurt

"Studies on ribosome-nascent chain-complexes at the example of γ-Crystallin B"

Expression and purification of native and NMR-labeled ribosomes, ribosome-nascent chain-complexes and target proteins.

04/2011-12/2011   **Research assistant**, Dötsch group, Institute of Biophysical Chemistry, Goethe University Frankfurt

02/2011-04/2011   **Internship**, Dötsch group, Institute of Biophysical Chemistry, Goethe University Frankfurt

"purification of stabilized TAp63α constructs for X-ray crystallography"

10/2010-09/2011   **Teaching Assistant**, undergrad classes Biophysical Chemistry I and II, BSc Biochemistry, Goethe University Frankfurt

Revision and sample calculations with a class of 20 students.

08/2007-05/2008   **Civil Service**, children's home Hossenhaus, Solingen.

Groundskeeping, tilling of agricultural land

Publications

2018   Krauskopf K*, **Gebel J***, Kazemi S, Tuppi M, Löhr F, Schäfer B, Koch J, Güntert P, Dötsch V & Kehrloesser S (2018) Regulation of the Activity in the p53 Family Depends on the Organization of the Transactivation Domain. *Structure* **26:** 1091-1100.e4

2018   Nemajerova A, Amelio I, **Gebel J**, Dötsch V, Melino G & Moll UM (2018) Non-oncogenic roles of TAp73: From multiciliogenesis to metabolism. *Cell Death Differ.* **25:** 144-153

2017   **Gebel J**, Tuppi M, Krauskopf K, Coutandin D, Pitzius S, Kehrloesser S, Osterburg C & Dötsch V (2017) Control mechanisms in germ cells mediated by p53 family proteins. *J. Cell Sci.* **130:** 2663-2671

2016   **Gebel J***, Luh LM*, Coutandin D*, Osterburg C, Löhr F, Schäfer B, Frombach AS, Sumyk M, Buchner L, Krojer T, Salah E, Mathea S, Güntert P, Knapp S & Dötsch V (2016) Mechanism of TAp73 inhibition by ΔNp63 and structural basis of p63/p73 hetero-tetramerization. *Cell Death Differ.* **23:** 1930-1940

2016   Coutandin D*, Osterburg C*, Srivastav RK, Sumyk M, Kehrloesser S, **Gebel J**, Tuppi M, Hannewald J, Schäfer B, Salah E, Mathea S, Müller-Kuller U, Doutch J, Grez M, Knapp S & Dötsch V (2016) Quality control in oocytes by p63 is based on a spring-loaded activation mechanism on the molecular and cellular level. *Elife* **5:** 1-22

2013   Luh LM*, Kehrloesser S*, Deutsch GB, **Gebel J**, Coutandin D, Schäfer B, Agostini M, Melino G & Dötsch V (2013) Analysis of the oligomeric state and transactivation potential of TAp73α. *Cell Death Differ.* **20:** 1008-16

*These authors contributed equally to the work.

Laboratory skills

Biochemistry	Immunoprecipitation, immunoblotting, protein production (E. coli, in vitro translation, sf9 insect cell culture), stable isotopic labeling, protein purification (affinity, ion exchange, size exclusion), FPLC, SDS PAGE, protein cross linking, enzyme mediated protein ligation, pulldown assays
Cell Biology	Cell culture, nucleic acid transfection, transactivation activity assays, protein silencing, application of small molecule inhibitors, in vitro differentiation of stem cells, Crispr/Cas9
Molecular Biology	Molecular cloning techniques, PCR, mutagenesis
Biophysics	NMR (1D-3D setup, analysis, structure calculation), ITC, protein crystallography, SPR, MS, CD

Animal Sciences	preparation of P8 mice ovaries, culture of mice ovaries
Legal	Eingeschränkte Sachkunde nach ChemVerbotsV
	certification of knowledge of chemical toxicity and the German regulatory framework for placing chemicals on the market
	FELASA certification category B
	certification allowing for independent handling of experimental animals

Talks and Seminars

2017   BMRZ Symposium, Bad Homburg, Germany
"Regulation of the TAp63α activity by phosphorylation"

2013   BMRZ Symposium, Bad Homburg, Germany
"Structure and Stability of the Heterotetrameric Complex of p63 and p73"

Poster Presentations

2018   28th International Congress on Magnetic Resonance in Biological Systems (ICMRBS), Dublin, Ireland
"TAp63α is activated via timed multistep phosphorylation and a "kinetic fuse"

2018   2nd Frankfurt Conference on Quality Control in Life Processes and 8th p63/p73 workshop, Frankfurt, Germany
"TAp63α is activated via timed multistep phosphorylation and a "kinetic fuse"

2016   1st Frankfurt Conference on Quality Control in Life Processes, Frankfurt, Germany
"Insight into the hetero-oligomieric interaction of ΔNp63α and TAp73 by structural and functional analysis"

2014   BMRZ evaluation, Frankfurt
"Structural investigations on p63/p73"

2013   Molecular Life Sciences 2013, International Symposium of the german society for biochemistry and molecular biology (GBM), Frankfurt, Germany
"Insight into the hetero-oligomieric interaction of ΔNp63α and TAp73 by structural and functional analysis"

2013   6th p63/p73 workshop, Chiba, Japan
"Insight into the hetero-oligomieric interaction of ΔNp63α and TAp73 by Structural and Functional Analysis"

Scholarships and Awards

08/2018	ICMRBS poster award
01/2014	Award for the best diploma thesis in Biochemistry
10/2011-10/2013	Scholarship "MainCampus Academicus" of the foundation of the Polytechnische Gesellschaft, Frankfurt
2004	Jugend forscht - special price in the national competition for the best work in the category "work environment"
	"Laptop-based lighting control for small theater stages"

Computer and language skills

Microsoft Office

Microsoft Visual Studio

Adobe Illustrator, Photoshop, Premiere

Scientific programs: Pymol, Origin, Unicorn, Prism, Bruker TopSpin, Sparky NMR, CCPN

German: native speaker

English: fluent in spoken and written (bilingual secondary education)

French/Finnish: basic knowledge

Extracurricular activities

01/2013-now	Board of the Alumni Association "FBCF"
	"Förderverein Biochemie in Frankfurt e.V."
	Responsibility on the Board: CTO, homepage
12/2009-08/2012	Head representative of the student council, Faculty 14 Biochemistry, Goethe University, Frankfurt
	Main organization of student activities, including representation of students during the development of new bachelor and master curricula, mediation between professors and students in the resolution of conflicts and organization of social activities on campus such as get-togethers with invited speakers, orientation week for first year students and parties.

Personal Interests/Activities

Electrical engineering

Rock climbing and hiking

Academic teachers

R. Abele, B. Averhoff, P. J. Bauer, G. Bruls, C. Buchholz, C. Büchel, V. Dötsch, G. Eckert, E. Egert, U. Ermler, K. Fendler, C. Glaubitz, M. Göbel, A. Gottschalk, J. Koch, B. Kolbesen, M. Kössl, W. Kühlbrandt, B. Ludwig, V. Müller, H. D. Osiewacz, H. Schwalbe, R. Tampé, M. Wagner, C. Ziegler, H. Zimmerman, M. Zörnig